Cleanup Efficiency of Hydraulically Fractured Vertical and Multiple Fractured Horizontal Wells

By

Hamid Reza Nasriani

Submitted for the degree of **Doctor of Philosophy** in

Petroleum Engineering

Heriot-Watt University

Energy, Geoscience, Infrastructure and Society / Institute of Petroleum Engineering

June 2016

Abstract

The initiation and propagation of fractures in unconventional tight and ultra-tight reservoirs are achieved through the injection of high volumes of fracturing fluid, FF. Several field experiences have shown that ineffective FF cleanup can significantly impair gas production.

In this thesis, results of 109 different sets of vertical well (VW) and multiple fractured horizontal well (MFHW) numerical simulations, each consisting of 4096 or 1000 runs depending on two different sampling approaches, are presented studying the impact of pertinent parameters during FF injection (stimulating), soaking (shut-in) and production periods for a total of 384,394 runs. In these sets I studied, the impact of a combination of various shut-in time, matrix permeability range, applied drawdown pressure and injected FF volume. For the MFHW case, the impact of fractures spacing and horizontal length were also investigated.

In each set, twelve pertinent parameters related to fracture and matrix relative permeability and matrix capillary pressure have been varied. Gas production loss (GPL) and produced FF (PFF), as the response terms, have been calculated based on two separate response surface statistical models. In each set, the correlation between parameters and GPL and PFF have then been established and compared with a base reference set and other similar sets but with one different variable. An extensive evaluation of capillary pressure (Pc) correlations available for tight and ultra-tight formations was performed to investigate the reliability of available Pc correlation models. Additionally, a comprehensive investigation was conducted on the unconventional relative permeability (Kr) with jail effect in unconventional formations. A practically attractive approach has been adopted to successfully model the weak and strong permeability jail effects to express unconventional Kr models.

DEDICATION

To my parents, my wife and my lovely son for their patience and continuous support throughout my study.

ACKNOWLEDGMENTS

I would like to express my deepest appreciation and gratitude to my supervisor, Prof Jamiolahmady who provided the opportunity, financial support and technical support.

You have been a tremendous supervisor for me. It would have been impossible to complete this thesis without your expertise, understanding and encouragement. I have always benefited from your expertise, supervision, brilliant ideas, invaluable advice and extensive knowledge.

I am very grateful to my examiners, Prof Eric Mackay and Dr Reza Fassihi for spending their valuable time in reading this thesis and sharing their insightful comments and suggestions.

I wish to extend special appreciation to my colleagues in Gas Condensate Recovery team at Heriot-Watt University for helpful discussions and suggestions regarding this work.

Finally, I would like to express my sincere gratitude to my loving wife and also my best friend, Leila, my devoted parents and my brilliant son, Amir Hossein, for their unconditional support, understanding and encouragement.

(Research Thesis Submission Form should be placed here)

TABLE OF CONTENTS

LISTS OF TABLES

LISTS OF FIGURES

LIST OF PUBLICATIONS

1) Jamiolahmady M., Alajmi E., **Nasriani H.R.**, Ghahri P., Pichestapong K., "A Thorough Investigation of Clean-up Efficiency of Hydraulic Fractured Wells Using Statistical Approaches", SPE-170862-MS, SPE Annual Technical Conference and Exhibition, Amsterdam, The Netherlands, 27–29 October 2014, http://dx.doi.org/10.2118/170862-MS

2) **Nasriani H.R.,** Jamiolahmady M., Alajmi E., Ghahri P., "A Study of Hydraulic Fracturing Clean-up Efficiency in Unconventional Gas Reservoirs Using Statistical Approaches", S.ID: 21646, ECMOR XIV 14th European Conference on the Mathematics of Oil Recovery, Catania, Sicily, Italy, 8 - 11 September 2014, DOI: 10.3997/2214-4609.20141797.

3) **Nasriani H.R.**, Jamiolahmady M., Alajmi E., "An Integrated Study of Clean-up Efficiency of Short Hydraulic Fractured Vertical Wells Using Response Surface Methodology", S.ID:21446, 76th European Association of Geoscientists and Engineers Conference and Exhibition 2014: Experience the Energy - Incorporating SPE EUROPEC 2014, Amsterdam RAI, Amsterdam, Netherlands, 16 - 19 June 2014, DOI: 10.3997/2214-4609.20141380.

List of Symbols

Nomenclature

a_i: coefficients of the equation

B_o: oil formation factor

h: reservoir thickness

J: productivity index

k: absolute reservoir permeability

k_v: vertical permeability

k_h: horizontal permeability

Kr: relative permeability

K_{max}: end point of the Corey relative permeability curve

Kmr: matrix permeability ratio, i.e., if Kmr=10 mean the Km variation range is reduced by a factor of 10.

L: length

M: mobility

n_g: exponent of the gas Corey relative permeability curve

n_w: exponent of the water Corey relative permeability curve

Nf: number of fractures

P: pressure

Pc: capillary pressure

P_d: threshold pressure

q: flow rate

r: radius

S_w: water saturation

Swi: initial water saturation

Swir: irreducible water saturation

Swc: critical water saturation

Sgr: residual gas saturation

Sgc: critical gas saturation

W_f: fracture width

X_f: half length of the fracture

x: x direction

y: y direction

z: z direction

Greek Letters:

ϕ: porosity

μ: viscosity

ρ: density

λ: pore size distribution index

σ: interfacial tension

Subscript

ave: average

bhp: bottom hole pressure

c: condensate

dew: dew point

f: fracture

g: gas

h: horizontal

HW: horizontal well

i: an index

j: an index

m: matrix

o: oil

r: residual

x: x-direction

y: y-direction

w: refers to well-bore

Abbreviations

AD%: absolute deviation (percentage)

AAD%: Average Absolute Percentage Deviation

CCE: constant composition expansion

CPU: computer processing unit

CVD: constant volume depletion

DP: pressure drawdown.

Dra: drainage

EOS: equation of state

FF: fracture fluid

FFPT: total fracturing fluid production

FFR: fracture fluid residue

FFV: fracture fluid volume

FFS: full factorial sampling

FGPT: total cumulative gas production

FVR: the ratio of injected fracture fluid to fracture volume

FQRSM: full quadratic response surface model

GCR: gas condensate research group

GPL: gas production loss

GPR: gas production rate

HF: hydraulic fracturing

HFW: hydraulically fractured well

HW: horizontal well

HWU: Heriot-Watt University

IFT: interfacial tension

Imb: imbibition

IPE: Institute of Petroleum Engineering

ILRSM: interactive linear response surface model

LGR: local grid refinement.

LHS: Latin hypercube sampling

LRM: linear response surface model

MEPO: MEPO Multiple Realization Optimizer software

MFHW: multiple fractured horizontal well.

OH: open-hole

PFF: produced fracturing fluid

PR: productivity ratio

PR3: 3 parameters Peng-Robinson equation of state

PQRSM: pure quadratic response surface model

IFT: interfacial tension

Python: Python Programming Language

RMSE: root mean square error

RSM: response surface model

SFVW: single fractured vertical well.

SL: single layer

TL: two layer

SRV: stimulated reservoir volume

ST: shut-in/soaking time.

TGP: total gas production

VW: vertical well

1-D: one dimensional

2-D: two-dimensional

3-D: three-dimensional

CHAPTER 1 INTRODUCTION

Tight and ultratight gas formations usually refer to low permeability gas bearing formations that predominantly produce dry gas. The most important issue with the development of tight and ultratight gas formations is that their production rate is not at economic flow rates without stimulation, i.e., hydraulic fracturing. In other words, commercially production of these unconventional resources involves the development of either hydraulically fractured vertical wells or multiple fractured horizontal wells.

Hydraulic fracturing is generally implemented to increase the productivity of the well in these unconventional formations. The initiation and propagation of fractures in unconventional reservoirs are achieved through the injection of high volumes of fracturing fluid, FF. Hydraulic fracturing, even though commonly a very effective well stimulating technique to enhance well productivity in tight and ultra-tight formations, frequently does not respond as expected. Ineffective fracture cleanup is one of the main reasons put forward to explain this underperformance (Jamiolahmady et al., 2009, Ghahri et al., 2011, Assiri and Miskimins, 2014, Jurus et al., 2013).

This thesis reports some of the numerical works of the Gas Condensate Recovery Joint Industry Project (JIP) at Heriot-Watt University. The broad objectives of this project are to investigate the flow of gas and condensate in conventional and unconventional reservoirs, to conduct a comprehensive investigation on the hydraulic fracturing cleanup, to study the improvement in relative permeability of low IFT systems as velocity increases and/or IFT decreases using a combined experimental and theoretical approach and to study near-wellbore effects.

Chapter 2 of this thesis presents a literature review on cleanup efficiency. The literature review gives an overview of the theoretical and numerical aspects of hydraulic fracturing treatment and post-fracturing cleanup efficiency. The main focus of this chapter is on the cleanup efficiency of hydraulic fractures. There are several experimental, numerical and field studies investigating the impact of the cleanup efficiency of hydraulic fractures on gas production and FF flowback in unconventional tight/ultratight formations. The assumptions and main findings of these studies are summarised.

In Chapter 3, following the encouraging results of the work conducted by Jamiolahmady et al. (2009) and Ghahri et al. (2011), I present the results of 66 different

sets of vertical well (VW) numerical simulations, studying the impact of pertinent parameters during FF injection (stimulating), soaking (shut-in) and production periods for total of 270,336 runs. In each set, twelve pertinent parameters related to fracture and matrix relative permeability and matrix capillary pressure have been varied. Additionally, the impact of shut-in time, matrix permeability range, applied drawdown pressure, injected FF volume, fracture spacing and horizontal well length have been investigated by running different sets. A 2-level full factorial statistical experimental design approach has been applied to sample a wide range of variation of 12 pertinent parameters covering many practical cases. Gas production loss (GPL), as the response terms, has been calculated and input into a response surface statistical model. In each set, the correlation between parameters and GPL has then been established and compared with a base reference set and other similar sets but with one different variable.

The details of the pre-fractured single fractured vertical well model will be presented in section 3.2. In section 3.3, a list of 66 different sets for long and short single fractured vertical well (SFVW) is presented. The ranges of variation of pertinent parameters that were investigated in the numerical simulations during this study will be presented in section 3.4. The details of governing equations for capillary pressure and gas and water relative permeabilities will also be discussed in section 3.4. Section 3.5 gives an introduction to the analysis approach adopted in this study and defines terminologies that are used in order to make it easier for the reader to follow the presented results and conclusions. In section 3.5.1, the main response in this study which is Gas Production Loss (GPL, %) is described. It is defined as a measure of unclean fracture cumulative production deviation from the cumulative production of the case with fully (100%) clean fracture. Section 3.5.2 discusses the response surface model which is used to analyse and express the sensitivity of the set of parameters pertinent to the main response. Section 3.5.3 presents the 12 pertinent parameters that have been considered in this study. There, a brief description of the physical impact that each parameter has on fluid flow is discussed.

Section 3.5.4 explains the two types of figures used in this study. The first type of figures is the histogram figure, which has been used to show the cumulative frequency of a certain range of the main response (GPL) for any numerical model (i.e. reference model, short fracture model, etc.). The second is Tornado chart figure; which is used to show the impact of the pertinent parameter on the main response (GPL). It shows the parameter's

direction of impact (negative or positive) and the relative importance which each parameter has on the behaviour of the main response.

In section 3.5.5, it is highlighted that considerable efforts were dedicated to fit equations that are more representative of the trends observed in the performed simulations. In this exercise, the main dependent variable (i.e. GPL) domain of the fitted response surface model (RSM) was changed. That is, without the domain change there were cases whereby the predicted GPL was very different from the actual value and sometimes giving unrealistic negative or greater than 100%, GPL values. However, with the domain change this issue was eliminated.

These 66 different sets for long and short fracture SFVW will be investigated comprehensively in sections 3.6 to 3.13. In these sections, I have analysed the results of the 66 different sets for long fracture SFVW, 400m, and short fracture SFVW, 100m. The results have been compared with those of a base reference set and other similar SFVW-Sets. These models have the same reservoir dimensions as those of the SFVW reference set but differ in the fracture fluid injection volume (FVR), shut-in time period (ST), matrix permeability variation range (Kmr), pressure drawdown (DP), initial water saturation (Swi) and length of the hydraulic fracture. The main conclusions of this chapter are in section 3.14.

Chapter 4 focuses on the cleanup efficiency of multiple fractured horizontal wells (MFHW). In this chapter, following the promising results of the work conducted on the cleanup efficiency of SFVWs, the line of research is extended to MFHWs. Similar to the work conducted on SFVWs, in these MFHW-Sets, twelve pertinent parameters related to fracture and matrix relative permeability and matrix capillary pressure have been varied. Additionally, the impact of shut-in time, matrix permeability range, applied drawdown pressure, injected FF volume, fracture spacing and horizontal well length have been investigated by running different sets. Gas production loss (GPL), as the response terms, has been calculated based on and input into a response surface statistical model. In each MFHW-Set, the correlation between parameters and GPL has been established and compared with a base reference set and other similar sets but with one different variable. Since MFHW-Sets require significantly more CPU time than the vertically fractured well model and in order to reduce the CPU time and to ensure achieving more accurate predictions for GPLs, the Latin hypercube sampling (LHS) method has been used in the

last 7 MFHW-Sets instead of two-level full factorial sampling (FFS) used in the first 22 MFHW-Sets.

It should be noted that the response surface model fitted to results based on the full factorial is linear whereas that fitted based on LHS could be either linear or quadratic, which increases the accuracy of the fitted response surface models. For these simulations using LHS, the Multiple Realization Optimizer, MEPO, (Schlumberger, 2013) has been used to link automatically different stages of the simulations conducted using ECLIPSE100 (Schlumberger, 2015) and to perform pre and post-processing stages. 7 MFHW base reference sets with different run numbers have been conducted and analysed to obtain the minimum (optimum) number of runs required for this new approach. The details of pre-fractured multiple fractured horizontal well model will be presented in section 4.1. In section 4.2, a list of 29 different sets for MFHW is presented. The ranges of variation of pertinent parameters that were investigated in the numerical simulations during this study will be similar to those of SFVW sets. These 29 different sets for MFHW will be investigated comprehensively in sections 4.3-4.11. In section 4.11, for the MFHW sets 23 to 29, instead of two-level FFS experimental design used in the previous simulations (MFHW sets 1 to 22), the LHS method has been used to decrease the required number of runs. It should be noted that the response surface model fitted to results based on the full factorial is a linear whereas that fitted based on LHS could be either linear or quadratic, which increases the accuracy of the fitted response surface models. For these simulations, the MEPO software has been used to link automatically different stages of the simulations conducted using ECLIPSE100 and to perform pre and post-processing stages. The main conclusions of this chapter will be found in section 4. 12.

In chapter 5, following the promising results of the work conducted on the cleanup efficiency of SFVWs and MFHWs, the line of research is extended to MFHWs with unconventional Pc and unconventional relative permeability. In section 5.1, a comprehensive evaluation of Pc correlations available for tight and ultra-tight formations is performed using Go2Flow software to investigate the reliability of available Pc correlations models for tight and ultra-tight formations. The result of the study suggested that that Brooks and Corey is a simple and accurate one-specific-parameter model to represent Pc data in tight and ultra-tight unconventional formations, but the range of pore size distribution index should be limited to 0.3 to 1.5, rather than the 1 to 4 used previously, to represent more realistically the unconventional tight/ultra-tight rock

behaviours. In section 5.3, the new pore size distribution range suitable for Pc of unconventional formations with different Kmr, DP and FVR has been applied and corresponding results were analysed, compared and discussed. The aim was to observe the impact of these parameters on cleanup efficiency while using unconventional Pc.

In section 5.4, a comprehensive investigation was conducted on the unconventional relative permeability (Kr) with relative permeability jail effect in unconventional formations. An attractive approach has been adopted to successfully model the weak and strong permeability jail effects in unconventional Kr models. Additionally, a new dimensionless term, similar to GPL, has also been defined to capture the impact of the same pertinent parameters on the production of FF, which is an important consideration for HF of unconventional reservoirs. 5 different MFHW-sets with unconventional Pc and Kr will be investigated comprehensively in sections 5.5-5.6. The main conclusions of this chapter will be presented in section 5.7. In section 5.8, the cleanup efficiency of the MFHWs in heterogeneous formations, while changing some of the pertinent parameters, was investigated. 5 different MFHW-Sets were modelled considering different injection volume (FVR=10), shut-in time (ST=20), applied pressure drawdown (DP) during production and Km range.

The main conclusions of this thesis are in chapter 6. This chapter also includes some recommendations for further investigations of the research areas discussed in this work.

1.1 References

ASSIRI, W. & MISKIMINS, J. L. 2014. The Water Blockage Effect on Desiccated Tight Gas Reservoir. SPE International Symposium and Exhibition on Formation Damage Control, 26-28 February, Lafayette, Louisiana, USA

GHAHRI, P., JAMIOLAHMADY, M. & SOHRABI, M. 2011. A Thorough Investigation Of Cleanup Efficiency Of Hydraulic Fractured Wells Using Response Surface Method. Society of Petroleum Engineers.

JAMIOLAHMADY, M., SOHRABI, M. & GHAHRI, P. 2009. Investigation of Cleanup Efficiency of Hydraulically Fractured Wells in Gas Condensate Reservoirs. Society of Petroleum Engineers.

JURUS, W. J., WHITSON, C. H. & GOLAN, M. 2013. Modeling Water Flow in Hydraulically-Fractured Shale Wells. Society of Petroleum Engineers.

SCHLUMBERGER (2013) 'MEPO Multiple Realization Optimizer; MEPO4.2.0; Build:2617; Date:2013-Apr-25_15-59', *SPT Group; A Schlumberger Company*.

SCHLUMBERGER (2015) 'Geoquest, ECLIPSE 100, Version 2015.1.0.0', *Simulation Launch Management Utility*.

CHAPTER 2 LITERATURE REVIEW ON POST-FRACTURING CLEANUP

Natural gas is considered to be the cleanest fossil fuel with least emissions. It is also considered to be one of the most substantial source of energy in future due to its abundance and environmental reliability. Natural gas plays a progressively important role in residential heating, industrial, commercial and electrical generation sectors across the world. Natural gas resources could be either conventional or unconventional. Unlike the conventional natural gas reserves that are considered to be one of the most economical and easiest reserves to extract, unconventional natural gas resources are much more problematic and less economically viable to develop. Coalbed methane, tight and ultra-tight gas sands, gas shales and gas hydrates are considered as unconventional gas resources. Significant demand growth on natural gas has resulted in the development of natural gas resources from tight and ultra-tight gas sands and shale gas plays. Tight and ultra-tight gas resources make up 57-59% of the worldwide unconventional resources with pronounced abundance in several parts of the world, i.e., Europe, Asia, North Africa, North America and the Middle East, (Dong et al., 2011).

Hydraulic fracturing is generally implemented to increase the productivity of the wells in these unconventional formations. The initiation and propagation of fractures in unconventional reservoirs are achieved through the injection of high volumes of fracturing fluid, FF. Several field experiences have shown that ineffective FF cleanup can significantly impair gas production. There are several experimental, numerical and field studies investigating the impact of the cleanup efficiency of hydraulic fractures on gas production and FF flowback in unconventional tight/ultra-tight formations.

Cooke (1975, 1973) implemented laboratory experiments showing the impact of fracturing fluid residue (FFR) and reservoir environment (the FF and the reservoir temperature) on the propped fracture conductivity during the cleanup process of vertically fractured wells. He also demonstrated that the fracture permeability can be affected by the existence of high-temperature brine. Using a predictive method he developed a theoretic model based on the volume of FFR (after it reduces the fracture porosity and impairs the fracture conductivity) to calculate fracture permeability (kf) reduction. He also obtained the fracture porosity decline as a function of closure pressure and temperature and demonstrated the results in the form of a chart. These charts could be

used to estimate the fracture permeability reduction due to those effects, by means of the same theoretical model, which was previously developed for estimation of kf reduction.

Tannich (1975) investigated the cleanup procedure using a numerical model and observed that FF flowback (also known as load recovery) and gas breakthrough period are functions of matrix permeability and fracture conductivity. He highlighted that larger fracture conductivity values will result in a better cleanup. However, he did not capture the impact of different matrix relative permeability qualities on the cleanup process.

Holditch (1979) conducted a study on the impact of damage to matrix grids in the vicinity of the fracture, by examining the effect of FF (considered as water) saturation increase and permeability decrease in this region, on the productivity of hydraulically fractured gas wells. He conducted his study by means of a finite difference numerical simulator. It was noted that the impact of capillary pressure, Pc, in tight formations (low permeability reservoirs) was evident in low pressure drawdown (DP) cases in which DP was not significantly larger than the matrix Pc. He described that the complete water blockage happens only when the matrix permeability of the region around the fracture decreases by 99.9% or DP does not overcome Pc in the region invaded by FF. He reported that the FF invasion depth in their matrix was up to 5 in, with uniform FF distribution in the matrix adjacent to the hydraulic fracture. He concluded that in low permeability formations, Pc and relative permeability in invaded zones are significantly important on cleanup efficiency but in his work, the effect of FFR on the fracture conductivity was not investigated.

Cinco-Ley and Samaniego-V (1981) studied hydraulic fracturing and fracture conductivity (Fcd) reduction of vertically fractured wells with two different damage zones, i.,e., damaged regions around and within the fracture. They observed that at early production stages, the impact of fracture conductivity and fracture face damage (as restricting factors to flow) on productivity are significantly different. They suggested a correlation for approximating the effect of fracture face skin on well productivity.

Pope et al. (1996) presented a positive relationship between load recovery and gas production from field data. They explained that as FF is produced back to the surface from HF, an equivalent space in the fracture becomes available to the flow of the gas toward the well. Therefore, the higher the load recovery, the more the gas production. They presented a correlation between FF flowback and gas production rates to support their theory. They also highlighted larger initial flow rates will result in load FF recovery.

May et al. (1997) considered a yield stress for polymer residue in a numerical model and investigated the effect of yield stress on FF cleanup efficiency. They reported that increasing DP has a minimal effect on cleanup of fracture whilst increasing Fcd can substantially increase the effective fracture length and consequently speed up the cleanup process.

Lolon et al. (2003) investigated the cleanup process of HFs using a numerical model. Their aim was to understand how FF production and effective fracture length affect the gas production. They noticed that the FF production rate and consequently the cleanup is substantially affected by the Fcd. i.e., the higher the Fcd the faster the cleanup. They also concluded that larger Fcd values result in longer effective fracture length, greater cumulative gas production and the faster fracture cleanup. They also highlighted that the impact of Fcd influencing effective fracture length is more significant than those of matrix permeability, fracture closure effects, or formation water mobility.

Friedel et al. (2004) used a fracturing simulator to model fracturing and then imported the results of the simulator into a reservoir simulator to investigate the cleanup. They considered a time-dependent mechanical matrix skin to better match the production rates using measured drainage matrix relative permeability curves.

Gdanski et al. (2005) extended the study conducted by Holditch (1979) on cleanup to further investigate the gas and FF two-phase flow and matrix permeability damage in the invaded region. For this study, they developed a numerical model and discussed that the fracture face damage extensively reduced gas production if the matrix permeability in the invaded region is reduced to 1% of the initial matrix permeability. They also reported that the larger the original matrix Pc, the more damage to the gas production. However, they did not consider the fact that in the case of larger Pc values the FF is imbibed more in the matrix, reducing the FF saturation in the fracture grids, increased gas effective permeability inside the fracture and consequently cleaner fractures.

Wang et al. (2009) developed a numerical model to simulate tight gas reservoirs, they investigated the impact of reservoir pressure, fracture length, DP, multiphase gas and FF flow, proppant crushing, polymer filter cake, and gel yield stress inside the fracture. They reported that the major factor that decreases FF cleanup and gas recovery is the gel strength of the FF inside the fracture after fracturing stimulation.

Jamiolahmady et al. (2009) studied the cleanup efficiency in single fractured vertical wells, SFVW, of gas and gas-condensate fields. They further investigated some of the uncertainty on the impact of pertinent parameters affecting the cleanup efficiency in tight

and ultra-tight formations. They also reproduced the numerical model results mentioned by Holditch (1979) which has been referred to in many cleanup simulation studies from then on. They conducted a wide-ranging sensitivity analysis to investigate the impact of Kf reduction due to FF residue and reservoir conditions, FF viscosity change, Pc, FF injection and imbibition into the matrix, matrix permeability (Km) reduction due to FF invasion in the invaded zone, an increase in Pc of the matrix invaded zone, initial water saturation (Swi), hysteresis, FF relative permeability and DP on the cleanup efficiency of a SFVWs.

They reported that the existence of FF in the invaded region affects the gas cumulative production by impairing the gas relative permeability, i.e., it results in a gas production loss compared to a case when no FF was injected. Decreasing the FF viscosity and consequently increasing FF mobility results in larger FF recovery at the production stage. They also highlighted that when Pc increases, the FF invades deeper into matrix due to capillary forces resulting in the better cleanup.

To study the cleanup process, Bazin et al. (2010) implemented Special Core Analysis Laboratory (SCAL) experiments to measure the reduced matrix permeability and the multi-phase flow across the core after core flooding by FF. The FF saturation distribution profile, retention and flowback were measured by X-ray in the experiment. They also conducted numerical simulations to study the impact of different parameters like DP and relative permeability hysteresis effect. They mentioned that during the FF injection, FF moves simultaneously by both displacement (viscous forces) and imbibition (capillary force) mechanisms. During the production stage after fracture stimulation, some water moves further into the matrix counter-current to the gas flow, which is toward the well due to capillary imbibition. Since the SCAL experiment was considered to model the cleanup process, it was not possible to fully capture the cleanup efficiency due to the limited length of the core sample whilst in the reservoir, the FF saturation in the matrix could reduce further (more cleanup) due to FF imbibition into much deeper zones inside the matrix.

Gdanski and Walters (2010) developed a two-dimensional model to simulate the fracture cleanup process and to study the physics of two-phase flow within the matrix and fracture. They ignored the gravity effects in their numerical model. They simulated a quarter of the reservoir by means of symmetry. They demonstrated that FF flow-back is a function of Pc, matrix permeability, matrix relative permeability to FF and gas, Swi, Shut-in time (ST), DP, and fracture dimensions and fracture permeability. They

highlighted that among these factors considered, the quality of the matrix relative permeability to gas and FF can significantly affect the impact of other factors on FF recovery whether it is a slight or significant impact on load recovery. They concluded that good-quality matrix relative permeabilities to FF and gas allow Pc to significantly decrease FF recoveries. This FF recovery reduction is more pronounced in cases with extended ST, lower Swi in the matrix, higher Pc and lower fracture conductivity. They mentioned that moderate-quality matrix relative permeabilities to FF and gas extensively decreased the impact of Pc as well as ST, Swi and fracture conductivity. Poor-quality matrix relative permeabilities to FF and gas substantially disabled the FF imbibition into the matrix.

Ghahri et al. (2011) extended the work conducted by Jamiolahmady et al. (2009). They conducted a wide-ranging investigation of variation of all pertinent parameters using experimental design combined with the response surface methodology (RSM). They demonstrated that gas production loss, GPL, is significantly affected by parameters linked to FF cleanup inside the fracture particularly Kf. In their study, sometimes increased FF flowback from the matrix into fracture increased GPL. At longer production periods, the impact of fluid mobility in the matrix became more distinct. The relative significance of pertinent parameters was less pronounced for lower FF injection volume and especially at longer production periods.

Jurus et al. (2013) studied the effect of water imbibition due to Pc as the main mechanism for retaining of FF in the matrix. They used the available conventional Pc and relative permeability models to capture the effect of Pc on retention of FF and gas production. They reported that capillary forces have a significant impact on FF flowback. They also mentioned that positive Pc increases the FF leak off into the matrix and improves FF retention whilst negative Pc does not have a major impact on retaining FF but may affect the injectivity of the well. They showed that once the initial water saturation, Swi, was less than the irreducible water saturation, Swir, water retention in the matrix could be stronger.

Assiri and Miskimins (2014) showed the FF blockage effect on the productivity of desiccated tight gas reservoirs. They simulated a single horizontal well (with the length of 2000 ft.) using a black oil commercial simulator. To capture the effect of a desiccating tight gas reservoir, they considered that Swi is less than Swir in the model. In this case injected FF during hydraulic fracturing is locked in the vicinity of the wellbore at water saturations up to Swir. Additionally, some FF could be retained at higher water saturations

than Swir due to capillary forces. They observed that the reduced gas productivity after hydraulic fracturing indicates an FF blockage. They showed that gas productivity could be dropped by up to 44%, and a delay in production could be experienced. They concluded that the cleanup procedure depends on how desiccating the tight gas formation is. However, hydraulic fractures, HFs, have not been included in their numerical model and their observations were based on a single horizontal well in a desiccated tight gas reservoir.

This thesis extends the line of the work conducted by Jamiolahmady et al. (2009) and Ghahri et al. (2011) to the areas which are not addressed in their work as below:

- Identifying the gaps in SFVW study and conducting new SFVW sets which were not addressed before to fill the gap (sets with different parameters, i.e., tight and very tight sets, shorter fracture, different Swi, DP, FVR….).
- Extending the cleanup efficiency study to MFHWs systems and conducting new MFHW-Sets.
- Applying new sampling approach to increase the accuracy of RSM and reduce CPU time (i.e., the Latin hypercube sampling (LHS) method rather than the old full factorial sampling) and conducting new MFHW-Sets using new approach
- Conducting a comprehensive evaluation of Pc correlations available for tight and ultra-tight formations.
- Conducting a comprehensive investigation on unconventional relative permeability (Kr) and permeability jail effects in unconventional formations and conducting new MFHW-Sets.

In this thesis, results of 109 different sets (a total of 384,394 runs) of the single fractured vertical well (SFVW) and multiple fractured horizontal well (MFHW) numerical simulations, are presented. These sets capture the impact of pertinent parameters during FF injection (stimulating), soaking (shut-in) and production periods. In each set, twelve pertinent parameters (matrix and fracture permeability, IFT, Lambda and end point and exponent of Corey gas and FF relative permeability curve in matrix and fracture) have been varied. In addition to those twelve pertinent parameters, the impact of shut-in time (ST), matrix permeability range, applied drawdown pressure, injected FF volume, fracture spacing and horizontal well length has been investigated by running different sets. Two response terms (Gas production loss (GPL) and produced FF (PFF)) have been calculated and input into a response surface statistical model. In each set, the correlation between parameters and GPL as well as PFF have then been

established and compared with a base reference set and other similar sets but with one different variable. A comprehensive evaluation of capillary pressure (Pc) correlations available for modelling tight and ultra-tight formations has been performed to identify a suitable Pc for the purpose of this study. Additionally, a comprehensive investigation has been conducted on the unconventional relative permeability (Kr) with jail effects. Accordingly, an approach has been implemented to successfully model the weak and strong permeability jail effects to represent unconventional Kr models.

It should be mentioned that the fracture face roughness is not included in this study, but it could increase FF retention due to additional pressure drop in the fracture relative to a smooth surface. It is also should be highlighted that the shape of the fracture is not always regular and this may affect the fracture cleanup efficiency.

2.1 Geomechanical Effects:

Economic production from extremely low permeability, insignificant porosity shale plays is not possible without stimulation techniques. Several studies are conducted to further understand the complex flow performance in tight and ultra-tight fields. But, with the intention of predicting the performance of shale gas fields, applying precise shale rock properties is important for developing a geologic model for the field.

The rock geomechanical properties have a huge impact on the principal stress profile of a field. The rock geomechanical properties consist of Poisson's ratio, total minimum horizontal stress, and bulk, Young, and shear modulus. These properties have a substantial impact on the development plans of shale plays compared to conventional formations. It should be highlighted that geomechanical data play an important role in assisting engineers and geoscientists during geomechanical modelling, hydraulic fracture operation design as well as reservoir modelling in shale gas fields.

There are two sets of variables for studying the geomechanical effects, the first set is the flow variables set including pressure and temperature and the second sets is variables associated with geomechanics like stress, strain and displacement. The equations for geomechanical effect are presented as follows:

$$\nabla . \boldsymbol{\sigma} - \boldsymbol{F} = \mathbf{0} \qquad \textbf{2.1}$$

$$\boldsymbol{\sigma} = \boldsymbol{C} : \boldsymbol{\varepsilon} + (\boldsymbol{\alpha p} + \boldsymbol{\eta} \Delta \boldsymbol{T}) \boldsymbol{I} \qquad \textbf{2.2}$$

$$\boldsymbol{\varepsilon} = \frac{\mathbf{1}}{\mathbf{2}} [\nabla \boldsymbol{u} + (\nabla \boldsymbol{u})^{\boldsymbol{T}}] \qquad \textbf{2.3}$$

Where in these equations σ is the total tensor and F is the body force, C the tangential stiffness tensor, α is the Biot's constant, η is the thermoelastic constant, ε is the strain tensor and u is displacement vector. If these three equation are combined together; the resulting equation will be as follows:

$$\boldsymbol{\nabla}.\left\{\boldsymbol{C}:\frac{\mathbf{1}}{\mathbf{2}}[\boldsymbol{\nabla u}+(\boldsymbol{\nabla u})^{\boldsymbol{T}}]\right\}=-\boldsymbol{\nabla}[(\propto \boldsymbol{p}+\boldsymbol{\eta}\Delta\boldsymbol{T})\boldsymbol{I}]+\boldsymbol{F} \qquad \textbf{2.4}$$

First the flow set is solved and the pressure is attained, then the pressure is used in Equation. 2.4 to determine the displacement vector. Once the displacement vector is obtained, the stress and strain tensor can be obtained using Equation. 2.2 and Equation 2.3, respectively.

Since the porosity is calculated using the geomechanical factors. Hence, porosity is not only a function of just pressure and temperature but it is also a function of rock stress and strain.

In several studies, pressure dependant properties were presented to consider the change in conductivity (Pedrosa Jr, 1986; Raghavan and Chin, 2002; Cho, Ozkan and Apaydin, 2013; Kim, Lee and Lee, 2016). Hence, in this thesis in SFVW-Sets 64, 65 and 66. In these SFVW-sets power law equations are used to obtain the stress dependent properties.

$$\frac{\emptyset}{\emptyset_{\boldsymbol{i}}}=\left(\frac{\boldsymbol{\sigma'}}{\boldsymbol{\sigma'}_{\boldsymbol{i}}}\right)^{-\boldsymbol{a}} \qquad \textbf{2.5}$$

$$\frac{\boldsymbol{K}}{\boldsymbol{K_i}}=\left(\frac{\boldsymbol{\sigma'}}{\boldsymbol{\sigma'}_{\boldsymbol{i}}}\right)^{-\boldsymbol{b}} \qquad \textbf{2.6}$$

Where σ' is the effective stress and a and b are the coefficients determined in the experiments.

It should be noted that the explicit modelling of the fracturing geo-mechanics and fracture propagation was outside of the scope of this thesis and the aim was to capture the dynamic of gas and FF in post-fracturing stage and the detrimental effect of FF on production. Therefore, micro-fractures are not explicitly modelled and permeability enhancement is studied in a few sets, i.e., SFVW-Sets 64, 65 and 66.

2.2 References

ALAJMI, E 2012. Modelling of Gas-Condensate Flow around Complex Well Geometries and Cleanup Efficiency in Heterogeneous Systems. PhD thesis, Heriot-Watt University Petroleum Engineering, Edinburgh, UK

ASSIRI, W. & MISKIMINS, J. L. 2014. The Water Blockage Effect on Desiccated Tight Gas Reservoir. Society of Petroleum Engineers.

BAZIN, B., BEKRI, S., VIZIKA, O., HERZHAFT, B. & AUBRY, E. 2010. Fracturing in Tight Gas Reservoirs: Application of Special-Core-Analysis Methods To Investigate Formation-Damage Mechanisms.

BENNION, D. B., THOMAS, F. B., SCHULMEISTER, B. E. & SUMANI, M. 2004. Determination of true effective in situ gas permeability in subnormally water-saturated tight gas reservoirs. *Journal of Canadian Petroleum Technology,* 43**,** 27-32.

BENTSEN, R. G. & ANLI, J. 1977. Using Parameter Estimation Techniques To Convert Centrifuge Data Into a Capillary-Pressure Curve.

BROOKS, R. H. & COREY, A. 1966. Properties of porous media affecting fluid flow. *Journal of the Irrigation and Drainage Division,* 92**,** 61-90.

BYRNES, A. P. 1996. Reservoir characteristics of low-permeability sandstones in the Rocky Mountains. *Mountain Geologist,* 34**,** 39-48.

BYRNES, A. P. 2008. Issues with gas relative permeability in low-permeability sandstones. *AAPG Hedberg Series, no. 3, p. 63–76.*

CHO, Y., OZKAN, E. & APAYDIN, O. G. (2013) 'Pressure-dependent natural-fracture permeability in shale and its effect on shale-gas well production', *SPE Reservoir Evaluation & Engineering*. Society of Petroleum Engineers, 16(2), pp. 216–228.

CINCO-LEY, H. & SAMANIEGO-V, F. 1981. Transient Pressure Analysis: Finite Conductivity Fracture Case Versus Damaged Fracture Case. Society of Petroleum Engineers.

CLUFF, R. M. & BYRNES, A. P. 2010. Relative Permeability In Tight Gas Sandstone Reservoirs - The Permeability Jailt; Model. *Society of Petrophysicists and Well-Log Analysts.* Society of Petrophysicists and Well-Log Analysts.

COOKE, C. E., JR. 1973. Conductivity of Fracture Proppants in Multiple Layers.

COOKE, C. E., JR. 1975. Effect of Fracturing Fluids on Fracture Conductivity.

DONG, Z., HOLDITCH, S. A., MCVAY, D. & AYERS, W. B. 2011. Global Unconventional Gas Resource Assessments. Society of Petroleum Engineers.

ECONOMIDES, M. J. & MARTIN, A. N. How to decide between horizontal transverse, horizontal longitudinal and vertical fractured completion. Proceedings - SPE Annual Technical Conference and Exhibition, 2010. 2474-2491.

FRIEDEL, T., MTCHEDLISHVILI, G., BEHR, A., VOIGT, H.-D. & HÄFNER, F. 2004. Numerical analysis of cleanup processes in german tight gas formations with fractured wells. *Erdöl, Erdgas, Kohle*, 120**,** OG133-OG136.

GDANSKI, R., WEAVER, J., SLABAUGH, B., WALTERS, H. & PARKER, M. 2005. Fracture Face Damage It Matters. *SPE 94649.*

GDANSKI, R. D. & WALTERS, H. G. 2010. Impact of Fracture Conductivity and Matrix Relative Permeability on Load Recovery. Society of Petroleum Engineers.

GHAHRI, P., JAMIOLAHMADY, M. & SOHRABI, M. 2011. A Thorough Investigation Of Cleanup Efficiency Of Hydraulic Fractured Wells Using Response Surface Method. Society of Petroleum Engineers.

GHAHRI, P 2010. Modelling of Gas-condensate flow around horizontal and deviated wells and cleanup efficiency of hydraulically fractured wells. PhD thesis, Heriot-Watt University Petroleum Engineering, Edinburgh, UK

HOLDITCH, S. A. 1979. Factors Affecting Water Blocking and Gas Flow From Hydraulically Fractured Gas Wells.

JAMIOLAHMADY, M., SOHRABI, M. & GHAHRI, P. 2009. Investigation of Cleanup Efficiency of Hydraulically Fractured Wells in Gas Condensate Reservoirs. Society of Petroleum Engineers.

JURUS, W. J., WHITSON, C. H. & GOLAN, M. 2013. Modeling Water Flow in Hydraulically-Fractured Shale Wells. Society of Petroleum Engineers.

KIM, T. H., Lee, J. H. & LEE, K. S. (2016) 'Integrated reservoir flow and geomechanical model to generate type curves for pressure transient responses of a hydraulically-fractured well in shale gas reservoirs', *Journal of Petroleum Science and Engineering*, 146, pp. 457–472. doi: 10.1016/j.petrol.2016.06.001.

LEVERETT, M. 1941. Capillary behavior in porous solids. *Transactions of the AIME,* 142**,** 152-169.

LOLON, E. P., MCVAY, D. A. & SCHUBARTH, S. K. 2003. Effect of Fracture Conductivity on Effective Fracture Length. Society of Petroleum Engineers.

MAY, E. A., BRITT, L. K. & NOLTE, K. G. 1997. The Effect of Yield Stress on Fracture Fluid Cleanup Nolte, SPE, Dowell. Society of Petroleum Engineers.

MCKAY, M. D., BECKMAN, R. J. & CONOVER, W. J. 1979. A Comparison of Three Methods for Selecting Values of Input Variables in the Analysis of Output from a Computer Code. *Technometrics,* 21**,** 239-245.

PEDROSA JR, O. A. (1986) 'Pressure transient response in stress-sensitive formations', in *SPE California Regional Meeting*. Society of Petroleum Engineers.

POPE, D., BRITT, L., CONSTIEN, V., ANDERSON, A. & LEUNG, L. 1996. Field Study of Guar Removal from Hydraulic Fractures. Society of Petroleum Engineers.

RAGHAVAN, R. & CHIN, L. Y. (2002) 'Productivity changes in reservoirs with stress-dependent permeability', in *SPE Annual Technical Conference and Exhibition*. Society of Petroleum Engineers.

RUSHING, J. A., NEWSHAM, K. E. & BLASINGAME, T. A. 2008. Rock Typing: Keys to Understanding Productivity in Tight Gas Sands. Society of Petroleum Engineers.

SHAFER, J. & NEASHAM, J. Mercury porosimetry protocol for rapid determination of petrophysical and reservoir quality properties. International Symposium of the Society of Core Analysts, SCA, 2000. 12.

SHANLEY, K. W., CLUFF, R. M. & ROBINSON, J. W. 2004. Factors controlling prolific gas production from low-permeability sandstone reservoirs: Implications for resource assessment, prospect development, and risk analysis. *AAPG bulletin,* 88**,** 1083-1121.

SHAOUL, J. R., VAN ZELM, L. F. & DE PATER, C. J. 2011. Damage Mechanisms in Unconventional-Gas-Well Stimulation--A New Look at an Old Problem.

SKELT, C. & HARRISON, B. 1995. An Integrated Approach To Saturation Height Analysis. Society of Petrophysicists and Well-Log Analysts.

TANNICH, J. D. 1975. Liquid Removal From Hydraulically Fractured Gas Wells.

THOMEER, J. H. M. 1960. Introduction of a Pore Geometrical Factor Defined by the Capillary Pressure Curve.

UNIVERSITY OF KANSAS CENTER FOR RESEARCH, I. & SURVEY., T. K. G. 2009. Analysis Of Critical Permeability, Capillary Pressure And Electrical Properties For Mesaverde Tight Gas Sandstones From Western U.S. Basins. *Final Scientific/Technical Report for United States Department of Energy and National Energy Technology Laboratory*.

WANG, J. Y., HOLDITCH, S. A. & MCVAY, D. 2009. Modeling Fracture Fluid Cleanup in Tight Gas Wells. Society of Petroleum Engineers.

WELLS, J. D. & AMAEFULE, J. O. 1985. Capillary Pressure and Permeability Relationships in Tight Gas Sands. Society of Petroleum Engineers.

CHAPTER 3 CLEANUP EFFICIENCY OF HYDRAULICALLY FRACTURED VERTICAL WELLS

3.1 Introduction

It is well documented that hydraulic fracturing, HF, even though commonly a very effective well stimulating technique to enhance well productivity in tight and ultra-tight formations, frequently does not respond as expected. Ineffective fracture cleanup is one of the main reasons put forward to explain this underperformance.

FF is one of the most important components of HF operations. It typically consists of water (95%), sand (4.5%) and some chemical additives (up to 0.5%) which are added to the mixture of FF to attain different goals such as enhancing of the fracturing, the prevention of corrosion, changing energy forces, changing the FF viscosity, adjusting the PH of FF, stabilizing clays, delaying breakdown of gel polymer chains, and preventing formation of scale deposits. Gelling agents are added to FF to make it viscous enough to carry the proppant (i.e., sands) efficiently to the hydraulic fractures to hold the Fracture aperture open and create a significantly conductive channel for the fluids to easily flow to the well. FF creates the fractures and transports the proppants, which in turn prevent the closure of the fractures after HF treatment. FF cleanup after HF treatment is meant to remove FF from the fracture and the matrix. FF impairs the productivity through various mechanisms by invasion into the matrix and fracture. During the last forty years, several studies have been conducted to investigate the impact of FF on the well performance of hydraulically fractured wells, which were mentioned in the previous chapter.

In this chapter, following the encouraging results of the work conducted by Jamiolahmady et al. (2009) and Ghahri et al. (2011) , the results of 66 different sets of vertical well (VW) numerical simulations, are presented studying the impact of pertinent parameters during FF injection (stimulating), soaking (shut-in) and production periods for total of 270,336 runs. In each set, twelve pertinent parameters related to fracture and matrix relative permeability and matrix capillary pressure have been varied. Additionally, the impact of shut-in time, matrix permeability range, applied drawdown pressure, injected FF volume and fracture length have been investigated by running different sets. Gas production loss (GPL), as the response term, has been calculated based on a response surface statistical model. In each set, the correlation between parameters and GPL has then been established and compared with a base reference set and other similar sets but with one different variable.

3.2 Single Fractured Vertical Well (SFVW) Model

For the case of single fractured vertical well, SFVW, a pre-fractured single well model was built using ECLIPSE 100 (Schlumberger, 2015) with dimensions of 2000 by 2000 by 40 m in x-, y- and z-directions. The Cartesian fine grid was optimised to minimise the numerical error. The initial reservoir pressure and matrix porosity were 7500 psi and 15% respectively. Table 3.1 shows fracture properties and reservoir dimensions for the reference model used here. The fracture half-length (Xf) was either 400m (long SFVW) or 100m (short SFVW). The fluid properties of the single-phase gas flowing through the model are tabulated in Table 3.2. The fracturing fluid, FF, was defined as water with a viscosity of 0.5 cp and compressibility of 5e-6 (1/psi). For the base set defined as a reference, FF volume of two times fracture volume was considered for the injection periods. Since a section of the system (a quarter of the system) was modelled (Figure 3.1), FF with a total injection volume of either 64 m^3 (long SFVW) or 16 m^3 (short SFVW) was considered. That is, the FF volume per fracture length, defined as (= Vinj / Lf, m^3/m) was equal to 0.16 m^3/m equivalent to 2 FVR (The ratio of injected fracture fluid to fracture volume) defined as FVR= Vinj / Vf, m^3/m^3. In the second period of simulation, gas and fracture fluid phases are produced under controlled bottom-hole pressure. After FF injection and before production, the well is shut-in for two days.

3.2.1 Validation of the developed Model of Single Fractured Vertical Well

To validate the model developed for SFVW cleanup operation, the predicted bottom hole pressures from the reservoir simulation outputs were compared with analytical models. It should be noted that cleanup period is during early time flow period i.e., transient period (MoradiDowlatAbad M, 2016).

In this section, the governing equations for early time flow period are discussed. It should be noted that the fracture linear flow period has been ignored in this study due to its short life span in comparison to the linear flow time towards the fracture.

the linear flow regime is considered as parallel flow lines that move toward a plane orthogonally. the linear flow regime could be identified by a half-slope in the derivative on a log-log diagnostic plot or by a straight line on a square root of time (linear flow specialized) plot.

Equation 8.1 has been generally used for describing the linear flow regimes:

$$P_{wf} = P_i - (\frac{8.128qB}{A}\sqrt{\frac{\mu t}{K_m \emptyset C_t}}) \qquad 3.1$$

where A is the area perpendicular to the linear flow, h is the formation thickness, t is the time, Pi is the initial reservoir pressure and q is the flowrate produced from one fracture.

At the early time flow period, the early linear flow is the main flow regime in most of SFVWs and MFHWs in tight reservoirs. For this flow regime, as the area perpendicular to the flow is the cross section of a fracture (2Xfh), the corresponding equation is as follows:

$$P_{wf} = P_i - \left\{\sqrt{\frac{16.52q^2B^2\mu}{h^2\emptyset C_t}}\frac{\sqrt{t}}{\sqrt{K_m X_f^2}} + \frac{141.2q\mu B}{K_m h}(S_D + S_c)\right\} \qquad 3.2$$

In Equation 3.2, S_D is the damage skin, S_c is the convergence skin in a fractured horizontal well.

For a multiple fractured horizontal well in a tight and ultratight reservoir, the total production rate, qt, in the early-time flow period can be calculated from Equation: 3.3.

$$q_t = \sum_{i=1}^{N} q_i \qquad 3.3$$

Considering a constant fracture spacing and homogeneous formation within the fractures as well as equal fractures properties, the total production rate of the well could be estimated by multiplying the production rate from a single fracture by the number of fractures during the early-time flow period, i.e., q in Equation 3.2 is (qt/Nf).

As soon as pressure perturbations of neighbouring fractures reach each other (i.e. fracture interference starts), The early linear flow regime ends. The corresponding time can be estimated by Equation 3.4.

$$t_{el} = 237\frac{\emptyset\mu C_t S_f^2}{K_m} \qquad 3.4$$

where ∅, μ, Ct and t_{el} are the porosity, viscosity, total compressibility and the time of interference respectively. It should be highlighted that the fracture interference time depends on the reservoir and fracture properties.

If the bi-linear flow happens rather than early linear flow in MFHWs, Equation 3.2 should be substituted by Equation 3.5.

$$P_{wf} = P_i - \left\{ \frac{44.13 q B \mu \sqrt[4]{t}}{h\sqrt{K_f W_f} * \sqrt[4]{K_m \emptyset \mu C_t}} + \frac{141.2 q \mu B}{K_m h} (S_D + S_c) \right\} \qquad 3.5$$

In this section, to validate the model developed for SFVW cleanup operation and in order to give confidence that the model is consistent, the predicted bottom hole pressures from the reservoir simulation outputs were compared with analytical models.

Figure 3.2 shows the predicated bottom hole pressure by simulation model and also the predicated bottom hole pressure by analytical model (Equation 3.2) versus production time, it should be noted that both graphs are overlapping and almost on top of one another which confirms the accuracy of the developed model. Figure 3.3 shows the predicated bottom hole pressure by analytical model (Equation 3.2) versus the one of simulation model where satisfactory R^2 of 0.9993 is noted.

3.3 Sets Analysed

In this chapter, the results of total of 66 different sets for long fracture SFVW, 400m, (40 sets), short fracture SFVW, 100m, (21 sets), two-layer long fracture, 400m, (4 sets), shorter fracture length SFVW base reference set, Xf=50m, (one set) are analyzed. The results have been compared with those of a base reference set and other similar sets. These models have the same reservoir dimensions as those of the SFVW reference set but differ in the fracture fluid injection volume (FVR), shut-in time period (ST), matrix permeability variation range (Kmr), pressure drawdown (DP), initial water saturation (Swi) and length of the hydraulic fracture. The SFVW sets that have been considered in this chapter are listed here for the reference and convenience.

The analysed SFVW sets in this chapter are listed in Table 3.4a to Table 3.4f.

For SFVW simulation sets, there is a Base Reference set with parameters in the ranges indicated in Table 3.4 as defaulted values. The other sets are cited based on the differences of the parameters variation range from the Base Reference set, i.e., in each SFVW-Set any parameter that has a tick mark has the defaulted values otherwise the parameter's value is stated in the table.

It should be noted that the results of each SFVW-Set are compared either with base reference set or with similar SFVW-Sets reported highlighting the impact of pertinent

parameters studied in this thesis. This means that set numbering might not be monotonic for sets reported in different sections.

3.4 Range and Number of Investigated Variables

Table 3.3 shows the ranges of variation of pertinent parameters that were investigated in the numerical simulations during this study. There are 12 parameters for the production period in this Table. These variables were selected based on the understanding of the process gained by the work of the GCR team, i.e., Ghahri (2010) and Alajmi(2012), literature data and support of Total as one of the sponsors of the project, which is gratefully appreciated. As shown in Table 3.3, the other remaining 6 parameters, i.e., porosity and critical gas and water saturations in the matrix and fracture and pressure drawdown (DP), were considered constant in each simulation set. Porosity was fixed at a value of 0.15 and both residual gas saturation in the matrix (Sgrm) and fracture (Sgrf) were fixed at a value of 0.1. Additionally, critical water saturation in the matrix (Swcm) and fracture (Swcf) were fixed at a value of 0.15.

In line with the team's investigation of the process and to reduce the otherwise unacceptable CPU time required, it was assumed that the FF fill in the fracture instantly during the injection period eliminating the need to consider the impact of parameters on this flow period. In this procedure, the FF saturation distribution within the matrix, which contributes to the performance of cleanup to a much greater extent, is obtained by the simulator but that within the fracture is assumed to happen instantly, which is somewhat consistent with what happens in reality and reported in the literature.

- Equations 3.6, 3.7, 3.8 and 3.9 describe the capillary pressure (Thomas, Katz and Tek, 1968)

  and relative permeability curves (Brooks and Corey, 1966) for data of Table 3.3.

$$\frac{Pd}{IFT} = 0.0075 \times K^{-0.5}$$

- Threshold pressure Pd ,bar, (Thomas, Katz and Tek, 1968) 3.6
- Interfacial tension IFT (dyne/cm)
- Matrix permeability (K (mD))

$$\left(\frac{Pd}{Pc}\right)^{\lambda} = \frac{Sw - Swr}{1 - Swr} \quad 3.7$$

$$k_{rw} = K_{\max w} \times \left(\frac{Sw - Swr}{1 - Swr - Sgr}\right)^{nw} \quad 3.8$$

$$k_{rg} = K_{\max g} \times \left(\frac{Sg - Sgr}{1 - Swr - Sgr} \right)^{ng} \quad 3.9$$

Equation 3.7 is used to calculate Pc. This equation is linked to Equation 3.6.

The impact of pressure drop (DP), which was considered constant, was treated separately, i.e. different sets of simulations were considered for each pressure drop. This brings the total number of variables from 16 in Ghahri's work (Ghahri (2010)) to 12 in Alajmi's work (Alajmi (2012)) and this work for both pre- and post-treatment simulations. Based on this number of parameters, each fracture well model (mentioned earlier) requires 4096 simulation runs (for a two-level full factorial sampling (FSS) design) bringing the total number of simulation runs for all the analysed 66 sets of 12-parameter models to 270,336 simulation runs. It should be noted that Panteha (Ghahri (2010)) had conducted 4 sets and Ebrahim (Alajmi (2012)) had 7 sets and those runs did not investigate the cases that are addressed in this thesis (i.e., Chapter 3).

It should be noted that in this study and to analysis the results more efficiently using the response surface method, described below, the parameters are scaled between 0 and 1 with zero corresponding to the lower limit of variation of a selected parameter and 1 corresponding to the maximum point. It also should be highlighted that in FFs approach, as one parameter changes and kept the other constant and due to the nature of the sensitivity analysis, I do not keep any correlation between the parameters that are dependent on one another (e.g., Permeability and porosity, or Swi and porosity)

3.5 Methodology

Analysing a huge number of numerical simulation runs is a real challenge and hence, should be presented in a very systematic and easy-to-follow way or it will lose its benefit. The aim of this section is to give an introduction to the analysis approach adopted in this study and to define terminologies that are used in order to make it easier for the reader to follow the presented results and conclusions.

3.5.1 Main Response

The main response in this study is Gas Production Loss (GPL, %), defined as a measure of unclean fracture cumulative production deviation from the cumulative production of the case with fully (100%) clean fracture.

$$GPL = 100 \times \left[\frac{FGPT_{clean} - FGPT_{un-clean}}{FGPT_{clean}}\right] \qquad 3.10$$

FGPT: total gas cumulative production

In reality, it is difficult (if not technically unfeasible) to get a fully clean fracture job. However, if we understand the impact of pertinent parameters on the cleanup process then we can provide practical guidelines to get closer to a 100% clean fracture job. One main advantage of GPL is that it is a normalised quantity, which allows us to compare different scenarios more simply and draw conclusions more properly. In this study, the impact of pertinent parameters on GPL are addressed. In this exercise, a parameter is considered to have a positive impact if increasing the value of the parameter reduces GPL while a negative impact parameter is the one, which increases GPL as its value is increased.

3.5.2 Response Surface Method (RSM)

RSM is a useful tool to analyse and express the sensitivity of a set of parameters pertinent to a particular output. It is a combination of statistical and mathematical methods to find an appropriate relationship between the main response y and independent variables x1, x2, x3... xn. It fits a polynomial function to the response y. This polynomial function (f(xi)) is called the response surface model. This model can be a linear or quadratic (with or without interaction term) and defined by Equation 3.11.

$$y = a_0 + \sum_{k=1}^{n} a_k x_k + \sum_{i=1}^{n} \sum_{j=i+1}^{n} a_i a_j x_i\, x_j + \sum_{l=1}^{n} a_l x_l^2 \qquad 3.11$$

In Equation 3.11 four different models could be considered:

- Linear Surface model, if constant (a_0) and linear terms ($a_k x_k$) are considered.
- Interactive Linear Surface model, if the interaction terms ($a_i a_j x_i x_j$) are also considered.
- Pure Quadratic Surface model, if constant & linear and quadratic terms ($a_l^2 x_l^2$) are considered.
- Full Quadratic Surface model, if constant& linear, interaction and quadratic terms are considered.

For the team's previous works, and because linear full factorial experimental design had been used, the linear response model with and without interaction terms was employed to describe the dependency of gas production loss (GPL) on parameters affecting the cleanup efficiency of an HFW. That is, to discuss the dependency of GPL on individual parameters the linear function without interaction terms was reported.

However, the fitted equations with interaction terms were used for GPL prediction and included in NEW-COIN. NEW-COIN (NEW-COIN, 2015) is an in-house software, developed by the Heriot-Watt Gas Condensate Recovery team, which calculates near wellbore relative permeability accounting for coupling and inertia; and estimates gas condensate well productivity for various completion strategies, it also estimates the cleanup efficiency of hydraulic fracturing in SFVWs and MFHWs.

A MATLAB code (The MathWorks, 2013) was developed for SFVW-Sets to link different stages of the simulation and to model the two-level full factorial sampling approach. The MATLAB code is included in Appendix 7.1.

3.5.3 Pertinent Parameters

As mentioned previously, 12 pertinent parameters have been considered in this study. Here I will give a brief description of the physical impact that each parameter has on fluid flow.

The exponent of Corey type (gas or fracture fluid) relative permeability curve (n_{gi} and n_{wi}, where i refer to inside fracture or inside matrix): Physically, increasing Corey exponent increases the curvature of relative permeability curve and thus reduces the relative permeability of fluid, as shown in Figure 3.4.

The end point of (gas or fracture fluid) relative permeability (K_{maxgi} and K_{maxwi}, where i refer to inside fracture or inside matrix): Increasing the end point of fluid relative permeability will increase the relative permeability value, as shown in Figure 3.5.

Capillary pressure: In this study, there are three parameters, which affect capillary pressure as demonstrated by Equations 3.6 and 3.7. These parameters are matrix permeability (Km, mD), interfacial tension (IFT, mN/m), and pore size distribution index (λ).

Interfacial tension (IFT): an increase in interfacial tension increases capillary pressure, as shown in Figure 3.5.

Pore size distribution index (λ): an increase in Pore size distribution index (λ) decreases capillary pressure, as shown in Figure 3.6.

Matrix permeability (Km): an increase in matrix permeability decreases capillary pressure, as shown in Figure 3.7.

3.5.4 Figures Used for Analysis of Our Results

There are two types of Figures used in this study. The first type of Figures is the Histogram Figure, which has been used to show the cumulative frequency of a certain range of the main response (GPL) for any numerical model (i.e. reference model, short fracture case-a model ...etc.). Here I use gas production loss of 20% (called hereafter GPL_{20}) as our reference line for comparison between different models. That is, knowing the frequency of cases, which have GPL_{20}, allows us to compare the severity of GPL between different fracture models. For instance, referring to Figure 3.8, which shows a cumulative frequency of GPL for two different models (model A and B), it can be noticed that model A has a GPL_{20} of 25% while model B has GPL_{20} of 60%. This means that 75% of the simulated cases in model A has a GPL of more than 20%, while the corresponding value in model B is 40%, in other words, faster cleanup is observed for model B compared to model A due to the larger cumulative frequency of runs with GPL less than 20%. This also suggests that the severity of GPL is more in model A compared to that in model B.

The second type of Figures is the Tornado chart figure; is used to show the impact of the pertinent parameter on the main response (GPL). It shows parameter's direction of impact (negative or positive) and the relative importance, which each parameter has on the behaviour of the main response. Figure 3.9 shows a tornado chart of two dimensionless pertinent parameters (A and B) effect on GPL. It should be mentioned that in Figure 3.9 the parameters values range from 0 to 1, this is due to the fact that all parameters coefficients values have been scaled to the parameter with the highest coefficient value. There are two sets of bars in this Figure corresponding to the response with and without interaction parameters.

From the first look at this tornado chart (Figure 3.9), one can draw a general qualitative conclusion about the impact of all pertinent parameters at a certain time of production. That is, parameters with a positive scaled value of the coefficient have a negative impact on the gas production. Thus as the parameter scaled value increases in the positive direction GPL increases. In the same manner, parameters with a negative scaled value of the coefficient have a positive impact on gas production; hence as the parameter absolute scaled value increases in the negative direction GPL decreases.

From this Figure, we can also observe the relative importance of each parameter. That is, the parameter with the highest absolute value has the highest impact on the main response. Based on this, we can conclude that parameter (A) has a negative impact on gas production (i.e. it has a scaled value of (0.5), which means that as its value increases GPL

will increase). In the opposite direction, the parameter (B) has a positive impact on gas production with a scaled value of (-0.7). Parameter (B) is more important than the parameter (A), as it has a higher absolute scaled value compared to that of the parameter (A).

Furthermore, from such tornado charts, one can determine the worst and best case scenario for a combination of pertinent parameters. That is, the best case scenario with the lowest GPL is the one for which all parameters (with a positive scaled coefficient value) are set to the minimum limit of their variation range while all other parameters (with a negative scaled coefficient value) are set to the maximum limit of their variation range. Conversely, the worst case scenario with the highest GPL is the one for which all parameters (with a positive scaled coefficient value) are set to their maximum limit of range while all other parameters (with a negative scaled coefficient value) are set to their minimum limit of the range. For simplicity, referring to Figure 3.9, and let us assume that parameter (A) ranges from (10 at minimum to 100 at maximum) and parameter (B) ranges from (5 at minimum to 50 at maximum). From the tornado chart analysis, we find that the best case scenario, with minimum GPL, is the one for which the parameter (A) is set to its maximum (i.e. a value of 100) and parameter (B) is set to its minimum (i.e. a value of 5). Conversely, the worst case scenario, with maximum GPL, is the one for which the parameter (A) is set to its minimum (i.e. a value of 10) and parameter (B) is set to its maximum (i.e. a value of 50). Nevertheless, any other combination of parameter (A and B) values is within our best and worst case scenario.

In this thesis, sometimes the saturation map of FF distribution in and around the fractures (Figure 3.10) are also produced and used to better interpret the results. It should be noted that the saturation map directly generated by Floviz cannot be used due to the grid refinements in the vicinity of fractures. Therefore, in order to have a better saturation map, which more clearly shows the effect of FF in/around the fracture, the output data for fracture grid blocks saturation and also adjacent grid blocks saturation were used in MATLAB software (The MathWorks, 2013) to develop a saturation map for the investigated case. Since we need to have all saturation maps consistent with respect to number of grids, size and also colour distribution, a MATLAB code has been developed which uses the adjacent grid blocks saturation as input and give the map in a standardised format. The MATLAB code is included in Appendix 7.2. It should be noted that to have a better visualisation of the saturation distribution, dimensions of grid blocks have not been selected to the same scale as those of the single-well model under study. To clarify

the information on these plots, the fracture length in the x-direction and grid block sizes in the y-direction has been added to these plots.

3.5.5 Domain Change

It should be highlighted that considerable efforts were dedicated to fit equations that are more representative of the trends observed in the performed simulations. In this exercise, the main dependent variable (i.e. GPL) domain of the fitted response surface model (RSM) was changed. That is, without the domain change there were cases whereby the predicted GPL was very different from the actual value and sometimes giving unrealistic negative or greater than 100%, GPL values. However, with the domain change this issue was eliminated.

Figure 3.11a shows that while real simulation results vary in the 0-100% range (x-axis), the calculated GPLs using normal RSM are in the range of -30% to 120% (y-axis). To overcome this difficulty and to obtain more accurate RSM and benefiting from the support of MATLAB mathematical package technical support team, the GPL variable has been transferred to a different domain. That is, instead of defining the model with the output as GPL, we have defined the regression model, which gives Log of (GPL/(101-GPL)) as the output. This ensures that GPL varies within the desired interval [0,100]. Figure 3.11b shows the same real simulation results (x-axis) versus the calculated GPL (y-axis), after the GPL domain change. It is noted that calculated GPL values using RSM in new domain correctly vary in the 0 to 100% range.

3.6 SFVW Base Reference Set

Ranges of parameters corresponding to the best case and worst case scenarios of the Base Reference Set are tabulated in Table 3.5. The impact of pertinent parameters on GPL is displayed graphically in the form of a tornado chart, Figure 3.12. Two saturation maps corresponding to this set are shown in Figure 3.13 and Figure 3.14. The corresponding histogram chart demonstrating the GPL cumulative frequency is shown in Figure 3.15.

From data of Figure 3.12, it is noted that fracture permeability (K_f), with the highest absolute coefficient value of 1, plays the most important role in cleaning the fracture, i.e. the higher the fracture permeability, the lower the GPL. This observation agrees with having a high coefficient for the Corey exponent and endpoint for fracturing fluid relative permeability curve (n_{wf} and K_{maxwf}), which are +0.63 and -0.61, respectively. That is, they

all show that cleanup performance is better if FF mobility inside the fracture improves (10 days production period is considered).

An increase in the Corey exponent of gas relative permeability in the fracture and the matrix (n_{gf} and n_{gm}) shows a negative impact on the cleanup efficiency with their coefficients being +0.58 and +0.51, respectively. That is, a decrease in gas mobility inside either the fracture or matrix causes an increase in GPL.

The impacts of interfacial tension (IFT), pore size distribution index (λ) and Matrix permeability (Km) with their coefficients being -0.38, +0.3 and -0.4, respectively, have a moderate impact on GPL. Based on these coefficients, an increase in IFT or a decrease in λ decreases GPL but based on the capillary pressure (Pc) equations, Equation 3.6 and 3.7, such changes increase Pc. Therefore, it can be concluded that both these two parameters are affecting the results such that if capillary pressure increases, there is a reduction in GPL or an improvement in the cleanup, as more FF is imbibed into matrix leaving fracture clean for gas to flow. However, it should be noted that km also affects Pc, which is discussed below.

The Pc effect can be more clearly seen in the saturation map that has been created using the MATLAB code. The saturation map of the best and worst case scenarios after two days of the shut-in period are shown in Figure 3.13 and Figure 3.14, respectively. As mentioned above, to have a better visualisation of the saturation distributions, dimensions of grid blocks have not been selected to the same scale as those of the single-well model under study. In the best case, maximum IFT and minimum λ, which tend to increase Pc have been considered. Figure 3.13 shows that in this set the fracture has low FF (defined as water) saturation, similarly to the un-invaded region, i.e. better cleanup. However, for the worst case scenario with the lowest IFT and highest λ, which tend to decrease Pc, FF saturation inside the fracture is still high, Figure 3.14, i.e. poor cleanup.

Matrix permeability (K_m) has a coefficient of -0.4, suggesting that the higher the Km the lower GPL. An increase in matrix permeability (K_m) influences GPL in two ways:

(i) It allows better mobility for fluids in the matrix during injection and production periods.

(ii) It reduces capillary pressure.

Based on the points mentioned above, a reduction of Pc should increase GPL. Hence, it can be concluded that in this set the contribution of Km in improving fluid mobility, particularly that of the fracture fluid flowing into the matrix, results in the better cleanup, i.e. lowering GPL. This also impacts the Pc values of the best and worst case scenarios

discussed above. That is, for the best case scenario and based on the impact of km in the Tornado chart; the highest km value (which reduces GPL) has been used. This suggests that because at this higher km value Pc is lower than that at the lower km value, Pc is not at its maximum for the best case. Conversely, for the worst case scenario, the lowest km value (which increase GPL) has been used, which suggests that the corresponding Pc is not at its minimum value. These trends also suggest that the impact of km on Pc is not important to the same extent as that of IFT and λ, both of which change in the direction of increasing Pc and decreasing GPL simultaneously.

These observations suggest that in SFVW-Set 1 base reference set, using chemicals (IFT reducing agents) to reduce Pc could increase GPL and impair cleanup efficiency.

The impact of rest of pertinent parameters (K_{maxgf}, K_{maxgm}, $K_{maxwm,}$ and n_{wm}) is considered small since the absolute values of their coefficients are less than 0.2.

After 30 days of production, the same trends are still observed but the values of the coefficients are slightly greater for most of the parameters. This is due to having lower GPL, which exaggerates the impact of parameters. However, still, K_f, as well as nwf and Kmaxwf, are the main dominant parameters. The absolute values of n_{gf}, n_{gm}, IFT and λ coefficients are more or less similar to those of the early production period. The effect of K_{maxgf}, K_{maxgm}, $K_{maxwm,}$ and n_{wm} are also small.

Comparison of results after one year with those after 10 days of production suggests an increase in coefficient of n_{wf}. This trend is due to a sizeable reduction in FF removed from fracture after one year of production, which makes the impact of FF relative permeability to be more noticed.

There is also a substantial decrease in the absolute value of the K_m coefficient from -0.37 after 30 days to -0.096 after 370 days of production. This suggests that improved mobility of fracture fluid in the matrix, when k_m is increased, does not significantly impact the results at low FF saturation.

From cumulative frequency data of histogram shown in Figure 3.15, it is noted that during the first 10 days of production, more than 83% of simulation runs have GPL greater than 20%, GPL_{20}=17%. It is noticeable that GPL declines significantly as production time increases. That is, the frequency of runs with GPL greater than 20% is about 68% and 28% after 30 and 370 days of production, respectively.

The main observation is that FF mobility in the fracture is the most important parameter; therefore, to improve cleanup efficiency, it is advised to create fracture with high permeability. This can also be accomplished by improving kf, by reducing nwf or

increasing Kmaxwf. Moreover, high Pc owing to higher IFT reduces GPL, in other words, two general practical guidelines can be drawn (i). Improvement in fracture permeability and FF mobility inside the fracture results in favourable cleanup efficiency (ii) maintaining high Pc by retaining high IFT results in a cleaner fracture.

3.7 SFVW-Sets with Injection volume increased (FVR=10)

In SFVW-set 2, the ratio of injected volume of FF to fracture volume (FVR) was increased from 2 in the base reference set to 10. As shown in the corresponding tornado chart, Figure 3.16, the general trends of this set are similar to those of the reference set but with smaller coefficients, which is due to the fact that larger amount of injected FF requires a longer time to produce. Accordingly, compared to the base reference set, higher GPL is experienced as seen in the corresponding histogram chart of the GPL cumulative frequency, Figure 3.17. Quite interestingly, coefficients (Figure 3.16) and frequency of GPL (Figure 3.17) of this set after 370 days of production are similar to those of the base reference set after 30 days of production, Figure 3.12 and Figure 3.15. This implies higher FF injected only results in a delay in the cleanup process, in other words, increasing FVR from 2 to 10 significantly increased GPL and delayed fracture cleanup resulting in overall poorer and slower cleanup performance, Figure 3.17.

The larger amount of injected FF results in higher GPL values and requires a longer time to flowback. This can clearly be seen in the water saturation map of the best case, Figure 3.18, after two days of a shut-in. Comparing data of this Figure with those of Figure 3.13 in the base reference set, it is noted that the FF saturation in the matrix and fracture is much greater than that of the base case. Similarly, the FF saturation in the matrix and fracture in the worst case, Figure 3.19, is much higher than that of the base case, Figure 3.14. Comparing the tornado charts of the SFVW base reference sets and that of SFVW-Set 2 with higher FVR, Figure 3.12 and Figure 3.16 respectively, shows that the relative importance of pertinent parameters when FVR=10 was less than those when FVR=2, especially at higher production periods.

20 additional SFVW-Sets, with a total of 81,920 simulation runs are also performed. These sets include studying the impact of a combination of increasing fracture volume ratio (FVR) with prolonging shut-in time, reducing matrix permeability range and decreasing or increasing DP on GPL in long SFVW-Sets (Xf=400m) and short SFVW-Sets (Xf=100m). The long SFVW-Sets are SFVW-Set 28 to 41 and the short SFVW-Sets are SFVW-Set 49 to 54.

In summary, injecting a high volume of FF, FVR=10, into a very tight formation significantly impairs production. The effect of varying other parameters such as extending soaking time or increasing pressure drawdown for such a case significantly reduce the negative impact of high FVR resulting in less GPL reduction.

In the case of sets 38 to 41, high FVR resulted in inconsistencies in the results because of high GPL close or equal to 100%, which resulted in killing the well. The common characteristic between sets 38, 39, 40 and 41 is that they all include very tight formations (Km=0.01-1μD). It is observed that as the matrix permeability range is reduced by a factor of a 100 (relative to the base reference set) in these sets, the tornado chart results (Figure 3.20) are significantly impaired, rendering comparison of pertinent parameters across sets unfeasible, as the parameter effects are masked by the high FVR damage.

In SFVW-Set 38, the histogram chart of the GPL cumulative frequency, Figure 3.21, shows that 54% of simulated runs (2212 out of 4096) have a GPL greater than 90% after one year of production. Similar results for SFVW-Set 39, 50% (2048 out of 4096), have a GPL greater than 90% after one year of production. Set 40 and 41 show similar results with 51% (2089 out of 4096) and 54% (2212 out of 4096), respectively, having a GPL greater than 90% after one year of production. That is, the majority of runs in these very tight formation sets have exceptionally high GPL which results in a poor response surface model and consequently a less reliable tornado chart. In other words, once a high volume of fracturing fluid is injected into the tight formation, the well is effectively killed. The effect of varying other parameters such as extending ST or increasing DP provides no major differences as excessive FF has been injected into a very low permeability formation. Therefore, it can be concluded that it is inadvisable to inject too much FF, particularly in tight formations as gas production is significantly impaired. According to our knowledge, this is a new result contributing to the fracture cleanup literature.

In short fractured wells and in line with what was observed in long fracture sets, an increased FVR from 2 to 10 leads to an increased GPL and poor cleanup efficiency, mainly due to the further invasion achieved by FF. Furthermore, when FVR was increased from 2 to 10 in short fractures, the parameters related to Pc became less important for the sets with a higher FVR. For both long and short fracture sets, it was observed that high DP (ΔP=4000psi) leads to an enhancement of the cleanup performance, reducing GPL and consequently, obtaining a greater production than in low drawdown sets.

In tight formations, comparing short and long fractured wells using an FVR of 10, it was found that the effect of an increased FVR has a greater impact on GPL in short

fractures at early times than in long fractures, being the other way around at later stages. IFT and ngf showed consistently greater values for long fractures.

If an extended ST was applied when using an increased FVR of 10, the results obtained for both (with and without increased ST) were, in some manner, the same, not improving GPL. Those parameters related with Pc have a greater impact after applying an extended ST.

3.8 SFVW-Set with increased soaking time (ST=20)

In SFVW-Set 3, the soaking time (ST) was increased from 2 in the base reference set to 20 days to give satisfactory time for capillary pressure (Pc) to allow imbibition of more FF into the matrix. This should result in a cleaner fracture for gas to flow. Comparing the tornado chart of this set with extended ST, Figure 3.22, with the base reference set, Figure 3.12, it is noted that despite longer shut-in period, the results seem more or less similar, i.e., most coefficients have approximately the same values. The exceptions are variables affecting Pc (i.e. IFT, λ and K_m), which show some discrepancies, particularly during the beginning of the production period. That is, after 10 days of production, there is an increase in the absolute value of the IFT coefficient from 0.38 in the base reference set to 0.56 in this set. For λ, it has increased from 0.3 to 0.41 and for $K_{m,}$ it has changed from 0.4 to 0.28. All these confirm the greater importance of Pc on improving fracture cleanup and reducing GPL in the set with increased ST. In other words, extending ST gives more time to FF to imbibe deeper into the matrix resulting in more distributed FF saturation inside the matrix. However, it seems this is limited only to the early production time.

Almost the same observation is noted when looking at the cumulative frequency of runs with a given GPL, Figure 3.23. That is, the corresponding curves for the base reference set and this set are almost overlapping except for 10 days production. It can be concluded that the extended shut-in time improves the cleanup efficiency only at the early production time.

It was mentioned that the extended ST results in more FF imbibing into the matrix which makes the impact of Pc parameters to be more important than that of the base reference set. This can clearly be seen in the water saturation map of the best case after twenty days of shut-in, Figure 3.24. Comparing data of this Figure with those of Figure 3.13 in the base reference set, it is noted that the FF saturation in the matrix and fracture is much smaller than that of the base case. Similarly, the FF saturation in the

matrix and fracture in the worst case, Figure 3.24, is smaller than that of the base case, Figure 3.14. In other words, extending ST from 2 days in the base reference set, SFVW-Set1, to 20 days in SFVW-Set 3 results in more distributed FF in the matrix and also cleaner fracture and consequently better cleanup.

3.9 SFVW-Sets with reduced Km range (Kmr=10 and 100)

In these sets, the range of matrix permeability variation was lowered from 1 μD-100 μD (Kmr=1) in the base reference set to 0.1 μD-10 μD in SFVW-Set 4, i.e. Kmr=10, and to 0.01 μD-1 μD in SFVW-Set 25, i.e. Kmr=100. The aim was to compare the results of these sets with the base reference set, SFVW-Set 1, with the only difference being a tighter/tightest formation by a factor of 10 and 100 in SFVW-Sets 4 and 25, to see the effect of Km reduction in moderate DP sets. Comparing the tornado charts of these sets with each other, Figure 3.26a and b, and also with that of the base reference set, Figure 3.12, demonstrates that most of the pertinent parameters show more or less the same trends in terms of direction of impact but, in these tight sets, the effect of fluid mobility in the matrix (i.e., K_m, K_{maxwm}, n_{wm}, K_{maxgm} and n_{gm}) is more important than that in the base reference set. From data of Figure 3.26 a and b, it is noted that as the formation becomes tighter/tightest in SFVW-Set 4 and 25 respectively, the coefficient values of K_m, K_{maxwm}, n_{wm} K_{maxgm}, n_{gm} become larger and also the most important affecting GPL in SFVW-Set 25, i.e. cleanup performance is better if fluid mobility (FF and Gas) inside the matrix improves. This observation highlights the fact that in tight formations, fluid mobility in matrix plays a very important role in the cleanup. Similarly, from data of Figure 3.26b, it is noted that fracture permeability has a moderate impact on GPL.

The saturation map of best and worst case scenarios of SFVW-Set 25 with Kmr=100 after two days of the shut-in period are shown in Figure 3.27 and Figure 3.28, respectively.

If one compares these saturation maps, with those of the base reference set, SFVW-Set 1, Figure 3.13 and Figure 3.14, it is noted that the fracturing fluid has gone deeper in the matrix (in Y direction) in SFVW-Set 1 than 25 due to larger value for Km in SFVW-Set 1 as a result of higher mobility. In other words, in tighter formations, due to having less FF mobility in the Y direction a bit more FF saturation in the X direction alongside the fracture is observed.

Figure 3.29 is the histogram chart that compares the GPL cumulative frequency of the runs in SFVW-Sets 25, 4 and, the base reference, SFVW-Set 1. It is noted that a decrease in matrix permeability variation range increases GPL and causes slower cleanup.

3.10 SFVW-Sets with reduced/increased DP (DP=100 and 4000 psi)

In these sets, the applied pressure drawdown (DP) of the base reference set was reduced & increased from 1000 to 100 psi & 4000 psi, respectively. The aim was to compare the impact of changing DP on cleanup.

Comparing the tornado charts of these set, i.e., SFVW-Set 6 with DP=100 and SFVW-Set 7 with DP=4000 with each other, Figure 3.30 and Figure 3.31 respectively, and also with that of the base reference set, Figure 3.12, highlights that still the same three main important parameters (i.e. Kf, Kmaxwf and nwf), overwhelmingly control the cleanup performance. However, in the SFVW-Set 6 with reduced DP (DP=100 psi), Figure 3.30, the impact of IFT and λ on GPL is more pronounced with greater coefficients than those of the base reference set, Figure 3.12, indicating greater significance of Pc on the cleanup efficiency in low DP SFVW-Sets. This trend emphasises that a decrease of GPL can be obtained through increasing IFT or reducing λ. This is also in agreement with the direction of the impact of the Km coefficient, which, opposite to the base reference set, is now positive, that is, an increase in Km increases GPL. In other words, in this SFVW-Set, the contribution of an increase in Km, which reduces Pc and increases GPL, is more dominant than that of improving fluid mobility and reducing GPL. This effect is more pronounced at later production periods when more of FF is produced. This trend is mainly due to the relative increase of Pc contribution when drawdown is decreased. In other words, it is more difficult for FF remaining inside matrix to flow out, consequently, the stronger the Pc, the larger the amount of FF invading into the formation and, the lesser the resistance for gas production inside the fracture. It is also noted that compared to the base reference set (Figure 3.12), here the absolute values of Kmaxwm and nwm coefficients have increased especially after 370 production days (Figure 3.30). In line with the explanations given above, this is because, at this low pressure drop, FF mobility in the matrix is more important.

In SFVW-Set 7, DP was fixed at 4000 psi, instead of the 1000 psi used for the base reference set. As noted in the corresponding tornado chart, Figure 3.31, and compared to the base reference set, increasing DP in this set has not resulted in major changes in the trends of data except for the more reduced impact of Pc. That is, here the absolute values

of the IFT and λ coefficients are smaller. The negative effect of an increase in Km on Pc is also smaller as the absolute value of its coefficient is higher. As mentioned above, an increase in Km influences GPL in two ways: (i) it allows better mobility for fluids and (ii) it reduces Pc. Considering that reduction of Pc should increase GPL, it can be concluded that in this set, the contribution of Km in improving fluid mobility, particularly that of fracture fluid flowing into the matrix, results in better cleanup and consequently lower GPL.

The histogram of cumulative GPL frequency for these SFVW-Sets, Figure 3.32, shows that the cleanup process is relatively slower in the low DP set (SFVW-Set 6). This shows that the cleanup process is severely delayed when DP is reduced. However, due to higher DP in SFVW-Set 7, greater reduction in GPL is observed as demonstrated by the histogram of cumulative GPL frequency.

3.11 SFVW-Sets with low Km range and different DPs and STs

In this section, the cleanup efficiency of FF in formations with very low matrix permeability while changing other pertinent parameters like DP and ST was investigated. 10 sets were simulated considering different applied DP during production, shut-in soaking time periods and Km range, i.e., SFVW-Sets 4, 14, 15, 16, 17, 23, 24, 25, 26 & 27.

3.11.1 Lower Km range (Kmr=10) & low DP (100psi) SFVW-Sets with different ST

In SFVW-Sets 14 and 15, the Km variation range was lowered from 1 μD-100 μD in the base reference set to 0.1 μD-10 μD (Kmr=10) and DP also decreased from 1000 psi in the base reference set to 100 psi. the only difference between the SFVW-Set 14 and 15 is ST, with its higher value allocated in SFVW-Set 15.

From data of SFVW-Set 14, Figure 3.33, it is noted that K_f with its coefficient values varying between -0.45 and -0.35 at the three production periods, is not as important as the base reference set. However, still it can be concluded that the higher the fracture permeability, the lower the GPL. This observation agrees with a relatively high coefficient for n_{wf} and K_{maxwf}. That is, they all show that cleanup performance is enhanced if FF mobility inside the fracture improves. In this set, the gas mobility in the matrix is the most important parameter. That is, n_{gm} has a positive coefficient of around 1 at all three production periods. This is because of reduced Km and DP. Furthermore, in this set, the effect of Pc on the imbibition of the FF into the matrix is an important factor due to the relatively high coefficient of IFT and λ, pertinent parameters affecting Pc.

If the tornado chart of SFVW-Set 14 shown in Figure 3.33 is compared with that of the previously reported SFVW-Set 6, with the higher Km variation range of 1 μD-100 μD, shown in Figure 3.30, it is noted that in the SFVW-Set 14, K_f is less and Km is more important. Similarly, the absolute values of the K_{maxgf}, n_{gf}, K_{maxwf} and n_{wf} coefficients of this set appear to be slightly lower than those of set 6. This means that GPL is less affected by gas and FF relative permeability inside the fracture. Due to having lower K_m values, which leads to the more important effect of fluid flow in the matrix, the absolute value of the n_{gm} and n_{wm} coefficients shown in Figure 3.33 are much higher, i.e. the impact of mobility of gas and FF in the matrix permeability is more pronounced here.

In order to study the impact of ST in sets with low Km range and low DP SFVW-Sets, the ST was extended from 2 days in SFVW-Set 14 to 20 days in SFVW-Set 15. In other words, SFVW-Set 14 and 15 are similar sets with the only difference being a longer ST of 20 days applied in SFVW-Set 15.

From data of Figure 3.34, corresponding to SFVW-Set 15, it is noted that IFT, λ and K_f with the coefficients of -1, +0.58 and -0.56 after 10 days of production, respectively, are relatively the most important parameters. That is, they all show that cleanup performance is improved if FF imbibition into the matrix and also mobility inside the fracture is improved. The gas mobility in the matrix is also important (n_{gm} with an absolute coefficient of +0.62) because the matrix permeability (k_m) is reduced by a factor of 10. This agrees with what was shown earlier for the previous SFVW-Set 14. If the tornado chart of this set, Figure 3.34, is compared with that of the previous set 14 with ST=2 days, Figure 3.33, it is noted that in this set IFT and λ are more important due to longer soaking time.

Looking at the histogram chart of the GPL cumulative frequency of SFVW-Sets 6, 14 & 15, Figure 3.35, slightly more severe GPL is observed at all production periods for set 14 compared to set 6 with the higher Km range. This increase in GPL is more pronounced at a later production period of 370 days. In other words, it is noted that the negative impact of reduced Km and DP in increasing the severity of gas production loss is small in this set. It is also noted that slightly less severe GPL is observed at early production periods for SFVW-Set 15 with longer ST compared to SFVW-Set 14. In other words, it seems at longer production period, this small difference is diminished.

3.11.2 Lower Km range & high DP SFVW-Sets with different ST

In SFVW-Set 16, the Km variation range was lowered from 1 μD-100 μD in the base reference set to 0.1 μD-10 μD (i.e. kmr=10) and DP increased from 1000 psi in the base reference set to 4000 psi.

Comparing the tornado chart of this set shown in Figure 3.36 with that of SFVW-Set 4 with lower DP of 1000 psi shown in Figure 3.26a, it can be concluded that as DP is increased the impact of fracture and its relevant parameters are much higher due to the good delivery of fluids from the matrix to the fracture. It can also be concluded that the effect of Km in this set is more pronounced than that of set 4 because higher DP in this set enables easier delivery of fluids from the matrix to fracture than before. If the absolute coefficients for λ and IFT for these two sets are compared, it is noted that the effect of these parameters is less pronounced for this set 16, with lower absolute values, confirming that the effect of Pc is much more important in lower DP sets. In other words, the higher the DP, the lower the impact of Pc on cleanup efficiency and vice versa.

When the ST was extended from 2 days in set 16 to 20 days in set 17, the observation was the same as that noted by comparing set 15 and set 14, i.e. the impact of IFT and λ is more important for longer ST. In other words, when ST is increased by a factor of ten, the fracturing fluid imbibition into the matrix is more effective and the parameters pertinent to capillary pressure, i.e. IFT and λ, have higher absolute coefficient values. The histogram chart of the GPL cumulative frequency also confirmed that this effect is limited only to early production periods.

3.11.3 The Lowest Km range & low DP SFVW-Sets with different ST

In this SFVW-Set 23, Kmr was 100 and DP was reduced to 100 psi compared to the corresponding base reference set values of Kmr=1 and DP=1000 psi, respectively.

The trends of parameters in the tornado chart of this set, Figure 3.37, contradict previous observations, i.e. increasing K_f increases GPL at early times. This trend suggested that there was an inconsistency in the results. After an extensive investigation, it was noted that this is due to negative GPLs obtained for many simulation runs of this significantly low Km and low DP set. It should be noted that these negative GPLs, due to overpressure effect, were excluded when fitting the RSM equation. This resulted in a poor surface model and inaccurate calculated results. It should be noted that according to the definition of GPL, negative GPL, as per Equation 3.10, means that there is more total

cumulative gas production in the unclean case than the clean one with FF presence, which is not possible.

My investigations indicated that these negative GPLs were due to over-pressurizing of fluids (typically up to 900 psi higher than the average reservoir pressure, Figure 3.38) in the grids adjacent to the fracture while injecting the fracturing fluid at the end of shut-in time. On the other hand, the resultant FF saturation increase in the matrix did not impair the gas relative permeability much, i.e. Less than 10%. Hence, at this low DP of 100 psi, a higher GPT, total cumulative gas production, compared to the clean case was recorded, resulting in negative GPL.

In order to further confirm this, the clean case was re-ran using the saturation map (Figure 3.39) at the end of soaking time for the unclean case, in this case, the overpressure effect in grids adjacent to the fracture was eliminated. Figure 3.40 show that by removing this synthetic overpressure effect from the model and using the unclean saturation map, positive GPL are obtained. In other words, some runs have more cumulative gas production for the clean case than the unclean one.

In order to ensure that this synthetic over-pressure effect, created by my simulation method, did not have any adverse effect on other sets results, an extensive investigation, was performed, which confirmed the effect was limited only to this set. If ST was extended from 2 days in SFVW-Set 23 to 20 days SFVW-Set 24, it was noted that by extending ST the overpressure effect was alleviated, which indicates that impact of ST is more important at this lower Km, DP set. In the next section, a solution to the over-pressure effect will be investigated.

3.11.4 SFVWs with Permeability Enhancement, SFVW-Sets 64, 65 and 66

In the previous section (Section 3.11.3), numerical issues were reported for SFVW-Sets when Km and applied DP were small. The impact of synthetic over-pressure created during the injection period was particularly pronounced for SFVW-Sets with Kmr = 100 when applied DP was 100 psi, compared to the base reference set. SFVW-Set 23, with Kmr=100 and DP=100 psi, was considered unreliable.

It was discussed that during FF injection, to honour the assumed injected FF volume, injection pressure was increased to unrealistically high values. The resultant overpressure effect in matrix grids adjacent to the fracture did not dissipate completely during the shut-in time. This overpressure effect resulted in negative GPL especially when the DP and Km were low. According to the definition of GPL, a negative GPL means that total

cumulative gas production for the unclean case is higher than that of the clean one, Equation 3.10. This occurred because in cases with negative GPL, and at the start of the production period, the overpressure value was added to the imposed DP, mostly at early production periods and at the same time, the presence of FF did not reduce Krg significantly. These two effects result in higher FGPT than that for the clean case.

In order to mitigate the overpressure effect, a model for stress dependent permeability changes was used for modelling of water injection but only during the hydraulic fracturing stage (i.e., FF injection). This allowed the pressure to drop to the original reservoir pressure. It should be noted that no permeability modification was applied below the initial reservoir pressure (during the production period).

The stress dependent transmissibility changes were applied to both fracture and matrix grids, i.e. the same permeability enhancement factor (m) was used for matrix cells (in x and y-directions) and for fracture cells. As described earlier, FF is injected in a pre-fractured model and hence the fracture initiation and propagation is not simulated.

As mentioned, stress dependent permeability was considered to apply permeability enhancement in the zone in the vicinity of the fracture face during FF injection allowing dissipation of the unrealistically high pressures reported previously. A model available in the literature (Jurus et al., 2013) to describe permeability enhancement versus changes of stress was applied. In the proposed model the ratio of the current permeability (k) to original permeability (ko) is expressed by a power function of stress (s), Equation 3.12. one can use the increase of net pore pressure instead of absolute stress. Net pore pressure is defined as the difference between the current pressure and initial reservoir pressure. An increase in net pore pressure is identical to the reduction of rock effective stress, i.e, $s=-p_{net}= p_{Ri}-p_{grid}$.

The function is expressed by a straight line plot of Log (k/ko) versus stress, with a slope defined by m (Permeability Enhancement Factor).

$$\frac{K}{K_o} = 10^{-m*s}=10^{m*p_{net}} \qquad 3.12$$

Where:

- K: enhanced permeability due to injection, md
- Ko: original permeability, md
- m: permeability enhancement factor, Psi^{-1}, in this work m is considered to be 10^{-3} psi^{-1}

As mentioned earlier, stress dependent changes of permeability is modelled only for pressure above the original reservoir pressure, i.e., during the FF injection period. During the production period, the permeability is assumed constant and equal to the original value.

To evaluate the effect of permeability enhancement on cleanup efficiency, three SFVW-Sets of long SFVW base reference set (SFVW-Set 64), long SFVW with Kmr=100 and DP=100 psi (SFVW-Set 65) and long SFVW with Kmr=100 (SFVW-Set 66) were studied, these SFVW-Sets are here compared to their relevant SFVW-Sets without permeability enhancement respectively (i.e., SFVW-Sets 1, 23 and 25).

Comparing the tornado chart of SFVW-Sets 1 and 64, Figure 3.12 and Figure 3.41, with each other with the only difference being inclusion of permeability enhancement in SFVW-Set 64, it is noted that the impact of some of the parameters are slightly different but the overall observed trends of all parameters in SFVW-Sets 1 and 64 are more or less the same. Figure 3.42 shows the histogram chart that compares the GPL cumulative frequency of the runs in SFVW-Sets 1 and 64. It is noted that the GPL cumulative frequency of both SFVW-Sets are almost the same (only the histogram charts for GPL-10 days are slightly different). These two observations (comparison of tornado charts and histogram charts of SFVW-Sets 1 and 64) indicate that the effect of considering permeability enhancement in the SFVW base reference set is minimal, this is in line with the fact that in SFVW-Set 1 very few negative GPL values were observed due to relatively high permeability range (Kmr=1) and moderate DP.

Permeability enhancement was considered in two more SFVW-Sets with (Kmr=100) and with either DP=100psi (SFVW-Set 65) or DP=1000 psi (SFVW-Set 66). The impact of over-pressure effect in SFVW-Set 65 was maximum due to the very tight formation and very low DP. The aim was to compare the results of the SFVW-Set 23 with those of the SFVW-Set 65, with the only difference being the inclusion of permeability enhancement in SFVW-Set 65. The tornado chart for SFVW-Set 23, Figure 3.37, suggested an inconsistency in results. This was due to several negative GPLs obtained for many simulation runs of this low permeability low pressure drawdown SFVW-Set. The tornado chart for SFVW-Set 65, Figure 3.43, on the other hand, suggests that the inclusion of permeability enhancement can mitigate the overpressure effect and significantly improve the LRSM and resulting tornado chart. It is noted from Figure 3.43 that the effect of Pc pertinent parameters is most important for this low DP, low-k SFVW-Set, a trend

which was also observed in other SFVW-Sets with either low DP or low–k (Sections 3.11.1 and 3.11.3).

Figure 3.44 shows the histogram chart that compares the GPL cumulative frequency of the runs in SFVW-Sets 23 and 65. If one considers the histogram chart for SFVW-Set 23, it is noted that the cumulative frequency for 1 year falls below those for 10 and 30 days. This was due to having many runs with negative GPL, which have not been included in this Figure since the histogram chart takes only positive GPL values into account. But this issue has been sorted in SFVW-Set 65 with the inclusion of permeability enhancement.

Figure 3.45 and Figure 3.46 also indicate an improvement in trends of LRSM and Histogram chart for SFVW-Set 66 compared to those for SFVW-Set 25.

Based on the results observed in these new SFVW-Sets with permeability enhancement (SFVW-Sets 64, 65 and 66), it is noted that although the effect of considering permeability enhancement in high permeability high/moderate DP SFVW-Sets was minimal, it significantly alleviated the overpressure effect in low permeability moderate/low DP SFVW-Sets.

3.12 SFVW-Sets with short fracture length

In this section, the results of 21 new SFVW-Sets (i.e., SFVW-Sets 10, 11, 18-22, 28, 49-61) were performed to investigate the cleanup efficiency when fracture length was decreased, is presented. It was mentioned previously that the fracture length was either 100 or 400 metres representing short and long fracture SFVW-Sets, respectively.

Figure 3.47 and Figure 3.30 show the tornado charts of two relevant SFVW-Sets with different fracture lengths, SFVW-Set 18 (100 m short fracture) and SFVW-Set 6 (400 m long fracture) respectively both with DP=100 psi, these two tornado charts are compared in order to observe how the effect of pertinent parameters on GPL changes with the hydraulic fracture length.

It is noted that in SFVW-Set 18, similar to the long fracture SFVW-Set6, K_f, K_{maxwf} and n_{gf} coefficients have high values indicating that the cleanup performance is enhanced if FF mobility inside the fracture improves. Furthermore, as production time increases the effect of all pertinent parameters on GPL declines.

Another important observation is that the Km fluid mobility effect is more dominant than its effect on Pc, i.e. increasing km, whilst reducing Pc, decreases GPL whilst the

opposite trend was observed in long fracture SFVW-Set 6, this shows that in shorter fracture SFVW-Set, fluid mobility within the matrix is more important.

The results of short and long fractures in Figure 3.47 and Figure 3.30 indicate that as the fracture length increases, the effect of fracture pertinent parameters (K_f, K_{maxwf}, K_{maxgf}, n_{wf} and n_{gf}) on GPL reduction increases whilst the effect of matrix pertinent parameters (K_m, K_{maxwm}, K_{maxgm}, n_{wm} and n_{gm}) on GPL reduction decreases. In other words, for longer fractures, fluid mobility within fracture is more important whilst for shorter fracture, fluid mobility within the matrix is more dominant. It is also noted that having a shorter fracture reduces the impact of Pc on GPL, i.e. the absolute values of IFT and λ coefficients are smaller.

Figure 3.48 compares the histogram charts of two other relevant SFVW-Sets, i.e., Set 28 (xf=100m) and Set 8 (xf=400m) with Kmr=100 and DP=4000 psi. This Figure similar to that for SFVW-Sets 18 and 6, shows that the longer the fracture, the slower the cleanup which is due to injecting higher FF volume, which requires more time to cleanup.

In the other 19 SFVW-Sets of simulations, the effect of pertinent parameters in the lower matrix permeability range (tighter formation), extended soaking time, moderate/high DP and increased injected FF volume have been studied and compared for different fracture length (100m and 400m). In these SFVW-Sets, observations similar to those of the above SFVW-Sets were noted (i.e. the effect of fracture (and matrix) pertinent parameters on GPL reduction increases (and decreases) as fracture length increases). In the short fracture, SFVW-Set with higher injected FF, the effect of matrix pertinent parameters (K_m, K_{maxwm}, K_{maxgm}, n_{wm} and n_{gm}) on GPL was more pronounced. This is due to the fact that higher volume of injected FF makes fluid mobility in the matrix more important. In the higher DP SFVW-Sets, the effect of fracture mobility parameters was more pronounced. This is because, at higher DP, the impact of matrix and Pc parameters are less. However, in high DP short fracture SFVW-Sets, as formation became tighter, the effect of matrix mobility parameters (K_m, K_{maxwm}, K_{maxgm}, n_{wm} and n_{gm}) were more important. This is because in tighter formation fluid mobility in the matrix is more difficult and hence the improvement at higher pressure is more evident.

3.13 Long SFVW, Swi=50%, SFVW-Set 62 and Swi=75%, SFVW-Set 63

In addition to the SFVW base reference set, SFVW-Set 1, two SFVW-Sets were run to capture the effect of mobile formation water on cleanup efficiency. In these two SFVW-Sets, initial water saturation (Swi) was increased from 15% in SFVW base

reference set, SFVW-Set 1, to 50% in SFVW-Set 62 and 75% in SFVW-Set 63. In all SFVW-Sets, irreducible water saturation (S_{wir}) as well as critical water saturation (Swc) were set to 15%, consequently, formation water was immobile in SFVW-Set 1 and mobile in SFVW-Set 62 and 63.

Comparing the tornado chart of these three SFVW-Sets 1, 62 & 63, Figure 3.12, Figure 3.49 & Figure 3.50 respectively, with each other with the only difference being a higher Swi in SFVW-Sets 62 and 63, it is noted that the observed trends of all parameters in SFVW-Sets 1 and 62 are more or less the same, apart from the fact that the impact of some of the parameters are slightly different. The main difference between trends in these two SFVW-Sets compared to the SFVW-Set 63 with highest Swi is that Kf is the most important parameter in SFVW-Sets 1 and 62 and second most important parameter after ngm in SFVW-Set 63. In SFVW-Set 63, due to the fact that formation water saturation is set to the largest value (Swi=75%), gas mobility in the matrix is the most critical parameter, in other words, ngm is the main controlling parameter on GPL. For the same reason, ngf/nwf is more/less important in SFVW-Sets 62 and 63 compared to those of SFVW-Set 1.

If one compares Pc pertinent parameters (IFT, λ and Km) in SFVW-Set 1 and 62 it is noted that the effect of Pc on GPL is less important in SFVW-Set 62 due to smaller absolute values for IFT and λ, i.e. keeping water in the matrix, due to its high water saturation, is not as important in improving the cleanup efficiency.

The other important observation in Figure 3.50 is the trend change in the IFT coefficient in SFVW-Set 63. That is, in this SFVW-Set 63, IFT has a positive value indicating that an increase in IFT increases GPL. However, it should be noted that IFT is not the only parameter affecting Pc, hence we need to see the effect of IFT, Km and λ all together to understand the effect of Pc on cleanup efficiency in this largest Swi SFVW-Set. In this SFVW-Set, the capillary pressure was calculated and plotted by selecting the corresponding values of IFT, Km and λ for best and worst cases from their relevant tornado charts and also using Equations 3.6 and 3.7.

Figure 3.51 shows that in SFVW-Set 63, Pc of the worst case is higher than the best case whilst in SFVW-Sets 1 and 62 Pc of the worst case is lower than the best case at all Sw. In other words, in SFVW-Set 1 and SFVW-Set 62, it was better to keep the FF in the matrix by having higher Pc, but in SFVW-Set 63, it was best to backflow the FF out of the matrix. This is due to large initial water saturation, which has a detrimental effect on

gas production especially noting that initial gas saturation is 25%, which is close to the residual trap gas saturation value of 10%.

Therefore, in SFVW-Set 63, unlike previous two SFVW-Sets (1 and 62), using chemicals (IFT reducing agents) to reduce Pc could reduce GPL and improve cleanup efficiency.

Figure 3.52 shows the histogram chart that compares the GPL cumulative frequency of the runs in SFVW-Sets 1, 62 and 63. Slower/slowest cleanup is observed for SFVW-Sets 62 and 63 with larger/largest initial water saturation due to the detrimental effect of mobile water on gas production.

3.14 Conclusions

An extensive investigation on the cleanup efficiency of SFVWs was conducted to further improve the current understanding of hydraulic fracturing treatment for practical field applications.

In this chapter, I have analysed the results of a total of 66 different sets for Long fracture SFVW, 400m, and Short fracture SFVW, 100m. The results have been compared with those of a base reference set and other similar SFVW-Sets. These models have the same reservoir dimensions as those of the SFVW reference set but differ in the fracture fluid injection volume (FVR), shut-in time period (ST), matrix permeability variation range (Kmr), pressure drawdown (DP), initial water saturation (Swi) and length of the hydraulic fracture.

A summary of the main conclusions is given below:

1. Fracture permeability (Kf), as well as endpoint and exponent of Corey relative permeability equation of FF in fracture (Kmaxwf and nwf), were the key drivers of GPL improvement at every production period and for all cases studied apart from SFVW sets with very low Km range (i.e. SFVW-Set 25), SFVW sets with very low Km range and low DP (i.e. SFVW-Set 14, 15, 63) and SFVW sets with high Swi (i.e. SFVW-Set 65 & 66).
2. Additionally, matrix permeability (Km) displayed a positive impact on GPL, i.e. an increase in km reduced GPL and improved fracture cleanup for all SFVW-Sets apart from SFVW-Sets with reduced pressure drawdown of 100 psi described below.
3. The coefficients of interfacial tension (IFT) and pore size index (λ) parameters controlling capillary pressure indicated that an improvement of cleanup

efficiency is attained when capillary pressure (Pc) is increased. This is achieved when IFT is increased and/or λ is decreased except for sets with very low km range and set with high Swi (SFVW-Set 63).

4. When the volume of fracture fluid injected increased from 2 to 10 times fracture volume, the cleanup was slower.
5. As soaking time was extended from 2 to 20 days, more FF invaded further into the matrix, leaving the fracture cleaner for producing gas. However, the favourable result lasted only after 10 days of production. In other words, no improvement of GPL was observed after 30 days and beyond. At the same early time, variables related to capillary pressure (IFT, λ and Km) also showed more pronounced effect of Pc in improving the cleanup performance. The more pronounced effect of Pc affected by coefficient values of IFT and λ was also noticed in sets with matrix permeability variation range reduced by a factor of 10. The impact of ST was more important in lower Km, DP sets.
6. When the pressure drawdown was reduced from 1000 to 100 psi, the impact of Pc became more pronounced. The contribution of an increase in Km, which reduces Pc and increases GPL, was evident, i.e. the Km coefficient was positive. This trend, which is in line with increased absolute values of IFT and λ coefficients resulting in higher Pc, was opposite to what was observed in the previous cases where the Km coefficient was negative.
7. Increasing the pressure drawdown, resulted in the faster cleanup.
8. The high applied pressure drawdown resulted in the lower effect of capillary pressure and the more pronounced effect of Km on mobility.
9. The effect of matrix capillary pressure in GPL reduction was more pronounced when drawdown was very low and/or soaking time was extended.
10. In tighter gas formations, generally more GPL and slower cleanup were observed.
11. There were inconsistencies in SFVW-Set 23 with low DP=100 psi & low Km. After an extensive investigation, this was attributed to removing many negative GPL cases present in these very low DP and Km simulations. Negative GPL occurred because in our simulation method, the fluid in grids adjacent to fracture was overpressurized during FF injection. It was confirmed that this effect was limited only to this set.

12. The inclusion of permeability enhancement in very low DP and Km simulations could alleviate the over-pressure effect with minimal effect in high Km range high/moderate DP sets.
13. As fracture length decreased the effect of fracture parameters (fracture permeability, end point and exponent of Corey gas and FF relative permeability curve in fracture) on GPL decreased and the effect of matrix parameters (matrix permeability and end point and exponent of Corey gas and FF relative permeability curve in the matrix) on GPL increased.
14. The effect of capillary pressure in reducing GPL was less pronounced in shorter fractures.
15. In shorter fractures, faster fracture cleanup was observed.
16. In the short fracture set with higher injected FF, the effect of matrix pertinent parameters (Km, Kmaxwm, Kmaxgm, nwm and ngm) on GPL was more pronounced.
17. In the higher DP sets, the effect of fracture mobility parameters was more pronounced. However, in high DP short fracture sets as formation became tighter, the effect of matrix parameters (Km, Kmaxwm, Kmaxgm, nwm and ngm) were more important.
18. Kf is the most important parameter in sets 1 and 62 with Swi of 15% and 50% and second most important parameter after ngm in set 63 with Swi of 75%. That is due to the fact that as formation water saturation is set to the largest value (Swi=75%), gas mobility in the matrix is the lowest among these 3 sets. In other words, n_{gm} is the main controlling parameter on GPL.
19. ngf/nwf is more/less important in mobile water formation (higher Swi) sets compared to that in set 1 with immobile Swi due to gas mobility restrictions.
20. Slower/slowest cleanup was observed for SFVW sets with larger/largest initial water saturation compared to the SFVW base reference set due to the detrimental effect of mobile water on gas production.
21. Unlike SFVW-Sets 1 and 62 with Swi=15% and 50%, respectively, using chemicals (IFT reducing agents) to reduce Pc could reduce GPL and improve cleanup efficiency in set 63 (Swi=75%).

3.15 References

ALAJMI, E 2012 ' Modelling of Gas-Condensate Flow around Complex Well Geometries and Cleanup Efficiency in Heterogeneous Systems' PhD thesis, Heriot-Watt University Petroleum Engineering, Edinburgh, UK

BROOKS, R.H. & COREY, A.T., 1966. Properties of porous media affecting fluid flow. *Journal of the Irrigation and Drainage Division*, 92(2), pp.61–90.

GHAHRI, P., JAMIOLAHMADY, M. & SOHRABI, M. 2011. A Thorough Investigation Of Cleanup Efficiency Of Hydraulic Fractured Wells Using Response Surface Method. Society of Petroleum Engineers.

GHAHRI, P 2010 'Modelling of Gas-condensate flow around horizontal and deviated wells and cleanup efficiency of hydraulically fractured wells' PhD thesis, Heriot-Watt University Petroleum Engineering, Edinburgh, UK

JAMIOLAHMADY, M., SOHRABI, M. & GHAHRI, P. 2009. Investigation of Cleanup Efficiency of Hydraulically Fractured Wells in Gas Condensate Reservoirs. Society of Petroleum Engineers.

JURUS, W. J., WHITSON, C. H. & GOLAN, M. 2013. Modeling Water Flow in Hydraulically-Fractured Shale Wells. Society of Petroleum Engineers.

MORADIDOWLATABAD, M. (2016) *New Approaches for Performance Evaluation and Design of Well Completions in Horizontal Wells*. Heriot-Watt University.

NEW-COIN (2015) 'Near Wellbore Coupling INertial (NEW-COIN) Version 3.7 Build 5609'. Gas Condensate Recovery (GCR) Team, Heriot-Watt University.

PYTHON SOFTWARE FOUNDATION (2013) 'Python Programming Language, Python v2.7.6', *Python Software Foundation*.

SCHLUMBERGER (2013) 'MEPO Multiple Realization Optimizer; MEPO4.2.0; Build:2617; Date:2013-Apr-25_15-59', *SPT Group; A Schlumberger Company*.

SCHLUMBERGER (2014) 'Petrel E&P Software Platform 2014.1 (64-bit)', *Schlumberger Company*.

SCHLUMBERGER (2015) 'Geoquest, ECLIPSE 100, Version 2015.1.0.0', *Simulation Launch Management Utility*.

THE MATHWORKS (2013) 'MATLAB and Statistics Toolbox Release 2014b (8.4.0.150421)', *Natick Inc.* Massachusetts, United States.

THOMAS, L. K., KATZ, D. L. and TEK, M. R. (1968) 'Threshold pressure phenomena in porous media', *Society of Petroleum Engineers Journal*. Society of Petroleum Engineers, 8(2), pp. 174–184.

3.16 Tables

Table 3.1 Basic properties of the SFVW (Xf is fracture half length) model

X_f(m)	w_f(m)	Xres(m)	Yres(m)	Zres(m)
100 or 400	0.004	2000	2000	40

Table 3.2 Fluid properties of gas used in this study.

P (psi)	Bg	$\mu(cp)$
14.65	260.21	0.0147
400	9.4295	0.0149
600	6.2505	0.015
800	4.6658	0.0152
1000	3.7189	0.0154
1500	2.4673	0.016
2000	1.8527	0.0168
2500	1.492	0.0177
3000	1.2574	0.0187
3500	1.0942	0.0198
4000	0.9749	0.021
5000	0.8137	0.0235
6000	0.7109	0.026
7000	0.6401	0.0283
7500	0.6124	0.0295
8000	0.5886	0.0306
8500	0.5677	0.0317

Table 3.3 The range of variation of uncertain parameters after fracturing.

	Parameter	Min	Max
Fracture Permeability	K_f (D)	1	30
Matrix Permeability	K_m	1 µD	100 µD
Matrix capillary pressure curve (Pc)	Pore size index λ	1	4
Matrix capillary pressure curve (Pc)	Threshold pressure	Eq. (3.11)	Eq. (3.11)
Matrix capillary pressure curve (Pc)	Interfacial Tension (mNm/m)	2	50
Matrix Krg curve	n_{gm}	1.5	5
Matrix Krw curve	n_{wm}	1.2	4
Matrix Krg curve	K_{maxg}(end point)	0.5	1.0
Matrix Krw curve	K_{maxw}(end point)	0.05	0.6
Fracture Krg curve	n_{gf}	1.5	5
Fracture Krw curve	n_{wf}	1.2	4
Fracture Krg curve	K_{maxg}(end point)	0.5	1.0
Fracture Krw curve	K_{maxw}(end point)	0.1	0.75
Pressure Drawdown	Δp (psi)	1000	1000
Porosity	ϕ	0.15	0.15
Matrix Krg curve	S_{grm}	0.1	0.1
Matrix Krw curve	S_{wrm}	0.15	0.15
Fracture Krg curve	S_{grf}	0.1	0.1
Fracture Krw curve	S_{wrf}	0.15	0.15

Table 3.4a SFVW-Sets analysed

Set Name	DP (Psi)	FVR	Shut-in time (days)	Frack Length (m)	Kf (D)	Km (µD)	lam	IFT	ngm	nwm	Kmaxgm	Kmaxwm	ngf	nwf	Kmaxgf	Kmaxwf
Default Values	1000	2	2	400	1-30	1-100	1-4	2-50	1.5-5	1.2-4	0.5-1	0.05-0.6	1.5-5	1.2-4	0.5-1	0.1-0.75
SFVW-Set 1	✓	✓	✓	✓	✓	✓	✓	✓	✓	✓	✓	✓	✓	✓	✓	✓
SFVW-Set 2	✓	10	✓	✓	✓	✓	✓	✓	✓	✓	✓	✓	✓	✓	✓	✓
SFVW-Set 3	✓	✓	20	✓	✓	✓	✓	✓	✓	✓	✓	✓	✓	✓	✓	✓
SFVW-Set 4	✓	✓	✓	✓	✓	0.1-10	✓	✓	✓	✓	✓	✓	✓	✓	✓	✓
SFVW-Set 5	✓	✓	20	✓	✓	0.1-10	✓	✓	✓	✓	✓	✓	✓	✓	✓	✓
SFVW-Set 6	100	✓	✓	✓	✓	✓	✓	✓	✓	✓	✓	✓	✓	✓	✓	✓
SFVW-Set 7	4000	✓	✓	✓	✓	✓	✓	✓	✓	✓	✓	✓	✓	✓	✓	✓
SFVW-Set 8	4000	✓	✓	✓	✓	0.01-1	✓	✓	✓	✓	✓	✓	✓	✓	✓	✓
SFVW-Set 9	✓	5	✓	✓	✓	✓	✓	✓	✓	✓	✓	✓	✓	✓	✓	✓
SFVW-Set 10	✓	✓	✓	100	✓	✓	✓	✓	✓	✓	✓	✓	✓	✓	✓	✓
SFVW-Set 11	✓	5	✓	100	✓	✓	✓	✓	✓	✓	✓	✓	✓	✓	✓	✓
SFVW-Set 12	100	✓	20	✓	✓	✓	✓	✓	✓	✓	✓	✓	✓	✓	✓	✓
SFVW-Set 13	4000	✓	20	✓	✓	✓	✓	✓	✓	✓	✓	✓	✓	✓	✓	✓
SFVW-Set 14	100	✓	✓	✓	✓	0.1-10	✓	✓	✓	✓	✓	✓	✓	✓	✓	✓

Table 3.4b SFVW-Sets analysed

Set Name	DP (Psi)	FVR	Shut-in time (days)	Frack Length (m)	Kf (D)	Km (μD)	lam	IFT	ngm	nwm	Kmaxgm	Kmaxwm	ngf	nwf	Kmaxgf	Kmaxwf
Default Values	1000	2	2	400	1-30	1-100	1-4	2-50	1.5-5	1.2-4	0.5-1	0.05-0.6	1.5-5	1.2-4	0.5-1	0.1-0.75
SFVW-Set 15	100	✓	20	✓	✓	0.1-10	✓	✓	✓	✓	✓	✓	✓	✓	✓	✓
SFVW-Set 16	4000	✓	✓	✓	✓	0.1-10	✓	✓	✓	✓	✓	✓	✓	✓	✓	✓
SFVW-Set 17	4000	✓	20	✓	✓	0.1-10	✓	✓	✓	✓	✓	✓	✓	✓	✓	✓
SFVW-Set 18	100	✓	✓	100	✓	✓	✓	✓	✓	✓	✓	✓	✓	✓	✓	✓
SFVW-Set 19	100	✓	20	100	✓	✓	✓	✓	✓	✓	✓	✓	✓	✓	✓	✓
SFVW-Set 20	✓	10	✓	100	✓	✓	✓	✓	✓	✓	✓	✓	✓	✓	✓	✓
SFVW-Set 21	4000	✓	✓	100	✓	✓	✓	✓	✓	✓	✓	✓	✓	✓	✓	✓
SFVW-Set 22	4000	✓	✓	100	✓	0.1-10	✓	✓	✓	✓	✓	✓	✓	✓	✓	✓
SFVW-Set 23	100	✓	✓	✓	✓	0.01-1	✓	✓	✓	✓	✓	✓	✓	✓	✓	✓
SFVW-Set 24	100	✓	20	✓	✓	0.01-1	✓	✓	✓	✓	✓	✓	✓	✓	✓	✓
SFVW-Set 25	✓	✓	✓	✓	✓	0.01-1	✓	✓	✓	✓	✓	✓	✓	✓	✓	✓
SFVW-Set 26	✓	✓	20	✓	✓	0.01-1	✓	✓	✓	✓	✓	✓	✓	✓	✓	✓

Table 3.4c SFVW-Sets analysed

Set Name	DP (Psi)	FVR	Shut-in time (days)	Frack Length (m)	Kf (D)	Km (μD)	lam	IFT	ngm	nwm	Kmaxgm	Kmaxwm	ngf	nwf	Kmaxgf	Kmaxwf
Default Values	1000	2	2	400	1-30	1-100	1-4	2-50	1.5-5	1.2-4	0.5-1	0.05-0.6	1.5-5	1.2-4	0.5-1	0.1-0.75
SFVW-Set 27	4000	✓	20	✓	✓	0.01-1	✓	✓	✓	✓	✓	✓	✓	✓	✓	✓
SFVW-Set 28	4000	✓	✓	✓	✓	0.01-1	✓	✓	✓	✓	✓	✓	✓	✓	✓	✓
SFVW-Set 29	✓	10	20	✓	✓	✓	✓	✓	✓	✓	✓	✓	✓	✓	✓	✓
SFVW-Set 30	100	10	20	✓	✓	✓	✓	✓	✓	✓	✓	✓	✓	✓	✓	✓
SFVW-Set 31	4000	10	20	✓	✓	✓	✓	✓	✓	✓	✓	✓	✓	✓	✓	✓
SFVW-Set 32	100	10	✓	✓	✓	✓	✓	✓	✓	✓	✓	✓	✓	✓	✓	✓
SFVW-Set 33	4000	10	✓	✓	✓	✓	✓	✓	✓	✓	✓	✓	✓	✓	✓	✓
SFVW-Set 34	✓	10	20	✓	✓	0.1-10	✓	✓	✓	✓	✓	✓	✓	✓	✓	✓
SFVW-Set 35	✓	10	✓	✓	✓	0.1-10	✓	✓	✓	✓	✓	✓	✓	✓	✓	✓
SFVW-Set 36	4000	10	20	✓	✓	0.1-10	✓	✓	✓	✓	✓	✓	✓	✓	✓	✓

Table 3.4d SFVW-Sets analysed

Set Name	DP (Psi)	FVR	Shut-in time (days)	Frack Length (m)	Kf (D)	Km (μD)	lam	IFT	ngm	nwm	Kmaxgm	Kmaxwm	ngf	nwf	Kmaxgf	Kmaxwf
Default Values	1000	2	2	400	1-30	1-100	1-4	2-50	1.5-5	1.2-4	0.5-1	0.05-0.6	1.5-5	1.2-4	0.5-1	0.1-0.75
SFVW-Set 37	4000	10	✓	✓	✓	0.1-10	✓	✓	✓	✓	✓	✓	✓	✓	✓	✓
SFVW-Set 38	✓	10	20	✓	✓	0.01-1	✓	✓	✓	✓	✓	✓	✓	✓	✓	✓
SFVW-Set 39	4000	10	20	✓	✓	0.01-1	✓	✓	✓	✓	✓	✓	✓	✓	✓	✓
SFVW-Set 40	4000	10	✓	✓	✓	0.01-1	✓	✓	✓	✓	✓	✓	✓	✓	✓	✓
SFVW-Set 41	✓	10	✓	✓	✓	0.01-1	✓	✓	✓	✓	✓	✓	✓	✓	✓	✓
SFVW-Set 42 Two-Layer	✓	✓	✓	✓	✓	✓	✓	✓	✓	✓	✓	✓	✓	✓	✓	✓
SFVW-Set 43 Two-Layer	100	✓	✓	✓	✓	✓	✓	✓	✓	✓	✓	✓	✓	✓	✓	✓
SFVW-Set 44 Two-Layer	✓	✓	20	✓	✓	✓	✓	✓	✓	✓	✓	✓	✓	✓	✓	✓
SFVW-Set 45 Two-Layer	✓	✓	20	✓	✓	0.1-10	✓	✓	✓	✓	✓	✓	✓	✓	✓	✓
SFVW-Set 46	✓	✓	✓	50	✓	✓	✓	✓	✓	✓	✓	✓	✓	✓	✓	✓
SFVW-Set 47 with/without Hysteresis	✓	✓	✓	✓	✓	✓	✓	✓	✓	✓	✓	✓	✓	✓	✓	✓

Table 3.4e SFVW-Sets analysed

Set Name	DP (Psi)	FVR	Shut-in time (days)	Frack Length (m)	Kf (D)	Km (μD)	lam	IFT	ngm	nwm	Kmaxgm	Kmaxwm	ngf	nwf	Kmaxgf	Kmaxwf
Default Values	1000	2	2	400	1-30	1-100	1-4	2-50	1.5-5	1.2-4	0.5-1	0.05-0.6	1.5-5	1.2-4	0.5-1	0.1-0.75
SFVW-Set 48 with/without Hysteresis	100	✓	✓	✓	✓	0.1-10	✓	✓	✓	✓	✓	✓	✓	✓	✓	✓
SFVW-Set 49	100	10	✓	100	✓	✓	✓	✓	✓	✓	✓	✓	✓	✓	✓	✓
SFVW-Set 50	4000	10	✓	100	✓	✓	✓	✓	✓	✓	✓	✓	✓	✓	✓	✓
SFVW-Set 51	✓	10	✓	100	✓	0.1-10	✓	✓	✓	✓	✓	✓	✓	✓	✓	✓
SFVW-Set 52	✓	10	✓	100	✓	0.01-1	✓	✓	✓	✓	✓	✓	✓	✓	✓	✓
SFVW-Set 53	4000	10	✓	100	✓	0.01-1	✓	✓	✓	✓	✓	✓	✓	✓	✓	✓
SFVW-Set 54	✓	10	20	100	✓	✓	✓	✓	✓	✓	✓	✓	✓	✓	✓	✓
SFVW-Set 55	100	✓	✓	100	✓	0.1-10	✓	✓	✓	✓	✓	✓	✓	✓	✓	✓
SFVW-Set 56	4000	✓	20	100	✓	✓	✓	✓	✓	✓	✓	✓	✓	✓	✓	✓
SFVW-Set 57	✓	✓	✓	100	✓	0.1-10	✓	✓	✓	✓	✓	✓	✓	✓	✓	✓
SFVW-Set 58	100	✓	20	100	✓	0.1-10	✓	✓	✓	✓	✓	✓	✓	✓	✓	✓

Table 3.4f SFVW-Sets analysed

Set Name	DP (Psi)	FVR	Shut-in time (days)	Frack Length (m)	Kf (D)	Km (μD)	lam	IFT	ngm	nwm	Kmaxgm	Kmaxwm	ngf	nwf	Kmaxgf	Kmaxwf
Default Values	1000	2	2	400	1-30	1-100	1-4	2-50	1.5-5	1.2-4	0.5-1	0.05-0.6	1.5-5	1.2-4	0.5-1	0.1-0.75
SFVW-Set 59	4000	✓	20	100	✓	0.1-10	✓	✓	✓	✓	✓	✓	✓	✓	✓	✓
SFVW-Set 60	✓	✓	20	100	✓	0.1-10	✓	✓	✓	✓	✓	✓	✓	✓	✓	✓
SFVW-Set 61	4000	✓	20	100	✓	0.01-1	✓	✓	✓	✓	✓	✓	✓	✓	✓	✓
SFVW-Set 62, Swi=50%	✓	✓	✓	✓	✓	✓	✓	✓	✓	✓	✓	✓	✓	✓	✓	✓
SFVW-Set 63, Swi=75%	✓	✓	✓	✓	✓	✓	✓	✓	✓	✓	✓	✓	✓	✓	✓	✓
SFVW-Set 64, with Permeability Enhancement	✓	✓	✓	✓	✓	✓	✓	✓	✓	✓	✓	✓	✓	✓	✓	✓
SFVW-Set 65, with Permeability Enhancement	100	✓	✓	✓	✓	0.01-1	✓	✓	✓	✓	✓	✓	✓	✓	✓	✓
SFVW-Set 66, with Permeability Enhancement	✓	✓	✓	✓	✓	0.01-1	✓	✓	✓	✓	✓	✓	✓	✓	✓	✓

Table 3.5 Parameters for the worst and the best scenarios for the Base Reference Set, Set 1.

No.	Parameter		Case	
			Worst	Best
1	Fracture Permeability	K_f (D)	1	30
2	Matrix Permeability	K_m (μD)	1	100
3	Matrix Capillary Pressure	Pore Size Index, λ	4	1
4		Interfacial Tension, IFT (mNm/m)	2	50
5	Exponent of the Corey gas relative permeability curve in matrix	n_{gm}	5	1.5
6	Exponent of the Corey fracture fluid (water) relative permeability curve in matrix	n_{wm}	4	1.2
7	End point of Corey gas relative permeability curve in matrix	K_{maxgm}	0.5	1.0
8	End point of Corey fracture fluid (water) relative permeability curve in matrix	K_{maxwm}	0.05	0.6
9	Exponent of the Corey gas relative permeability curve in fracture	n_{gf}	5	1.5
10	Exponent of the Corey fracture fluid (water) relative permeability curve in fracture	n_{wf}	4	1.2
11	End point of Corey gas relative permeability curve in fracture	K_{maxgf}	0.5	1.0
12	End point of Corey fracture fluid (water) relative permeability curve in fracture	K_{maxwf}	0.1	0.75
13	Porosity	ϕ	0.15	
14	Residual water saturation in fracture	S_{wrf}	0.15	
15	Residual water saturation in matrix	S_{wrm}	0.15	
16	Residual gas saturation in fracture	S_{grf}	0.1	
17	Residual gas saturation in matrix	S_{grm}	0.1	

3.17 Figures

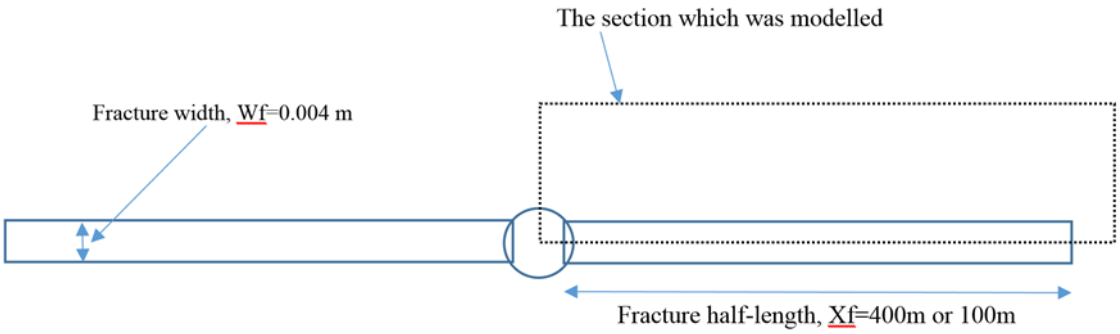

Figure 3.1 The section that is modelled for SFVW sets.

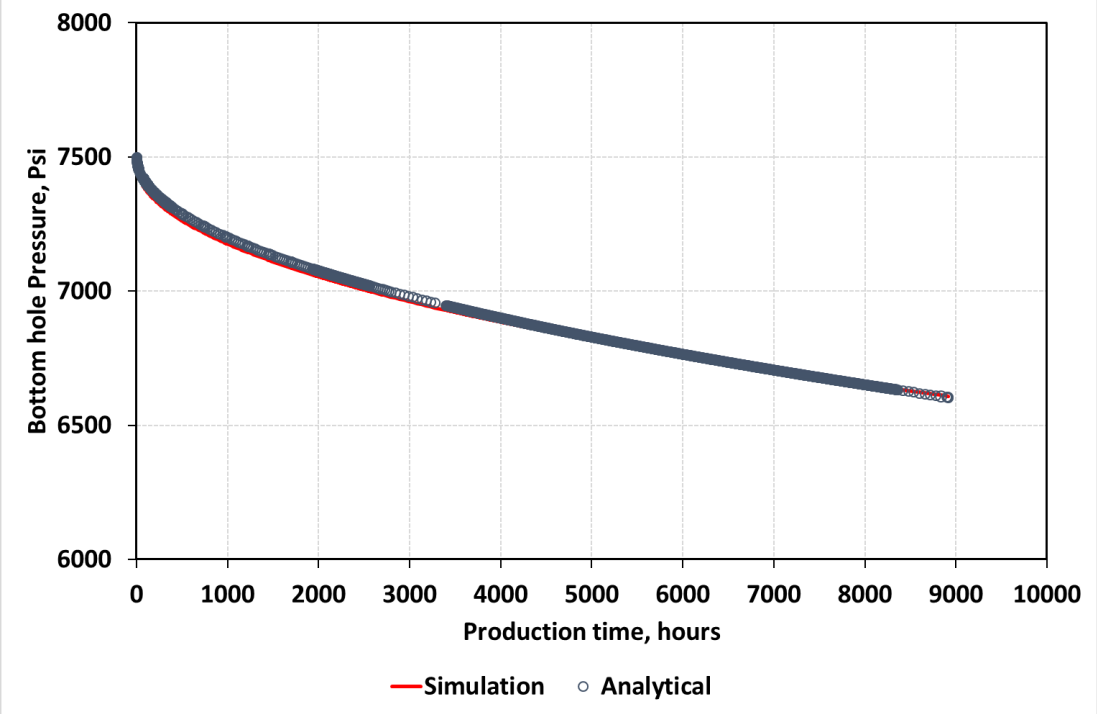

Figure 3.2 Predicated bottom hole pressure by simulation model and analytical model (Equation 3.2) versus production time.

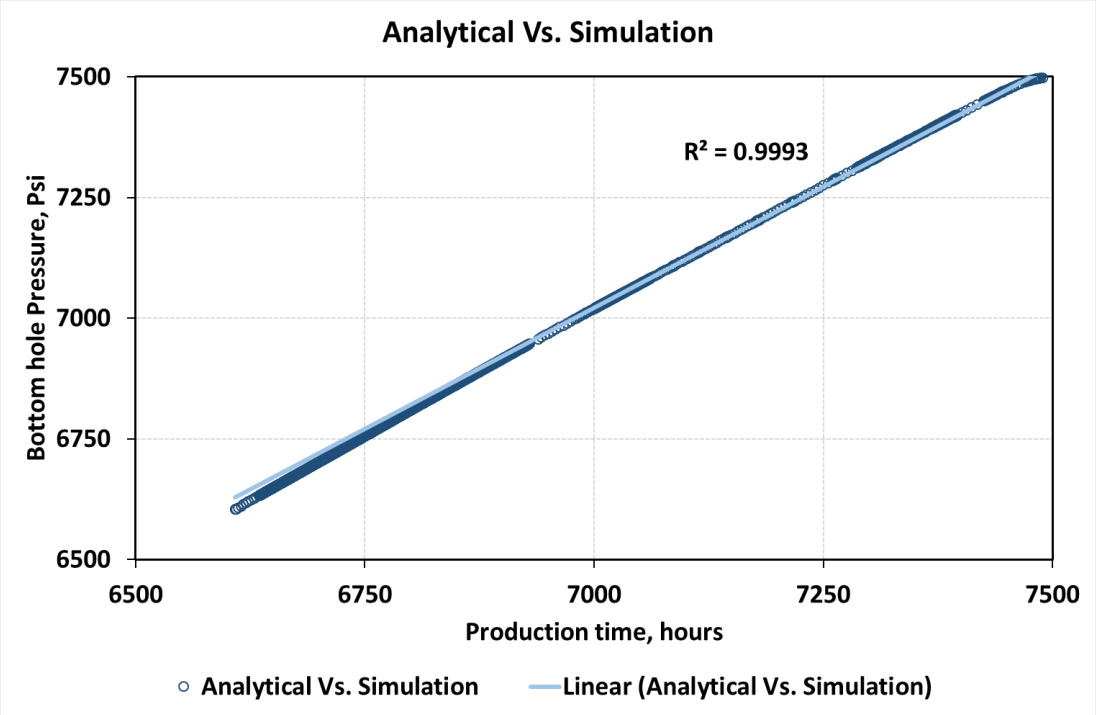

Figure 3.3 Predicated bottom hole pressure by analytical model (Equation 3.2) vs the one of simulation model.

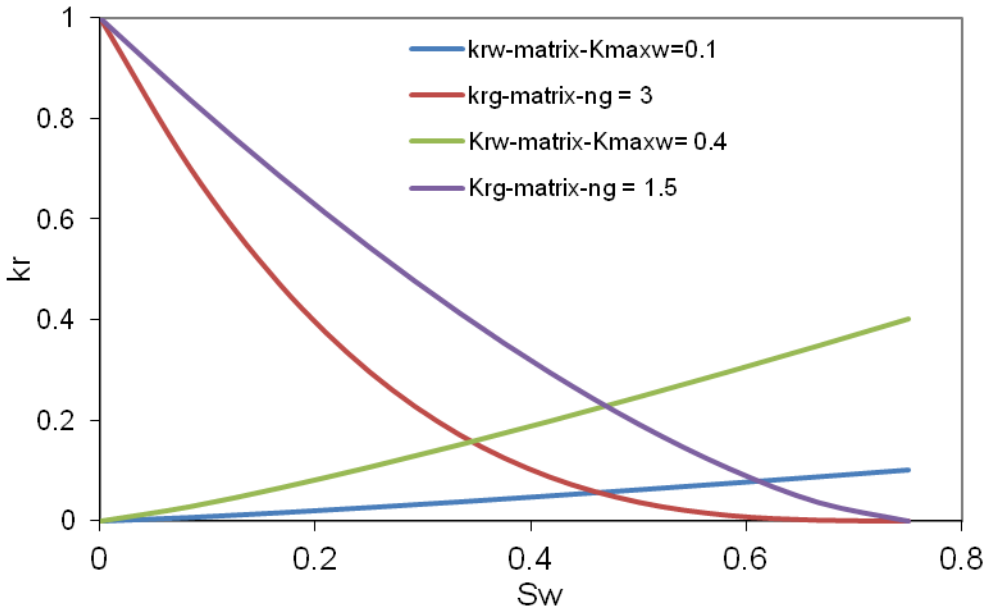

Figure 3.4 The variation of Krg and Krw vs Sw by changing the Corey endpoints and exponents.

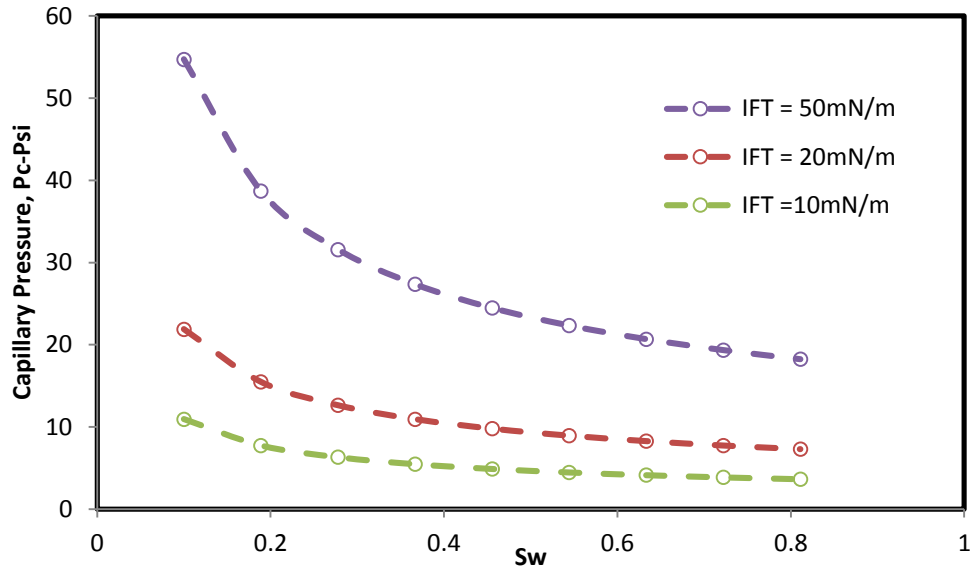

Figure 3.5 The variation of Pc by changing IFT.

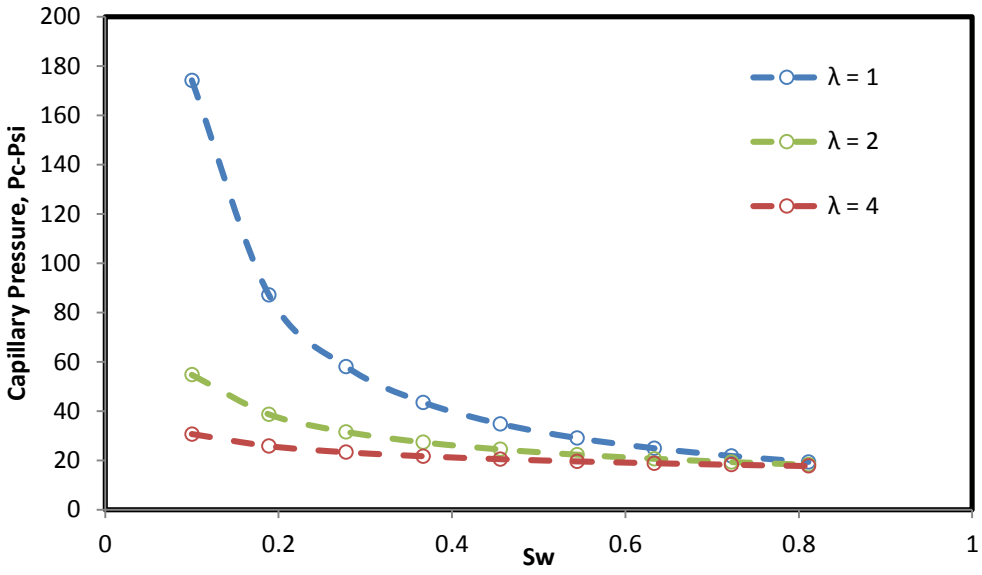

Figure 3.6 The variation of Pc by changing λ.

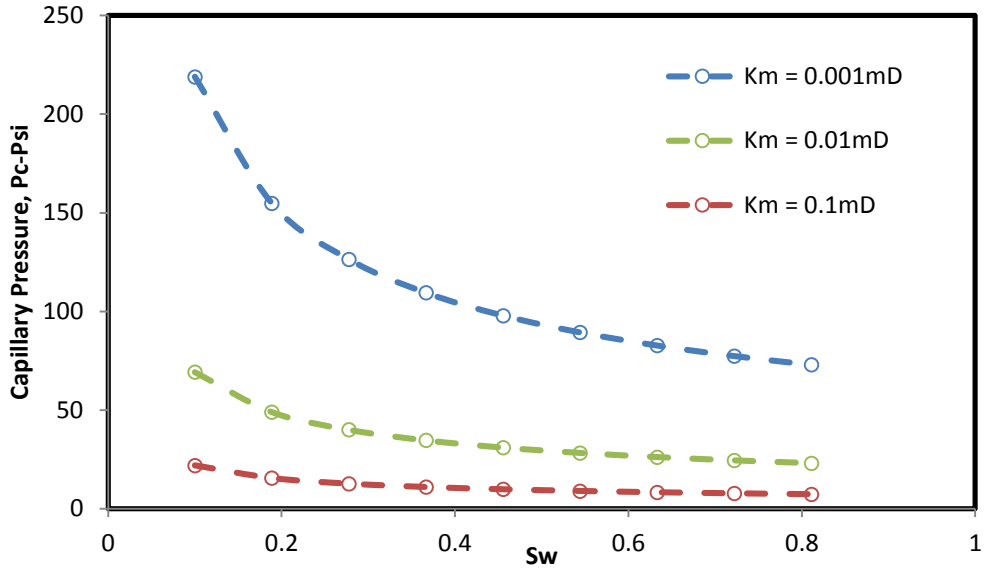

Figure 3.7 The variation of Pc by changing Km.

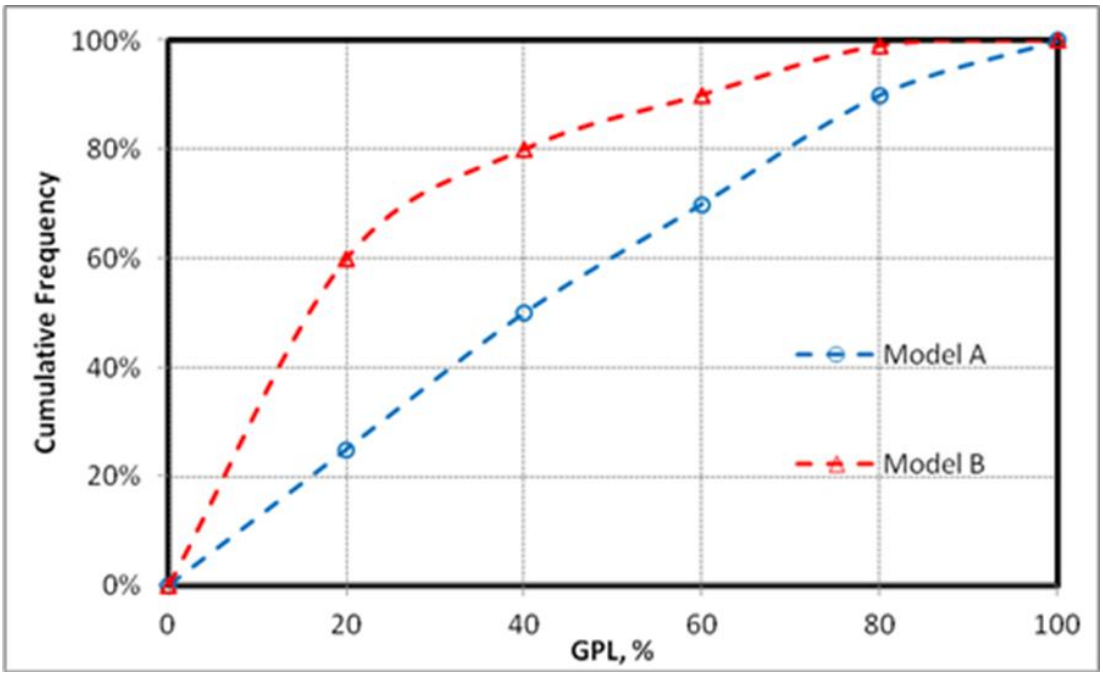

Figure 3.8 Histogram chart demonstrating the percentage of the cumulative frequency of the runs for (model A and B) versus GPL%. (For demonstration purposes).

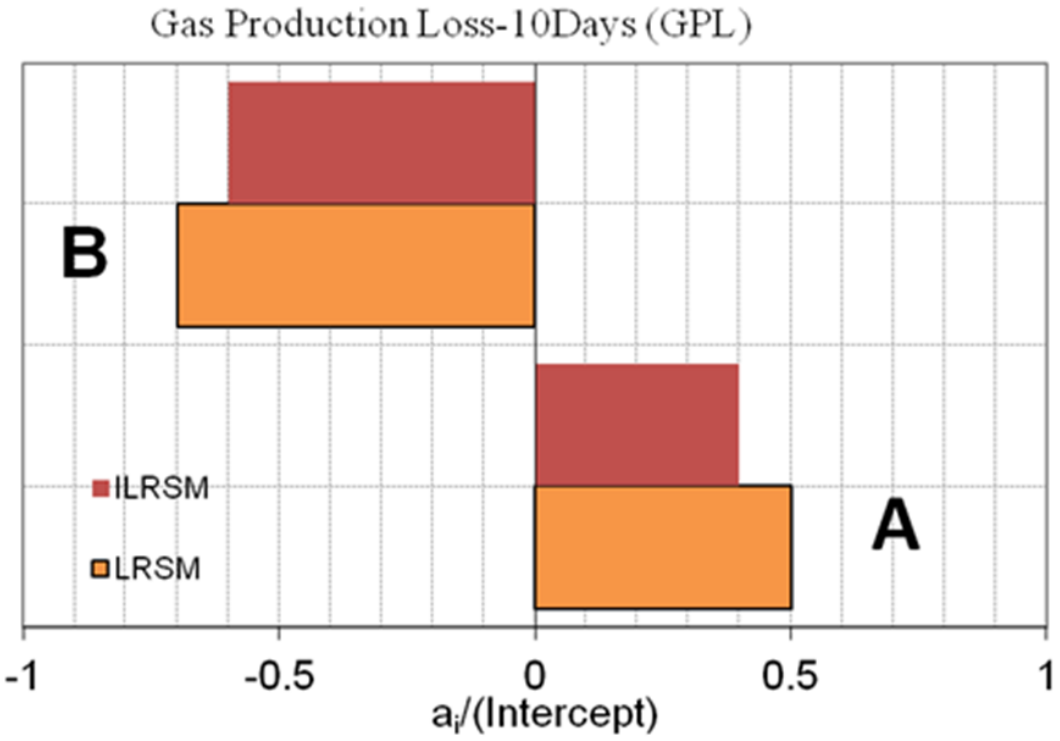

Figure 3.9 Tornado chart of primary coefficients of all pertinent parameters on gas production loss (Linear Response Surface Model, without interaction) for (Model A and B). (For demonstration purposes).

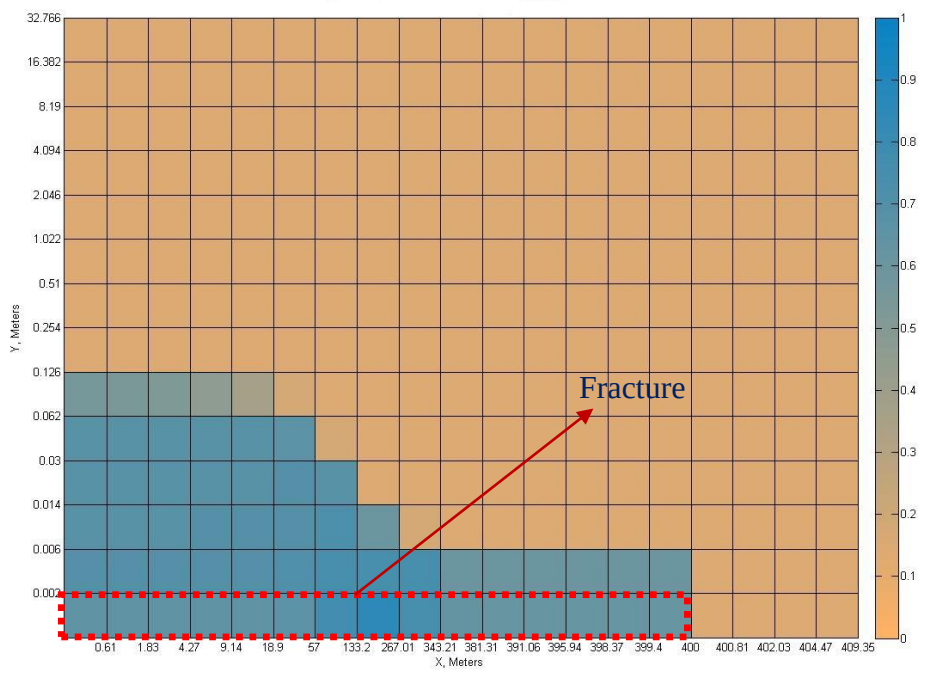

Figure 3.10 The saturation map of FF distribution in and around the fractures.

a. Normal RSM

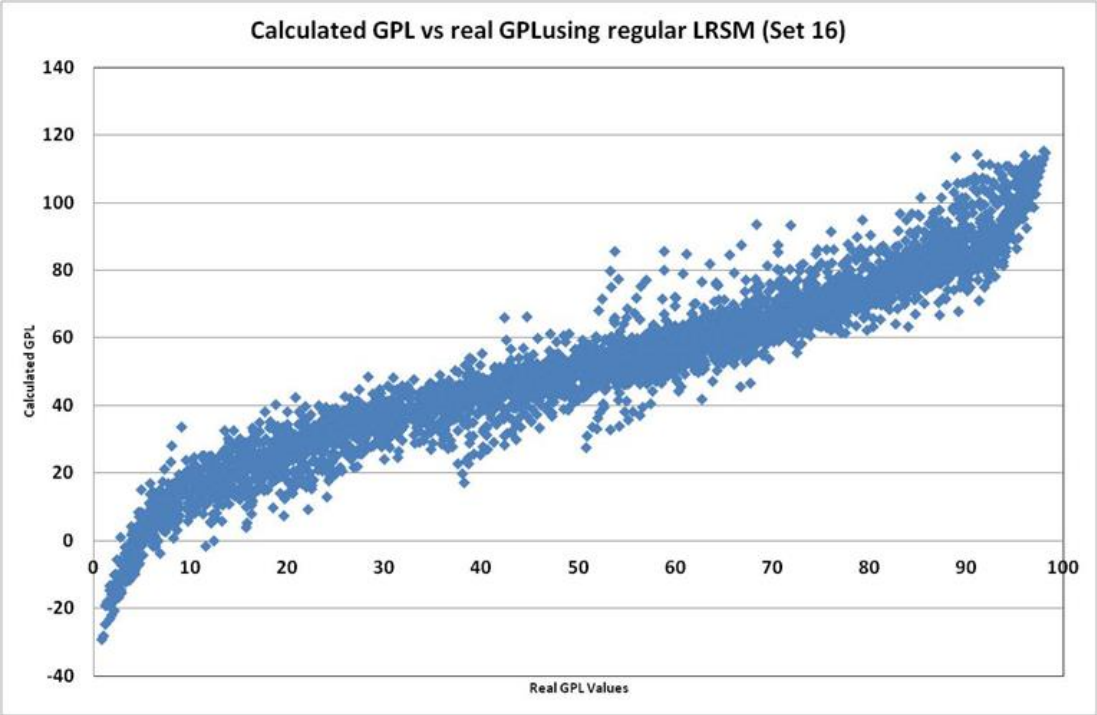

b. RSM with Domain change

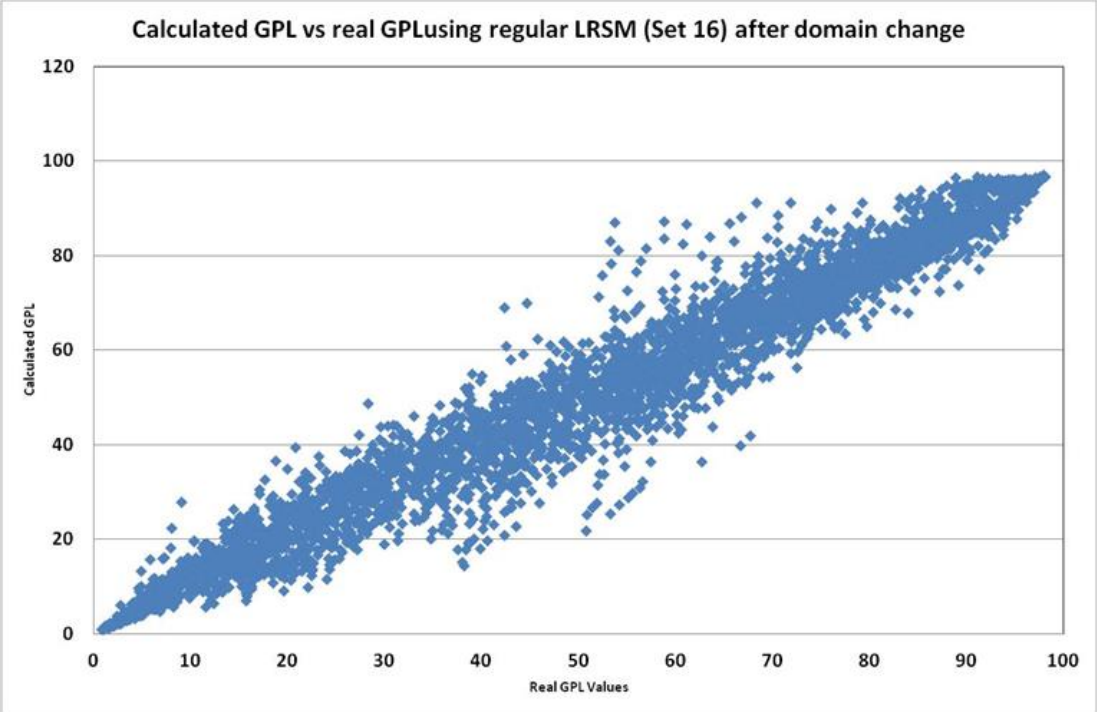

Figure 3.11 Calculated GPL using RSM versus real GPL results, a. Normal RSM, b. RSM with a domain change.

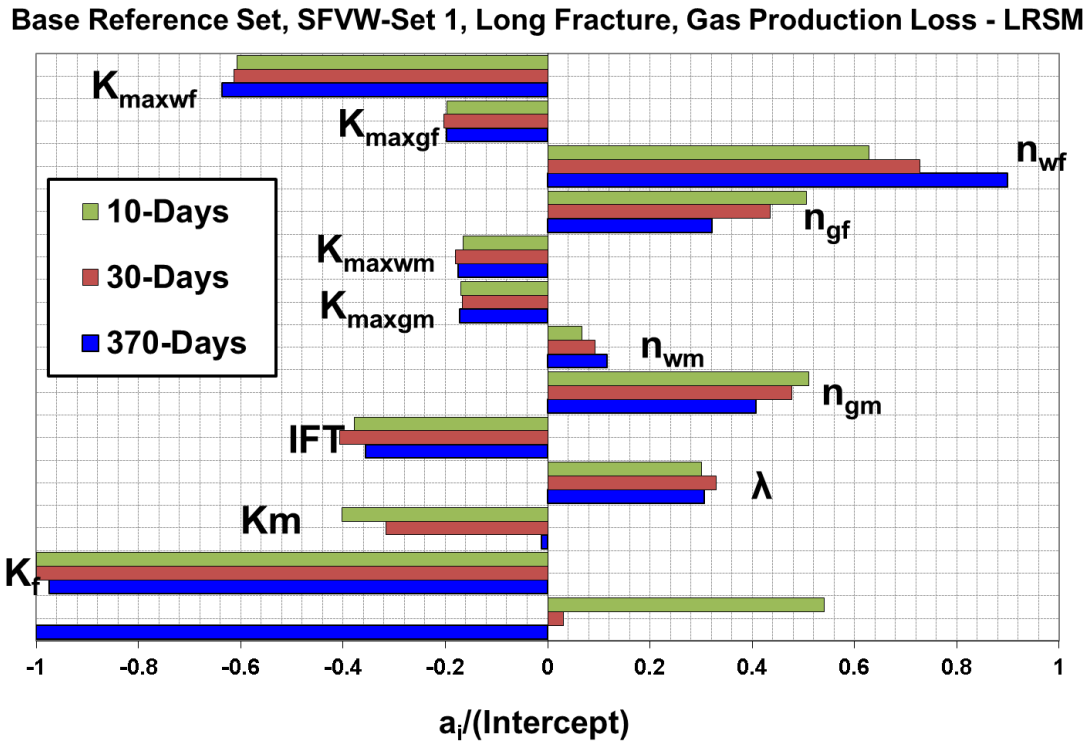

Figure 3.12 Tornado chart showing LRSM coefficients of all pertinent parameters in the Base Reference Set (BC) at three production stages, (FVR=2, DP=1000 psi, ST=2 days and Kmr=1).

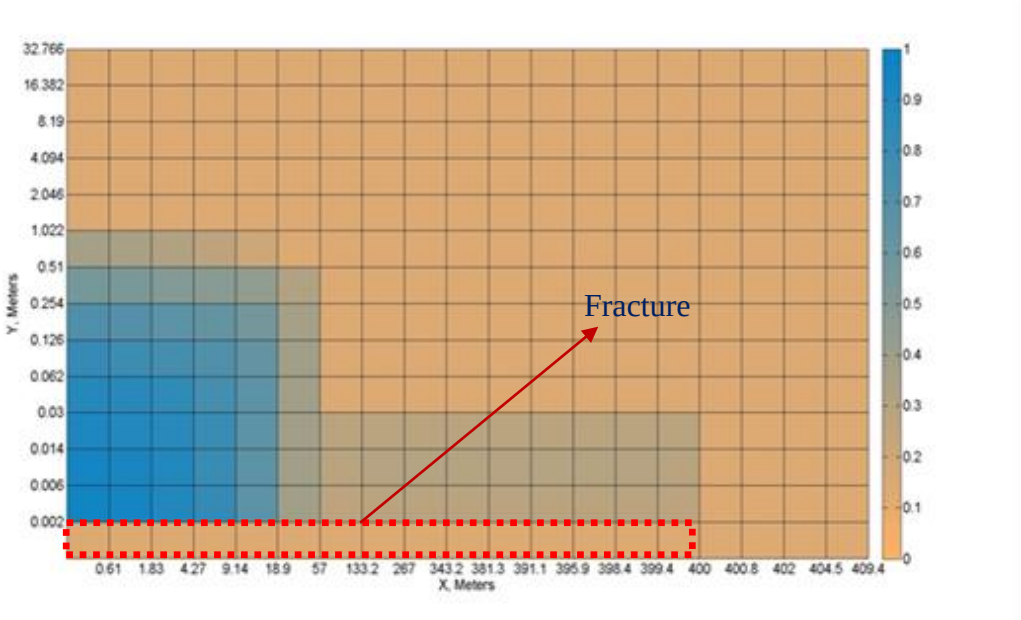

Figure 3.13 Fracturing Fluid saturation map of the best scenario of the Base Reference Set after 2 days of the shut-in period.

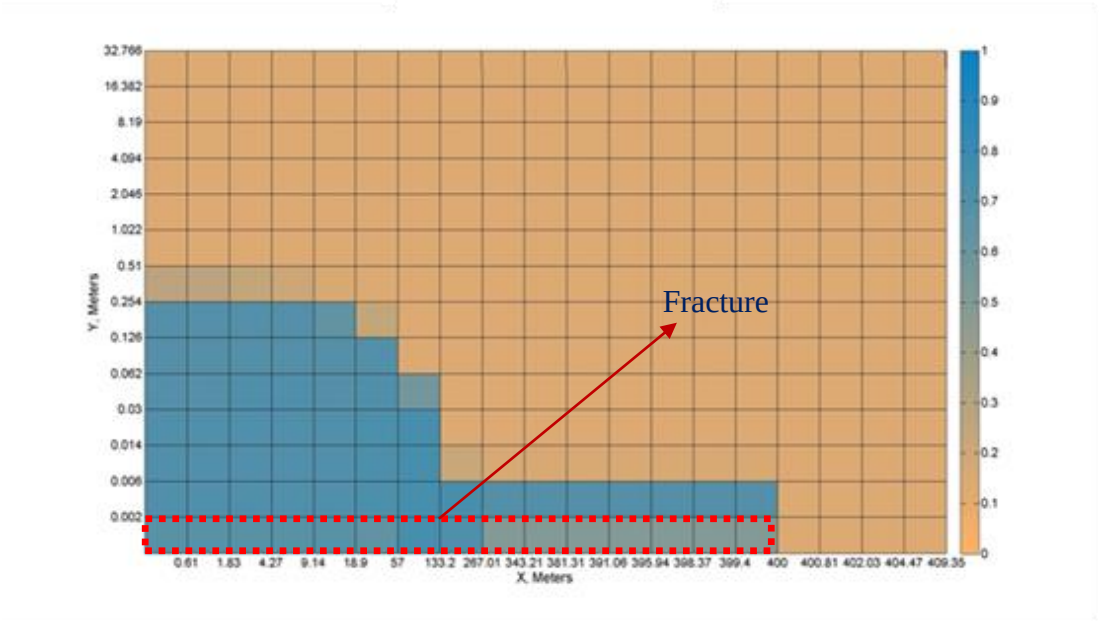

Figure 3.14 Fracturing Fluid saturation map of the worst scenario of the Base Reference Set after 2 days of the shut-in period.

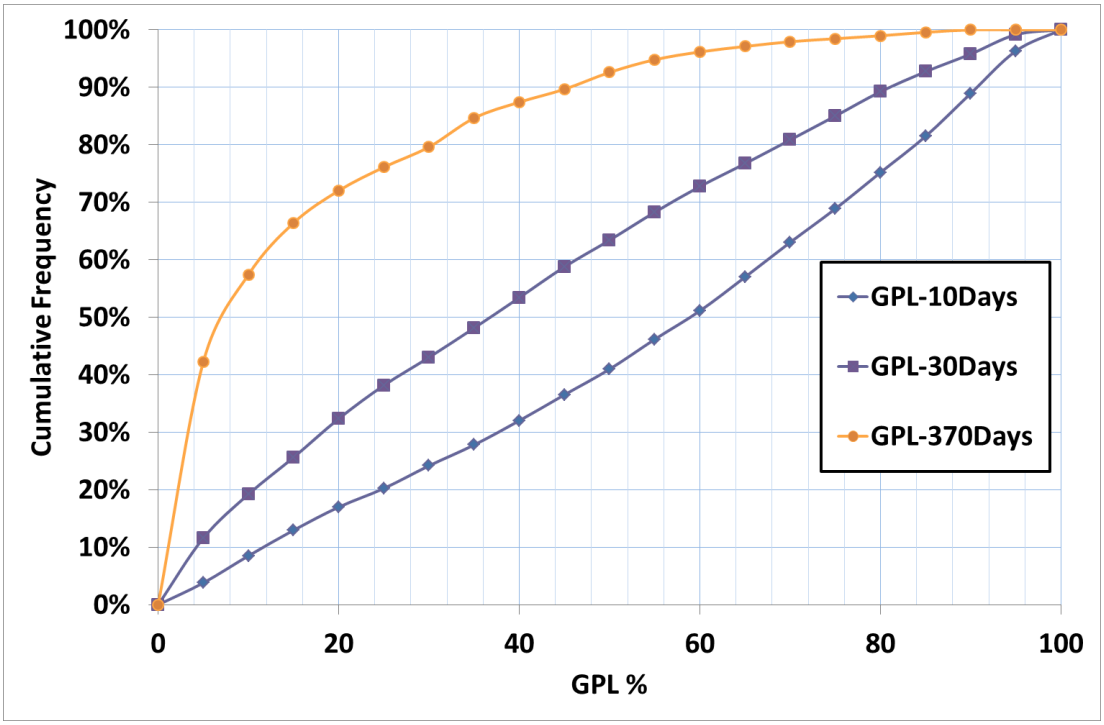

Figure 3.15 Histogram chart displaying cumulative frequency of the Base Reference Set (BC) at three production stages.

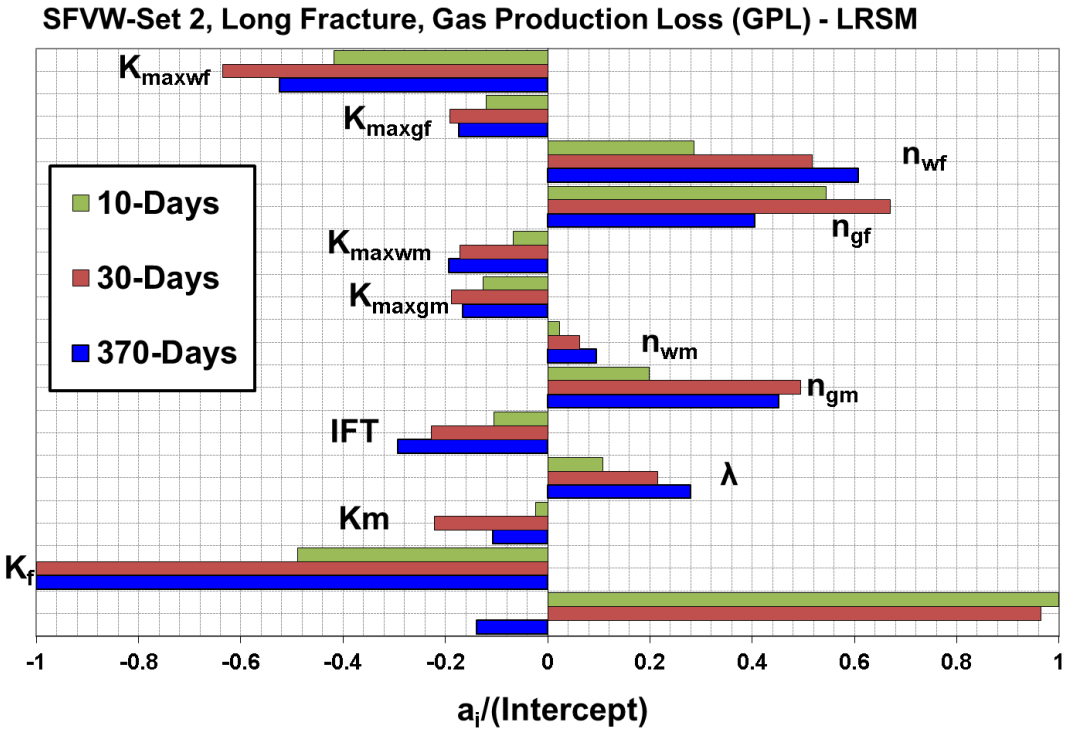

Figure 3.16 Tornado chart showing LRSM coefficients of all pertinent parameters in SFVW-Set 2 with higher FVR at three production periods, (FVR=10, DP=1000 psi, ST=2 days and Kmr=1).

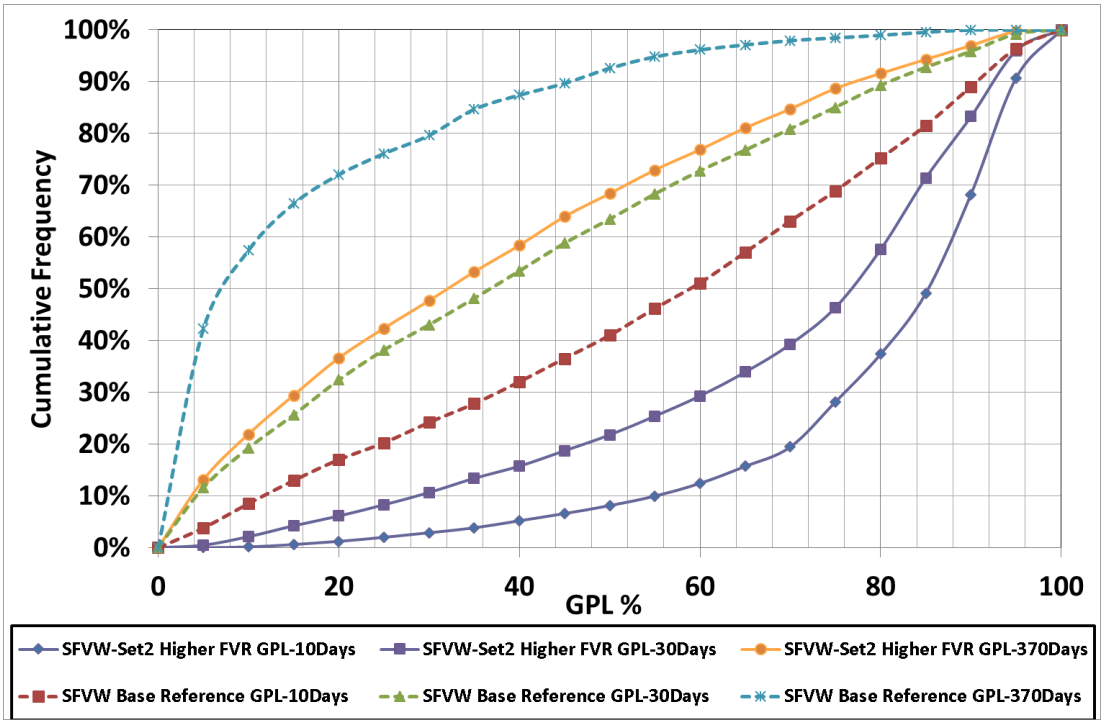

Figure 3.17 Histogram chart comparing the cumulative frequency of SFVW-Set 2 with FVR=10 and SFVW Base Reference Set (BC) at three production periods.

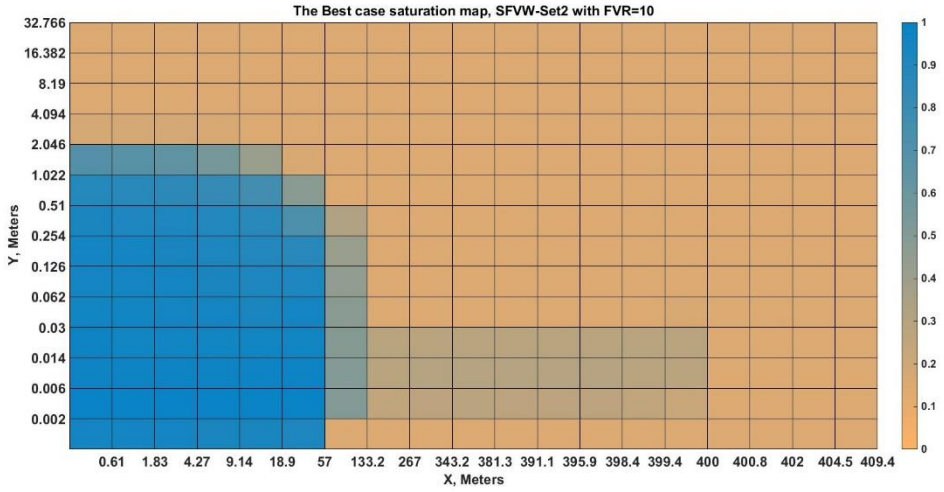

Figure 3.18 Fracturing Fluid saturation map of the best scenario of the SFVW-Set2 (FVR=10) after 2 days of the shut-in period.

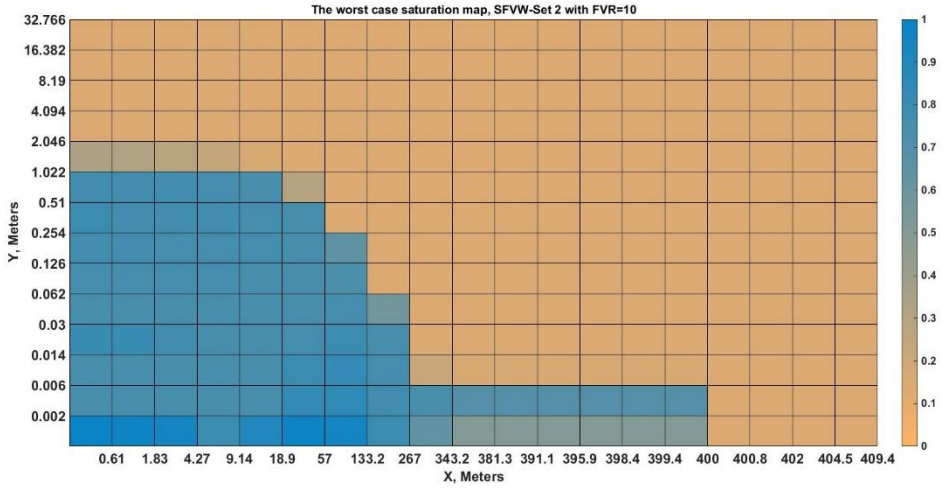

Figure 3.19 Fracturing Fluid saturation map of the worst scenario of the SFVW-Set2 (FVR=10) after 2 days of the shut-in period.

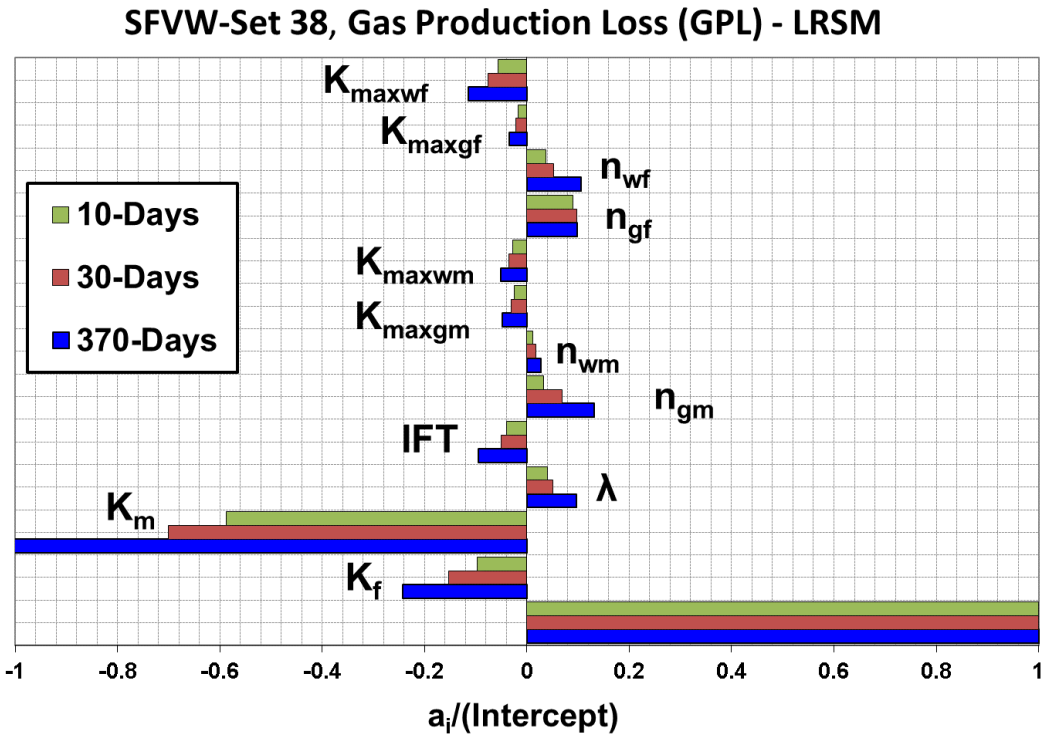

Figure 3.20 Tornado chart comparing LRSM coefficients of all pertinent parameters at three production stages, in the Set with FVR=10, Kmr= 100, ST=20 days, Long Fracture.

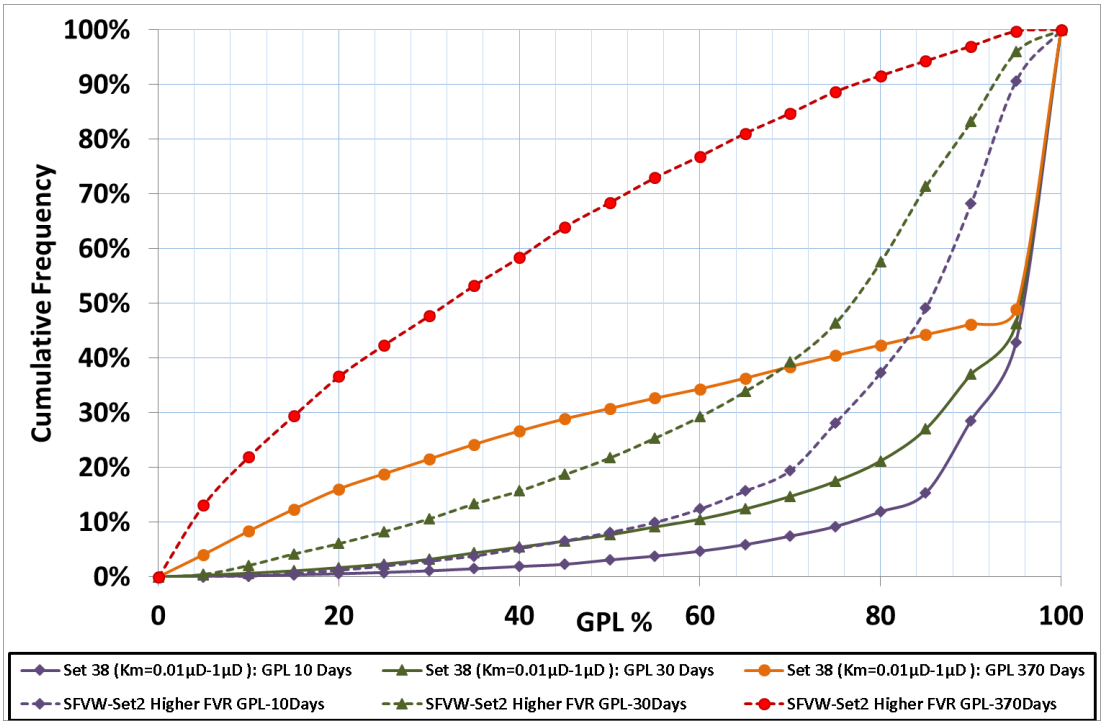

Figure 3.21 Histogram chart comparing the cumulative frequency of SFVW-Set 38 with FVR=10, Kmr=100 and ST=20 and SFVW-Set 2 with FVR=10 at three production periods.

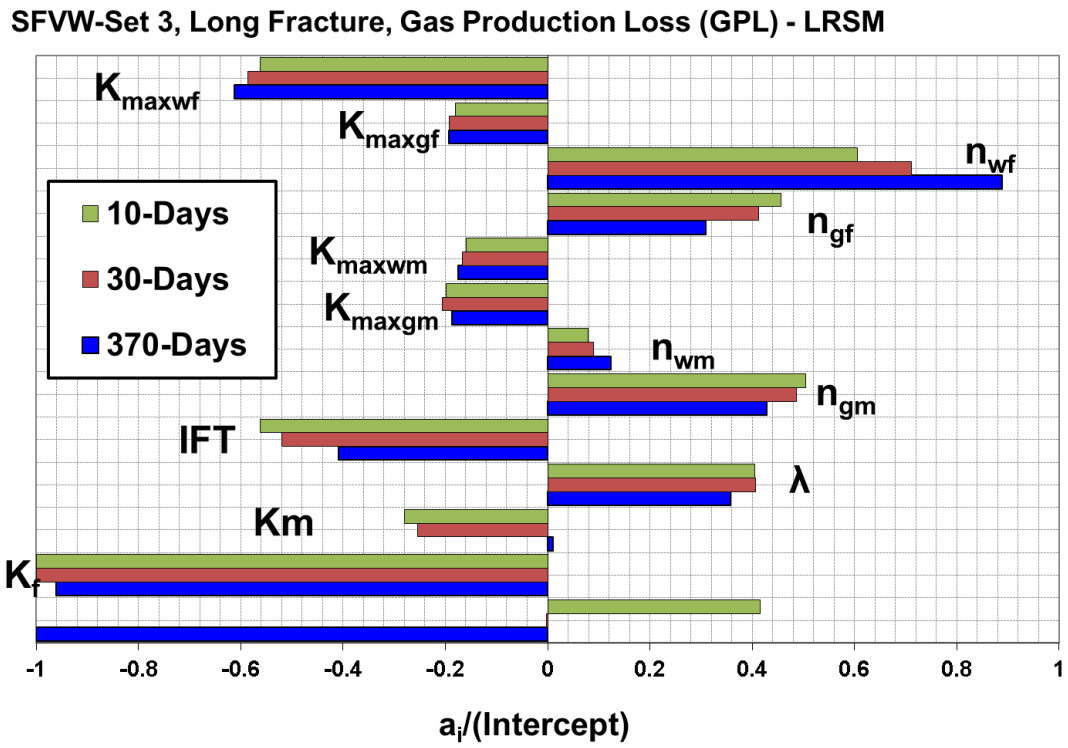

Figure 3.22 Tornado chart comparing LRSM coefficients of all pertinent parameters at three production stages, in the SFVW- Set with ST=20 days, Long Fracture.

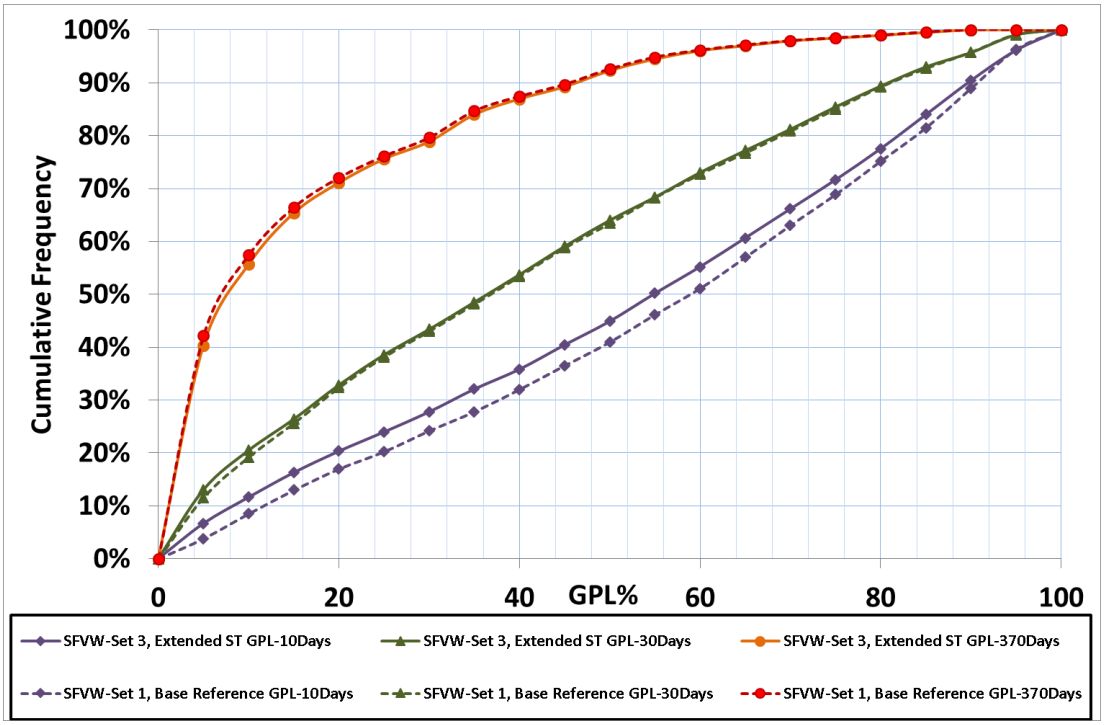

Figure 3.23 Histogram chart comparing the cumulative frequency of SFVW-Set 3 with ST=20, and SFVW-Set 1 base reference set at three production periods.

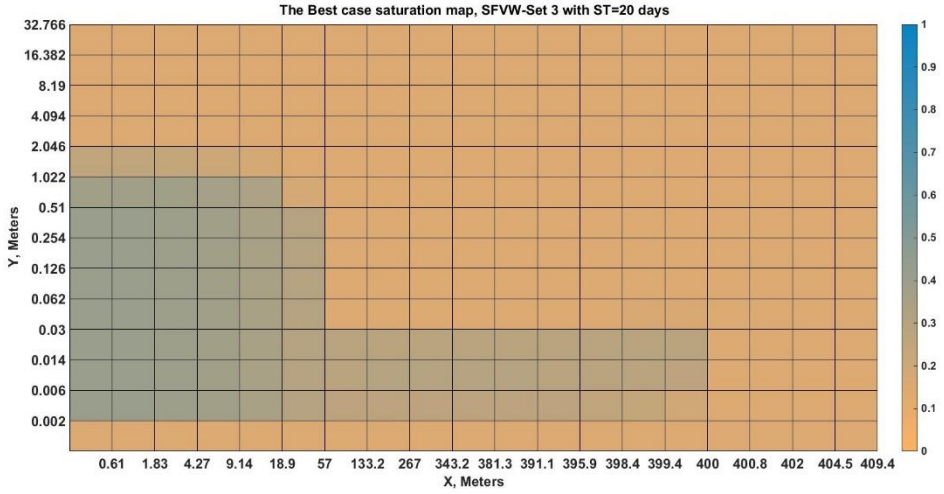

Figure 3.24 Fracturing Fluid saturation map of the best scenario of the SFVW-Set 3 after 20 days of the shut-in period.

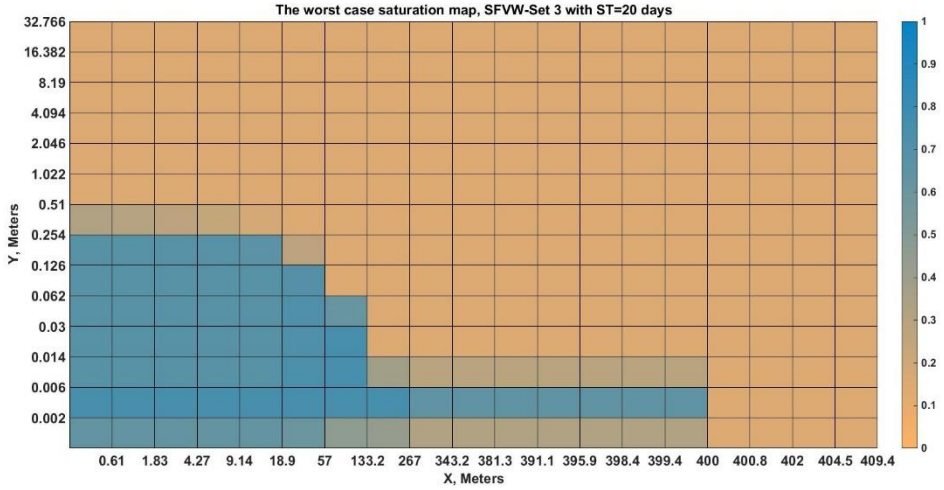

Figure 3.25 Fracturing Fluid saturation map of the worst scenario of the SFVW-Set 3 after 20 days of the shut-in period.

a. SFVW-Set 4, Kmr=10

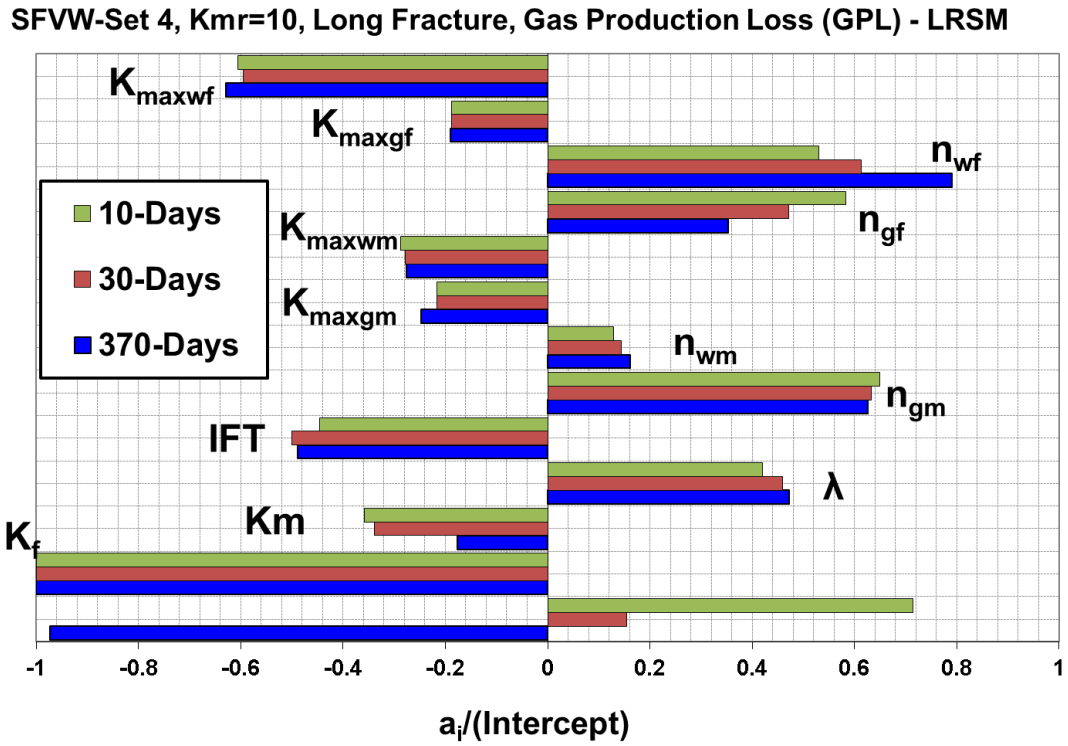

b. SFVW-Set 25, Kmr=100

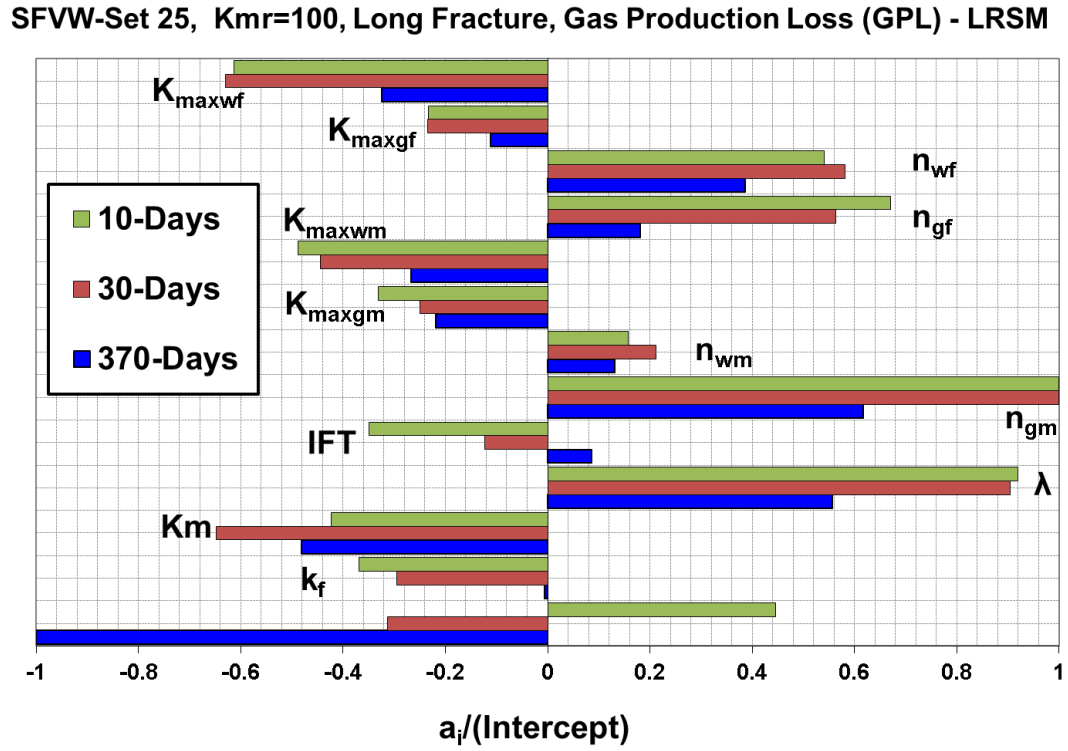

Figure 3.26 Tornado chart comparing LRSM coefficients of all pertinent parameters at three production stages, in a. SFVW-Set 4 with Kmr=10 and b. SFVW-Set 25 with Kmr=100., Long Fracture.

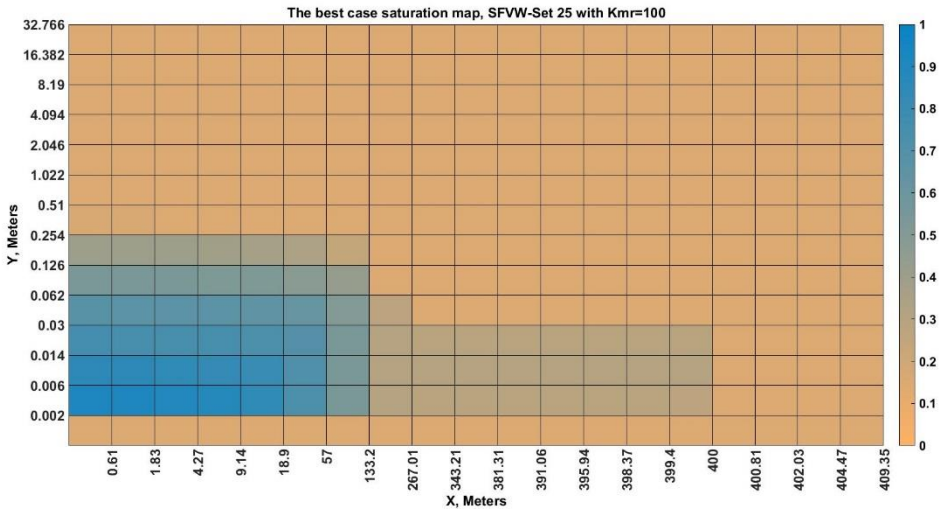

Figure 3.27 Fracturing Fluid saturation map of the best scenario of the SFVW-Set 25 after 2 days of the shut-in period.

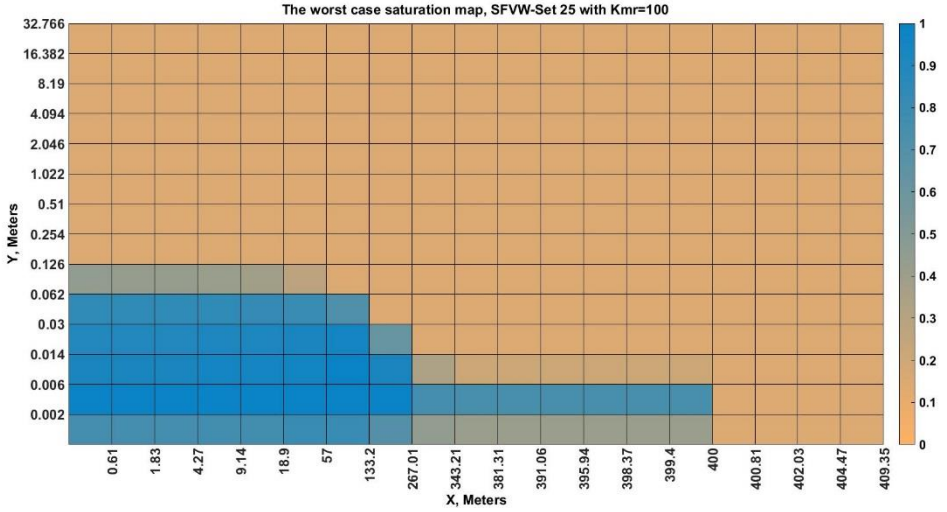

Figure 3.28 Fracturing Fluid saturation map of the worst scenario of the SFVW-Set 25 after 2 days of the shut-in period.

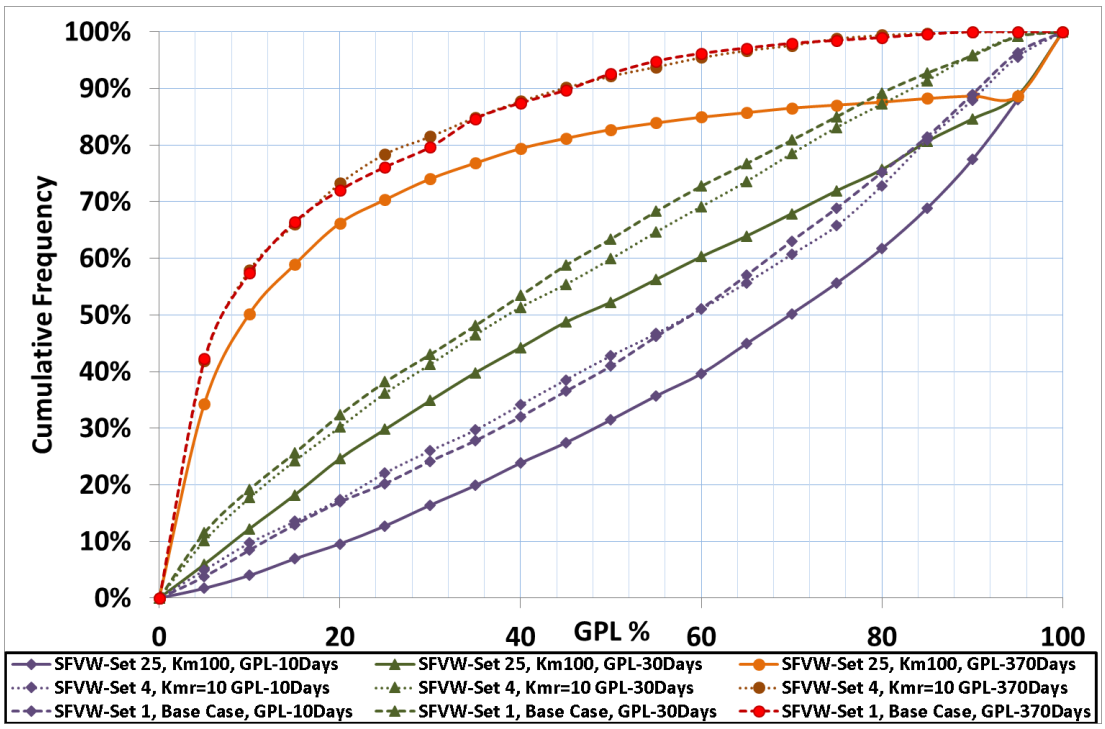

Figure 3.29 Histogram chart comparing the cumulative frequency of SFVW-Set 25, 4 and 1 with Kmr=100, 10 and 1 respectively at three production periods.

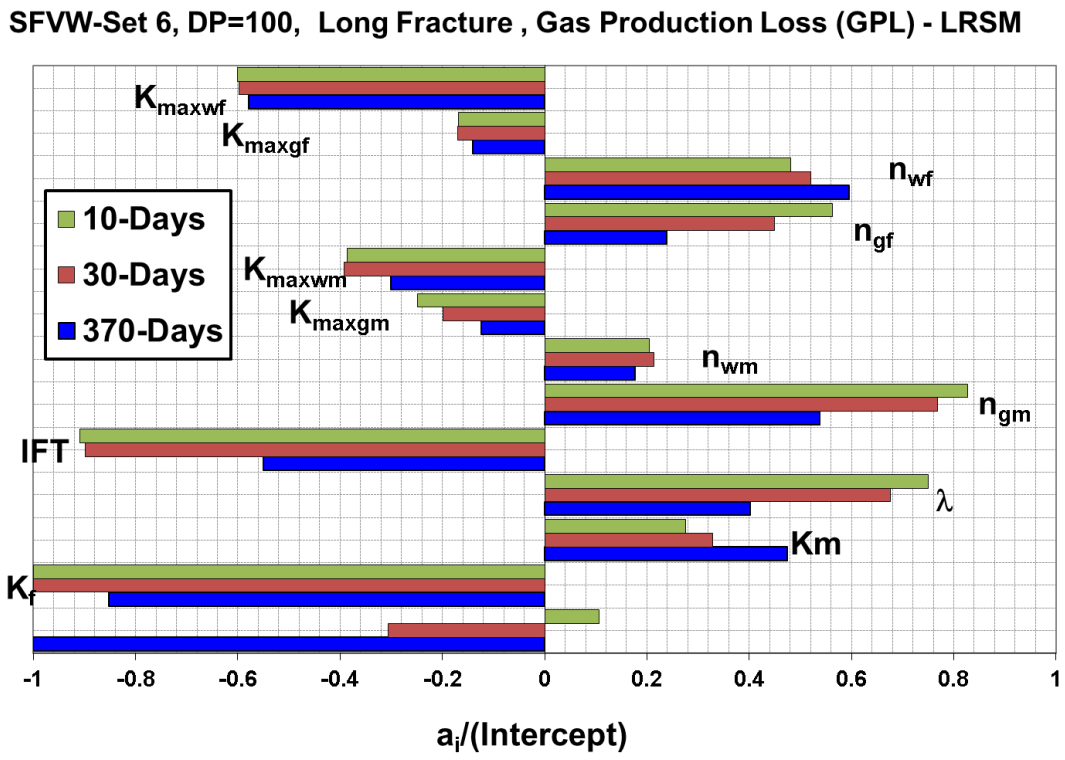

Figure 3.30 Tornado chart comparing LRSM coefficients of all pertinent parameters at three production stages, in SFVW-Set 6 with DP=100 psi, Long Fracture.

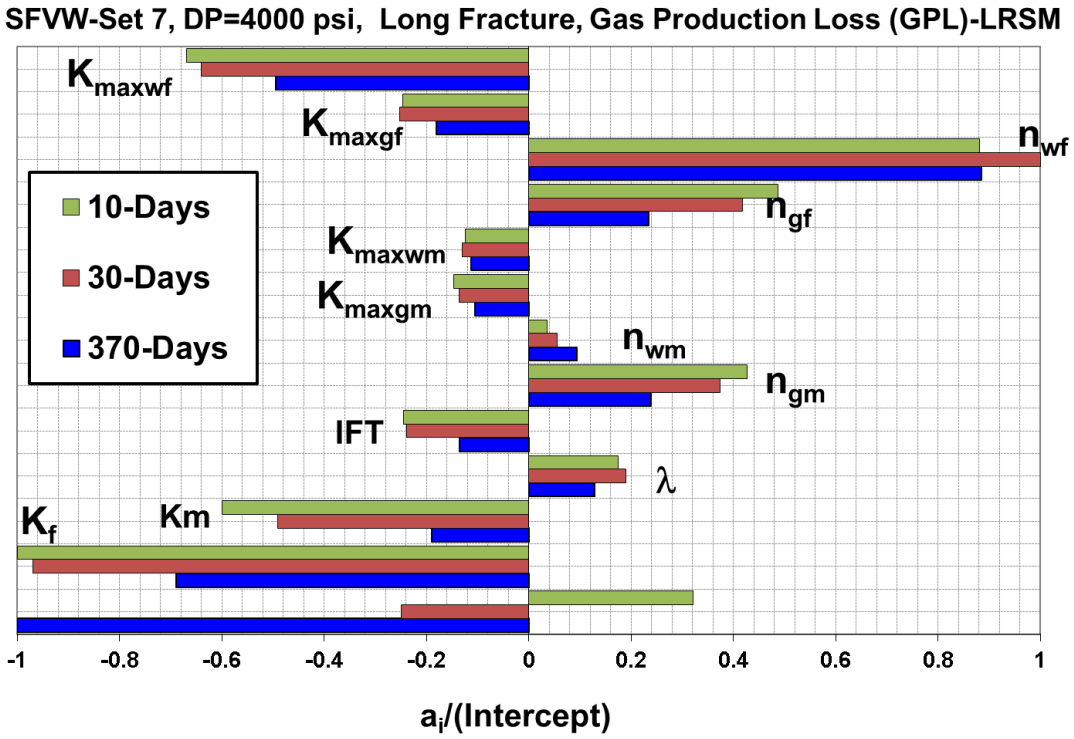

Figure 3.31 Tornado chart comparing LRSM coefficients of all pertinent parameters at three production stages, in SFVW-Set 7 with DP=4000 psi, Long Fracture.

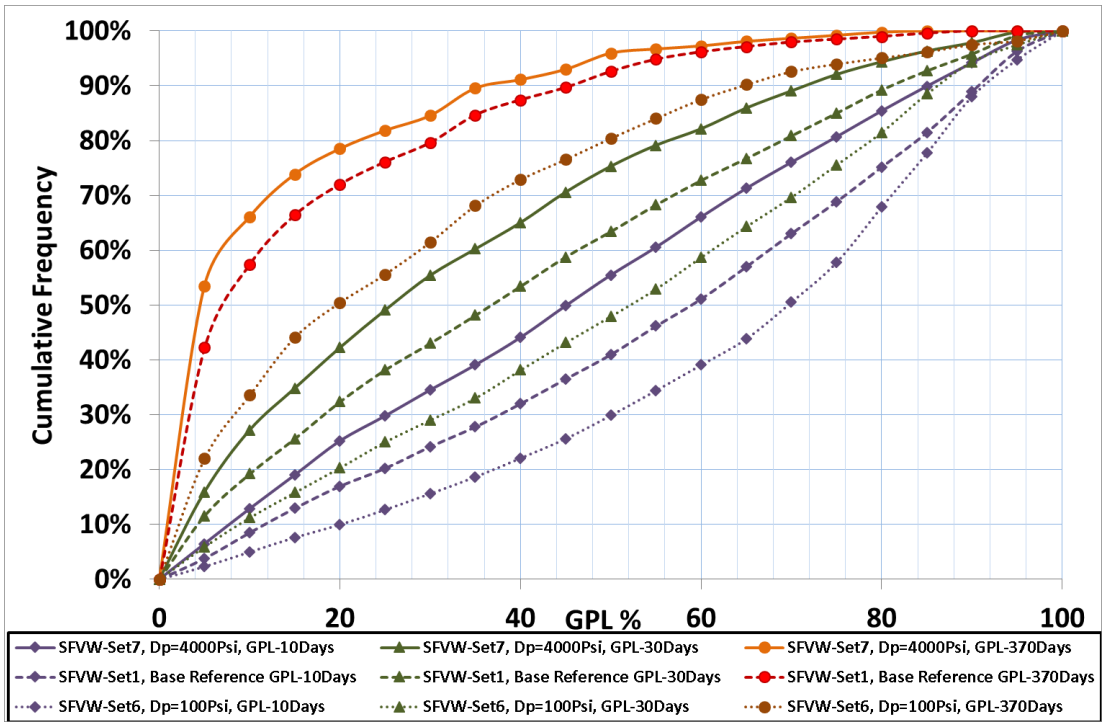

Figure 3.32 Histogram chart comparing the cumulative frequency of SFVW-Set 6, 1 and 7 with DP=100, 1000 and 4000 respectively at three production periods.

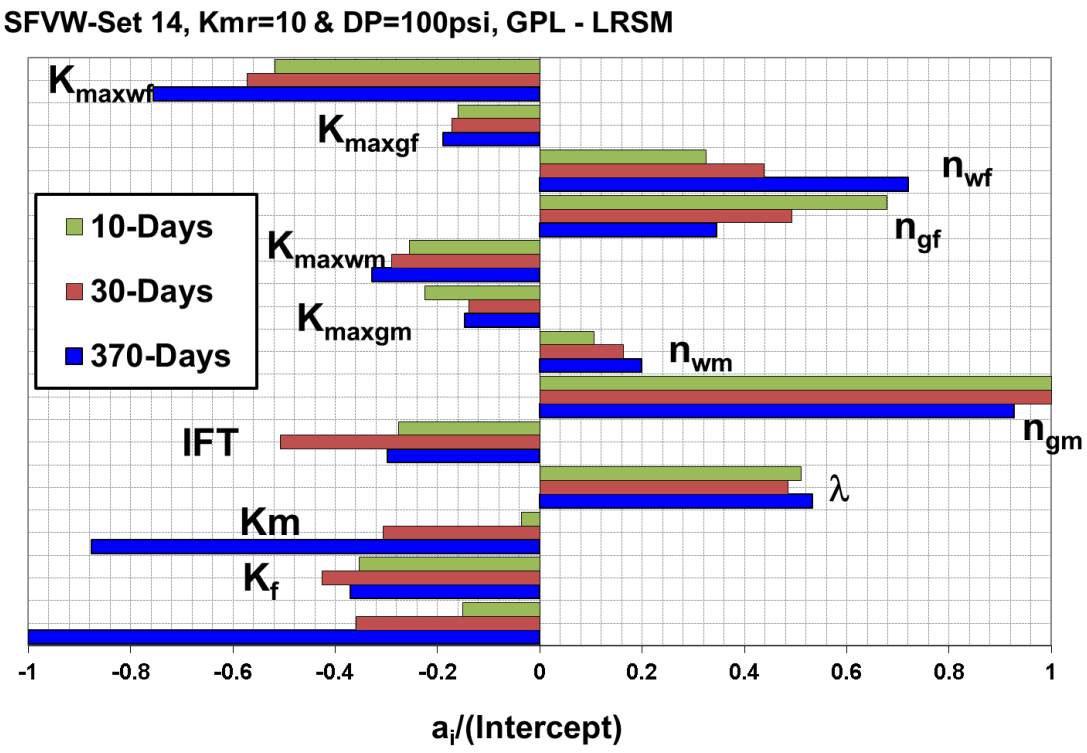

Figure 3.33 Tornado chart comparing LRSM coefficients of all pertinent parameters at three production stages, in SFVW-Set 14 with Kmr=10 &DP=100 psi, Long Fracture.

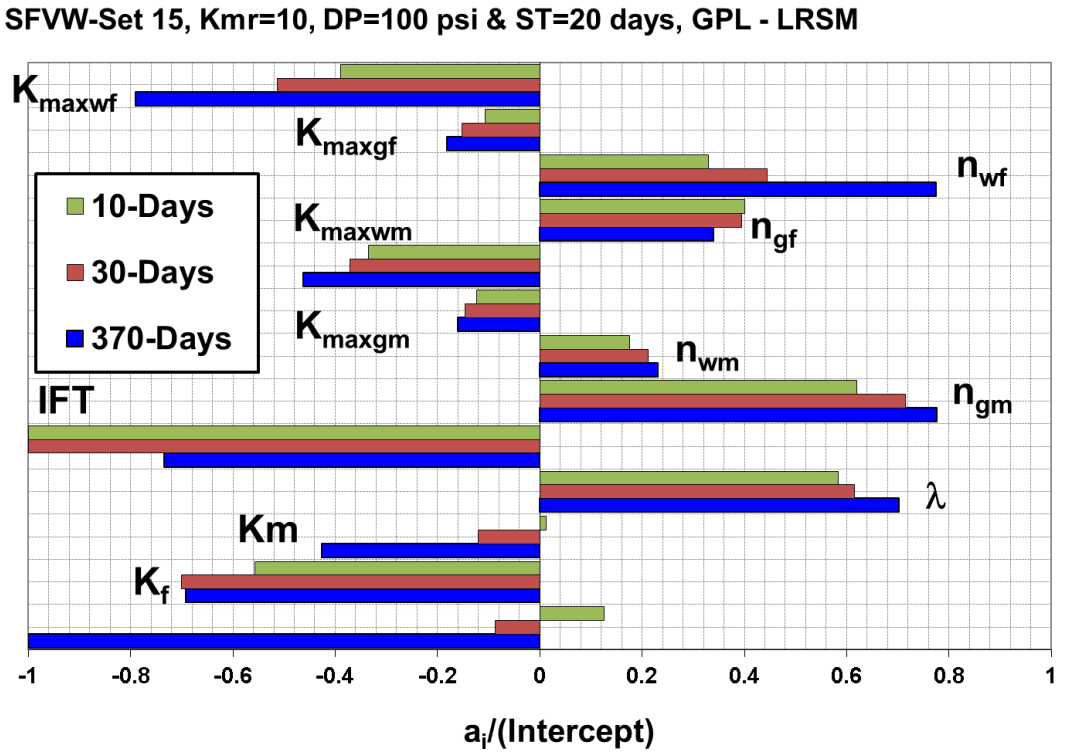

Figure 3.34 Tornado chart comparing LRSM coefficients of all pertinent parameters at three production stages, in SFVW-Set 15 with Kmr=10, DP=100 psi & ST=20 days, Long Fracture.

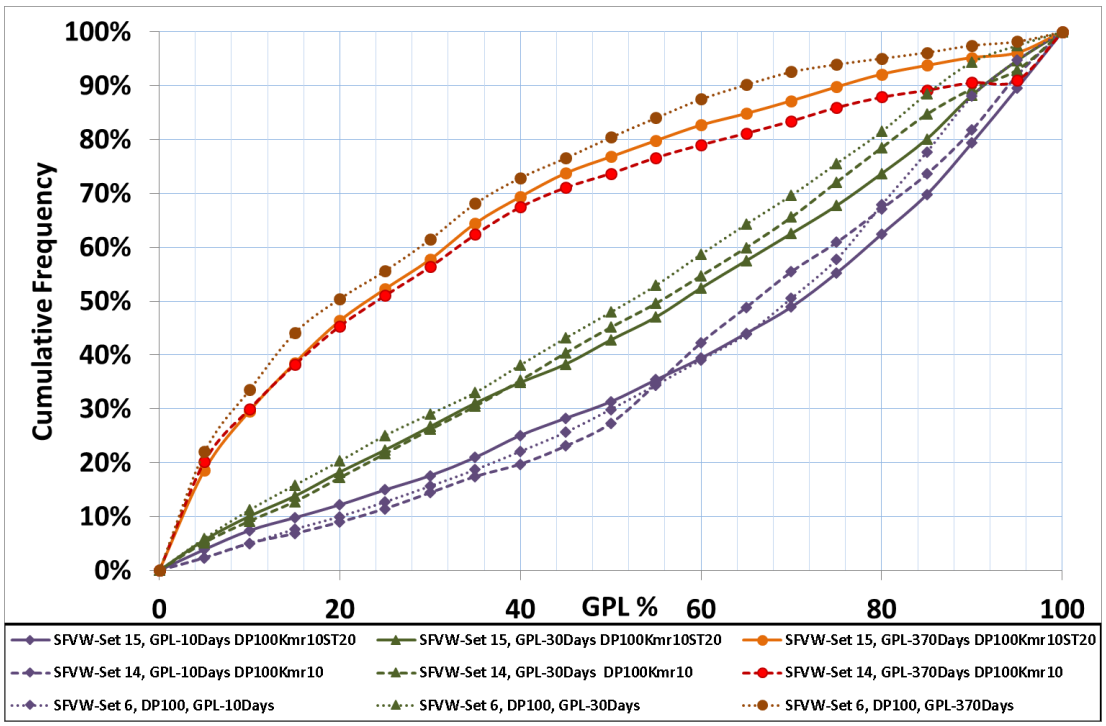

Figure 3.35 Histogram chart comparing cumulative frequency of SFVW-Set 6, 14 and 15 with DP=100, Kmr=10 & DP=100 and Kmr=10, DP=100 psi & ST=20 respectively at three production periods

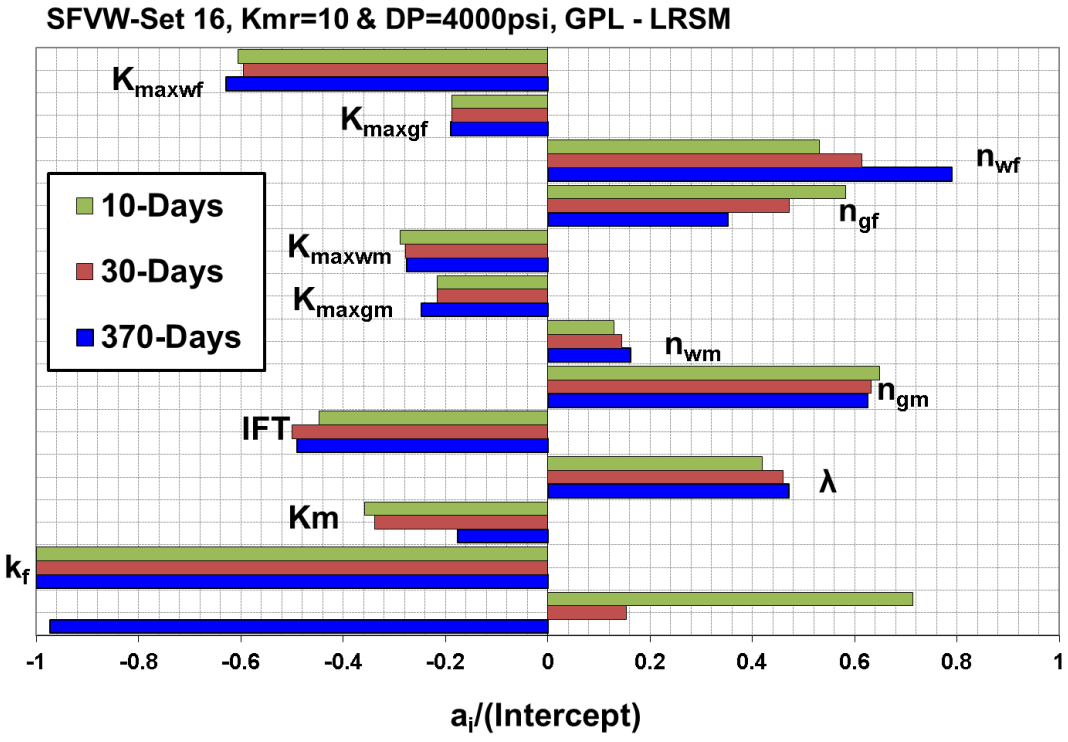

Figure 3.36 Tornado chart comparing LRSM coefficients of all pertinent parameters at three production stages, in SFVW-Set 16 with Kmr=10 & DP=4000, Long Fracture.

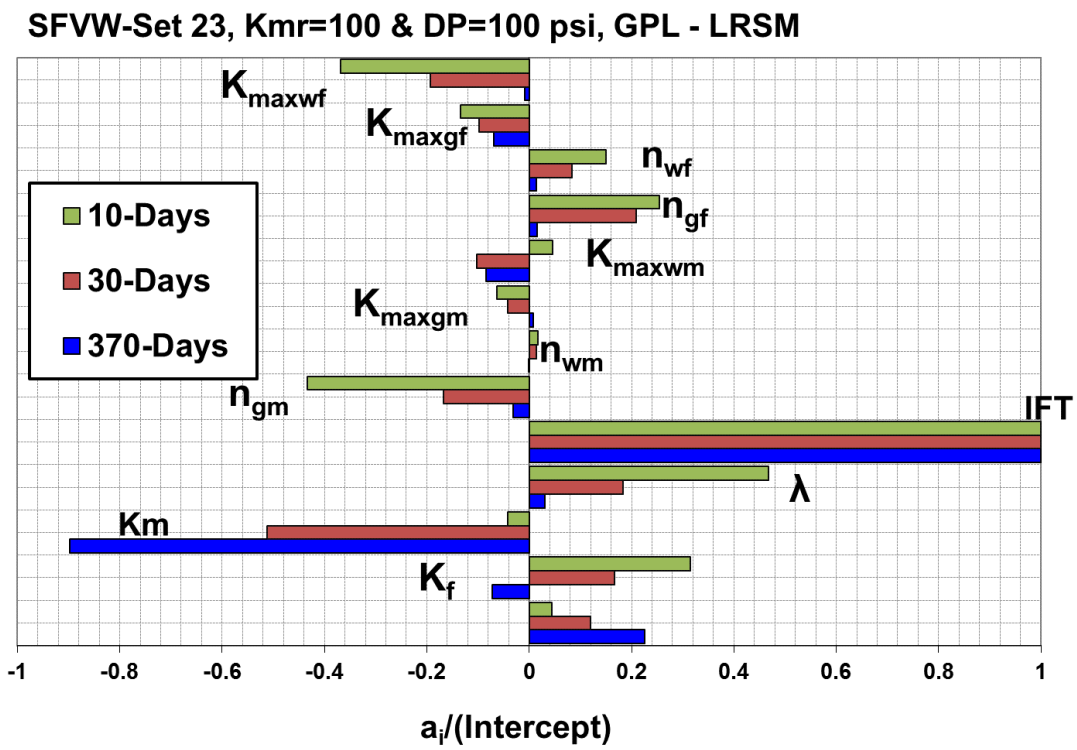

Figure 3.37 Tornado chart comparing LRSM coefficients of all pertinent parameters at three production stages, in SFVW-Set 23 with Kmr=100 & DP=100, Long Fracture.

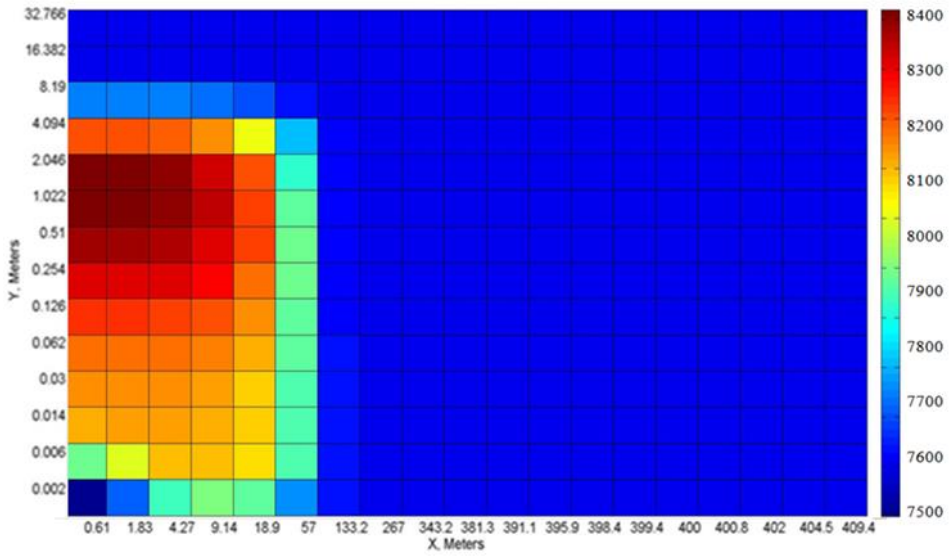

Figure 3.38 Pressure distribution Map at the End of Soaking time for SFVW-Set 23.

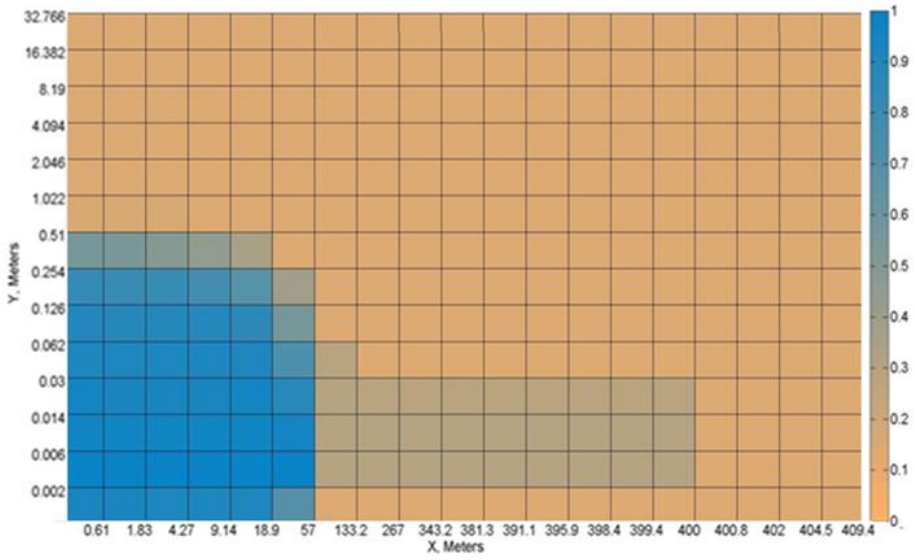

Figure 3.39 FF Saturation distribution Map at the End of Soaking time for SFVW-Set 23.

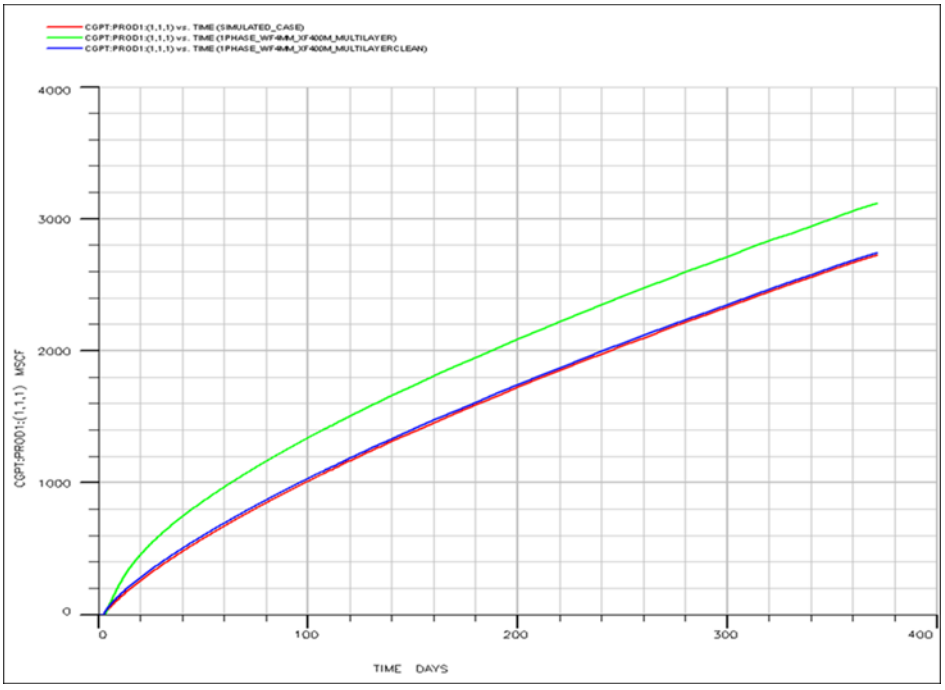

Figure 3.40 GPT (total cumulative gas production) plot for the three cases, clean, unclean and clean with unclean saturation map

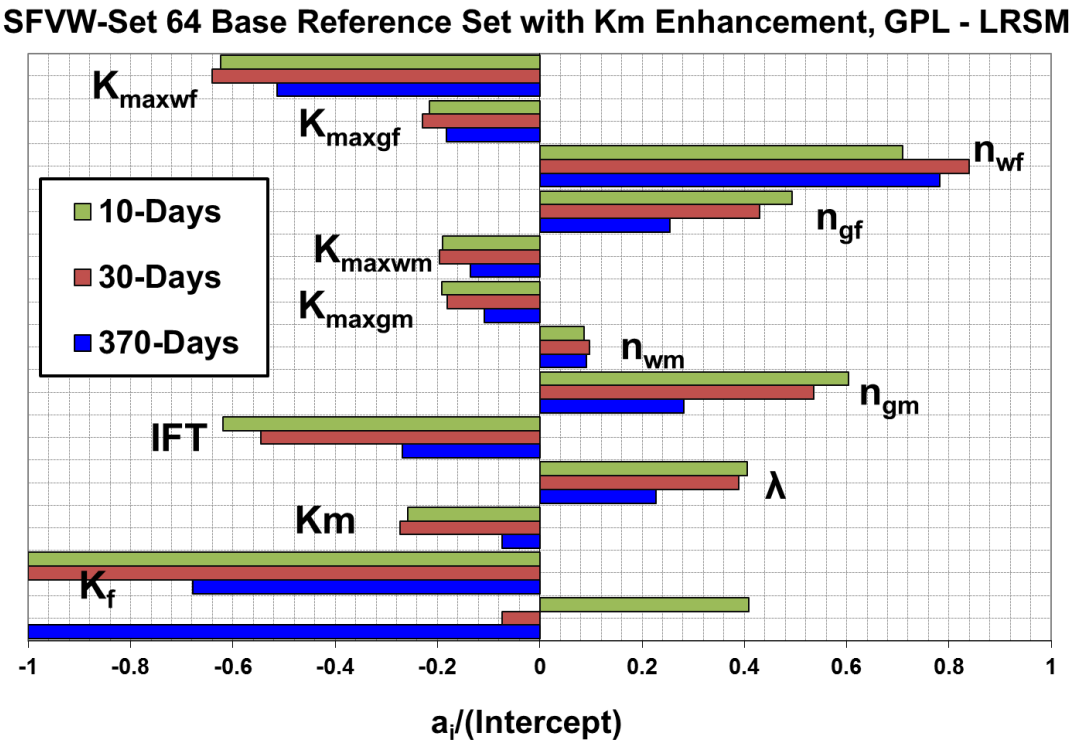

Figure 3.41 Tornado chart comparing LRSM coefficients of all pertinent parameters at three production stages, in SFVW-Set 64 base reference set with K enhancement, Long Fracture.

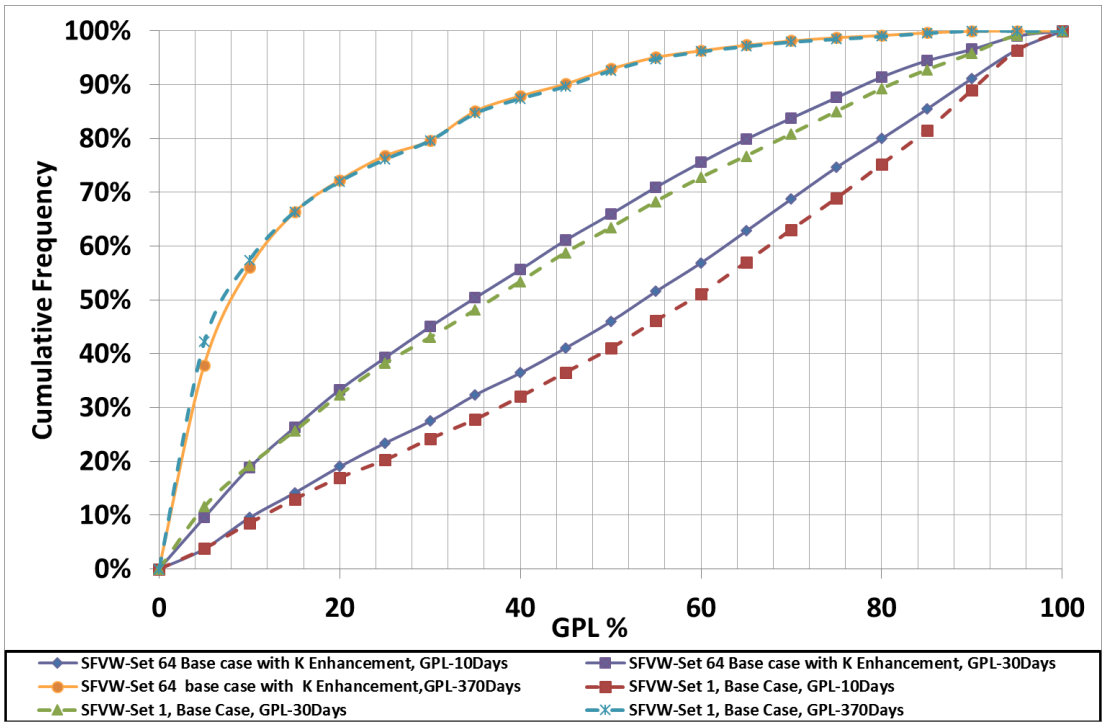

Figure 3.42 Histogram chart comparing cumulative frequency of SFVW-Set 64 and 1 with the only difference being inclusion of K enhancement in SFVW-Set 64 at three production periods

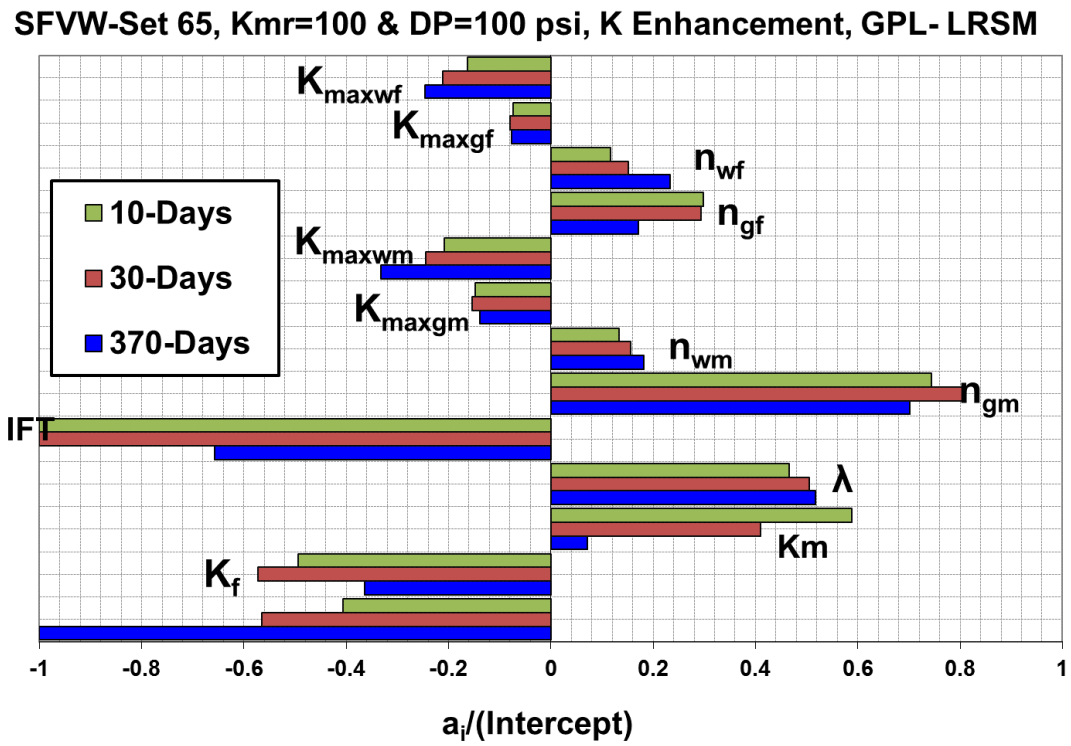

Figure 3.43 Tornado chart comparing LRSM coefficients of all pertinent parameters at three production stages, in SFVW-Set 65 (Kmr=100 & DP=100 psi) with K enhancement, Long Fracture.

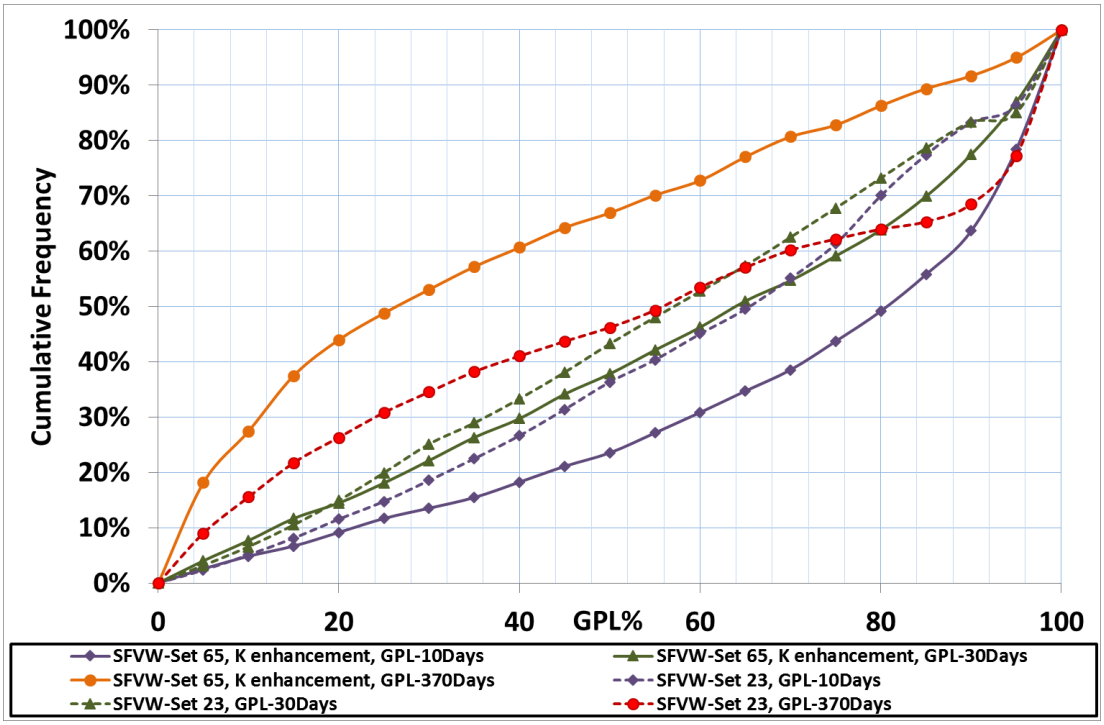

Figure 3.44 Histogram chart comparing cumulative frequency of SFVW-Set 65 and 23 with the only difference being inclusion of K enhancement in SFVW-Set 65 at three production periods

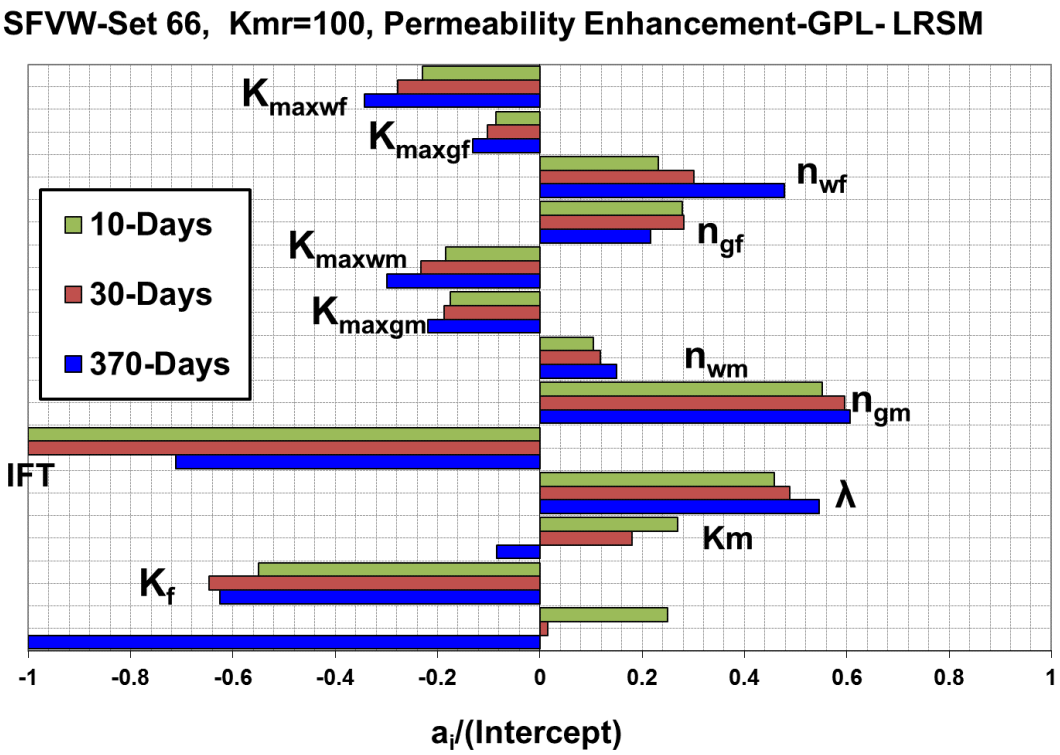

Figure 3.45 Tornado chart comparing LRSM coefficients of all pertinent parameters at three production stages, in SFVW-Set 66 (Kmr=100) with K enhancement, Long Fracture.

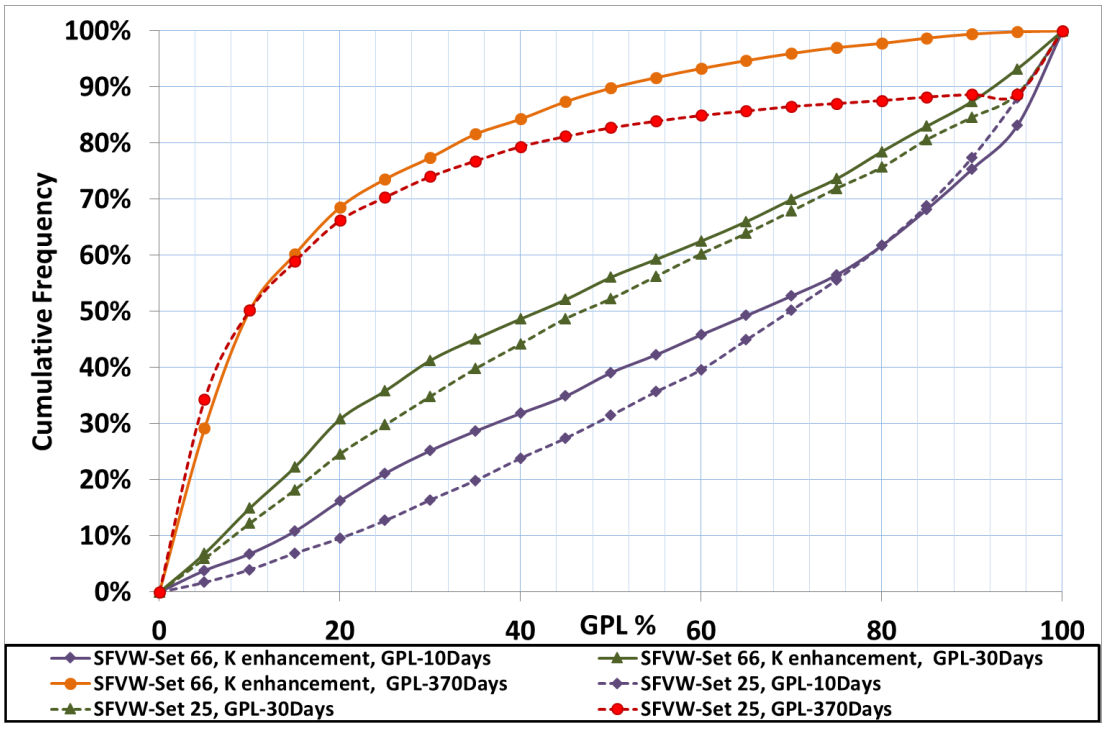

Figure 3.46 Histogram chart comparing cumulative frequency of SFVW-Set 66 and 25 with the only difference being inclusion of K enhancement in SFVW-Set 66 at three production periods

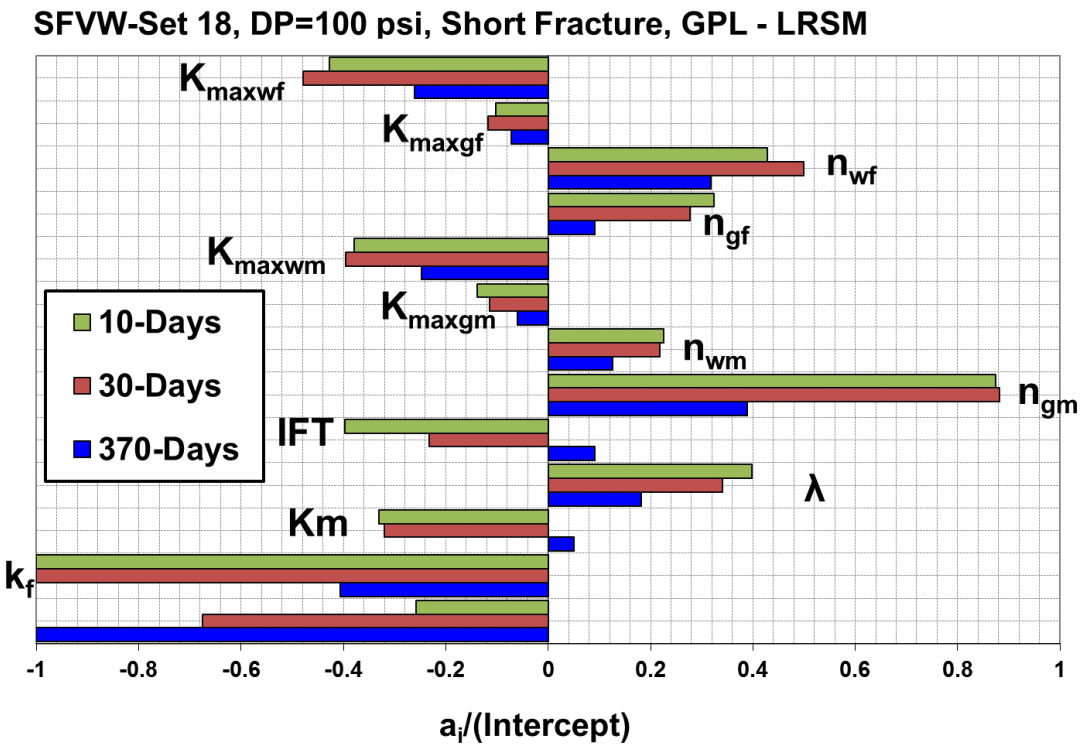

Figure 3.47 Tornado chart comparing LRSM coefficients of all pertinent parameters at three production stages, in SFVW-Set 18 (DP=100 psi), Short Fracture

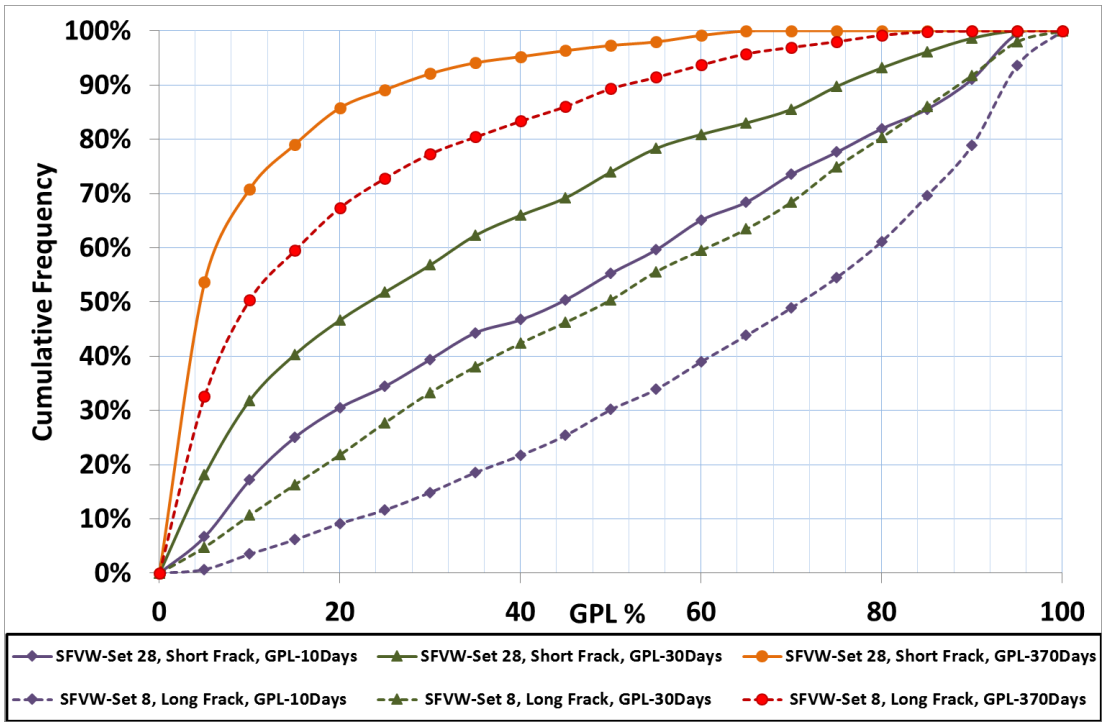

Figure 3.48 Histogram chart comparing cumulative frequency of SFVW-Set 28 and 8 with the only difference being a shorter fracture in SFVW-Set 28 at three production periods

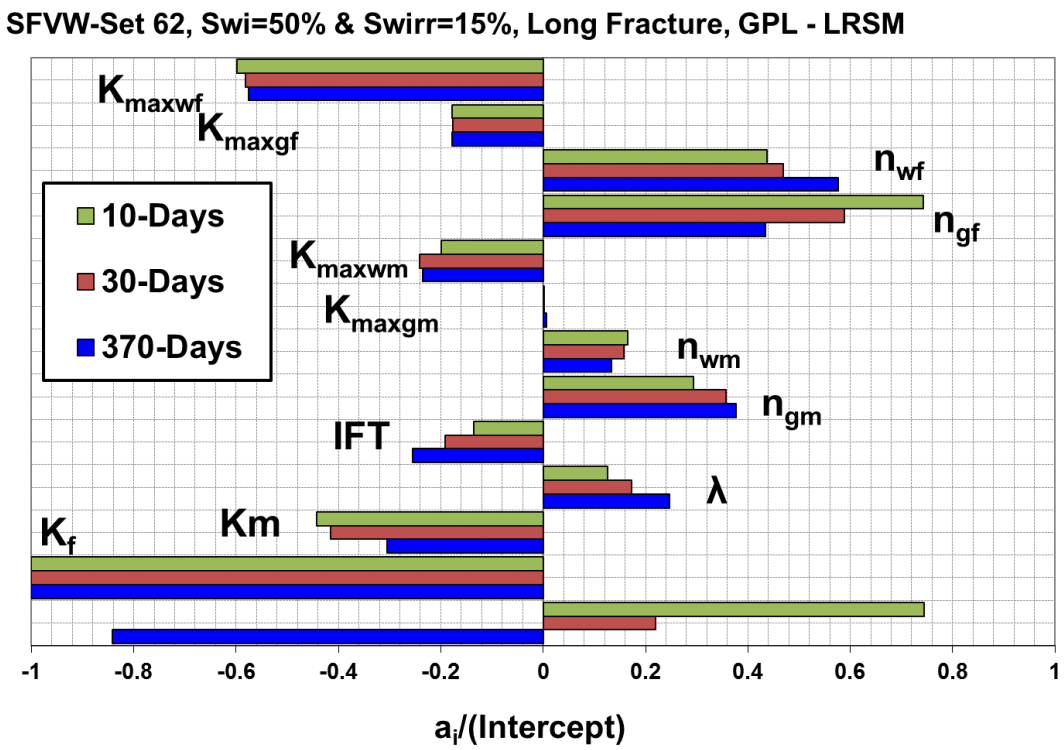

Figure 3.49 Tornado chart comparing LRSM coefficients of all pertinent parameters at three production stages, in SFVW-Set 62 (Swi=50% & Swirr=15%), Long Fracture

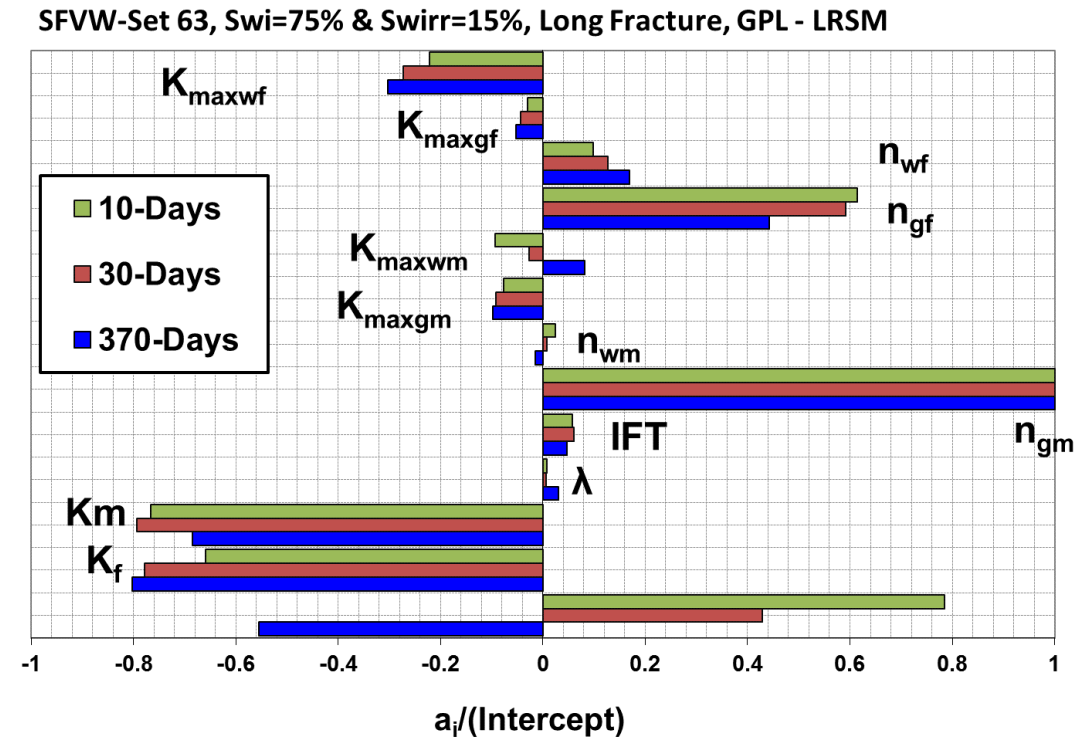

Figure 3.50 Tornado chart comparing LRSM coefficients of all pertinent parameters at three production stages, in SFVW-Set 63 (Swi=75% & Swirr=15%), Long Fracture

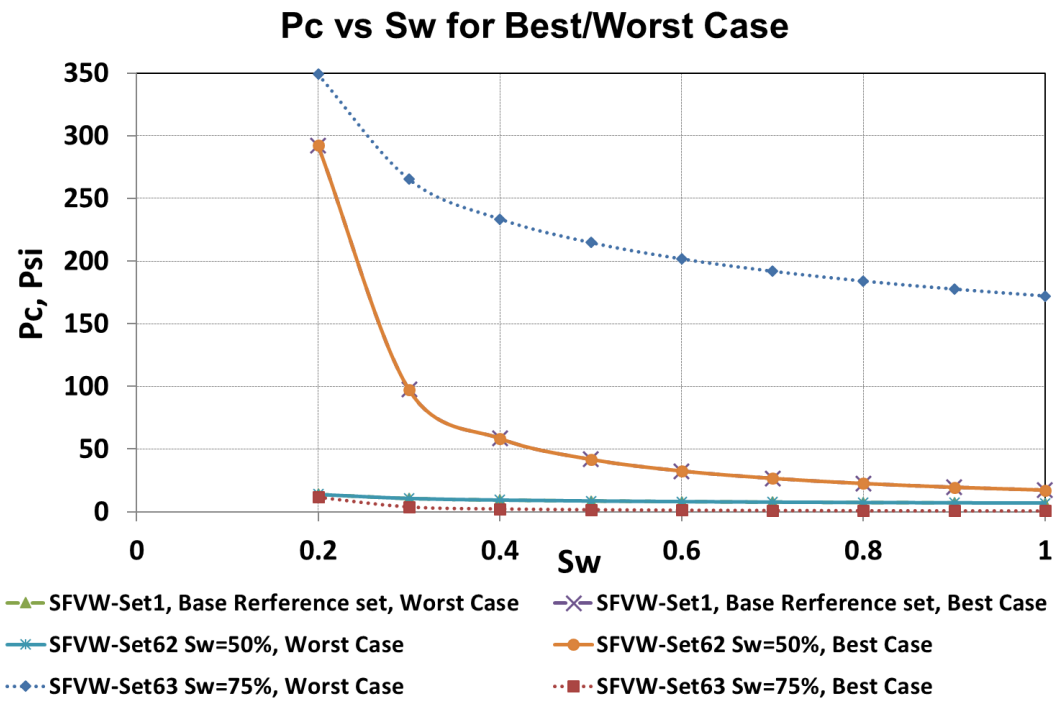

Figure 3.51 Capillary pressure curves for Best/Worst case Base reference set, SFVW-Set 1, Long SFVW-Set 62, Sw=50%, and Long SFVW-Set 63, Sw=75%,

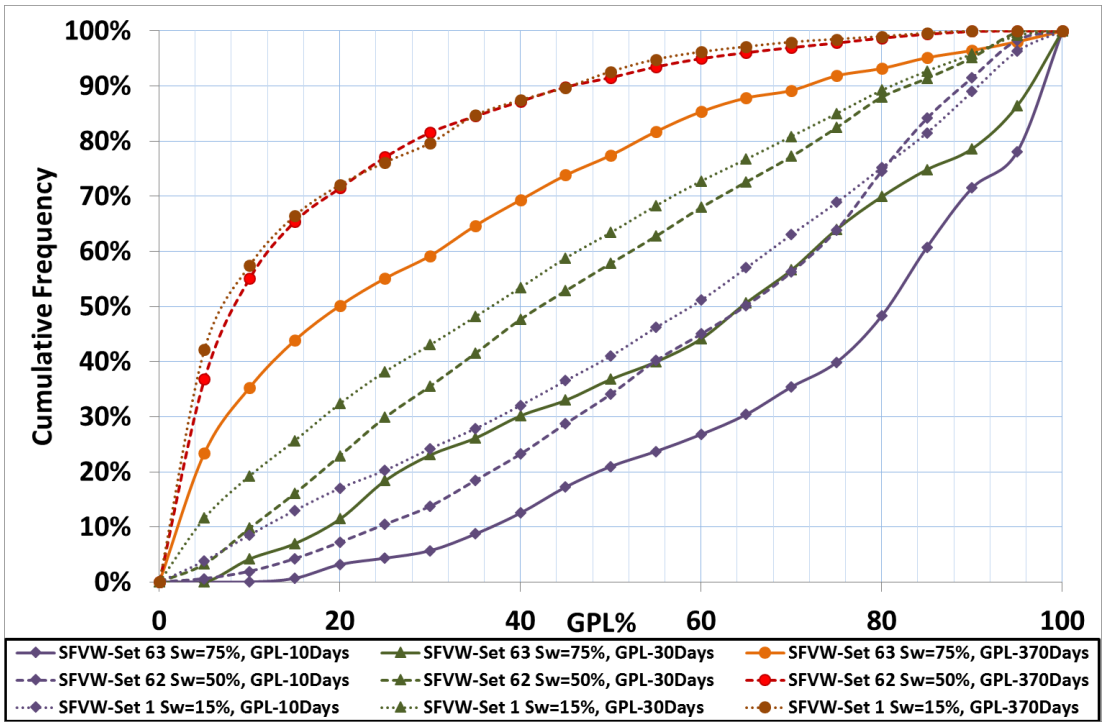

Figure 3.52 Histogram chart comparing GPL cumulative frequency of the Base reference set, SFVW-Set 1, SFVW-Sw=50%, Set 62 and SFVW-Sw=75%, Set 63.

CHAPTER 4 CLEANUP EFFICIENCY OF MULTIPLE FRACTURED HORIZONTAL WELL MODEL, MFHW

Tight and ultra-tight formations are described by extremely low permeability, low porosity and complex pores. Traditional fracturing technology of Single fracture vertical wells (SFVWs) in extremely tight and ultra-tight formations cannot result in effective and economic production. Successful development of such unconventional gas resources has proven that using the multiple fractured horizontal wells (MFHW) is an effective/economic way for the production of natural gas from tight and ultra-tight formations economically. In other words, MFHWs are essential in tight and ultra-tight formations to increase the gas production effectively and to achieve economical production, therefore, MFHWs are extensively applied in the development of unconventional gas formations.

In this chapter, following the promising results of the work conducted on the cleanup efficiency of SFVWs, the line of research is extended to MFHWs. Similar to the work conducted on SFVWs, in these MFHW-Sets, twelve pertinent parameters related to fracture and matrix relative permeability and matrix capillary pressure have been varied. Additionally, the impact of shut-in time, matrix permeability range, applied drawdown pressure, injected FF volume, fracture spacing and horizontal well length have been investigated by running different sets. Gas production loss (GPL), as the response term, has been calculated and input into a response surface statistical model. In each MFHW-Set, the correlation between parameters and GPL has then been established and compared with a base reference set and other similar sets but with one different variable. It should be noted that in this chapter the same Pc and Kr as those ones for SFVWs are used whereas in the next chapter unconventional Pc and Kr are considered, this was done to study the impact of pertinent parameters in a stepwise manner.

Since MFHW-Sets require significantly more CPU time than the vertical fractured well model and in order to reduce the CPU time and to ensure achieving more accurate predictions for GPLs, instead of the two-level full factorial sampling (FFS) used in the first 22 MFHW-Sets, the Latin hypercube sampling (LHS) method has been used in the last 7 MFHW-Sets.

It should be noted that the response surface model fitted to results based on the full factorial is linear whereas that fitted based on LHS could be either linear or quadratic, which increases the accuracy of the fitted response surface models. For these simulations

designed by LHS, the Multiple Realization Optimizer (MEPO) software has been used to automatically link different stages of the simulations conducted using ECLIPSE100 and to perform pre and post-processing stages. MEPO is a suitable software to design, perform and post-process many simulation runs in different simulation engines. It allows the user to choose different sampling approaches including Latin Hypercube and full factorial design. MEPO utilises a robust run management and enables the user to attain faster results more easily. It should be noted that the pre and post-processing stages are performed in MEPO using Python scripts, hence a new computer code has been developed using the Python Programming Language (Python Software Foundation, 2013), which generates different include-files for each simulation case. 7 MFHW base reference sets with different run numbers have been conducted and analysed to obtain the minimum (optimum) number of runs required for this new approach.

4.1 Multiple Fractured Horizontal Wells, MFHW

For the case of MFHW, a new model was set-up with three fractures placed on the 600 m horizontal well length. Fracture half-length was 90 m rather than 400 m corresponding to the VW reference set. The local grid refinement, LGR, (rather than global refinement) was used around fractures to capture the variation of flow parameters in this area whilst not increasing the CPU time significantly. Table 4.1 shows fracture properties and reservoir dimensions for the reference model used for MFHW. The fluid properties and the reservoir and fracture parameters and the variation range of all 12 parameters were similar to those of the SFVW-Sets as shown in Table 3.2 and Table 3.3. The MATLAB code (The MathWorks, 2013) that links different stages of the simulation had to be modified to handle the difference in the flow geometry The MATLAB code is included in Appendix 7.3. On the other hand, a new Python code was developed for those sets using LHS method.

4.1.1 Validation of the developed Model of Multiple Fractured Horizontal Well

To validate the model developed for MFHW cleanup operation, the same approach, as that of SFVW which was explained in Section 3.2.1, was conducted. The predicted bottom hole pressures from the reservoir simulation outputs were compared with analytical models. It should be noted that cleanup period is shorter that the early time flow period i.e., transient period, since the early linear flow regime period (i.e., 60 months according to Equation 3.4) is longer that the maximum cleanup period (1 year) which was

studied in this thesis. Therefore, the early linear flow equation (Equation 3.2) was used as analytical model.

In this section, to validate the model developed for MFHW cleanup operation and in order to give confidence that the model is consistent, the predicted bottom hole pressures from the reservoir simulation outputs were compared with analytical models.

Figure 4.1 shows the predicated bottom hole pressure by simulation model and also the predicated bottom hole pressure by analytical model (Equation 3.2) versus production time, it should be noted that both graphs are overlapping and almost on top of one another which confirms the accuracy of the developed model. Figure 4.2 shows the predicated bottom hole pressure by analytical model (Equation 3.2) versus the one of simulation model where satisfactory R^2 of 0.9978 is noted.

4.2 MFHW-Sets Analysed

In this chapter, the results of a total of 29 different sets for MFHW-Sets have been analysed. The results have been compared with those of a base reference set and other similar sets as well as SFVW-Sets. These models have the same reservoir dimensions as those of the MFHW reference set but differ in the fracture fluid injection volume (FVR), shut-in time period (ST), matrix permeability variation range (Kmr), pressure drawdown (DP), fracture spacing and horizontal length. The MFHW sets that have been considered in this chapter are listed in Table 4.2 first for reference and convenience.

For MFHW simulation sets, there is a Base Reference set with parameters in the ranges indicated in Table 4.2 as default values. The other sets are cited based on the differences of the parameters variation range from the Base Reference set, i.e., in each MFHW-Set, any parameter that has a tick mark has the default values otherwise the parameter's value is stated in the table. It should be noted that the parameters variation range of IFT, ngm, nwm, Kmaxgm, Kmaxwm, ngf, nwf, Kmaxgf and Kmaxwf are not listed in Table 4.2 since they are similar to those of Table 3.3 and Table 3.4.

For these MFHW simulation sets, there is a base reference set with parameters in the ranges indicated in Table 3.3. The other sets are cited based on the differences of the parameters variation range from the Base Reference set.

4.3 Multiple Fractured Horizontal Well, MFHW-Set 1, Base Reference Set

In this part the clean-up of the MFHW base reference set is discussed. As mentioned above, a new model was set-up with three 90 m fractures placed on the 600 m horizontal well length. Initially, to verify the new MFHW model, its results were compared with those of the corresponding SFVW base reference set.

To achieve this in addition to the MFHW, the corresponding tornado charts have been compared with that of the previously reported SFVW base reference set (having one fracture with Xf=400 m).

Comparing the tornado charts of the SFVW-Set 1 (Figure 3.12) and MFHW base reference sets (Figure 4.3), it is noted that the direction of impact of parameters is similar except for Km. That is, in the MFHW base reference set the effect of Km on Pc is more dominant than that on fluid flow whilst the reverse is observed for the SFVW base reference set. The SFVW and MFHW are different in two ways. First the number and volume of fractures and second the position of a fracture with respect to the well resulting in different flow geometries.

In order to identify which of these two resulted in this trend change, a new vertical well base reference model (with well competed in the Y-direction, Y-VW) was set-up. That is, this model is similar to the base reference SFVW set up (the same fracture volume) but with the well completed in the Y-direction (rather than Z-direction used for the SFVW base reference set, (Figure 4.4) to mimic similar well trajectory as that of MFHW.

Comparing tornado charts of the SFVW-Set 1 (Figure 3.12) and Y Direction-SFVW base reference sets (Figure 4.5), it is noted that the K_m trend in the Y-SFVW case, with the well completed in the Y-direction, is different from that of the SFVW Base Reference Set (the well was completed in the Z direction) confirming that the trend change is due to the flow geometry change and how the well is completed. It should be noted that in the Y-SFVW set the area perpendicular to flow at the wellbore is $2\pi r_w.w_f$, which is much less than that, i.e. $H*w_f$, for the Z-direction VW base reference set, Figure 4.4. In other words, the connection area between fracture and well is significantly restricted in the Y Direction-SFVW case. Hence for the Y-SFVW set, the effect of flow from the matrix towards fracture during the backflow clean-up is less important and rather imbibition of fracture fluid governed by matrix capillary pressure, which depends on K_m, is more important.

In literature, a similar observation was captured when productivity index of different completion was studied. Economides and Martin (2010) investigated the productivity index of different completions, i.e., horizontal transverse, horizontal longitudinal and vertical fractured completions. They referred to the negative effect of the restricted connection area of fracture and well as the near well bore choking effect. They mentioned that the near well bore choking effect is caused by the very limited area of contact between fracture and wellbore and it can seriously affect the productivity of gas wells.

Looking at the results of GPL and the gas to FF flow rate ratio vs. numbers of run confirms that due to a smaller flow area for the Y-direction VW set, there is more GPL whilst there is more gas production for the Z-direction VW set at the same FF production rate (Figure 4.6 and Figure 4.7).

Figure 4.8 is the histogram chart that compares the GPL cumulative frequency of the runs in MFHW-Sets 1 and SFVW-Set 1. Faster clean-up is observed for the MFHW base reference set compared to the SFVW base reference set, this is due to the higher production rate of the MFHW resulting in a faster and more efficient clean-up, i.e. number of cases with smaller GPL are more for the MFHW set. This trend was observed for almost all MFHW sets presented in this report.

In Figure 4.8, it is also noted that at GPL values larger than 60%, the corresponding cumulative frequencies are almost the same for both sets, i.e. the cumulative frequency of cases with GPL > or = 60% for these two sets is equal.

4.4 Increased FVR MFHW-Set 2

In MFHW-Set 2, the fracture volume ratio has been increased from 2 in the MFHW base reference set to 5. Comparing the tornado chart of MFHW-Set 2, Figure 4.9a, with that of MFHW-Set 1 (FVR=2) with the only difference being a higher FVR for MFHW-Set 2, Figure 4.5, it is noted that the observed trends are more or less the same.

The fracture permeability in both cases has the most significant impact on GPL and the sequences of the importance of other parameters are somewhat similar. If this high FVR MFHW set is compared with the relevant set in vertical well sets, i.e., SFVW-Set 9, the same trend is observed for all parameters except for K_m, which has been discussed earlier (Figure 4.9a and Figure 4.9b). It is also noted that Pc pertinent parameters are more important in the MFHW set whilst end points and exponents of Corey type relative permeability curves for gas and FF in the matrix and fracture are more important in the SFVW set. These observations are due to the fact that FF production has a more

detrimental effect on gas production in the MFHW set due to smaller area perpendicular to flow at the wellbore (also known as near well bore choking effect). Hence for the MFHW set the effect of flow from the matrix towards fracture during the backflow clean-up is less important and rather imbibition of fracture fluid governed by matrix capillary pressure, which depends on Km is more important. This trend was observed for all MFHW sets presented in this exercise.

Figure 4.10 is the histogram chart that compares the GPL cumulative frequency of the runs in MFHW -Sets 2 (MFHW with FVR=5) and MFHW base reference set. Similar to what was reported previously (Chapter 3) for the VW sets, faster clean-up is observed for the MFHW base reference set compared to the MFHW FVR=5. This is due to less FF injected in the MFHW base reference set, which requires less time to clean.

4.5 Extended ST MFHW-Set 3

In MFHW-Set 3, the shut-in time has been extended from 2 days in the MFHW base reference set to 20 days. Comparing the tornado chart of MFHW-Set 3 (ST=20) with that MFHW-Set 1 (ST=2) with the only difference being a longer soaking time for MFHW-Set 3, shows the same observation that was noted in chapter 3 for VW sets, i.e., the observed magnitude and trends of all pertinent parameters are more or less the same. However, the absolute value of Pc Pertinent parameters, i.e. IFT and λ, are larger than those of MFHW-Set 1, confirming the observation reported for the VW sets that extending soaking time makes the effect of Pc on GPL to be more important (Chapter 3).

The histogram chart that compares the GPL cumulative frequency of the runs in MFHW-Set 3 (MFHW with ST=20 days) and MFHW-Set 1 (MFHW base reference set), shows that faster clean-up is observed for the extended ST MFHW set compared to the MFHW base reference set but only at early production time, the same observation as the one noted for SFVWs.

4.6 Tighter Formations by a Factor of 10 and 100 MFHW-Sets 4 & 7

In this section, the range of matrix permeability variation has been lowered from 1 μD-100 μD in the MFHW base reference set to 0.1 μD-10 μD and 0.01 μD-1 μD in MFHW-Sets 4 & 7 respectively.

Comparing the tornado charts of MFHW-Set 4 (Kmr=10), Figure 4.11 with that of MFHW-Set 1 (Kmr=1) with the only difference being tighter formations by a factor of

10 for MFHW-Sets 4, Figure 4.3, it is noted that the observed trends are the same except for the Km coefficient. That is, in this MFHW-Set with the tighter formation, the first effect of Km on GPL (i.e. an increase in Km that improves fluid mobility and reduces GPL) is dominant whilst in MFHW-Set 1 the second effect (i.e. an increase in Km that reduces Pc and increases GPL) was dominant. Since in this tighter set, i.e., MFHW-Set 4, the matrix permeability range has been reduced by a factor of 10, Pc is already high enough and hence the effect of km on mobility is more important.

If MFHW-Set 4 is compared with the corresponding VW set, SFVW-Set 4, the same observation as that highlighted in previous sets, is noted.

Comparing the tornado chart of MFHW-Set 7 (Kmr=100), Figure 4.12, with that of MFHW-Set 1 (Kmr=1) with the only difference being a tighter formation by a factor of 100 for MFHW-Set 1, Figure 4.3, it is noted that the observed trends are the same except for the Km and IFT coefficients. In this very tight formation the first effect of Km on GPL (i.e. an increase in Km that improves fluid mobility and reduces GPL) is dominant whilst in MFHW-Set 1 the second effect (i.e. an increase in Km that reduces Pc and increases GPL) is dominant, i.e. the same observation as that in MFHW-Set 4 with Km variation range reduced by a factor of 10. Since in the current MFHW-Set 7, the matrix permeability range has been reduced substantially by a factor of 100, fluid mobility in the matrix is significantly difficult, hence the effect of km on mobility is more important. Figure 4.12 shows that the value of the Km coefficient is almost -1 at all production periods (in MFHW-Set 4, Figure 4.11, the value of Km was almost -0.1) indicating that as the formation gets tighter the first effect of Km on GPL is most pronounced.

It is noted that in MFHW-Sets 7, the IFT coefficient trend changes as production time increases, this highlights that using IFT reducing agent could improve the cleanup efficiency. This observation will be discussed in details in Section 4.10.

Considering the histogram charts that compare the GPL cumulative frequency of the runs in MFHW-Set 4 & 7 (MFHW with Kmr=10 &100) and MFHW-Set 1 (MFHW base reference set) shows the same observation similar to what was reported previously for the VW sets (Chapter 3), i.e., slower clean-up is observed for the tighter formation compared to the MFHW base reference set.

4.7 MFHW-Sets with reduced/increased DP (DP=100 and 4000 psi)

In this section, DP has been changed from 1000 psi in the MFHW base reference set to 100 and 4000 psi in MFHW-Sets 5 & 6 respectively.

Comparing the tornado chart of MFHW-Set 5 (DP=100), Figure 4.13, with that of MFHW-Set 1 (DP=1000) with the only difference being a lower DP by a factor of 10 for MFHW-Set 5, Figure 4.3, it is noted that the observed trends of pertinent parameters are the same with the exception of an increase in the absolute value of Pc pertinent parameters. This is in line with what was reported previously for low DP VW sets, i.e., in low DP sets the effect of Pc on GPL is more pronounced (Chapter 3).

In MFHW-Set 5, the impact of the end points and exponents of Corey type relative permeability curves for gas and FF in the matrix is more pronounced than that of these parameters in MFHW-Set 1 confirming the observation noted in the corresponding VW sets. That is, in low DP sets, it is more important how fluid (Gas and FF) flows from the matrix to fracture than how it flows from fracture to the wellbore. Figure 4.13 shows a small value for the Km coefficient of 10 days indicating that at this period the effect of Km on GPL is small but because it is negative, it can be concluded that the first effect of Km on GPL is dominant.

In MFHW-Set 6, DP has been increased from 1000 psi in the MFHW base reference set to 4000 psi.

Comparing the tornado chart of MFHW-Set 6 (DP=4000), Figure 4.14, with that of MFHW-Set 1 (DP=1000) with the only difference being a higher DP by a factor of 4 for MFHW-Set 6, Figure 4.3, it is noted that the observed trends of pertinent parameters are more or less similar with the exception of a decrease in the absolute value of Pc pertinent parameters. This is in line with what was reported previously for high DP VW sets, i.e., in high DP sets the effect of Pc on GPL is less pronounced. (Chapter3)

The impact of the end points and exponents of Corey type relative permeability curves for gas and FF in the matrix is less pronounced than that of these parameters in MFHW-Set 1 confirming the observation noted in the VW sets, that is, in high DP sets it is less important how fluid (Gas and FF) flows from the matrix to fracture than how it flows from fracture to the wellbore. This follows the same trend as what was observed above for the low DP set, MFHW DP=100 (MFHW-Set 5).

Figure 4.15 is the histogram chart that compares the GPL cumulative frequency of the runs in MFHW-Set 5 with DP=100 psi, MFHW base reference set with DP=1000psi and MFHW-Set 6 with DP=4000psi. Slower/faster clean-up is observed for this lower/higher DP set compared to the MFHW base reference set.

4.8 Impact of Hydraulic Fractures Interference on Clean-up Performance

In this section, the number of fractures is increased from three in MFHW-Set 1 to seven, nine and thirteen fractures on the same horizontal length in MFHW-Set 8, MFHW-Set 12 and MFHW-Set 13 respectively. In these sets, new models were set-up with seven, nine and thirteen 90 m fractures placed on the 600 m horizontal well length and the MATLAB code was changed accordingly. By doing this, the fracture spacing has been decreased from 300 in MFHW-Set 1 to 100, 75 and 50 m in MFHW-Set8 (MFHW Nf7 L600 Base Reference set), MFHW-Set12 (MFHW Nf9 L600 Base Reference set) and MFHW-Set13 (MFHW Nf13 L600 Base Reference set) respectively. The aim of running these MFHW-Sets with different fracture spacing was to observe the clean-up efficiency of MFHWs when the number of fractures (fracture spacing) is increased (decreased) on the same horizontal length.

Comparing the tornado chart of MFHW-Set1 (Figure 4.3) and the other MFHW base reference sets with different Nfs, MFHW Nf7 L600 base reference sets (Figure 4.16), MFHW Nf9 L600 base reference sets (Figure 4.17) and MFHW Nf13 L600 base reference sets (Figure 4.18), it is noted that the direction and magnitude of impact of all parameters are almost similar including that of Km. The same observations as the one reported for the MFHW Nf3 L600 base reference set (MFHW-Set 1) are observed for these sets. That is, in these MFHW base reference sets with different Nfs, the effect of Km on Pc is still more dominant than that on fluid flow whilst the reverse is observed for VW. As mentioned earlier, this trend change is due to the flow geometry change. Similar tornado charts for these MFHW-Sets with different fracture spacing shows that the change in fracture spacing does not affect the cleanup efficiency of MFHWs.

It should be noted that due to introducing several fractures to the model from three to 13 fractures on the same horizontal length and to remove the issues associated with convergence errors during simulation, smaller time steps were used in this set. In order to verify that this time step change does not affect our results and corresponding tornado charts, the set-up was run with old time steps and noted that the resulting tornado chart, Figure 4.19, is almost similar to Figure 4.18, confirming the integrity of our modelling approach.

Figure 4.20 is the histogram chart that compares the GPL cumulative frequency of the runs in sets, MFHW-Set1 (MFHW Nf3 L600), MFHW-Set8 (MFHW Nf7 L600), MFHW-Set12 (MFHW Nf9 L600) and MFHW-Set13 (MFHW Nf13 L600). It is noted that histogram charts for Nf=3 to 13 are almost the same. It should be noted that as one

increases Nf from 3 to 13 the clean-up is very slightly faster (except for Nf3, which is very slightly faster than Nf9) but generally very small differences are observed when changing Nf. This observation again reconfirms that the change in fracture spacing does not affect the cleanup efficiency of MFHWs.

These four MFHW sets (MFHW-Set1, MFHW-Set8, MFHW-Set12 and MFHW-Set13) with different fracture spacing (300, 100, 75 and 50 m all on the same 600m horizontal length) were investigated when the Km variation range was 1 μD-100 μD. The results indicated that Clean-up efficiency of MFHWs, when the number of fractures (fracture spacing) was increased (decreased) on the same horizontal length was almost the same. In other words, it could be concluded that the fracture interference did not affect the clean-up performance, when Km variation range was 1 μD-100 μD.

Here, the impact of fracture interference on clean-up performance of 3 new MFHW sets (MFHW-Set20, MFHW-Set21 and MFHW-Set22) with different fracture spacing (100, 75 and 50 m all on the same 600m horizontal length corresponding to 7, 9 and 13 fractures) was studied. In all these three sets, the Km variation range was increased by a factor of 100 (i.e., 100 μD-10000 μD) to increase the fracture interference and hence to observe its probable impact on clean-up.

Comparing the tornado charts of these three sets (Figure 4.21, Figure 4.22 and Figure 4.23), it is noted that the magnitude and direction of impact of all parameters are almost similar. That is, the same observation is made as the one presented in the previous four sets (MFHW-Set1, MFHW-Set8, MFHW-Set12 and MFHW-Set13) with Km variation range of 1 μD-100 μD.

Figure 4.24 is the histogram chart that compares the GPL cumulative frequency of the runs in sets MFHW-Set20, MFHW-Set21 and MFHW-Set22. It is noted that histogram charts for Nf=7 to 13 are the same and almost overlaying each other. This shows that although, as described below, the impact of fracture interference on flow is profound, its impact on clean-up performance is minimal. This is due to the fact that the injected FF is spreading within the fracture and matrix in the vicinity of fractures, just a few meters away from fracture i.e., at most 2-4 meters when FVR=10, which is much smaller than the fracture spacing.

Figure 4.25 which is from Chapter 5 of Gas Condensate Recovery Project Progress Report (Gas Condensate Recovery Project' Progress Report GCRP/15/1, Oct. 2014-Apr. 2015, April 2015, Heriot-Watt University, Institute of Petroleum Engineering, Chapter 5: Flow around MFHWs) highlights the effect of Nf and fracture spacing on productivity

index, PI. An increase in Nf generally results in an increase in PI, however, due to a higher degree of interference at shorter fracture spacing, the impact of increasing Nf on PI is not linear. Pressure distribution map in Figure 4.26, which corresponds to MFHW-Set22, confirms that pressure disturbance has been observed by adjacent fractures affecting flow performance.

Figure 4.27 shows the gas production rates of these 3 sets (MFHW-Set20, MFHW-Set21 and MFHW-Set22 with the corresponding Nf=100, 75 and 50 m) after 30 days of production for runs numbered between 3100 and 4000. The reason the runs were filtered was that gas production changes significantly from 1000 to 140000 MSCFD for all 4096 runs, which if included in one Figure would mask the Fracture spacing/Nf effect. It should be noted that the following observations were noted for all runs. Looking at the data of Figure 4.27, it is noted that:

- As Nf from 7 in MFHW-Set20 was increased to 9 and 13 in MFHW-Set21 and MFHW-Set22 respectively, gas production rate increases.
- If one considers any run number e.g., 3500, gas production rates are 106000, 118600 and 137800 MSCFD in MFHW-Set20, MFHW-Set21 and MFHW-Set22 with the corresponding Nf=100, 75 and 50 m. Gas production rates per Nf for these sets are 15142, 13178 and 10600 MSCFD per fracture in MFHW-Set20, MFHW-Set21 and MFHW-Set22 respectively. This confirms that fracture efficiency decreases when fracture spacing decreases and this is due to a higher degree of fracture interference for cases with the higher number of fractures. In other words, gas production rates have not been increased by the same factor as that of increasing the number of fractures due to a higher degree of fracture interference in MFHW-Set 22 compared to MFHW-set 20.

Following these results, the main conclusion of this section is that although the impact of fracture interference on flow is significant, its impact on clean-up performance is minimal.

4.9 MFHW-Sets with Different Horizontal Length

In order to observe the effect of horizontal well length on the clean up efficiency of MFHWs, when fracture spacing is the same, a new model was set-up with ten 90 m fractures placed on the 900 m horizontal well length. By doing this, the fracture spacing is the same as the one for MFHW-Set8 (MFHW Nf7 L600 Base Reference set) but with

longer horizontal length. That is, here there are ten fractures placed on the HW in this new MFHW-Set.

A comparison of the corresponding tornado chart, Figure 4.28 with the relevant tornado chart, Figure 4.16, of MFHW-Set 14, shows the same observation indicating that an increase in the horizontal well length while the fracture spacing is the same, does not change the fracture clean-up efficiency. Figure 4.29 is the histogram chart that compares the GPL cumulative frequency of the runs in MFHW-Set8 (MFHW Nf7 L600 and MFHW-Set14 (MFHW Nf10 L900). It is noted that histogram charts for these two sets are the same and overlap each other. This again shows that an increase in the horizontal well length while the fracture spacing is the same, does not change the fracture clean-up efficiency.

4.10 MFHW-Sets with Nf7 and L600m with different Km ranges

Following the IFT trend change which was observed in Section 4.6 for MFHW-Set 7 with the tightest formation range i.e., Kmr=100, three different MFHW-Sets (with Nf=7 rather than sets with Nf=3 discussed in section 4.6) with different Km ranges were studied. In this section, the range of matrix permeability variation was lowered from 1 μD-100 μD in the MFHW-Set8 Nf7 L600 base reference set to 0. 1 μD-10 μD and 0.01 μD-1 μD in MFHW-Set9 and MFHW-Set10, respectively.

Comparing the tornado chart of MFHW-Set 8 (Kmr=1), Figure 4.16, MFHW-Set9 (Kmr=10), Figure 4.30, and MFHW-Set10 (Kmr=100), Figure 4.31, it is noted that the observed trends of all parameters are more or less the same, including the trend of the Km coefficient. However, in MFHW-Set10, Km is the most important parameter at 30 and 370 days and second most important parameter after Kf at 10 days. That is, due to the fact that in the current set, MFHW-Set10, Km range has been reduced by a factor of 100, fluid mobility in the matrix is very important. If one compares the absolute values of Km, Kmaxwm, Kmaxwm, nwm and ngm in MFHW-Set8, MFHW-Set9 and MFHW-Set10, it is noted that fluid mobility in the matrix is more/most important in tighter/tightest formations (Kmr=10/ Kmr=100), i.e., the tighter the formation the more important the effect of fluid mobility on clean-up efficiency.

The other important observation in Figure 4.31, is the trend change in the IFT coefficient. That is, in this set, IFT has a positive value indicating that an increase in IFT increases GPL. However, it should be noted that IFT is not the only parameter affecting Pc, hence, it is important to see the effect of IFT, Km and λ all together to understand the

effect of Pc on clean-up efficiency in this section for these three MFHW-Sets. Capillary pressure of these three MFHW-Sets was calculated by selecting the corresponding values of IFT, Km and λ for best and worst cases from their relevant tornado charts and also using Equations 3.6 and 3.7. Table 4.3, which includes the calculated Pc data for these three MFHW-Sets, shows that in this set, MFHW-Set10, Pc of the worst case is much higher than the best case whilst in MFHW-Set8 and MFHW-Set9, Pc of the best case is higher than the worst case. This observation highlights that in MFHW-set 8 and MFHW-set-9, it is better to keep the FF in the matrix by having higher Pc, but in the tightest formation set, MFHW-Set10, it is best to backflow the FF out of the matrix. This is due to very tight nature of the formation (in MFHW-Set10) in which keeping the FF in the matrix has a more detrimental effect on production than its negative effect once it is produced through the fracture.

Figure 4.32 shows Pc versus water saturation, Sw, for those aforementioned sets (MFHW-Set8, MFHW-Set9 and MFHW-Set10). It is demonstrated that although higher Pc values were observed for best case than worst case at all Sw in Sets MFHW-Set8 and MFHW-Set9 (indicating that keeping FF in matrix is better and results in less GPL), higher Pc values were observed in MFHW-Set10 for worst case than best case at all Sw (it is best to backflow the FF out of the matrix). In other words, in MFHW-Set 10, unlike previous two sets, using chemicals (IFT reducing agents) to reduce Pc could reduce GPL.

According to results of these three sets (MFHW-Set 8, MFHW-Set 9 and MFHW-Set 10), matrix permeability plays an important role in hydraulic fracturing design. For those sets with matrix permeability variation 1 μD-100 μD and 0.1 μD-10 μD, using chemicals (IFT reducing agents) could increase GPL. In very tight sets with matrix permeability variation 0.01 μD-1 μD, it is recommended to use chemicals (IFT reducing agents) in order to reduce Pc and consequently reduce GPL.

All these runs were at moderate DP of 1000 psi. In order to confirm that this observation is also valid at low and high DP values, six new MFHW-Sets were conducted.

Three new sets (MFHW-Set15 Nf7-L600m DP4000, MFHW-Set17 Nf7-L600m Kmr10 DP4000 and MFHW-Set19 Nf7-L600m Kmr100 DP4000) is conducted to capture the effect of Km at high DP=4000 psi. In these sets, the range of Km variation is 1 μD-100 μD in MFHW-Set15, 0.1 μD-10 μD in MFHW-Set17 and 0.01 μD-1 μD MFHW-Set19 with DP=4000 psi in all of these sets.

A comparison of the tornado charts of these sets, Figure 4.33, Figure 4.34 and Figure 4.35, shows that Kf is the most important parameter affecting GPL for all three

sets at all production periods. Other fluid mobility parameters in the fracture (Kmaxwf, Kmaxwf, nwf and ngf) are the second most important set of parameters affecting GPL for MFHW-set15 and MFHW-set17 at all production periods and the third most important parameter for MFHW-set19. As the Km variation range is reduced by a factor of 10 and 100 in MFHW-set17 and MFHW-set19, the effect of Km and fluid mobility in the matrix become progressively more important. This is due to the fact that in tighter (tightest) formation, the fluid mobility inside the matrix becomes more (most) difficult.

Figure 4.35 shows that the trend of IFT has changed in MFHW-set19 compared to the other two sets. In order to fully understand the effect of Pc in these sets, the same approach as the one conducted for the three previous sets, i.e., MFHW-set8, 9 & 10, was followed by preparing the corresponding Pc values versus Sw for the best/worst scenarios, Figure 4.36. Data in this Figure confirms that for those sets with Kmr of 1 and 10, having higher Pc, corresponding to the best case scenario, is more favorable and using chemicals (IFT reducing agents) could increase GPL, whilst in the very tight set (Kmr=100) with higher Pc for the best case scenario, it is recommended to use chemicals (IFT reducing agents) in order to reduce Pc and consequently reduce GPL.

Following the results of the previous sets with moderate and high DP, here in MFHW-Sets 11, 16 and 18, DP was reduced to 100 psi. Here, the range of matrix permeability variation is 1 μD-100 μD in the MFHW-Set11, 0.1 μD-10 μD in MFHW-Set16 and 0.01 μD-1 μD MFHW-Set18 with DP=100 psi in all of these sets.

The tornado charts of these three low DP sets, i.e., Figure 4.37, Figure 4.38 and Figure 4.39, and their Pc plots versus Sw for the best/worst cases of these sets (Figure 4.40) show the same results as the ones observed in high and moderate DP.

Comparing the results of all 9 sets (MFHW-Set11, MFHW-Set16 and MFHW-Set18 with DP=100psi and MFHW-Set8, MFHW-Set9 and MFHW-Set10 with DP=1000psi and MFHW-Set15, MFHW-Set17 and MFHW-Set19 with DP=4000 psi) confirms that regardless of DP, for those MFHW sets with matrix permeability (Km) variation ranges of 1 μD-100 μD and 0.1 μD-10 μD, using chemicals (IFT reducing agents) could increase GPL whilst in very tight sets with the Km variation range of 0.01 μD-1 μD it is recommended to use chemicals (IFT reducing agents) in order to reduce Pc and consequently reduce GPL. In other words, it is best to retain FF in the matrix in sets with Km variation ranges of 1 μD-100 μD and 0.1 μD-10 μD. However, the positive effect of retaining FF in the matrix weakens in sets with the Km variation range of 0.1 μD-10 μD compared to the sets with the Km variation range of 1 μD-100 μD. In fact, in sets with

the Km variation range of 0.01 μD-1 μD this trend becomes opposite, i.e., it is best to backflow the FF.

If the tornado charts of the three low DP sets (Figure 4.37, Figure 4.38 and Figure 4.39) are compared with the relevant high DP sets (Figure 4.33, Figure 4.34 and Figure 4.35), it is noted that fluid mobility pertinent parameters (Kmaxgm, ngm, Kmaxwm and nwm) in the matrix are more important at low DP sets compared to the relevant ones in high DP sets, this is due to the fact that as DP decreases, fluid mobility in the matrix becomes more critical and consequently plays a more important role in the GPL reduction.

4.11 New MFHW sets Using a New Sampling approach, Latin hypercube sampling (LHS)

In previous sets, the full factorial linear experimental design was used to study the cleanup efficiency. Using FFS approach used to take a relatively long CPU time to conduct a large number of simulation runs (i.e. 4096 runs for each set). Introducing more complexity to the models made the CPU time even longer. In order to decrease the required number of runs and to reduce the CPU time, Latin Hypercube Sampling (LHS) method was used. It should be highlighted that the RSM fitted to results based on the FFS is linear whereas that fitted based on LHS could be either linear or quadratic, which increases the accuracy of the fitted RSMs. For these simulations, the Multiple Realization Optimizer (MEPO) software has been used to automatically link different stages of the simulations conducted using ECLIPSE100 and to perform pre and post-processing stages. MEPO (Schlumberger, 2013) is a proper software to design, perform and post-process many simulation runs in different simulation engines. MEPO utilises a powerful run management and provides faster results more easily. MEPO utilises Python script to perform the pre and post-processing stages, hence a new computer code was developed using the Python Programming Language (Python Software Foundation, 2013). The developed Python script creates different include-files for each simulation run. The new Python code is included in Appendix 7.4. 7 MFHW Nf7 L600m base reference sets with different run numbers were conducted and analysed to obtain the minimum (optimum) number of runs required for the LHS approach.

The results of this new approach with different run numbers of LHS MFHWs with the original MFHW base reference set have been compared and discussed. The discussion indicates that by using LHS, reduction of run numbers retained the main trends in tornado charts whilst reducing CPU time. It also ensures achieving more accurate predictions for

GPLs using both fitted linear and quadratic response methods. Finally, a different number of runs has been compared to obtain the minimum number of runs with a reasonable error.

4.11.1 Latin Hypercube Sampling (LHS)

McKay et al. (1979) were first to introduce Latin hypercube sampling (LHS). As a statistical method, LHS creates a sample of possible collections of parameter values from a multidimensional distribution. The LHS method is widely used to reduce the number of runs and CPU time. LHS is based on an arbitrary number of dimensions, whereby each sample is the only one in each axis-aligned hyperplane.

In this method and when sampling a function of n variables, the range of each variable is divided into m equally probable intervals. M sample points are then placed in m intervals to satisfy the Latin hypercube requirements. This equally spaced interval sampling technique is one of the main advantages of this LHS sampling. Another advantage is that random samples can be taken one at a time, remembering which samples were taken so far.

4.11.2 MEPO Multiple Realization Optimizer

MEPO (Schlumberger, 2013) was used in this study due to the fact that this software enables the user to choose between different sampling approaches, i.e., Latin Hypercube, full factorial design, fractional factorial, Plackett-Burman and OVAT. On the other hand, in the previous MATLAB code, the results for each simulation run were read and exported to an excel-file (or a text-file) for each run, i.e., in addition to the simulation run done by Eclipse, pre and post-processing were performed at the end of each run by MATLAB. However, in MEPO, the results are stored and at the end, the results of all runs could be exported once into an excel-file. In other words, post processing stage is faster using MEPO, this also results in less CPU time compared to the previous MATLAB code.

In order to conduct the LHS approach, the MEPO software was used. MEPO is a suitable software to design, perform and post-process many simulation runs in different simulation engines. The MEPO multiple realization optimizer utilises a robust run management arrangement and allows the user to attain faster results with relative ease.

4.11.3 Python Programming Code

Python (Python Software Foundation, 2013) has been used in this study since MEPO performs pre- and post-processing using Python scripts. Hence, a new Python code has been developed to generate include-files for each run. Python is a powerful programming language, which has efficient high-level data structures and a simple but effective approach to object-oriented programming. Python's stylish syntax and dynamic typing make it a perfect language for scripting and rapid application development in many areas on most platforms. The Python interpreter, with new functions and data types, also allows it to be implemented in C or C++ or other languages callable from C.

4.11.4 New MFHW sets Using MEPO and LHS (MFHW-Sets 23 to 29 Nf7 L600m & Base Reference Set)

In this section, the results of MFHW Nf7L600m base reference set (i.e. MFHW-Set 8) re-run with different run numbers using the LHS approach are discussed. The first aim for running MFHW Nf7L600m base reference set using LHS was to conduct a sensitivity analysis on run numbers and to decrease the required number of runs and consequently to reduce the CPU time. The second aim was to increase the accuracy of the fitted response surface models. MFHW Nf7L600m base reference set was conducted with different run numbers of 4096, 3000, 2000, 1000, 500, 250 and 100 using the LHS approach. Here, the results of these sets and those of the original two level full factorial MFHW Nf7L600m base reference set are analysed and compared with each other and a comprehensive error analysis is conducted to obtain the optimum (minimum) required number of runs. Finally based on the error analysis, the most accurate response surface model (full quadratic surface model) is selected. For the new MFHW sets, which are based on the LHS experimental design approach, in order to have a consistent assessment with results reported previously, the impact of individual parameters in the tornado charts, are still studied based on the linear surface model without interaction. However, the full quadratic surface model is used for prediction of GPL and will be included in the NEW-COIN.

Here the tornado chart of MFHW-set 23 Nf7 L600m Base Reference set using LHS with 4096 run numbers (Figure 4.41) with that of the two-level full factorial sampling (FFS) MFHW-Set 8 Nf7 L600m Base Reference set (Figure 4.16) with the only difference being different sampling approaches was compared. The same trend is observed in both tornado charts for all pertinent parameters. This observation ensures that changing the

sampling approach from two-level FFS design to LHS retained the main trends in tornado charts.

Comparing the tornado chart of MFHW Nf7 L600m Base Reference Set -Sets 23, 24, 25, 26, 27, 28 and 29, with different run numbers of 4096, 3000, 2000, 1000, 500, 250 and 100 respectively, Figure 4.41, Figure 4.42, Figure 4.43, Figure 4.44, Figure 4.45, Figure 4.46 and Figure 4.47, with each other with the only difference being reducing run numbers from 4096 to 100 runs indicated that the same trend and values were observed in all tornado charts for all pertinent parameters. These results indicate that by using LHS and reduction of run numbers the main trends in tornado charts has been retained whilst reducing CPU time.

Figure 4.48 is the histogram chart that compares the GPL cumulative frequency of the runs in 7 different sets with different run numbers (MFHW-Set23 to MFHW-Set29). Almost the same clean-up efficiency is observed for all run numbers. However, it is noted that as the run numbers are decreased (below 500), the curves obtained are not as smooth as those obtained with larger run numbers (Figure 4.48 and Figure 4.49). This suggests that decreasing run numbers to values of 250 and 100 could not result in consistent histogram charts.

At this stage, in order to obtain the optimum (minimum) required number of runs as well as the best response surface model to predict GPL values, a comprehensive error analysis was conducted as described in the next section.

4.11.4.1 Error Analysis of Fitted Linear Response Surface Method

One of the main reasons for conducting the MFHW set with different run numbers using LHS approach was to evaluate the level of improvement in the predictive capability of the fitted surface functions compared to those fitted to that using the two-level FFS technique. For this purpose, the errors of predicted GPL values of the MFHW with different run numbers (run numbers of 4096, 3000, 2000, 1000, 500, 250 and 100) using fitted linear response surface functions, with interactive parameters, (ILRSM) and those of the relevant two-level FFS MFHW set were compared.

The root mean square error, RMSE, Equation 4.1and relative RMSE %, Equation 4.2, were used for this purpose with the results presented in Table 4.4.

$$RMSE = \sqrt{\frac{\sum_{i=1}^{n}\left[GPL_{predict} - GPL_{sim}\right]^2}{n}} \qquad 4.1$$

$$relative\ RMSE\% = \frac{RMSE_i - RMSE_{run\ number\ of 4096}}{RMSE_{run\ number\ of 4096}} * 100 \qquad 4.2$$

RMSE and also relative RMSE% in Table 4.4 show that ILRSMs fitted to MFHW set using LHS approach with different run numbers predict GPL results more accurately than the relevant ILRSM using two-level FFS (except for LHS with run number 100). This observation suggests that generally, ILRSMs fitted to LHS runs predict GPLs better compared to those GPLs predicted by ILRSMs fitted to the data obtained using two-level FFS.

Figure 4.50 shows RMSE of ILRSMs versus run numbers at three production stages for MFHW Nf7 L600m Base Reference sets with different sampling approaches, i.e., LHS, and two-level FFS. From Figure 4.50, in addition to the observation of having more accurate results for LHS runs, it is also noted that as the run numbers are decreased (below 1000), there is a significant increase in RMSE at all three production stages. This suggests that decreasing run numbers to values less than 500 (i.e., 250 and 100) result in less accurate ILRSMs and consequently higher RMSEs compared to larger run numbers. This observation is in line with what was previously indicated in histogram charts, i.e., decreasing run numbers to the value of 250 and 100 resulted in less consistent charts than the ones for larger run numbers. Therefore, based on these results 1000 is considered as the optimum number of runs.

4.11.4.2 Error Analysis of Pure and Full Quadratic Response Surface Models

The main reason to conduct this error analysis for different run numbers using LHS approach in addition to that presented in section 4.11.4.1 is to investigate the accuracy of pure quadratic response surface models (PQRSM) and full quadratic response surface models (FQRSM) fitted to LHS results.

In order to evaluate the reliability of these two models, the RMSE and relative RMSE of predicted GPL values of the MFHW set with different run numbers (run numbers of 4096, 3000, 2000, 1000, 500, 250 and 100) using fitted PQRSM and FQRSM have been calculated.

Table 4.5 and Table 4.6 show RMSE and relative RMSE% of PQRSMs and FQRSMs fitted to the results of MFHW set using LHS approach with different run numbers. It is noted that the error of the predicted GPL values by FQRSM fitted to GPL values are less than the relevant ones for the predicted GPL values by PQRSM. In other words, the fitted FQRSMs predict the GPL values more accurately than the fitted PQRSMs except for the

set with 100 run numbers. For this latter case, larger errors in predicted GPL values by FQRSMs compared to the same GPL values predicted by PQRSMs is observed, because for FQRSMs, 91 surface model coefficients are calculated based on just 100 data points whereas for PQRSMs, just 25 surface model coefficients are calculated based on the same 100 data points, that is, using 100 as the number of data points to fix the large number of the FQRSMs' coefficients is not desirable. These results confirm that FQRSM with a larger number of coefficients predict GPL more accurately if the number of data points are larger than 100.

Figure 4.51 show RMSE of ILRSM, PQRSM and FQRSM models versus run numbers at three production stages for MFHW Nf7 L600m Base Reference sets with different sampling approaches, i.e., LHS and two-level FFS. From Figure 4.51, it is noted that the two-level FFS design is the least accurate sampling design and FQRSM is the most accurate design. It also indicates that the accuracy of the models with interaction terms (i.e. ILRSMs and FQRSMs with 79 and 91 coefficients, respectively) decreases significantly in small run numbers (i.e., 100 and 250) due to very few data points.

The results suggest that generally LHS approach is a more realistic and reliable approach compare to two-level FFS design. Using LHS with optimum run numbers compared to two-level FFS sets reduces the CPU time significantly. The response surface model which best predicted GPL values was FQRSM, in other words, FQRSM best describes the real physics of clean-up performance. The optimum (minimum) required number of MFHW-Nf7L600 runs for FQRSMs was 1000 run numbers.

4.12 Conclusions

Following the extensive investigation on clean-up efficiency of SFVWs and in order to further improve the current understanding of hydraulic fracturing treatment for practical field applications, this study has expanded the previous work that has been done in chapter 3 to MFHWs systems with different fracture spacing (300m, 100m, 75m and 50m), different fracture length (600m and 900m), different permeability variation range (Kmr=0.01, 1,10 and 100), different pressure drawdowns (DP=100, 1000 and 4000psi) and different STs. It should be noted that in this Chapter, conventional Pc and Kr, the same as those used in SFVW sets, were used whereas in the next chapter, unconventional ones are used

In this chapter, 29 MFHW-Sets with a total of 101058 runs have been studied. In each set, twelve pertinent parameters were varied based on either the two-level full factorial

statistical method or Latin Hypercube approach. Gas production loss (GPL) was calculated and input into a Response Surface Method as the response term. Correlation between parameters and GPL in each sensitivity study was then established and compared with the one obtained for the base reference set and other similar sets but with one different variable.

For the MFHW sets23 to 29, instead of two-level full factorial linear (FFS) experimental design used in the previous simulations (MFHW sets 1 to 22), the Latin hypercube sampling (LHS) method has been used to decrease the required number of runs. It should be noted that the response surface model fitted to results based on the full factorial is a linear whereas that fitted based on LHS could be either linear or quadratic, which increases the accuracy of the fitted response surface models. For these simulations, the Multiple Realization Optimizer (MEPO) software has been used to automatically link different stages of the simulations conducted using ECLIPSE100 and to perform pre and post-processing stages.

A summary of the main conclusions is given below:

1. The K_m trend in the MFHW case was different from that of the VW Base Reference Set confirming that the K_m trend change (from having a negative to a positive coefficient value) in the MFHW base reference set was due to the flow geometry change and how the well was completed. This is also in line with the more important Pc effect for the MFHW set, which is described next.
2. It was noted that Pc pertinent parameters were more important in the MFHW sets whilst end points and exponents of Corey type relative permeability curves for gas and FF in the matrix and fracture were more important in the VW sets. This observation suggests that FF production had a more detrimental effect on gas production in the MFHW set. In other words, having a higher Pc that results in more FF imbibition into the matrix and less resistance to the gas flow, is more important in MFHWs.
3. Faster clean-up was observed for MFHW compared to VW. This was due to having a higher production rate in MFHW sets.
4. In the reduced matrix permeability range MFHW sets (MFHW-Set 4 (Kmr=10) and MFHW-Set 7 (Kmr=100)), the first effect of Km on GPL (i.e. an increase in Km that improves fluid mobility and reduces GPL) was dominant (i.e. Km coefficient was negative) whilst in MFHW-Set 1 (MFHW base reference set) the second effect (i.e. an increase in Km that reduces Pc and increases GPL) was dominant (i.e. Km

coefficient was positive). Since in these two sets (MFHW-Set 4 and 7), the matrix permeability range had been reduced, Pc was already high enough and hence the effect of km on mobility was more important.

5. In low (high) DP MFHW sets the effect of Pc on GPL was more (less) pronounced. This trend is similar to what was previously reported for the corresponding low (high) DP VW sets.
6. In reduced DP MFHW set, the impact of the end points and exponents of Corey type relative permeability curves for gas and FF in the matrix were more pronounced than those of the MFHW base reference set, confirming the observation noted in the VW sets that in low DP sets, it is more important how fluids (Gas and FF) flow from the matrix to fracture than how it flows from fracture to wellbore, in other words, it is more crucial to transfer gas and FF from the matrix to fracture.
7. In Reduced (increased) DP MFHW sets, slower (faster) clean-up was observed; this is similar to what was previously reported for the corresponding VW sets.
8. Pc was more important and faster clean-up was observed for the extended soaking time set. The same trends were previously reported for the VW sets.
9. When the number of fractures (fracture spacing) was increased (decreased) on the same horizontal well length and compared to the previous MFHW Nf3 L600 base reference set, it was noted that the direction of impact of all parameters was almost similar including that of Km. That is, in the MFHW Nf7 L600 base reference set the effect of Km on Pc was still more dominant than that on fluid flow whilst the reverse was observed for VW.
10. Clean-up efficiency of MFHWs when the number of fractures (fracture spacing) was increased (decreased) on the same horizontal length was almost the same (i.e. very small changes up to 3-4% in the cumulative frequency of runs was noted).
11. Increasing horizontal well length while the fracture spacing was fixed, did not change the fracture clean-up efficiency at all.
12. In tighter set (MFHW Nf7 L600m Kmr10, MFHW-Set9), the first effect of Km on GPL (i.e. an increase in Km that improves fluid mobility and reduces GPL) was more dominant whilst in MFHW-Set8 (MFHW Nf7 L600 base reference set) the second effect (i.e. an increase in Km that reduces Pc and increases GPL) was more dominant. This change was attributed to the fact that since the matrix permeability range has been reduced by a factor of 10, fluid mobility in the matrix is more crucial in the low permeability set. In line with this, the absolute values of Kmaxwm,

Kmaxwm, nwm and ngm were larger in this tighter set compared to those in the base reference set) and Pc was not as important as before.

13. In line with the previous observation, the less important effect of Pc in tighter formation (MFHW Nf7 L600m Kmr10, MFHW-Set9) compared to the one for MFHW-Set8 was observed.
14. In the tightest formation set (MFHW Nf7 L600m Kmr100, MFHW-Set10), the first effect of Km on GPL (i.e. an increase in Km that improves fluid mobility and reduces GPL) was dominant and the effect of Km on clean-up efficiency was the most important at 30 and 370 days and second most important after Kf at 10 days. That is due to the fact that in MFHW-Set10, matrix permeability range has been reduced by a factor of 100, fluid mobility in the matrix is the most crucial factor between MFHW-Set8, MFHW-Set9 and MFHW-Set10 sets. In line with this, the absolute values of Kmaxwm, Kmaxwm, nwm and ngm were even larger in this set compared to those in the MFHW-Set9 set).
15. According to these three sets (MFHW-Set8, MFHW-Set9 and MFHW-Set10), matrix permeability plays an important role in hydraulic fracturing design, for those sets with matrix permeability variation 1 μD-100 μD and 0.1 μD-10 μD. Furthermore, using chemicals (IFT reducing agents) to reduce Pc could increase GPL whilst in very tight formation sets with matrix permeability variation 0.01 μD-1 μD it is recommended to utilise chemicals (IFT reducing agents) in order to reduce Pc and consequently reduce GPL.
16. Slower clean-up is observed for the MFHW-Set10 (and MFHW-set9) compared to MFHW-Set8 due to lower production rate of the tightest (and tighter) formation resulting in a slower and less efficient clean-up.
17. In MFHW Nf7 L600m DP100, MFHW-Set11, IFT was the most important parameter affecting GPL at 10 and 30 days and second most important after Kf at 370 days. This is in line with what was reported previously for low DP VW sets and low DP MFHW Nf3 set. Moreover, the impact of the end points and exponents of Corey type relative permeability curves for gas and FF in the matrix was more pronounced and clean-up was slower in this low DP set compared to that in MFHW-Set8.
18. Regardless of DP (100 or 1000 or 4000psi), for the MFHW sets with matrix permeability variation ranges of 1 μD-100 μD and 0.1 μD-10 μD, using chemicals (IFT reducing agents) could increase GPL whilst in very tight sets with the matrix

permeability variation range of 0.01 μD-1 μD, it is recommended to use chemicals (IFT reducing agents) in order to reduce Pc and consequently reduce GPL.

19. If the tornado charts of low DP MFHW-sets are compared with the relevant high DP sets, it is noted that fluid mobility pertinent parameters (Kmaxgm, ngm, Kmaxwm and nwm) are more important at low DP sets compared to the relevant ones in high DP sets. This is due to the fact that as DP decreases, fluid mobility in the matrix becomes a more critical and consequently more important controlling factor on GPL reduction.
20. Although the impact of fracture interference/fracture spacing on flow is significant, its impact on clean-up performance is minimal even when the permeability variation range was increased from 1 μD-100 μD by a factor of 100 to 100 μD-10000 μD in MFHWs systems with different fracture spacing (100m, 75m and 50m) corresponding to sets with 7, 9 and 13 fractures.
21. The results of MFHW sets with LHS suggest that generally LHS approach is a more realistic and reliable sampling approach compared to the two-level FFS experimental design.
22. Using LHS with an optimum run number reduces the CPU time significantly compared to two-level FFS sets.
23. The response surface model, which best predicted GPL values was FQRSM. In other words, FQRSM describes the real physics of clean-up performance better.
24. The optimum (minimum) required number of MFHW-Nf7L600 runs for FQRSMs was 1000 run numbers.

4.13 References

ECONOMIDES, M. J. & MARTIN, A. N. How to decide between horizontal transverse, horizontal longitudinal and vertical fractured completion. Proceedings - SPE Annual Technical Conference and Exhibition, 2010. 2474-2491.

GAS CONDENSATE RECOVERY PROJECT' Progress Report GCRP/15/1, Oct. 2014-Apr. 2015, April 2015, Heriot-Watt University, Institute of Petroleum Engineering.

MCKAY, M. D., BECKMAN, R. J. & CONOVER, W. J. 1979. A Comparison of Three Methods for Selecting Values of Input Variables in the Analysis of Output from a Computer Code. *Technometrics,* 21**,** 239-245.

PYTHON SOFTWARE FOUNDATION. 2013. Python Programming Language, Python v2.7.6, *Python Software Foundation*.

SCHLUMBERGER. 2013. MEPO Multiple Realization Optimizer; MEPO4.2.0; Build:2617; Date:2013-Apr-25_15-59', *SPT Group; A Schlumberger Company*.

4.14 Tables

Table 4.1 MFHW Model geometry in X, Y & Z direction (Xf is fracture half length)

Horizontal well length (m)	**Number of Hydraulic Fractures**	**X_f(m)**	**w_f(m)**	**Xres(m)**	**Yres(m)**	**Zres(m)**
600	3	90	0.004	2000	2000	40

Table 4.2 MFHW-Sets analysed

Set Name	No. of fracks	Horizontal Length (m)	DP (Psi)	FVR	Shut-in time (days)	Kf (D)	Km (µD)	lam	Sampling Approach	Number of Runs
Default Values	3	600	1000	2	2	1-30	1-100	1-4	FFS	4096
MFHW-Set 1	✓	✓	✓	✓	✓	✓	✓	✓	✓	✓
MFHW-Set 2	✓	✓	✓	5	✓	✓	✓	✓	✓	✓
MFHW-Set 3	✓	✓	✓	✓	20	✓	✓	✓	✓	✓
MFHW-Set 4	✓	✓	✓	✓	✓	✓	0.1-10	✓	✓	✓
MFHW-Set 5	✓	✓	100	✓	✓	✓	✓	✓	✓	✓
MFHW-Set 6	✓	✓	4000	✓	✓	✓	✓	✓	✓	✓
MFHW-Set 7	✓	✓	✓	✓	✓	✓	0.01-1	✓	✓	✓
MFHW-Set 8	7	✓	✓	✓	✓	✓	✓	✓	✓	✓
MFHW-Set 9	7	✓	✓	✓	✓	✓	0.1-10	✓	✓	✓
MFHW-Set 10	7	✓	✓	✓	✓	✓	0.01-1	✓	✓	✓
MFHW-Set 11	7	✓	100	✓	✓	✓	✓	✓	✓	✓
MFHW-Set 12	9	✓	100	✓	✓	✓	✓	✓	✓	✓
MFHW-Set 13	13	✓	100	✓	✓	✓	✓	✓	✓	✓
MFHW-Set 14	10	900	100	✓	✓	✓	✓	✓	✓	✓
MFHW-Set 15	7	✓	4000	✓	✓	✓	✓	✓	✓	✓
MFHW-Set 16	7	✓	100	✓	✓	✓	0.1-10	✓	✓	✓
MFHW-Set 17	7	✓	4000	✓	✓	✓	0.1-10	✓	✓	✓
MFHW-Set 18	7	✓	100	✓	✓	✓	0.01-1	✓	✓	✓
MFHW-Set 19	7	✓	4000	✓	✓	✓	0.01-1	✓	✓	✓
MFHW-Set 20	7	✓	✓	✓	✓	✓	100-10000	✓	✓	✓
MFHW-Set 21	9	✓	✓	✓	✓	✓	100-10000	✓	✓	✓
MFHW-Set 22	13	✓	✓	✓	✓	✓	100-10000	✓	✓	✓
MFHW-Set 23	7	✓	✓	✓	✓	✓	✓	✓	LHS	✓
MFHW-Set 24	7	✓	✓	✓	✓	✓	✓	✓	LHS	3000
MFHW-Set 25	7	✓	✓	✓	✓	✓	✓	✓	LHS	2000
MFHW-Set 26	7	✓	✓	✓	✓	✓	✓	✓	LHS	1000
MFHW-Set 27	7	✓	✓	✓	✓	✓	✓	✓	LHS	500
MFHW-Set 28	7	✓	✓	✓	✓	✓	✓	✓	LHS	250
MFHW-Set 29	7	✓	✓	✓	✓	✓	✓	✓	LHS	100

Table 4.3 Calculated Pc of Sets MFHW-Set8, MFHW-Set9 and MFHW-Set10 for Best/Worst Case.

		IFT	Km, mD	λ	Sw	Swr	Pd bar	Pc bar
MFHW Nf7 Base Reference Set, MFHW-Set8	Worst Case	2	0.1	4	0.2	0.15	0.047	0.10
	Best Case	50	0.001	1	0.2	0.15	11.86	201.60
MFHW Nf7 Kmr10, MFHW-Set9	Worst Case	2	0.0001	4	0.2	0.15	1.50	3.05
	Best Case	50	0.01	1	0.2	0.15	3.75	63.75
MFHW Nf7 Kmr100 Set, MFHW-Set10	Worst Case	50	0.00001	4	0.2	0.15	118.59	240.79
	Best Case	2	0.001	1	0.2	0.15	0.47	8.06

Table 4.4 RMSE and relative RMSE of interactive linear surface models (ILRSM) at three production stages for various MFHW Nf7 L600m Base Reference sets with different run numbers and sampling approaches, i.e., Latin Hypercube, LHS, and two-level Full Factorial Sampling, FFS.

	Run Numbers	LHS RMSE IL, 10 Days	Relative error % compare to LHS 4096 runs, 10 days	LHS RMSE IL, 30 Days	Relative error % compare to LHS 4096 runs, 30 days	LHS RMSE IL, 365 Days	Relative error % compare to LHS 4096 runs, 365 days
LHS 4096 Runs	4096	6.88	0.00	7.17	0.00	4.72	0.00
LHS 3000 Runs	3000	7.02	1.93	7.30	1.83	4.74	0.39
LHS 2000 Runs	2000	7.14	3.72	7.45	3.99	4.77	1.02
LHS 1000 Runs	1000	7.40	7.51	7.53	5.13	4.72	-0.04
LHS 500 Runs	500	7.87	14.27	7.78	8.64	4.69	-0.68
LHS 250 Runs	250	8.62	25.30	8.59	19.87	4.91	4.07
LHS 100 Runs	100	15.79	129.43	15.17	111.68	7.39	56.64
	Run Numbers	FF RMSE IL, 10 Days	Relative error % compare to LHS 4096 runs, 10 days	FF RMSE IL, 30 Days	Relative error % compare to LHS 4096 runs, 30 days	FF RMSE IL, 365 Days	Relative error % compare to LHS 4096 runs, 365 days
Full Factorial (4096 Runs)	4096	13.56	97.02	15.15	111.41	9.15	93.80

Table 4.5 RMSE and relative RMSE of the pure quadratic (PQ) model in run numbers at three production stages for MFHW Nf7 L600m Base Reference sets with LHS approach.

	Run Numbers	LHS RMSE PQ, 10 Days	Relative error % compare to LHS 4096 runs, 10 days	LHS RMSE PQ, 30 Days	Relative error % compare to LHS 4096 runs, 30 days	LHS RMSE PQ, 365 Days	Relative error % compare to LHS 4096 runs, 365 days
LHS 4096 Runs	4096	5.63	0.00	5.38	0.00	4.28	0.00
LHS 3000 Runs	3000	5.68	0.93	5.47	1.73	4.28	-0.07
LHS 2000 Runs	2000	5.68	0.93	5.46	1.48	4.27	-0.14
LHS 1000 Runs	1000	5.76	2.29	5.44	1.23	4.25	-0.76
LHS 500 Runs	500	5.75	2.09	5.45	1.35	4.28	0.00
LHS 250 Runs	250	5.94	5.47	5.58	3.71	4.30	0.57
LHS 100 Runs	100	6.03	7.02	5.95	10.69	4.33	1.08

Table 4.6 RMSE and relative RMSE of the full quadratic (FQ) model in run numbers at three production stages for MFHW Nf7 L600m Base Reference sets with LHS approach.

	Run Numbers	LHS RMSE FQ, 10 Days	Relative error % compare to LHS 4096 runs, 10 days	LHS RMSE FQ, 30 Days	Relative error % compare to LHS 4096 runs, 30 days	LHS RMSE FQ, 365 Days	Relative error % compare to LHS 4096 runs, 365 days
LHS 4096 Runs	4096	4.13	0.00	4.49	0.00	4.26	0.00
LHS 3000 Runs	3000	4.22	2.27	4.59	2.22	4.26	0.02
LHS 2000 Runs	2000	4.35	5.44	4.67	3.92	4.27	0.20
LHS 1000 Runs	1000	4.41	6.80	4.74	5.45	4.20	-1.42
LHS 500 Runs	500	4.58	10.95	4.85	7.84	4.24	-0.42
LHS 250 Runs	250	5.74	38.94	5.52	22.84	4.39	3.04
LHS 100 Runs	100	13.32	222.62	10.88	142.17	4.33	1.62

4.15 Figures

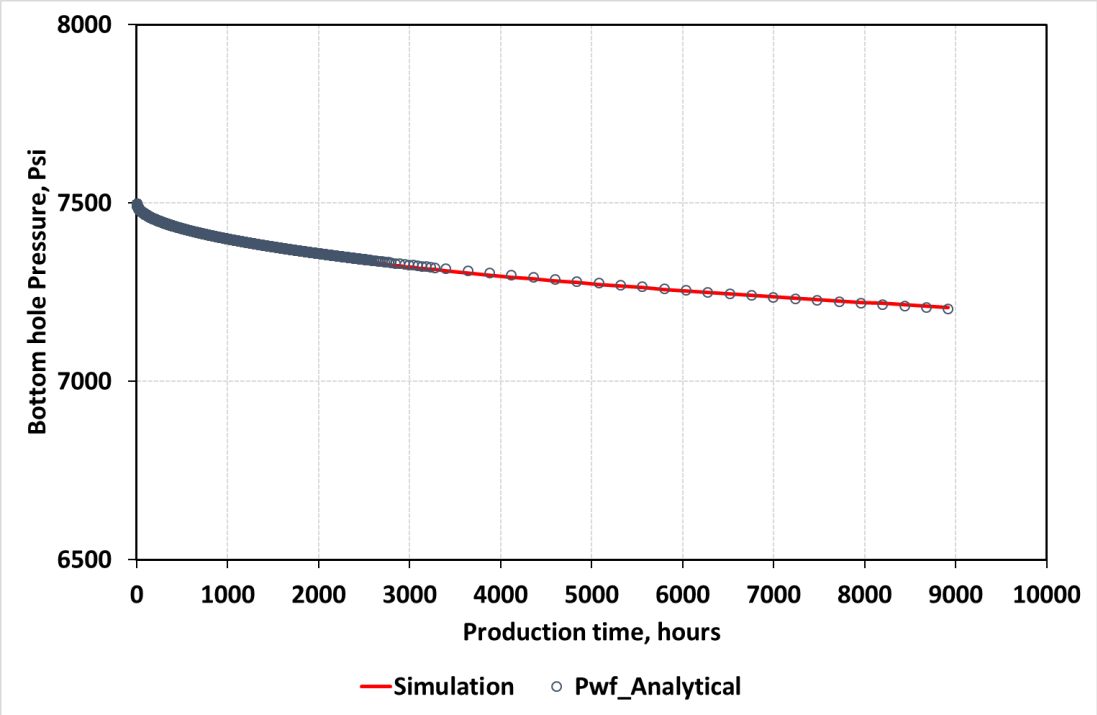

Figure 4.1 Predicated bottom hole pressure by simulation model of MFHW and analytical model (Equation 3.2) versus production time.

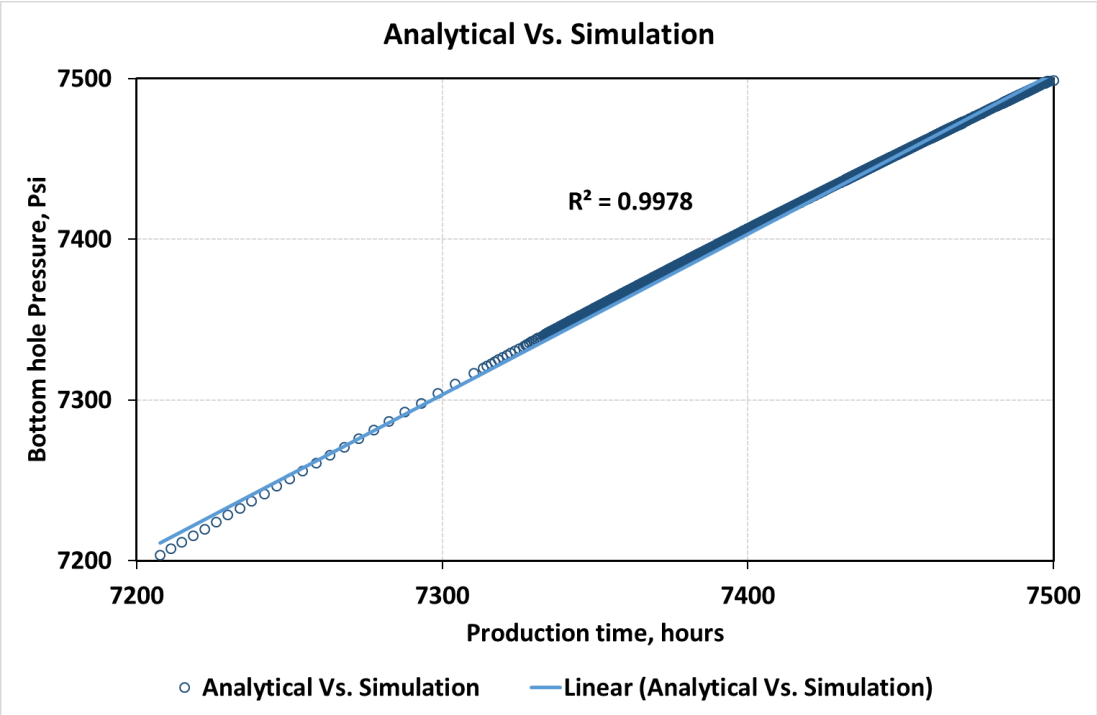

Figure 4.2 Predicated bottom hole pressure by analytical model (Equation 3.2) vs the one of simulation model of MFHW..

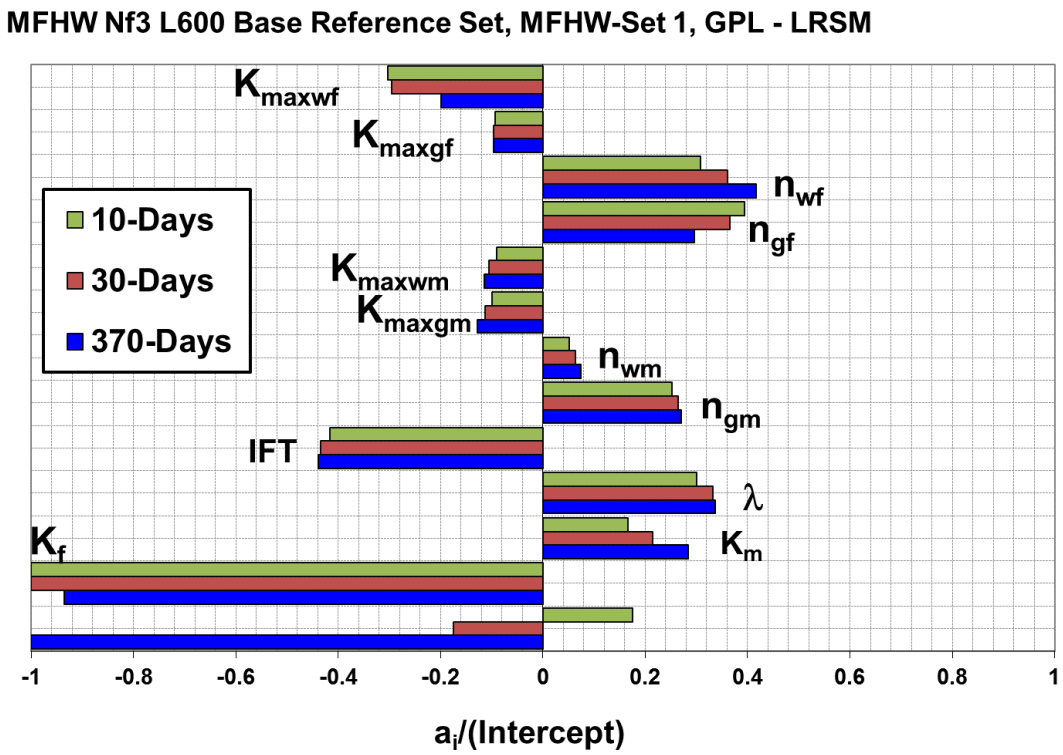

Figure 4.3 Tornado chart comparing LRSM coefficients of all pertinent parameters at three production stages for Multiple Fractured Horizontal Well, MFHW-Set1 Nf3 L600, Base Reference Set,

a. Single Fracture Vertical Well (SFVW) Base Reference Set, SFVW-Set 1

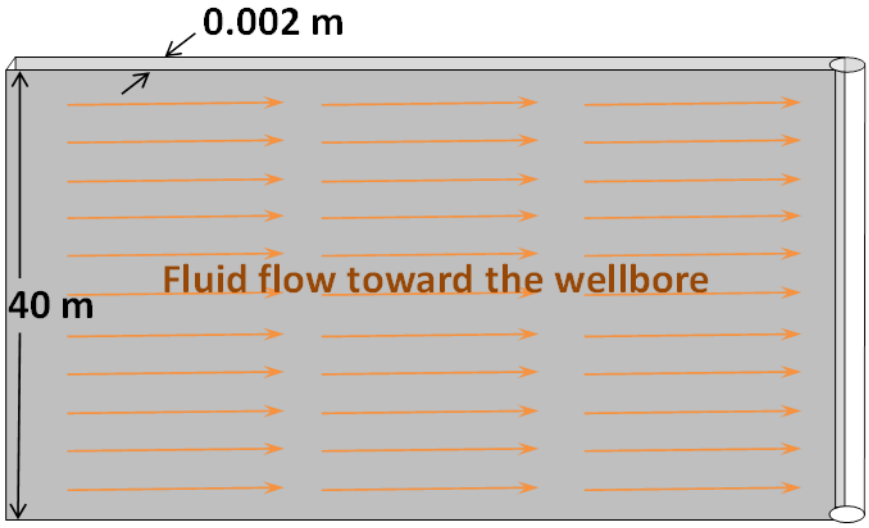

b. New Y- Direction SFVW Base Reference set

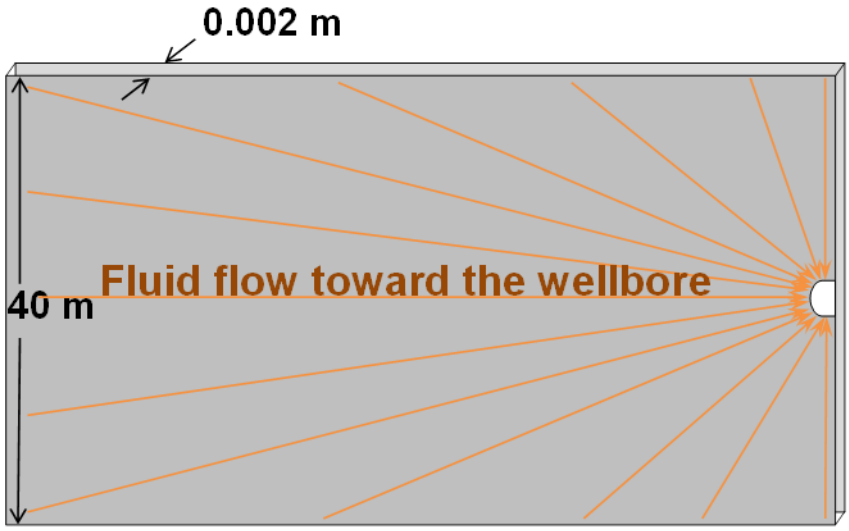

Figure 4.4: Well trajectory and flow geometry of (a) Single Fracture Vertical Well (SFVW) Base Reference Set, and (b) New Y- Direction SFVW Base Reference set.

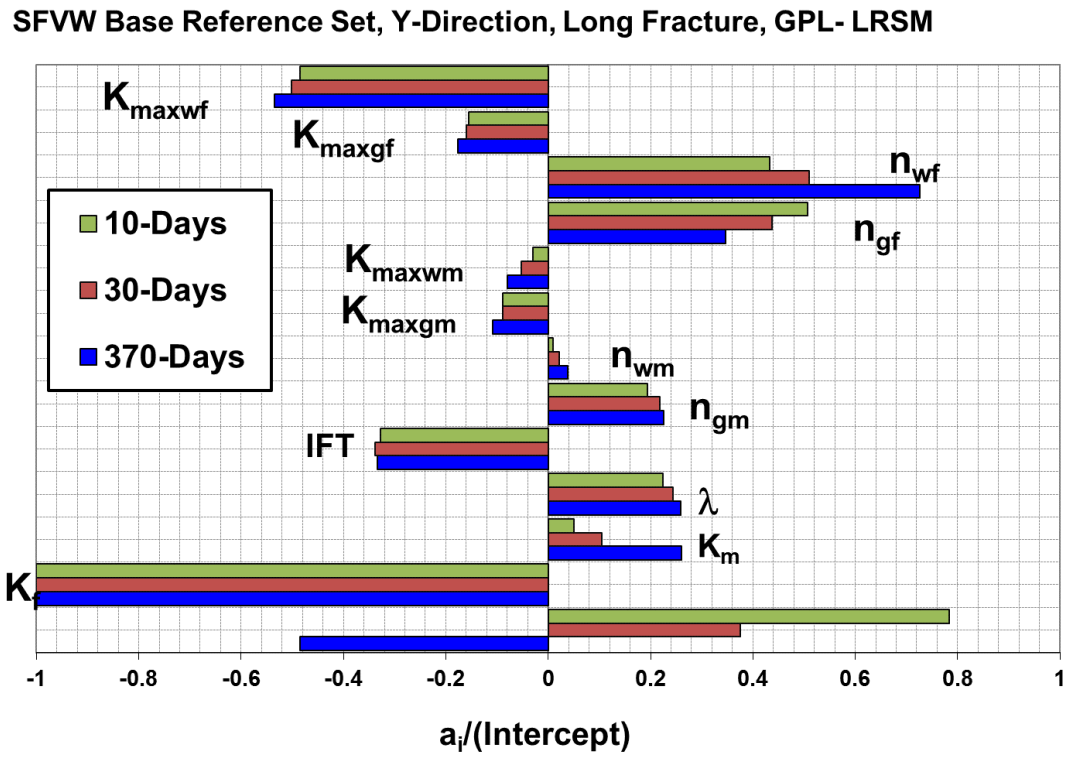

Figure 4.5 Tornado chart comparing LRSM coefficients of all pertinent parameters at three production stages for New Y- Direction SFVW Base Reference set.

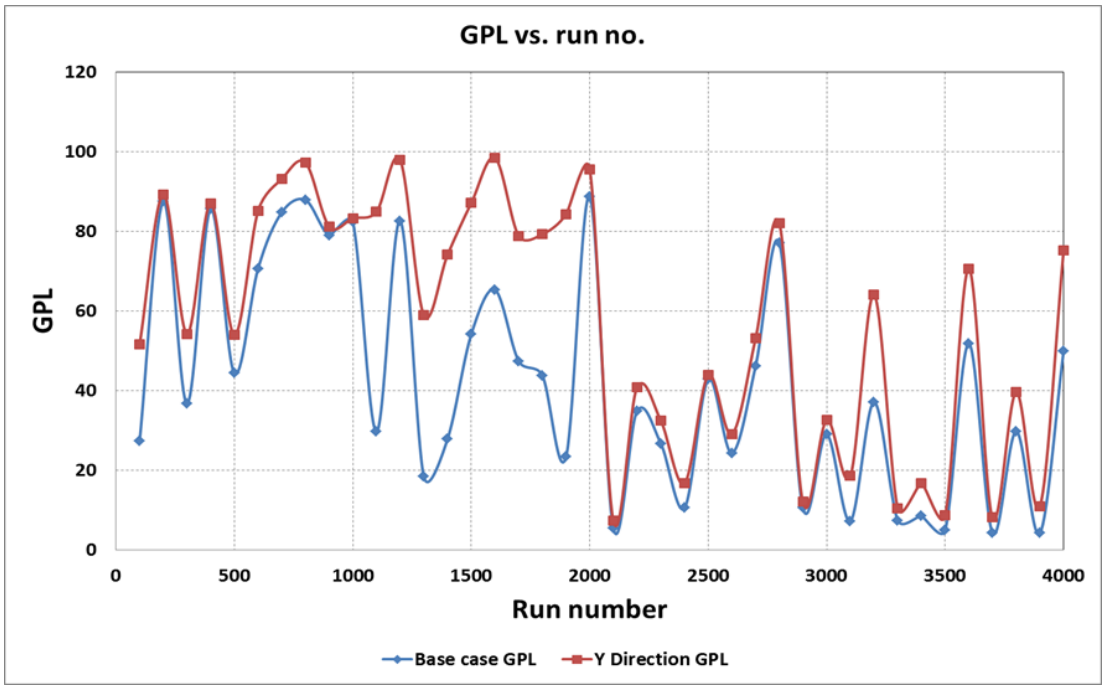

Figure 4.6 GPL vs Run Number for Z (SFVW) and Y Direction completion in Base Reference set,

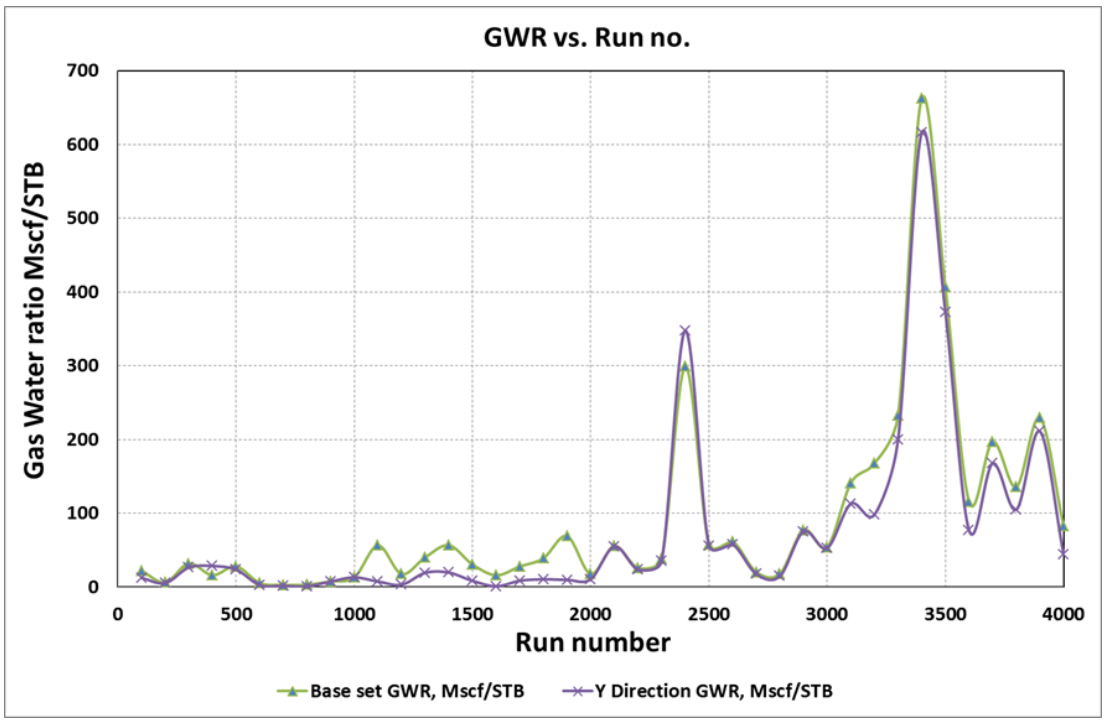

Figure 4.7 Gas Water Ratio vs Run Number for (SFVW) Z and Y Direction completion in Base Reference set,

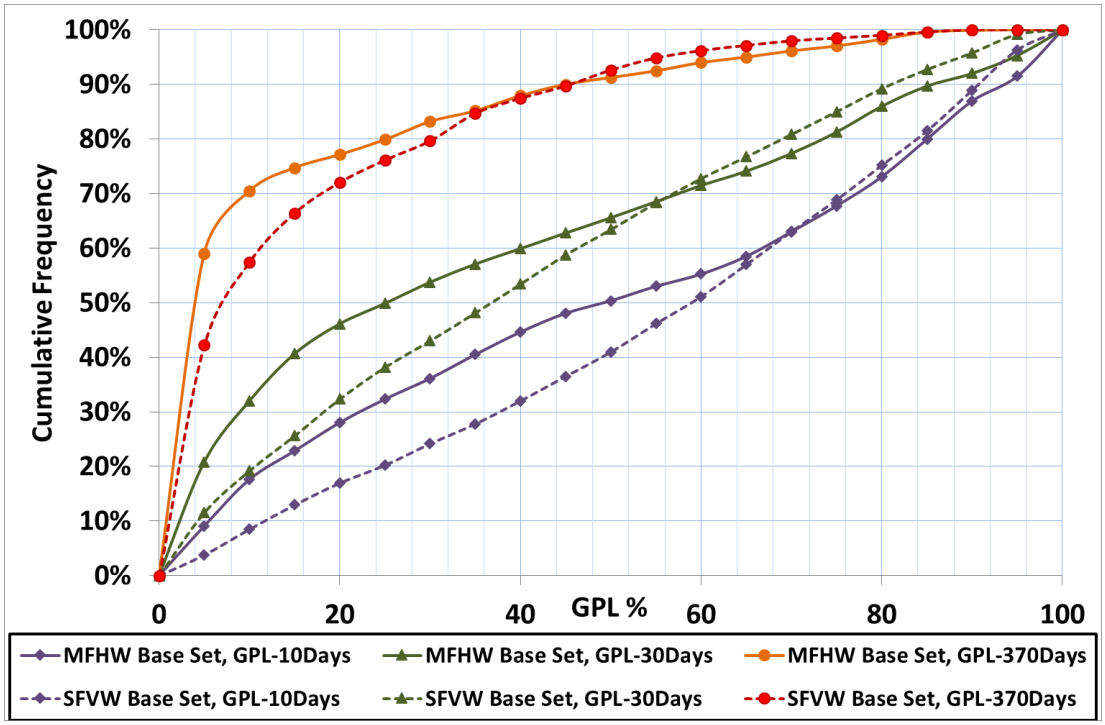

Figure 4.8 Histogram chart comparing GPL cumulative frequency of the MFHW Base Reference set, MFHW-Set 1, and SFVW Base Reference Set, SFVW-Set 1 at three production stages.

a. MFHW-Set2 FVR=5

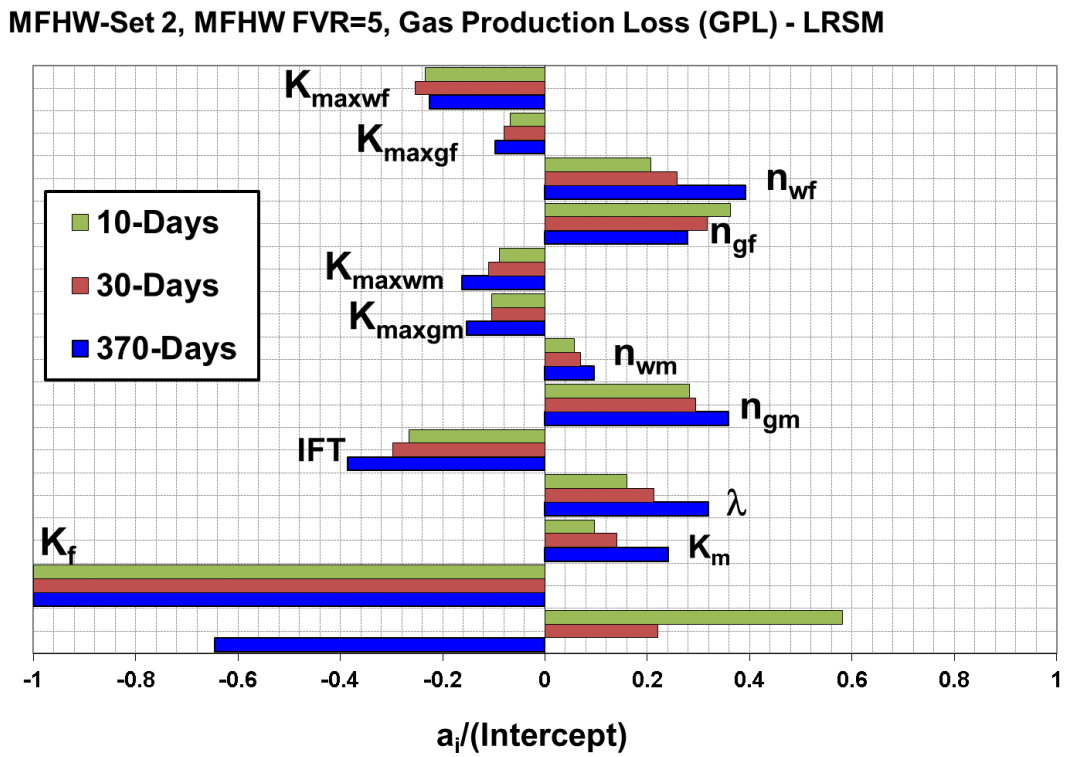

b. SFVW-Set 9 FVR=5

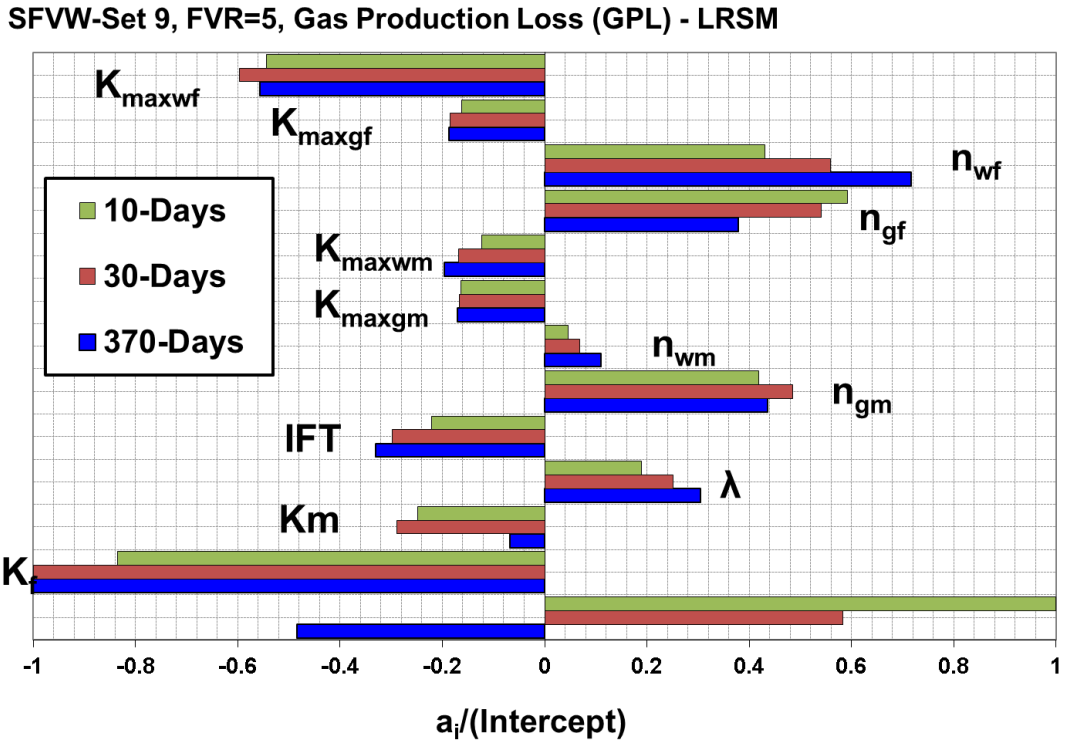

Figure 4.9 Tornado chart comparing LRSM coefficients of all pertinent parameters at three production stages for (a)MFHW- Set 50 FVR=5 & (b) SFVW-Set9 FVR=5

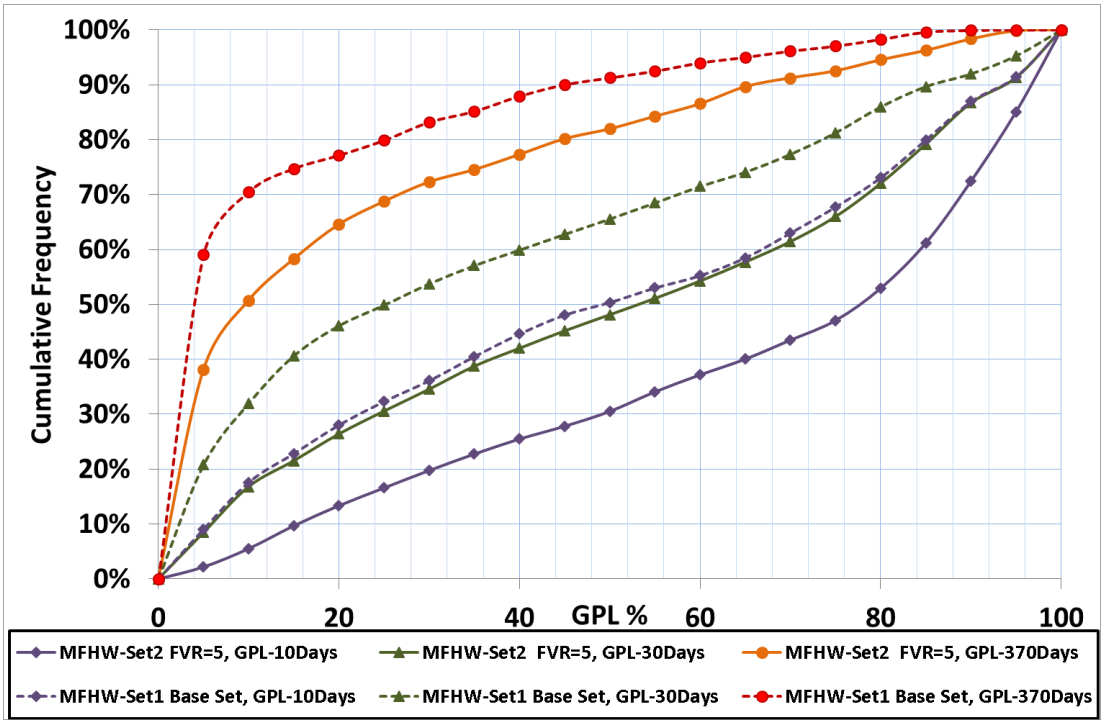

Figure 4.10 Histogram chart comparing GPL cumulative frequency of MFHW-Set2 FVR=5 and MFHW-Set1 Base Reference set at three production stages.

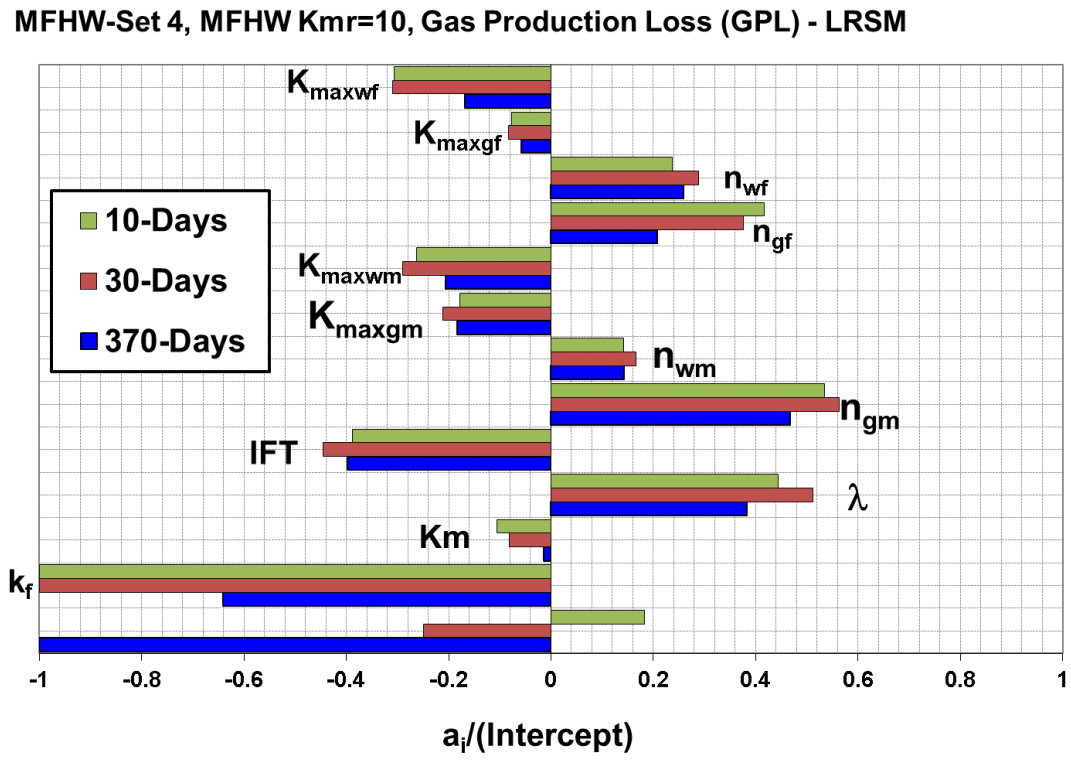

Figure 4.11 Tornado chart comparing LRSM coefficients of all pertinent parameters at three production stages for MFHW Kmr= 10, MFHW-Set 4

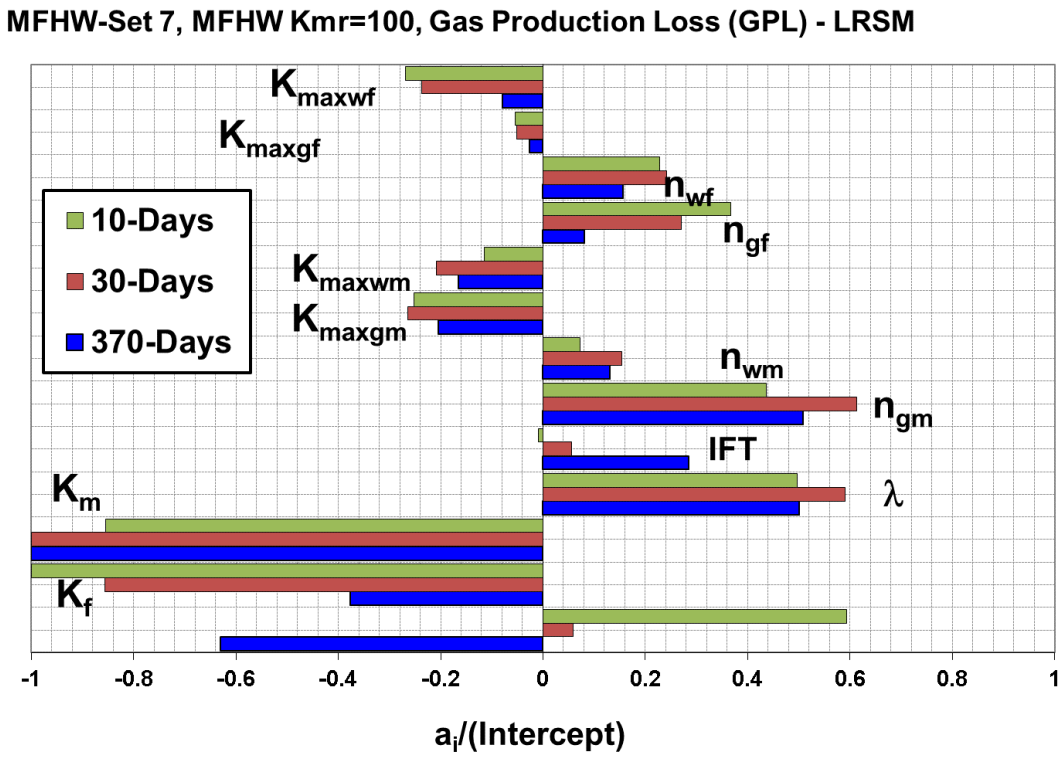

Figure 4.12 Tornado chart comparing LRSM coefficients of all pertinent parameters at three production stages for MFHW Kmr= 100, MFHW-Set 7

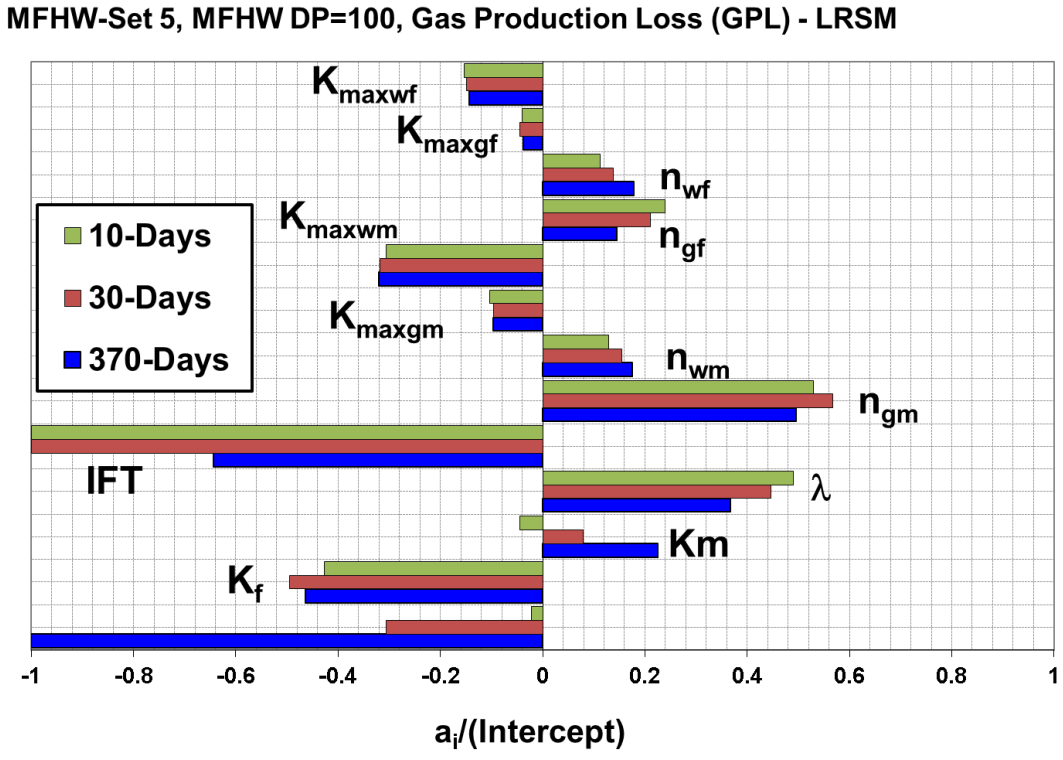

Figure 4.13 Tornado chart comparing LRSM coefficients of all pertinent parameters at three production stages for MFHW DP=100, MFHW-Set 5

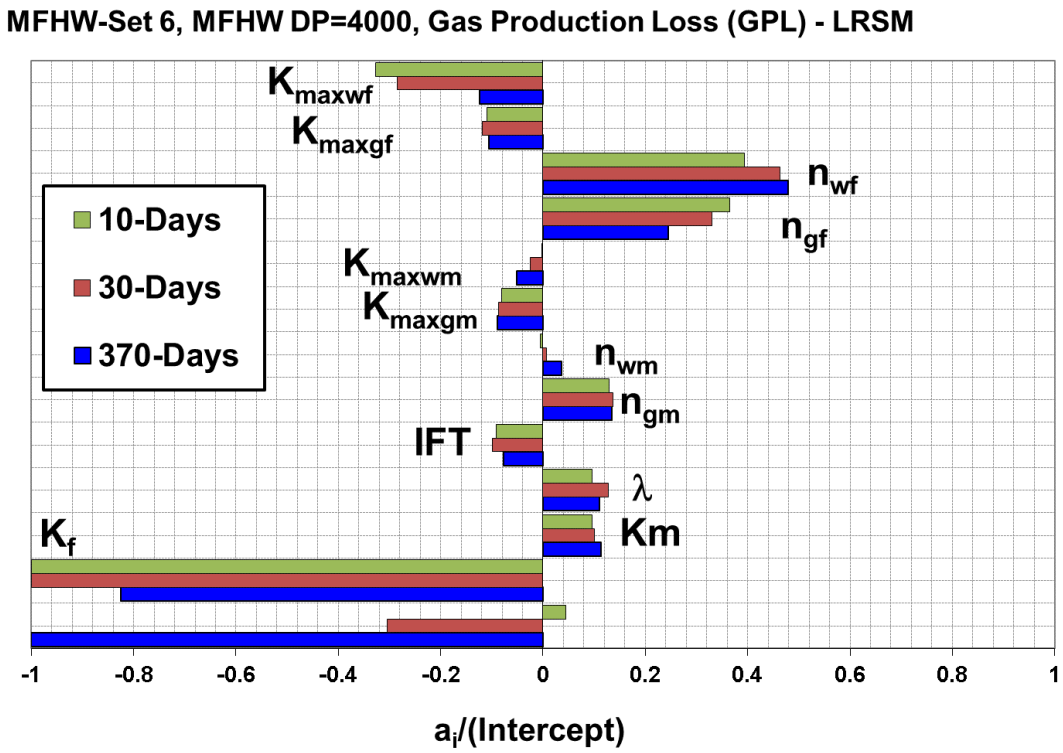

Figure 4.14 Tornado chart comparing LRSM coefficients of all pertinent parameters at three production stages for MFHW DP=4000, MFHW-Set 6

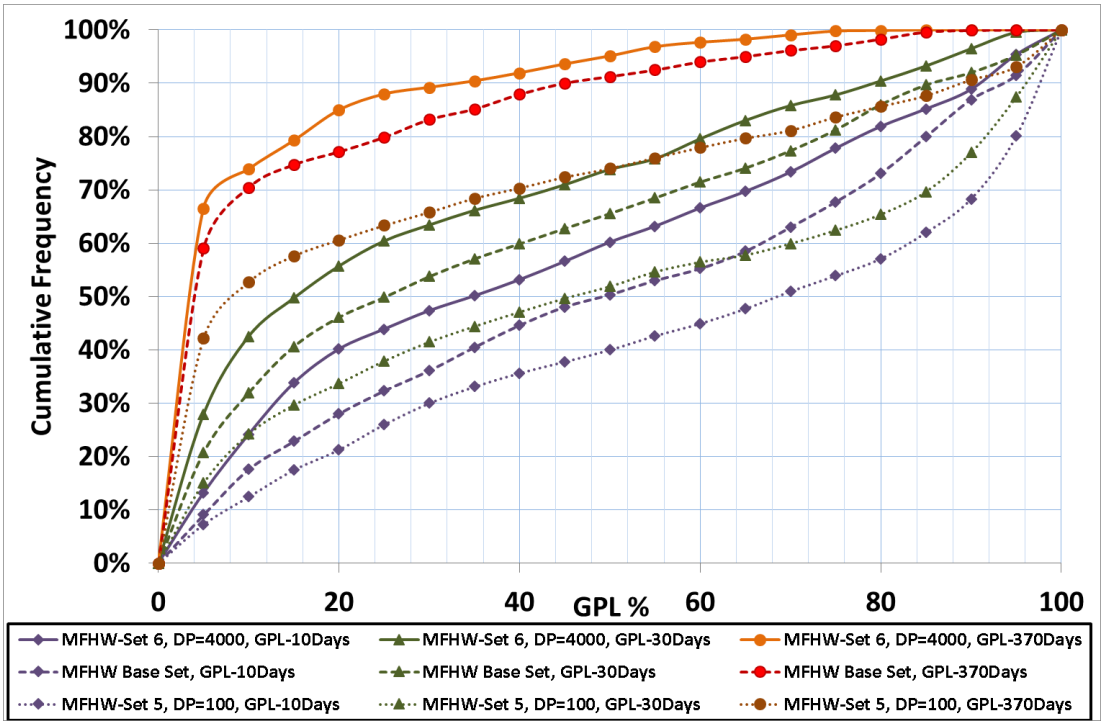

Figure 4.15 Histogram chart comparing GPL cumulative frequency of MFHW-Set 5 with DP=100, MFHW-Set 1 Base Reference set with Dp=1000 and MFHW-Set 6 with DP=4000 at three production stages.

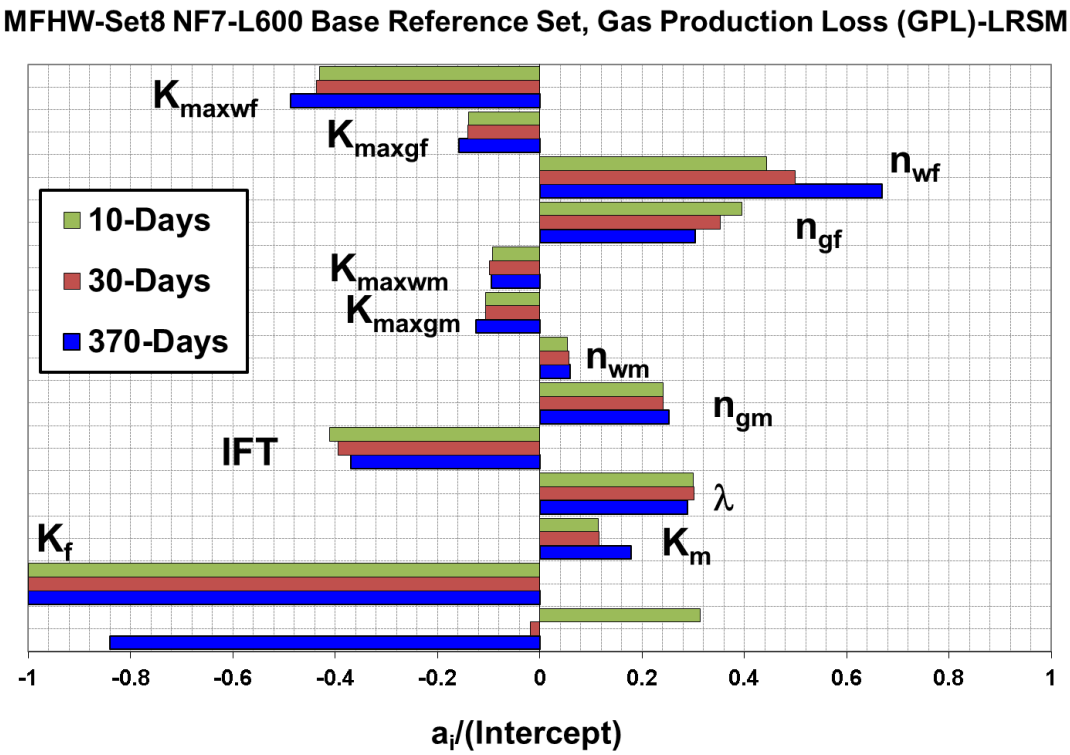

Figure 4.16 Tornado chart comparing LRSM coefficients of all pertinent parameters at three production stages for MFHW-Set8 Nf7 L600, Base Reference Set,

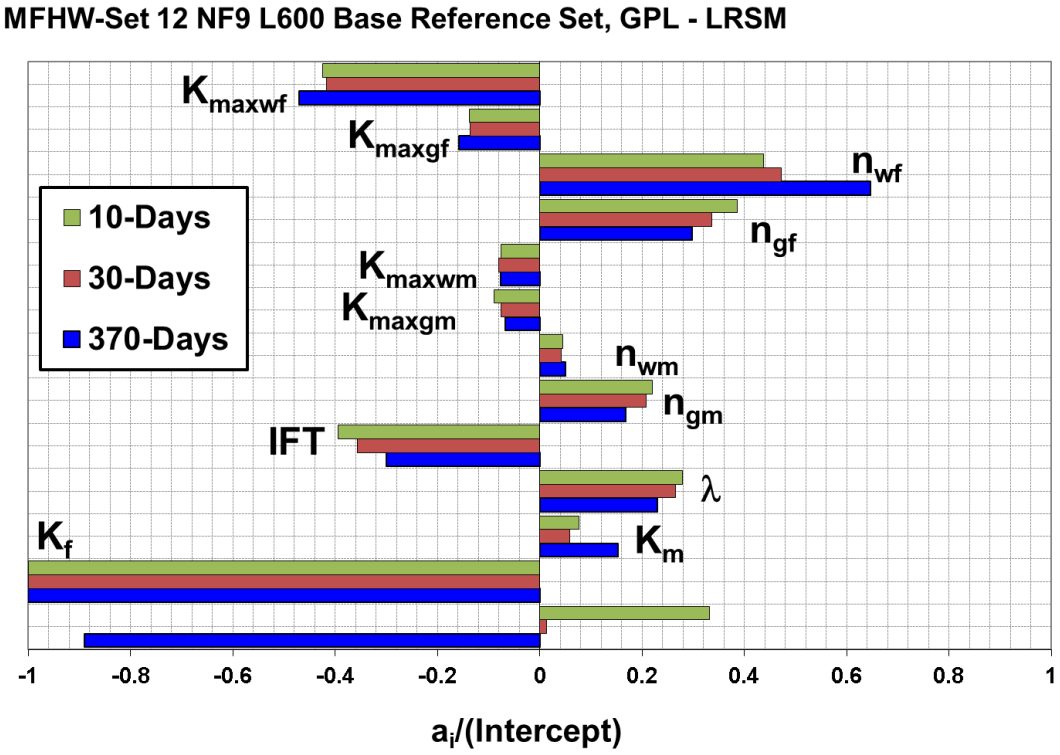

Figure 4.17 Tornado chart comparing LRSM coefficients of all pertinent parameters at three production stages for MFHW-Set12 Nf9 L600, Base Reference Set

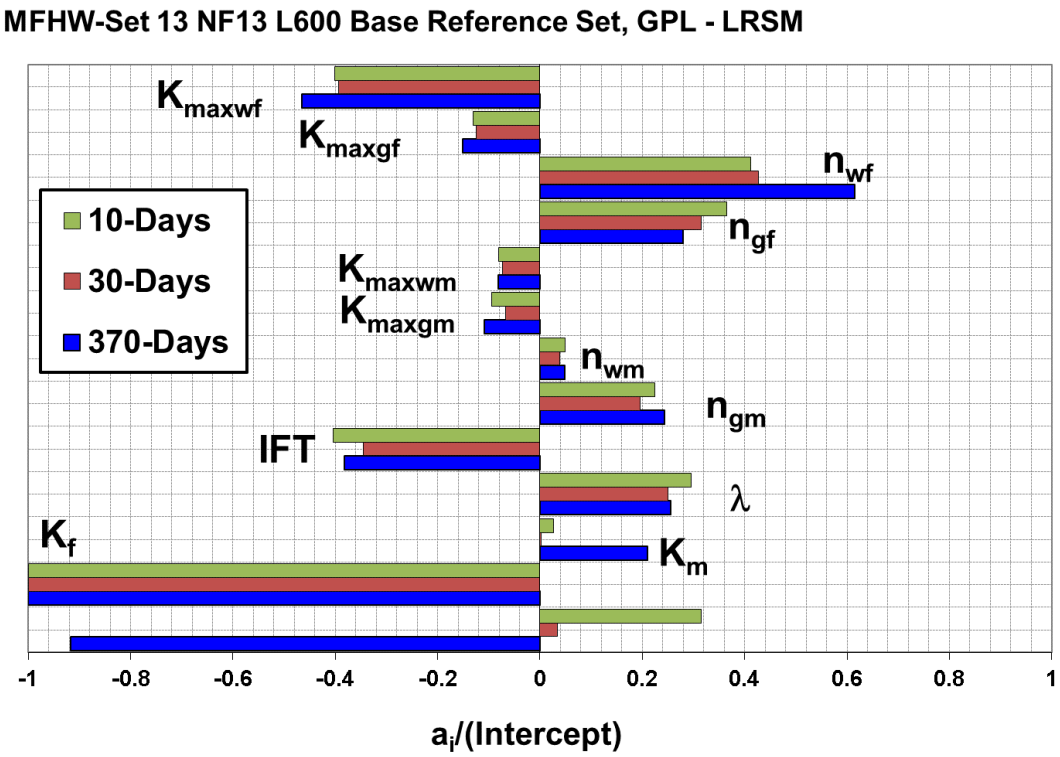

Figure 4.18 Tornado chart comparing LRSM coefficients of all pertinent parameters at three production stages for MFHW-Set13 Nf13 L600, Base Reference Set

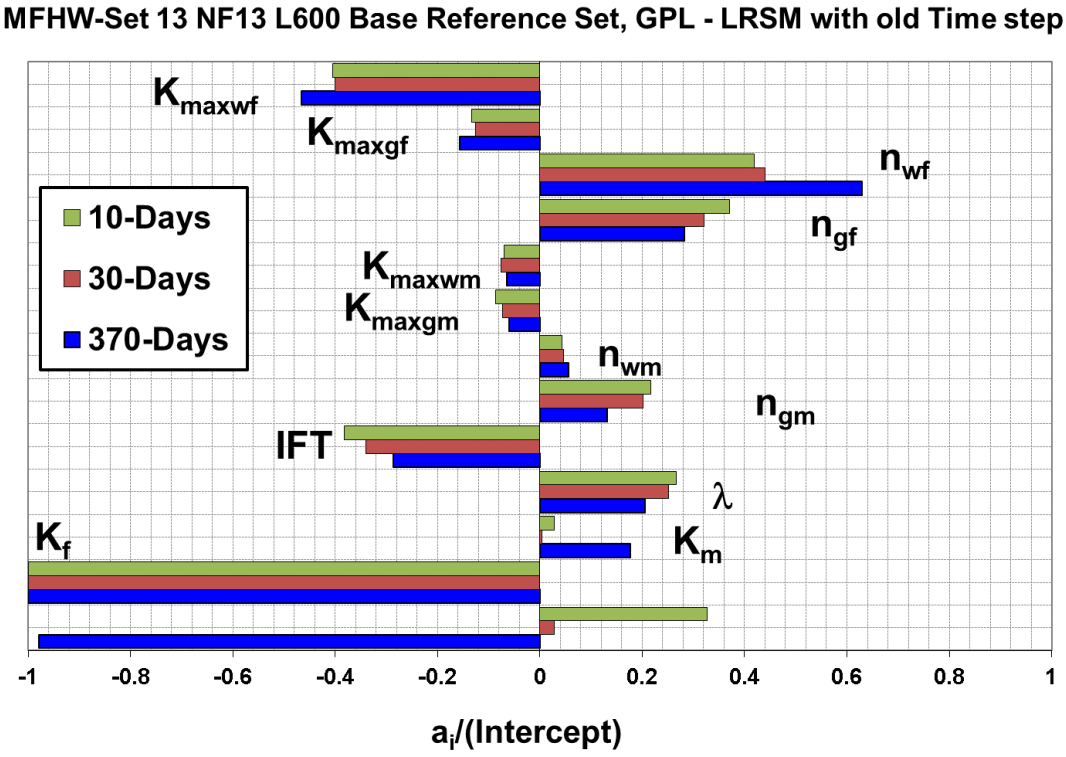

Figure 4.19 Tornado chart comparing LRSM coefficients of all pertinent parameters at three production stages for MFHW-Set13 Nf13 L600, Base Reference Set with the old time step

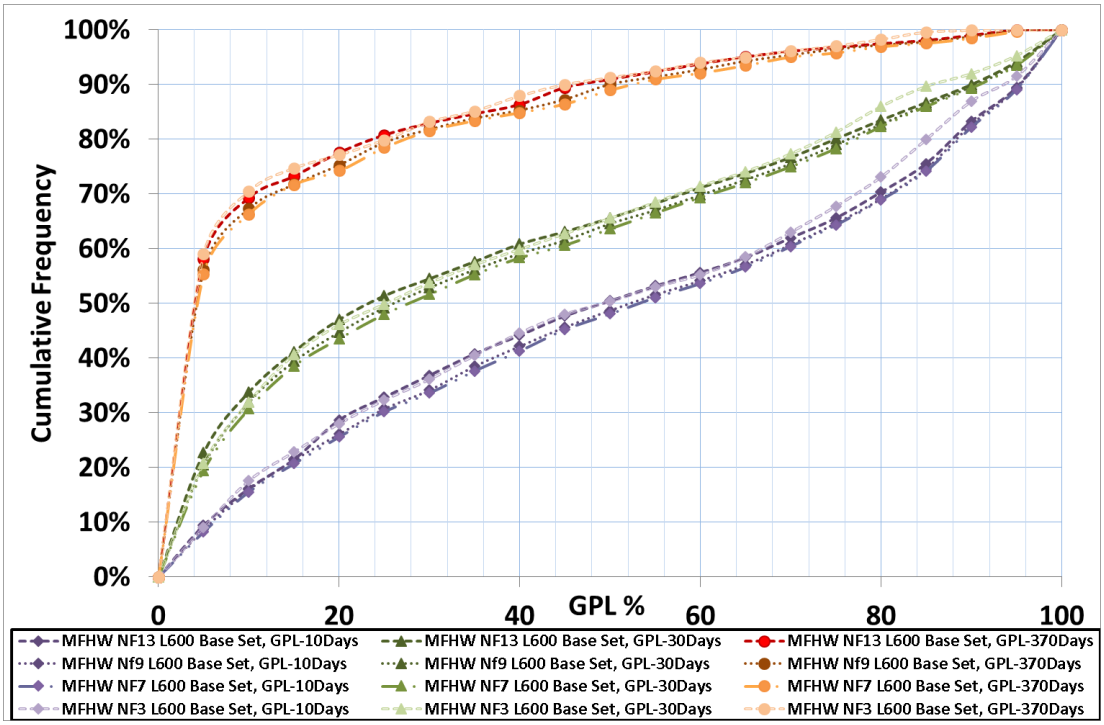

Figure 4.20 Histogram chart comparing GPL cumulative frequency of MFHW-Set 1Nf=3 with MFHW-Set 8 Base Reference set with Nf=7, MFHW-Set 12 with Nf=9 and MFHW-Set 13 with Nf=13 at three production stages.

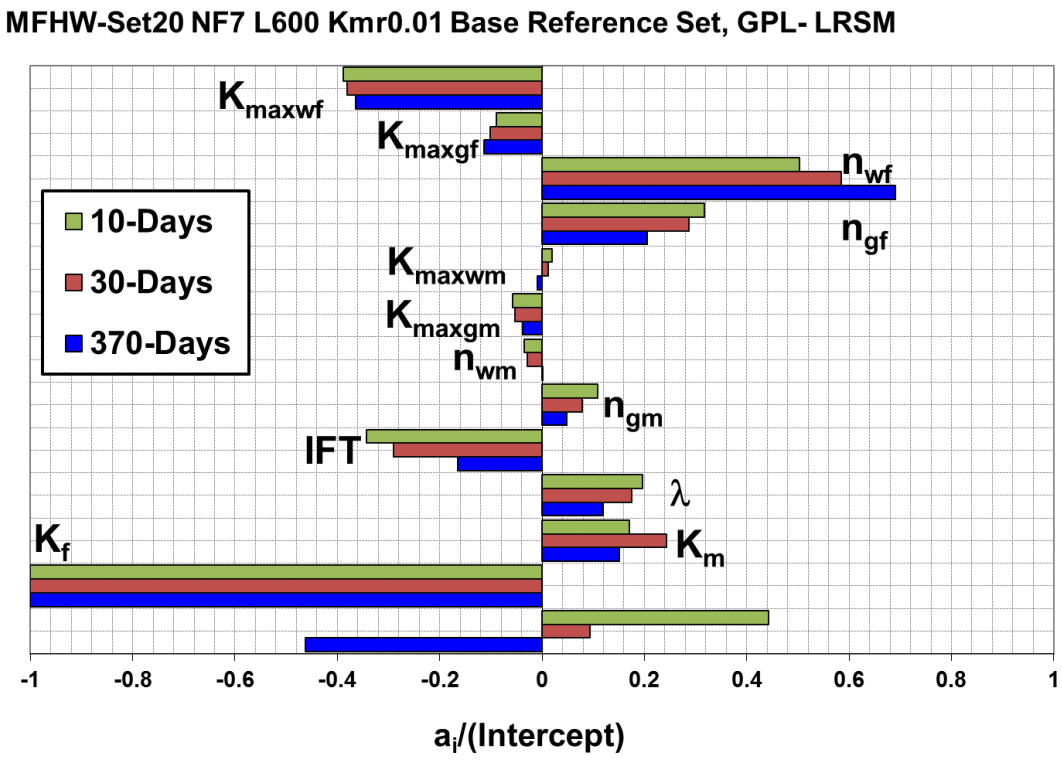

Figure 4.21 Tornado chart comparing LRSM coefficients of all pertinent parameters at three production stages for MFHW-Set20 Nf7-L600m Kmr0.01

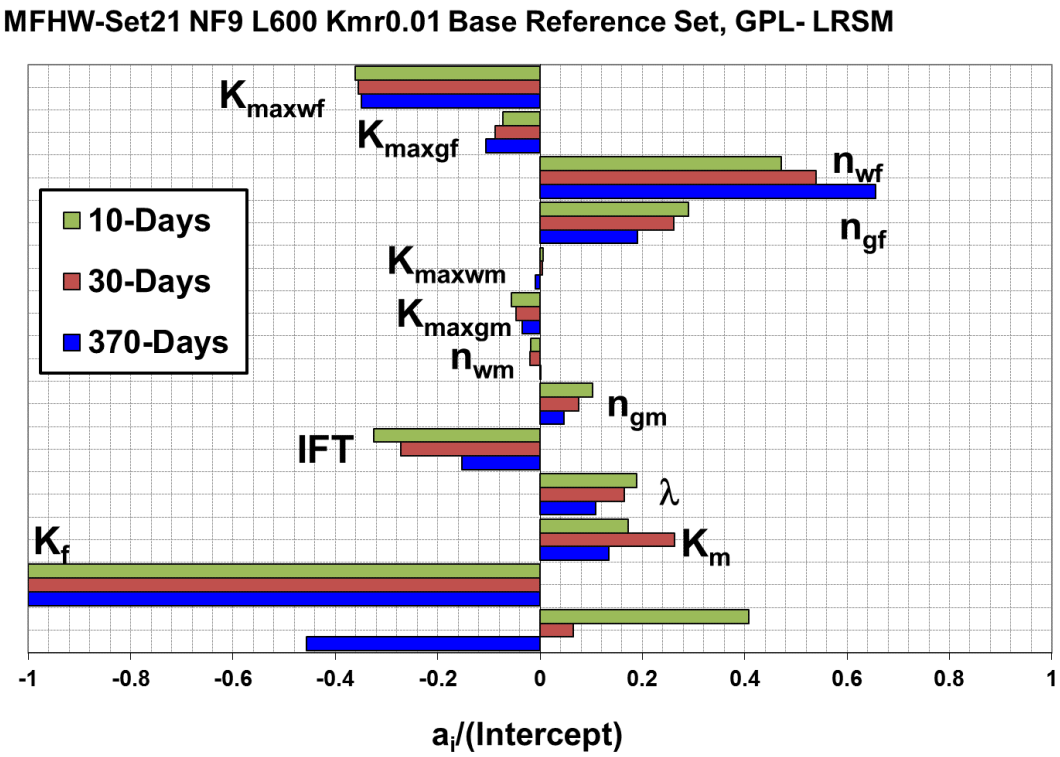

Figure 4.22 Tornado chart comparing LRSM coefficients of all pertinent parameters at three production stages for MFHW-Set21 Nf9-L600m Kmr0.01

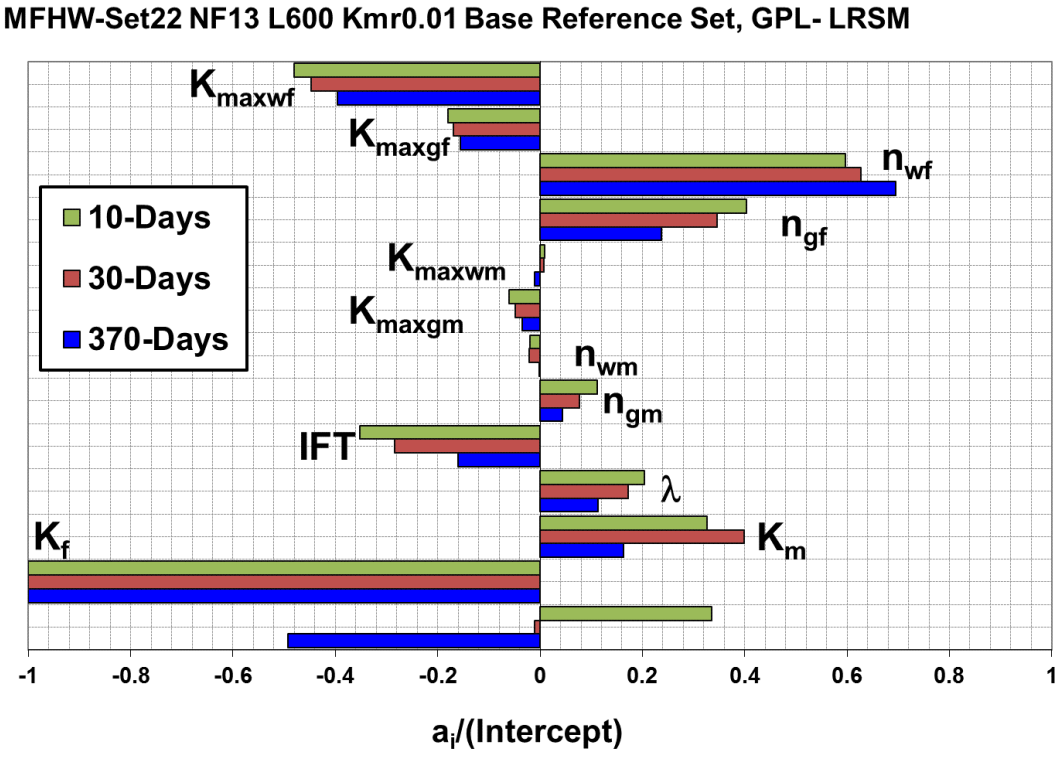

Figure 4.23 Tornado chart comparing LRSM coefficients of all pertinent parameters at three production stages for MFHW-Set22 Nf13-L600m Kmr0.01

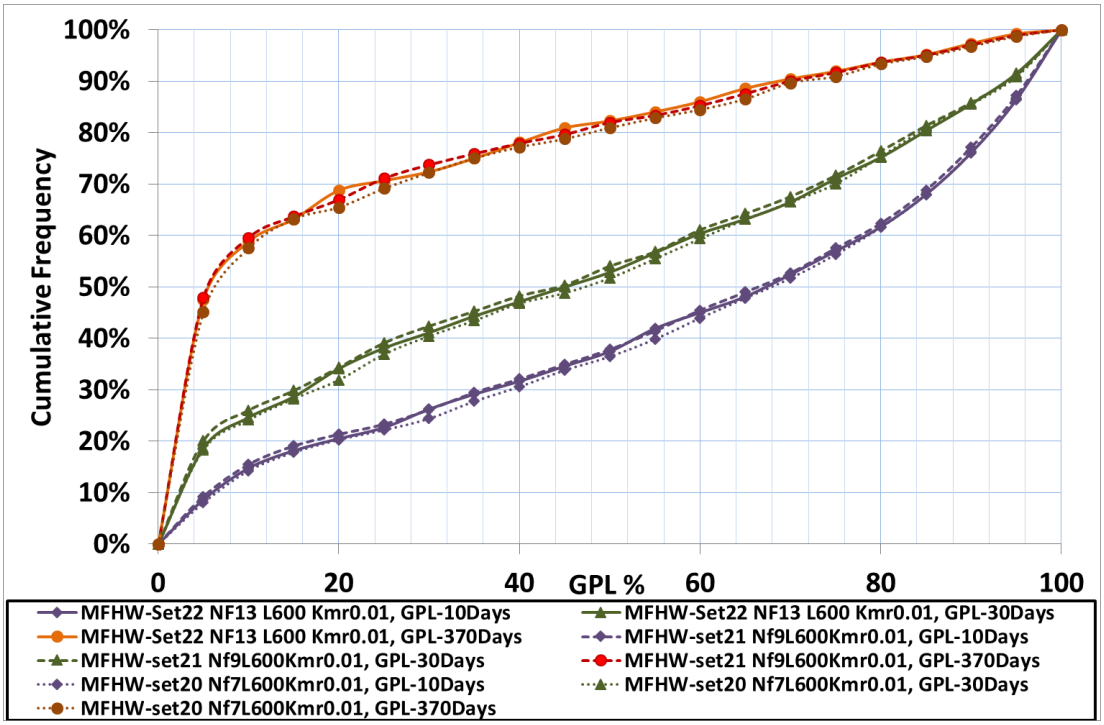

Figure 4.24 Histogram chart comparing GPL cumulative frequency of MFHW-Set20 Nf7-L600m Kmr0.01, MFHW-Set21 Nf9-L600m Kmr0.01 and MFHW-Set22 Nf13-L600m Kmr0.01 at three production stages.

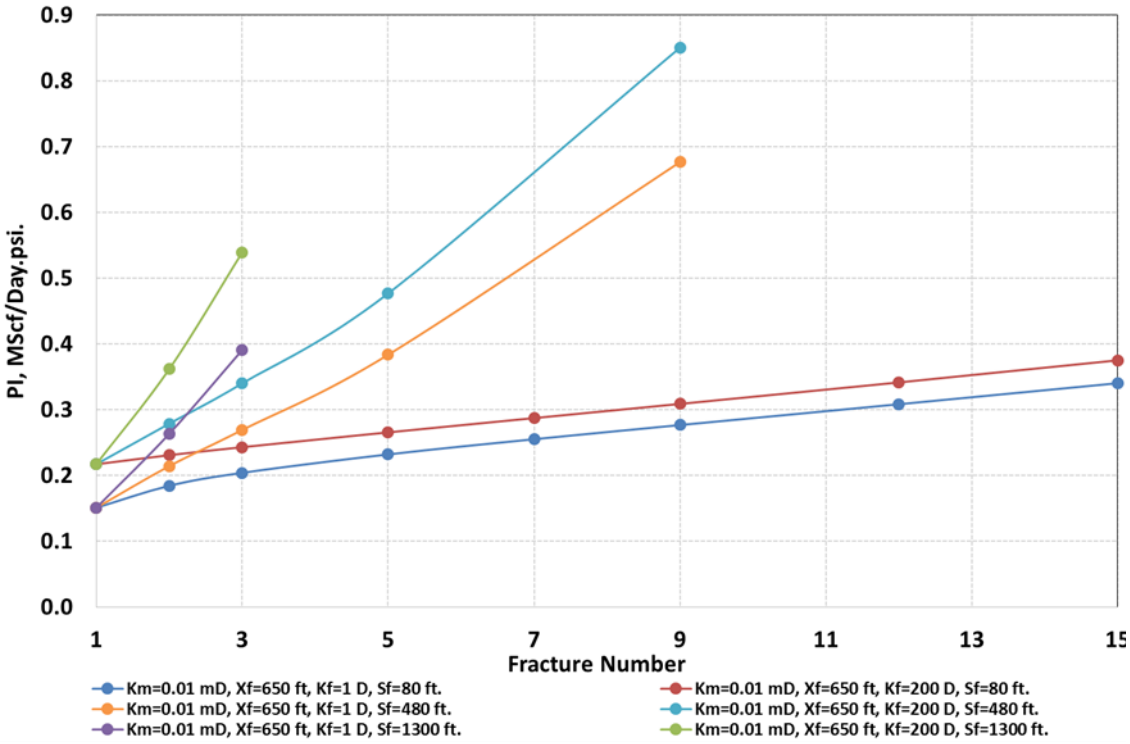

Figure 4.25 Impact of number of fracture on relative PI for various cases with Xf=110 ft. .(Ref to Gas Condensate Recovery Project' Progress Report GCRP/15/1, Oct. 2014-Apr. 2015, April 2015, Heriot-Watt University, Institute of Petroleum Engineering, Chapter 5, Figure 5.6)

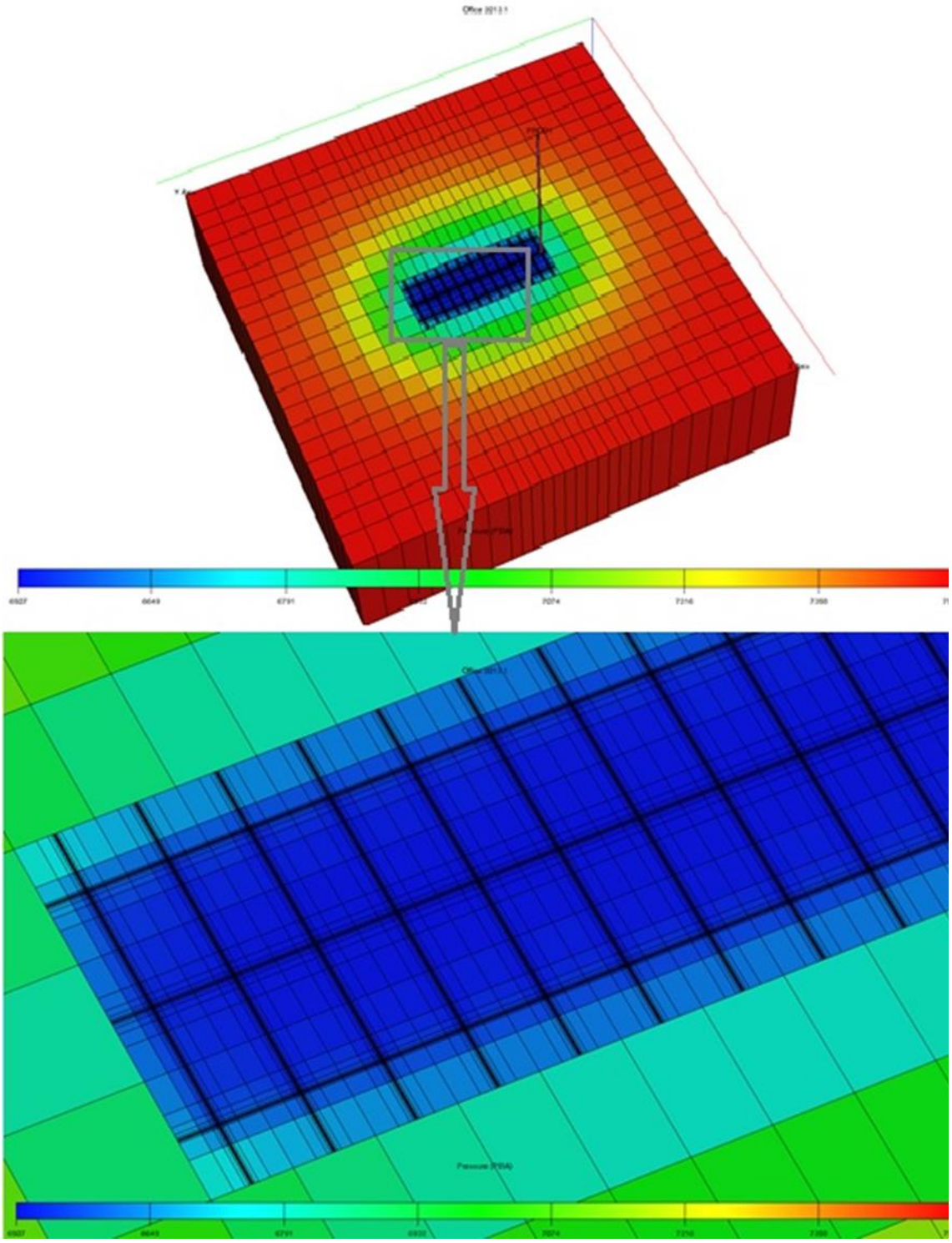

Figure 4.26 Pressure distribution map of MFHW-Set22 after one year of production (Red is 7500 psi and Blue is 6500 psi), the pressure disturbance is observed by adjacent fractures.

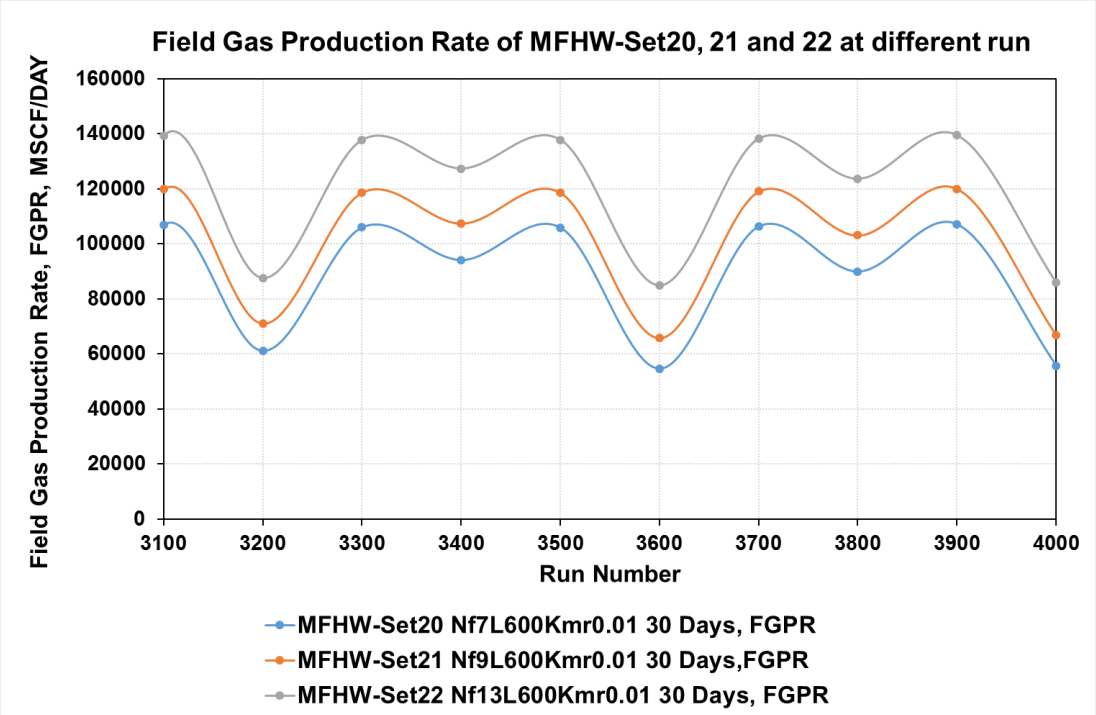

Figure 4.27 Comparison of Gas production rates vs run number in MFHW-Set20 Nf7-L600m Kmr0.01, MFHW-Set21 Nf9-L600m Kmr0.01 and MFHW-Set22 Nf13-L600m Kmr0.01 at 30 days production.

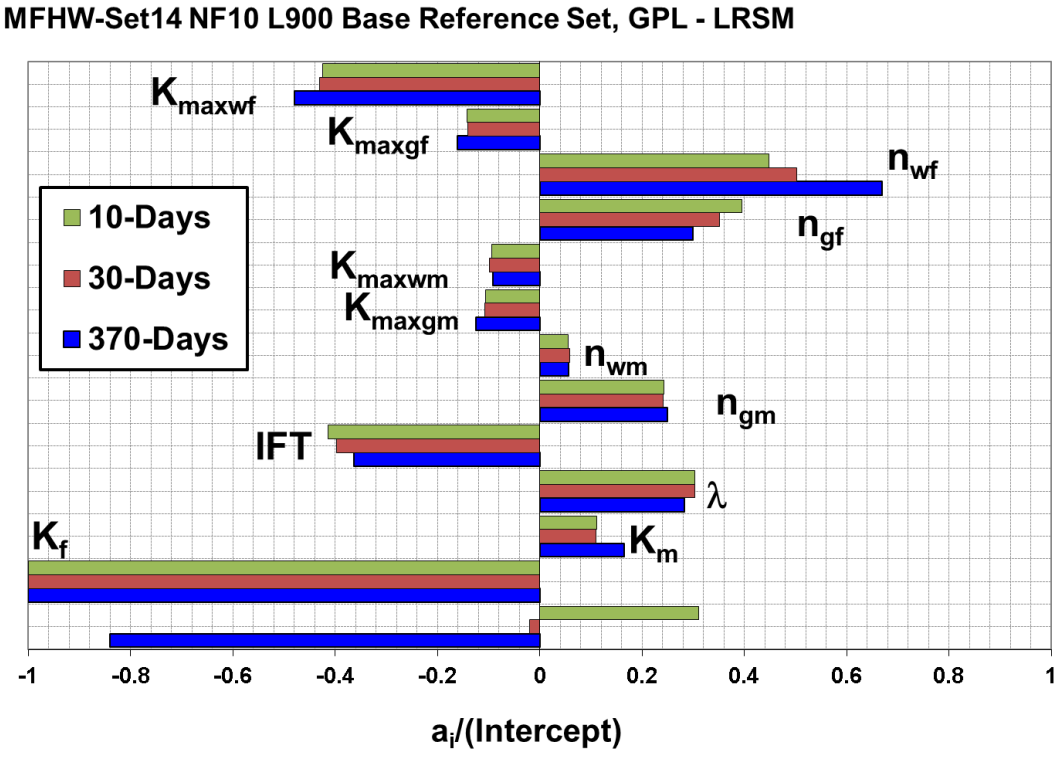

Figure 4.28 Tornado chart comparing LRSM coefficients of all pertinent parameters at three production stages for MFHW-Set14 Nf10 L600, Base Reference Set

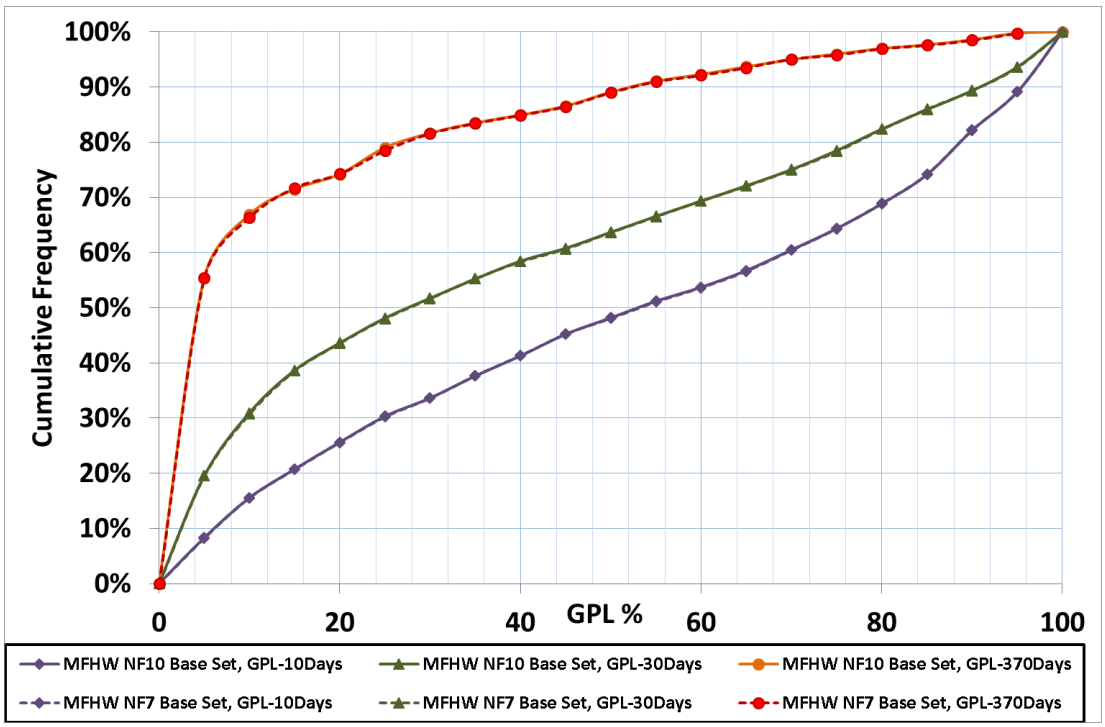

Figure 4.29 Histogram chart comparing GPL cumulative frequency of MFHW-Set 8 Base Reference set with Nf=7 with MFHW-Set 14 with Nf=10 at three production stages.

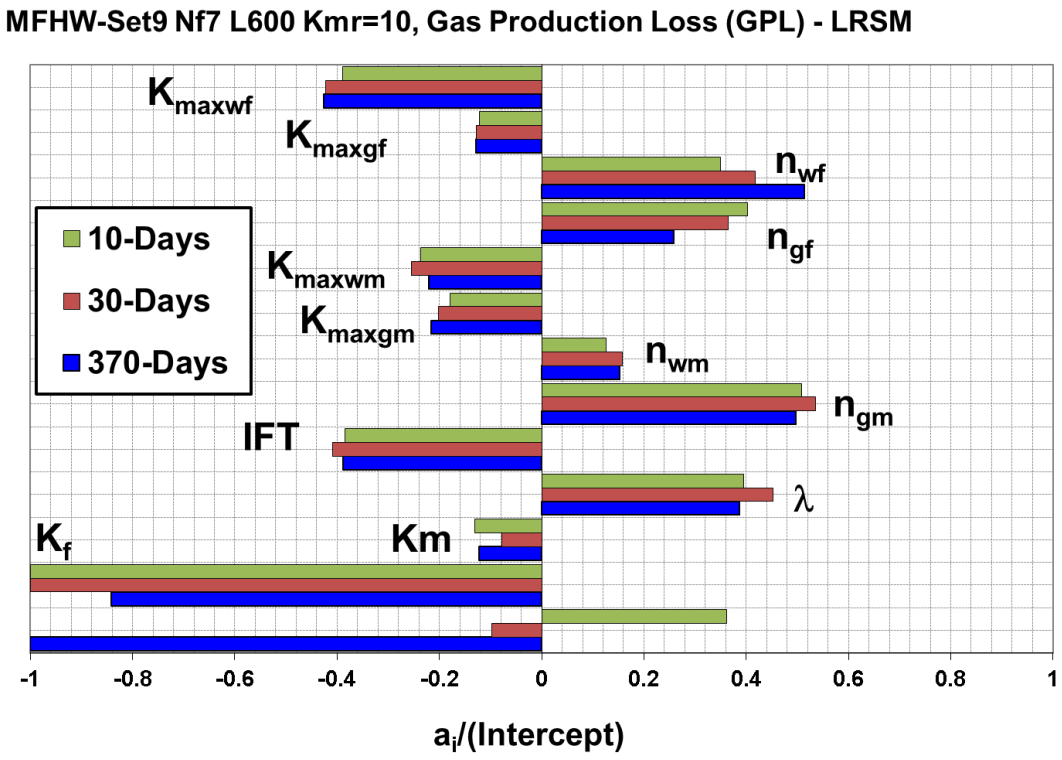

Figure 4.30 Tornado chart comparing LRSM coefficients of all pertinent parameters at three production stages for MFHW-Set9 Nf7 L600 Kmr=10, Base Reference Set

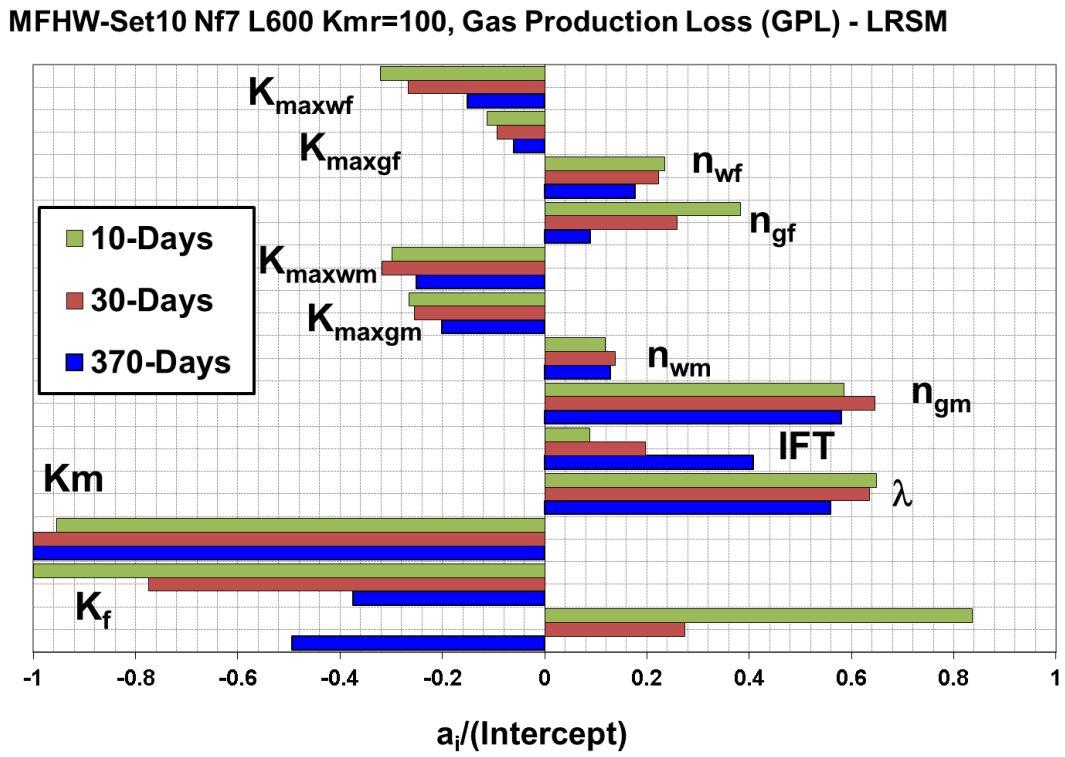

Figure 4.31 Tornado chart comparing LRSM coefficients of all pertinent parameters at three production stages for MFHW-Set10 Nf7 L600 Kmr=100, Base Reference Set

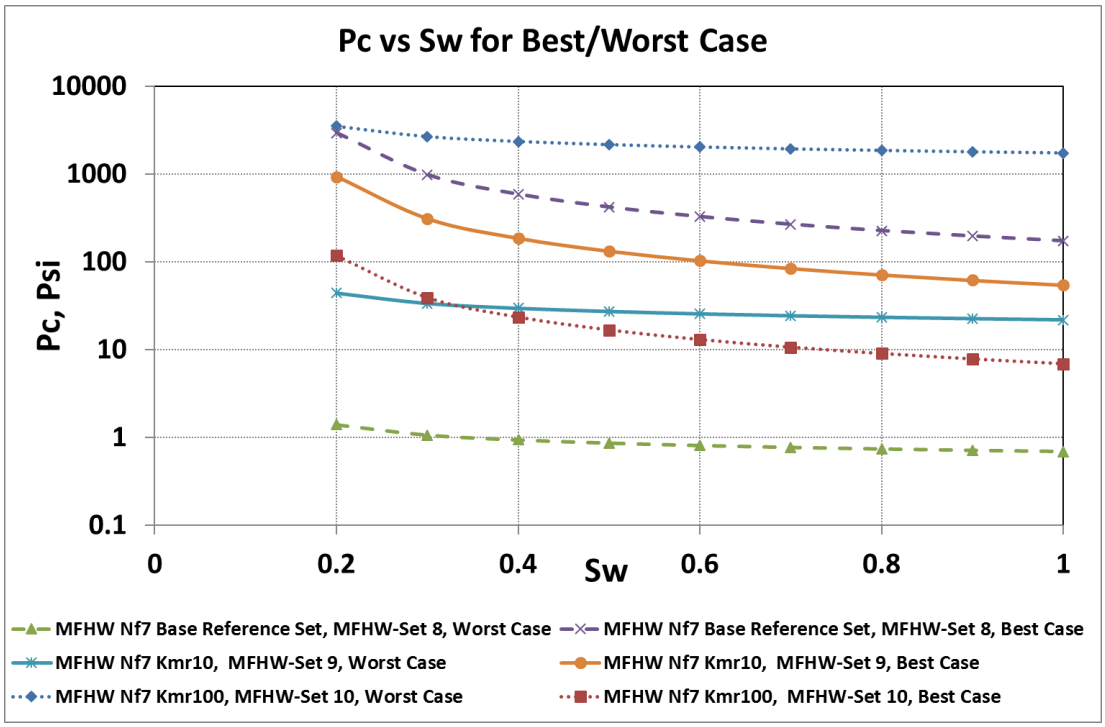

Figure 4.32 Pc vs. Sw for best/Worst Case of Sets MFHW-Set8, MFHW-Set9 and MFHW-Set10.

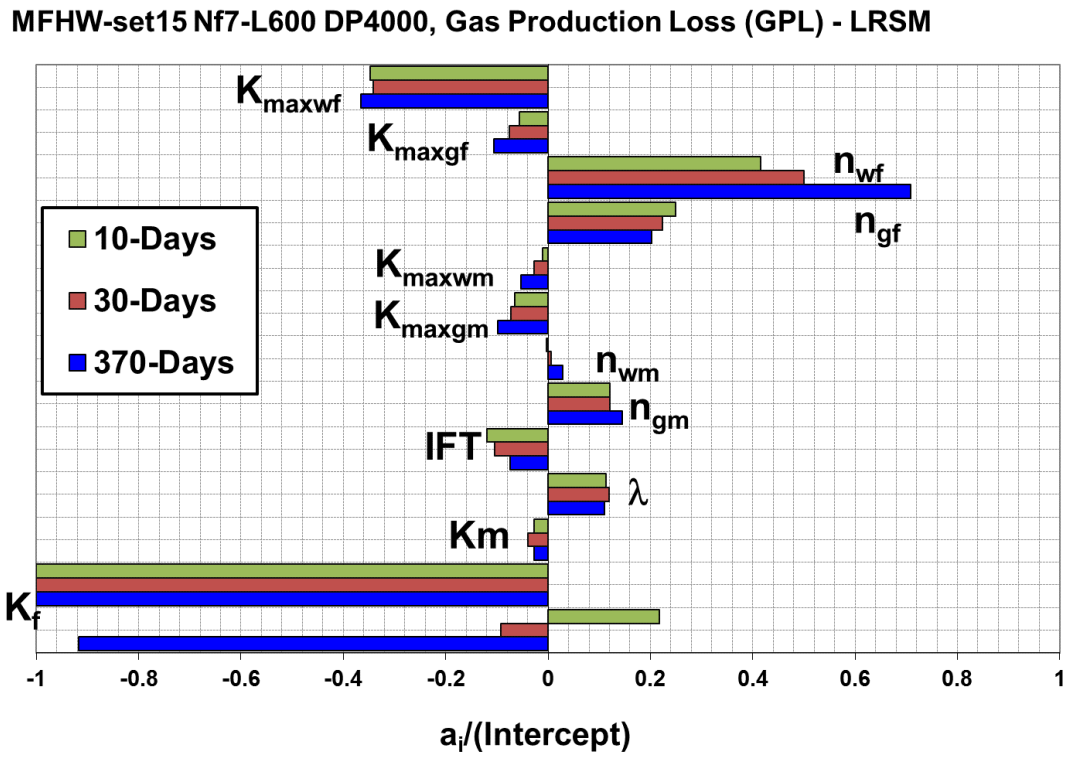

Figure 4.33 Tornado chart comparing LRSM coefficients of all pertinent parameters at three production stages for MFHW-Set15 Nf7-L600m DP4000

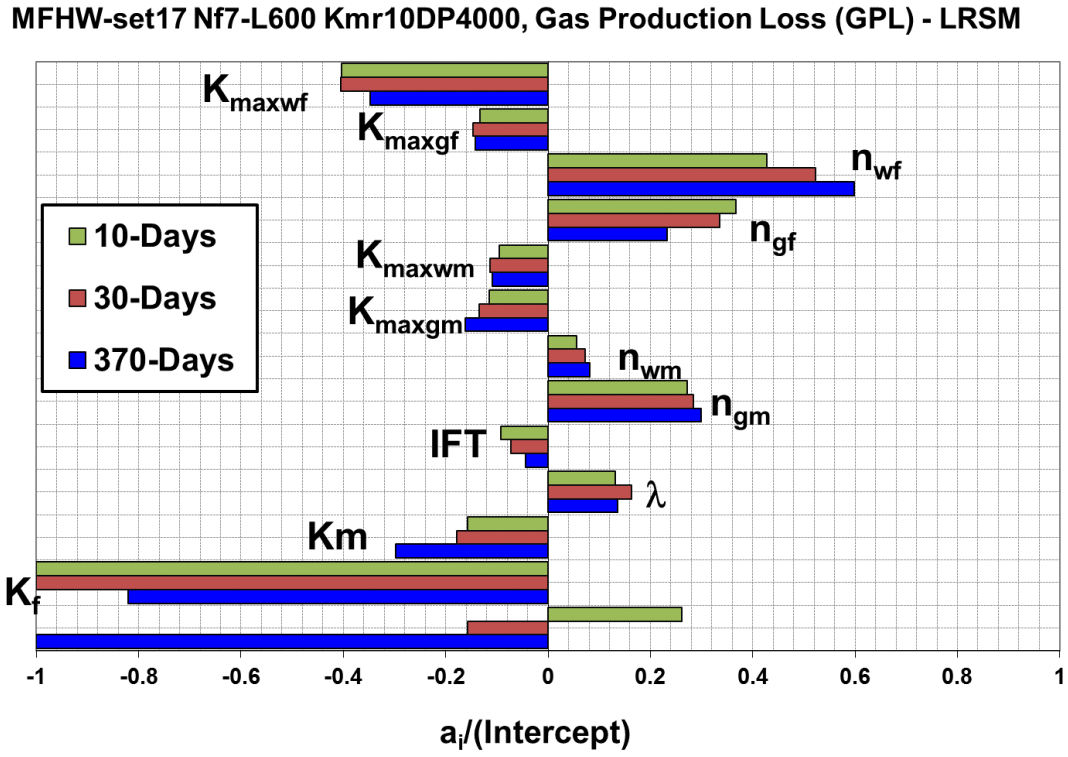

Figure 4.34 Tornado chart comparing LRSM coefficients of all pertinent parameters at three production stages for MFHW-Set17 Nf7-L600m Kmr10DP4000

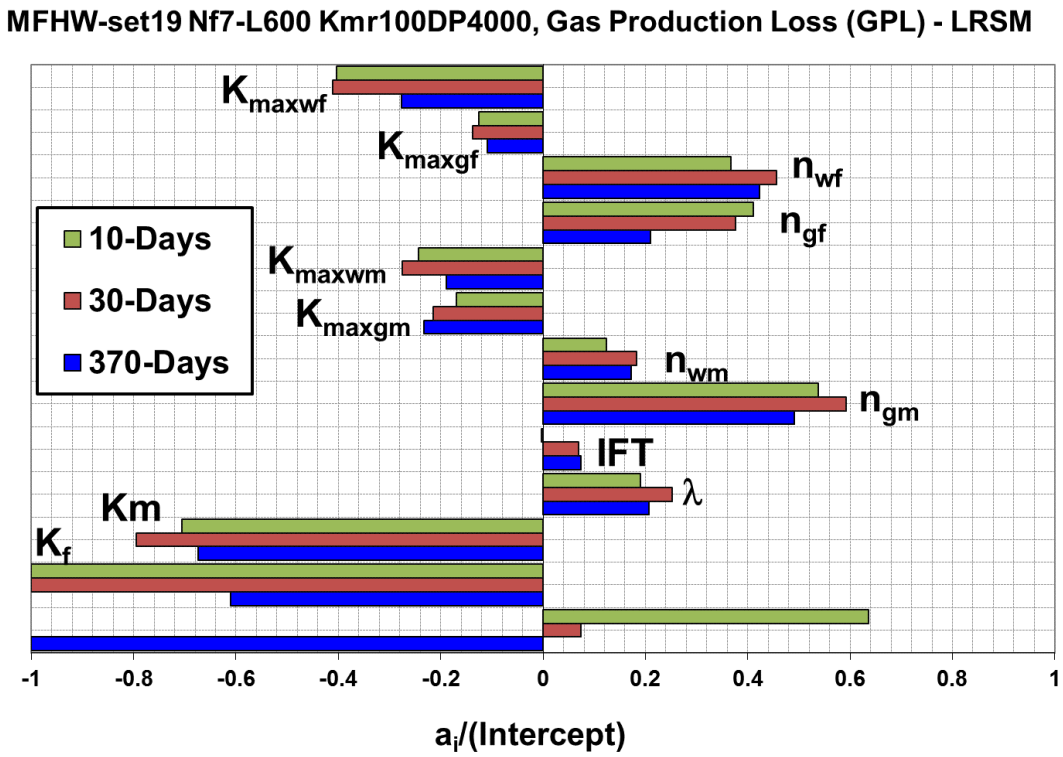

Figure 4.35 Tornado chart comparing LRSM coefficients of all pertinent parameters at three production stages for MFHW-Set19 Nf7-L600m Kmr100 DP4000

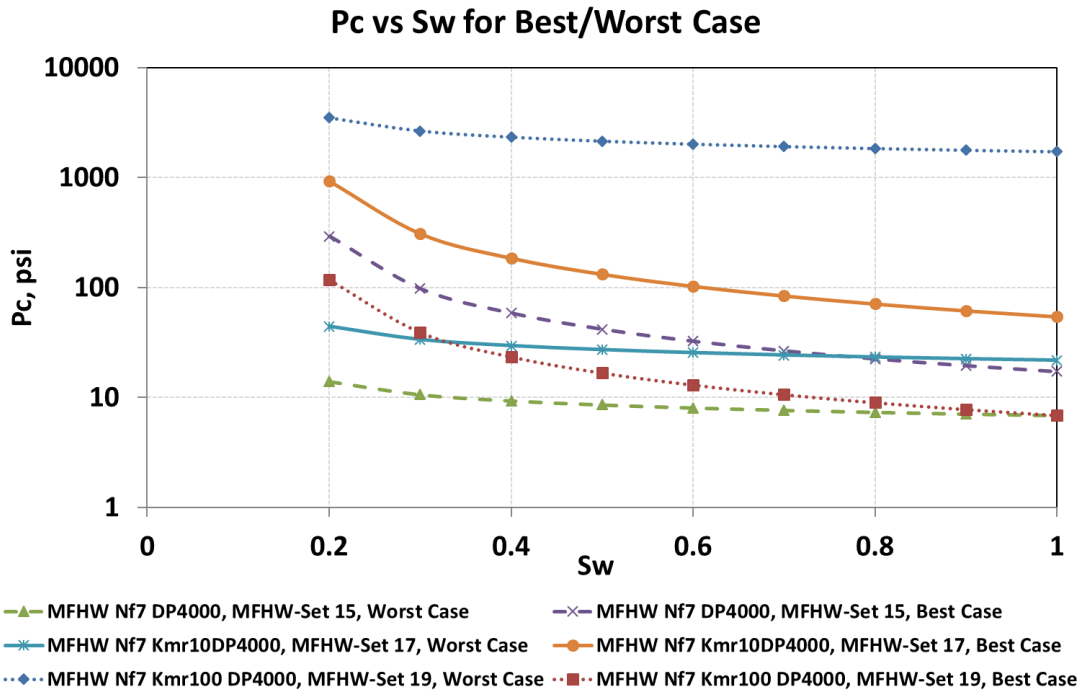

Figure 4.36 Pc vs. Sw for best/Worst Case of MFHW-Set15, MFHW-Set17 and MFHW-Set19

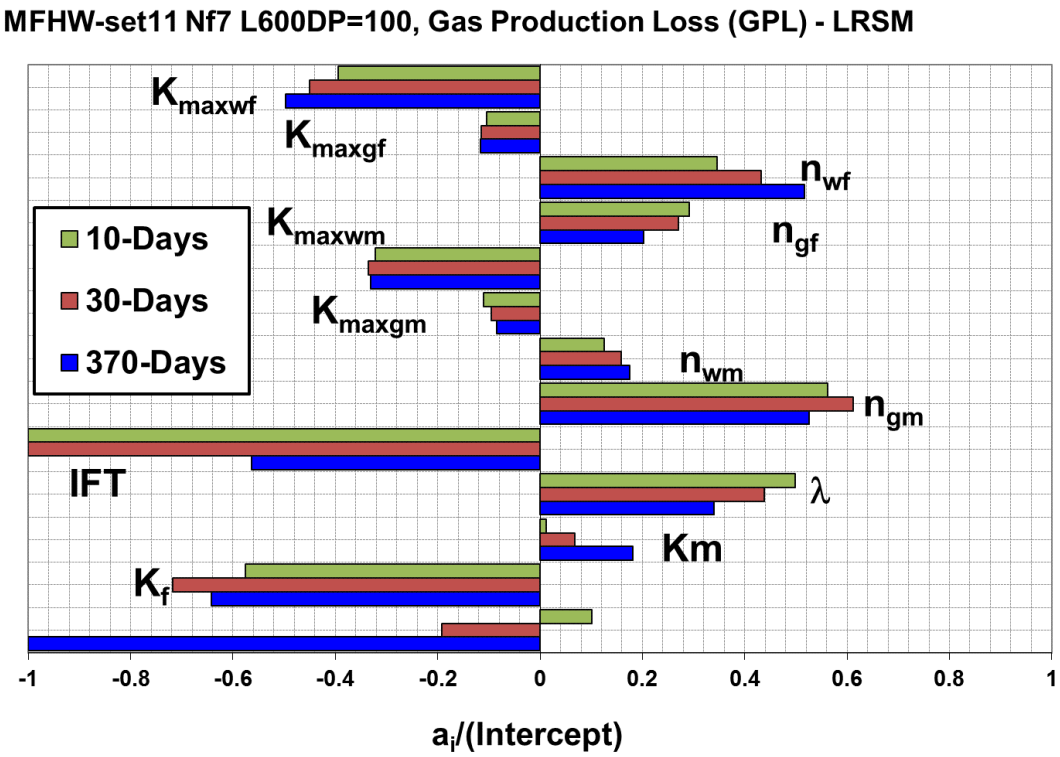

Figure 4.37 Tornado chart comparing LRSM coefficients of all pertinent parameters at three production stages for MFHW-Set11 Nf7-L600m DP100

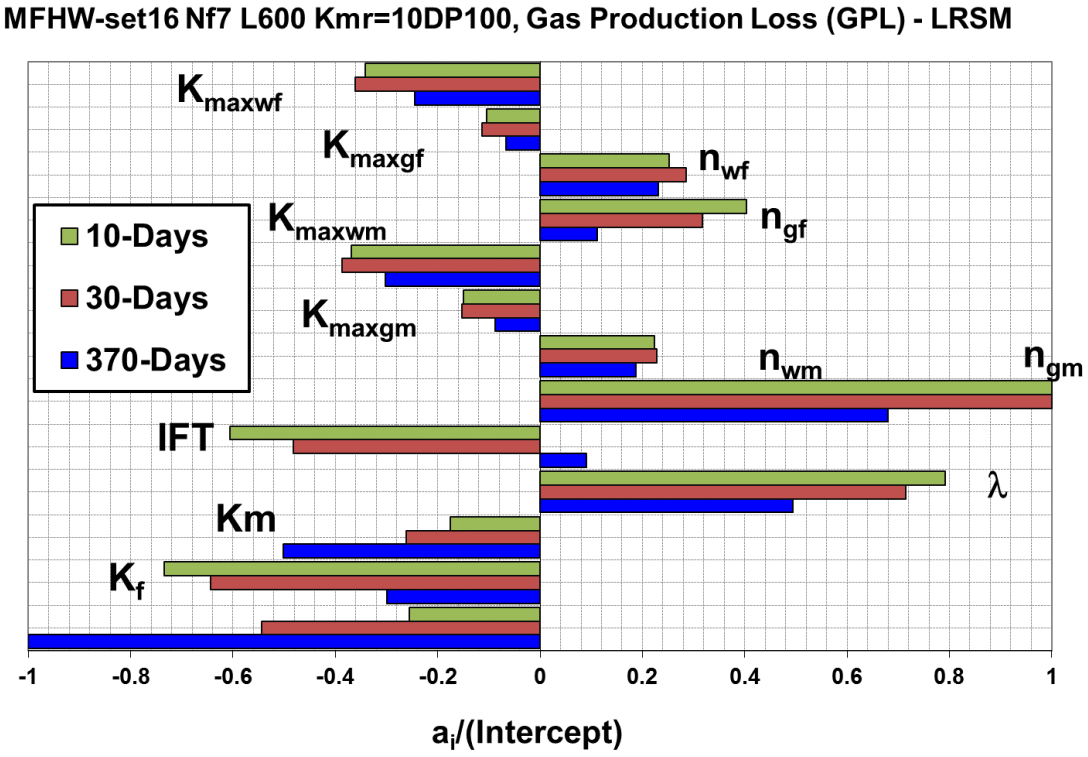

Figure 4.38 Tornado chart comparing LRSM coefficients of all pertinent parameters at three production stages for MFHW-Set16 Nf7-L600m Kmr10DP100

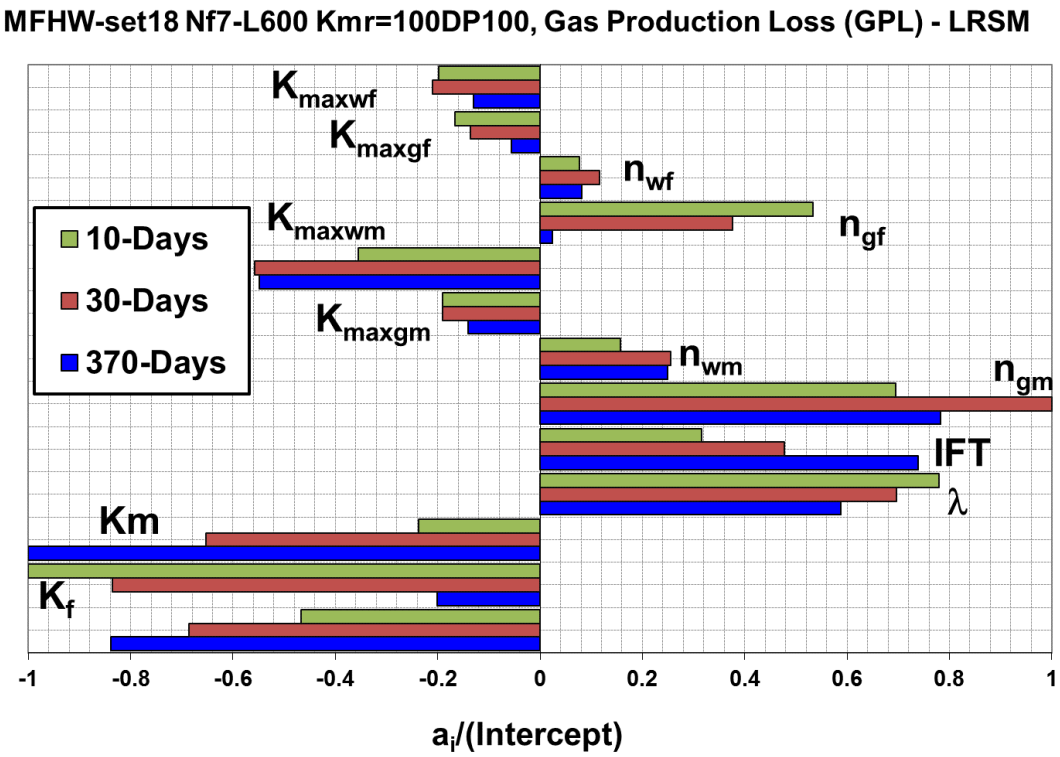

Figure 4.39 Tornado chart comparing LRSM coefficients of all pertinent parameters at three production stages for MFHW-Set18 Nf7-L600m Kmr100DP100

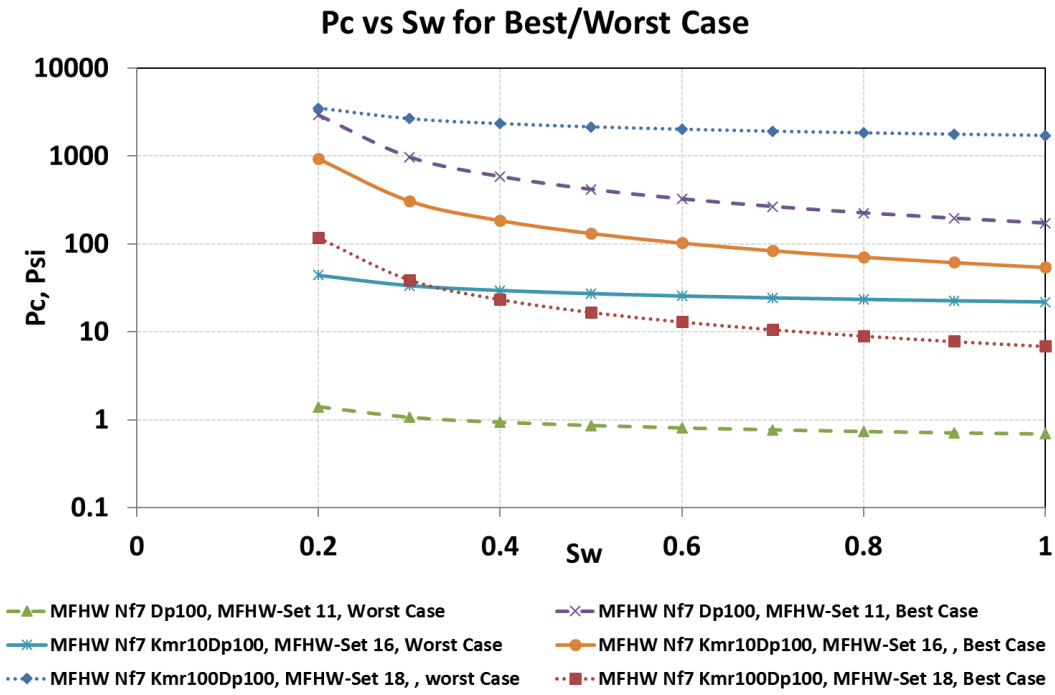

Figure 4.40 Pc vs. Sw for best/Worst Case of MFHW-Set11, MFHW-Set16 and MFHW-Set18

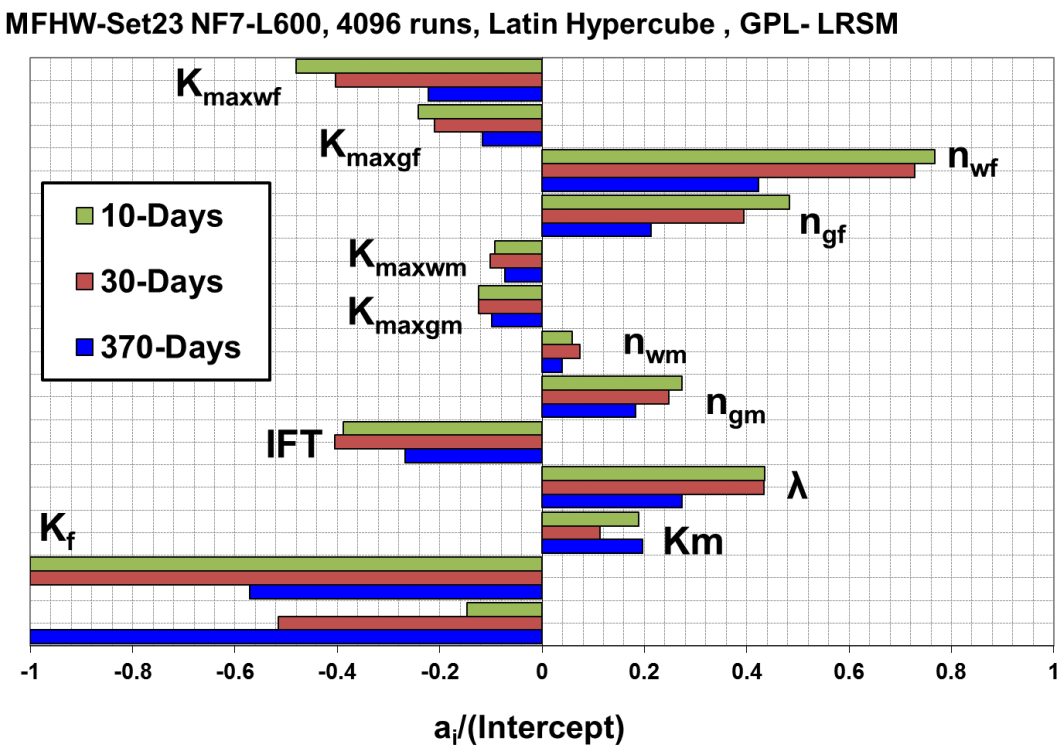

Figure 4.41 Tornado chart comparing LRSM coefficients of all pertinent parameters at three production stages for MFHW-Set23 Nf7 L600m Base Reference sets with LHS with 4096 Runs

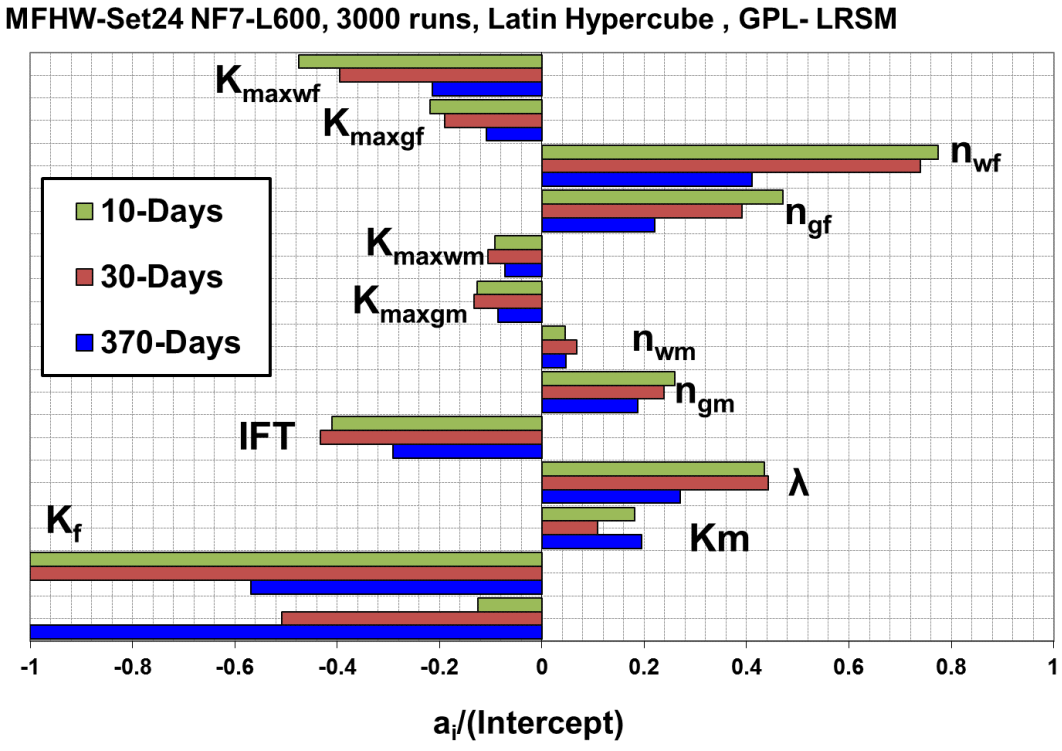

Figure 4.42 Tornado chart comparing LRSM coefficients of all pertinent parameters at three production stages for MFHW-Set24 Nf7 L600m Base Reference sets with LHS with 3000 Runs

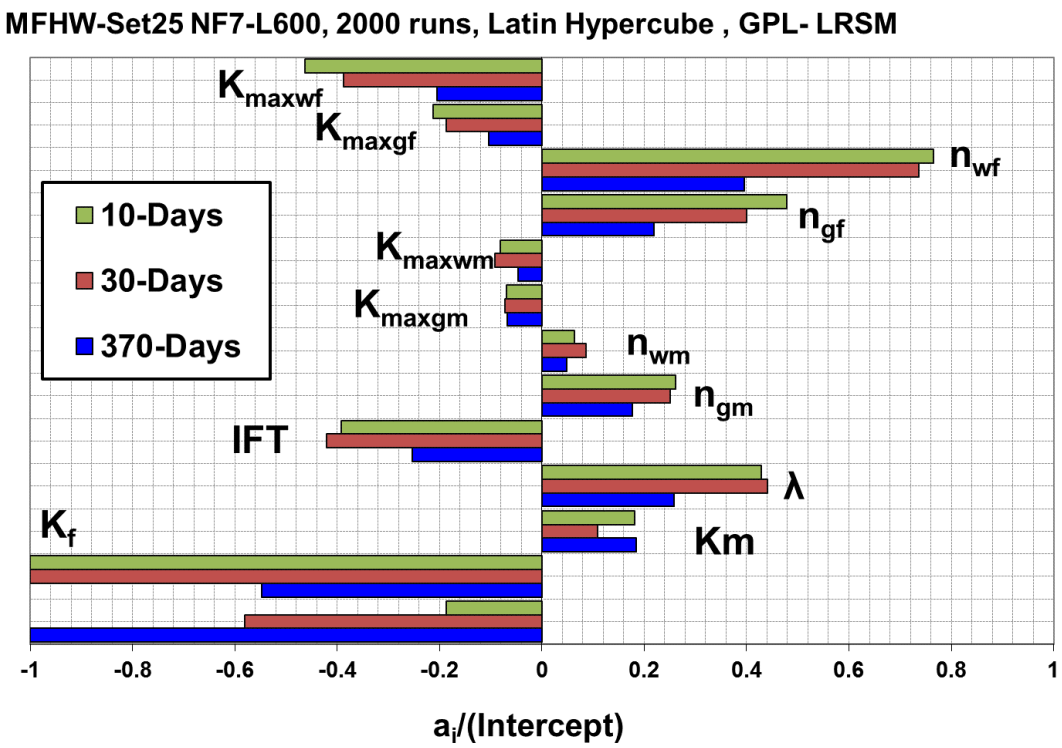

Figure 4.43 Tornado chart comparing LRSM coefficients of all pertinent parameters at three production stages for MFHW-Set25 Nf7 L600m Base Reference sets with LHS with 2000 Runs

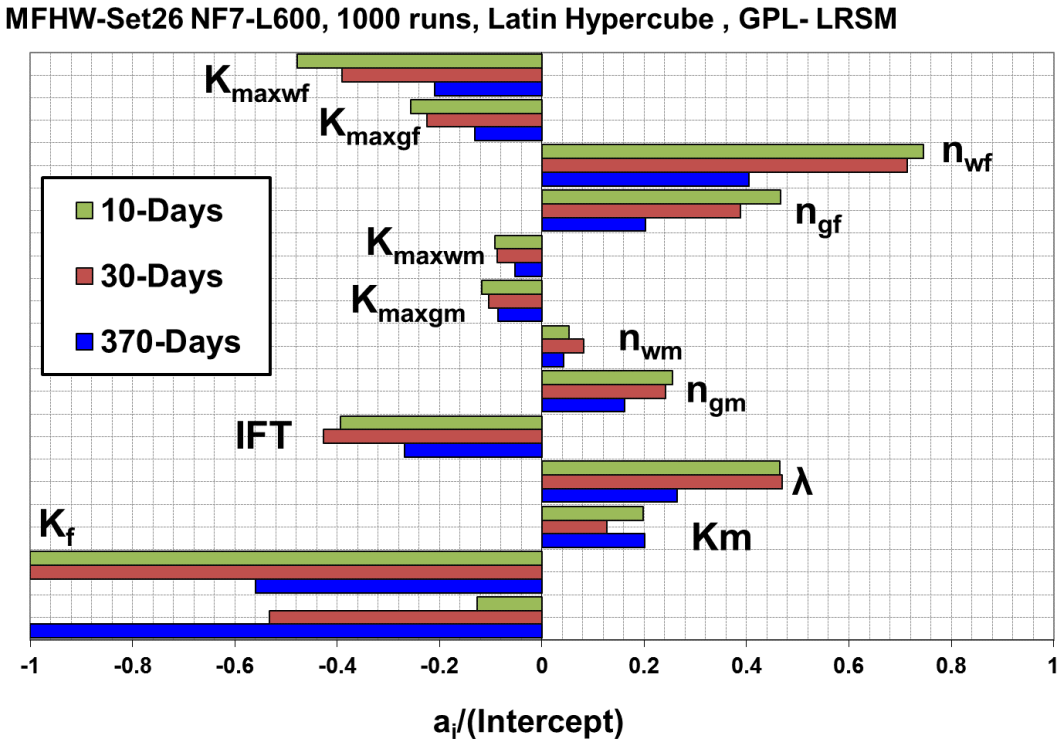

Figure 4.44 Tornado chart comparing LRSM coefficients of all pertinent parameters at three production stages for MFHW-Set26 Nf7 L600m Base Reference sets with LHS with 1000 Runs

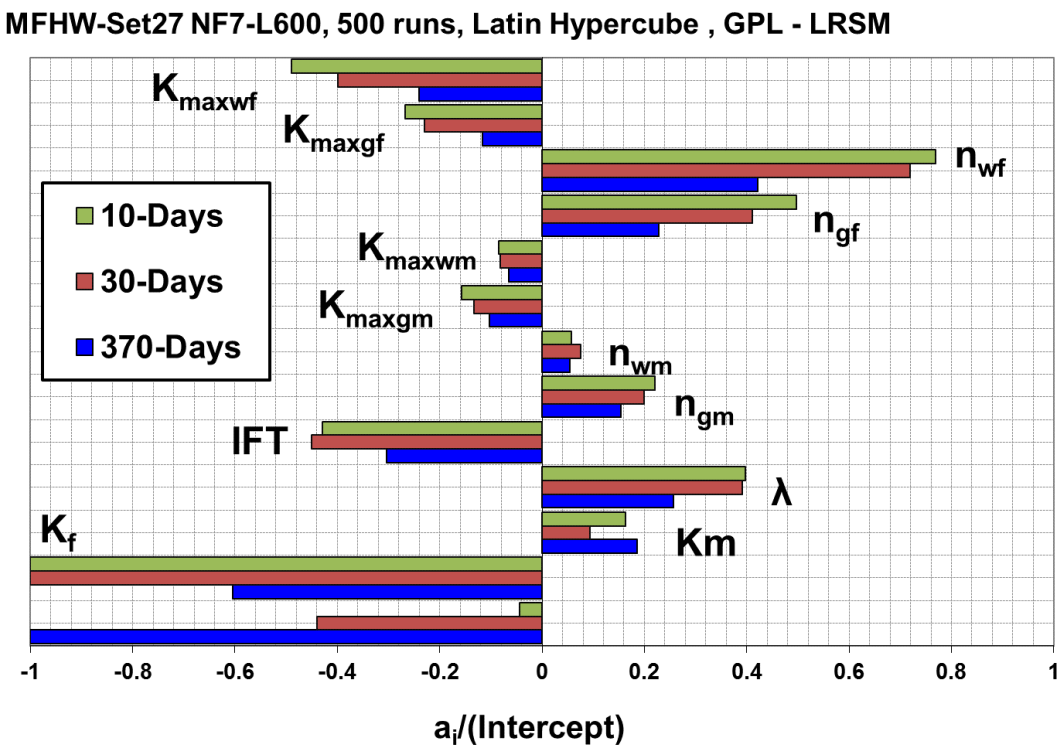

Figure 4.45 Tornado chart comparing LRSM coefficients of all pertinent parameters at three production stages for MFHW-Set27 Nf7 L600m Base Reference sets with LHS with 500 Runs

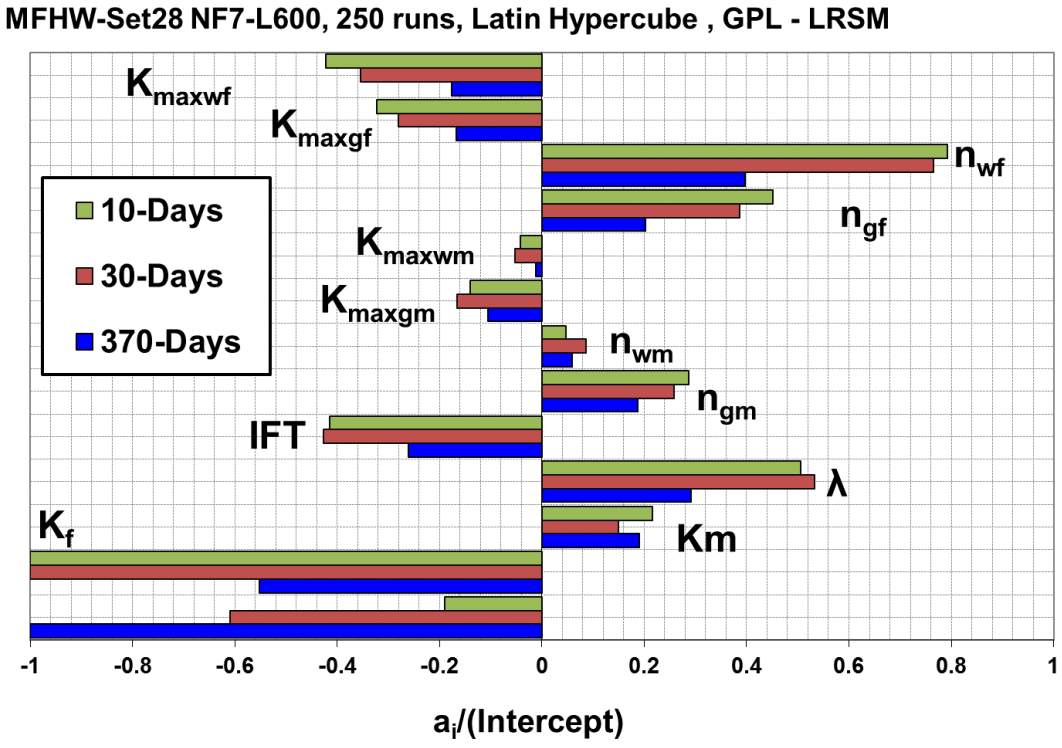

Figure 4.46 Tornado chart comparing LRSM coefficients of all pertinent parameters at three production stages for MFHW-Set28 Nf7 L600m Base Reference sets with LHS with 250 Runs

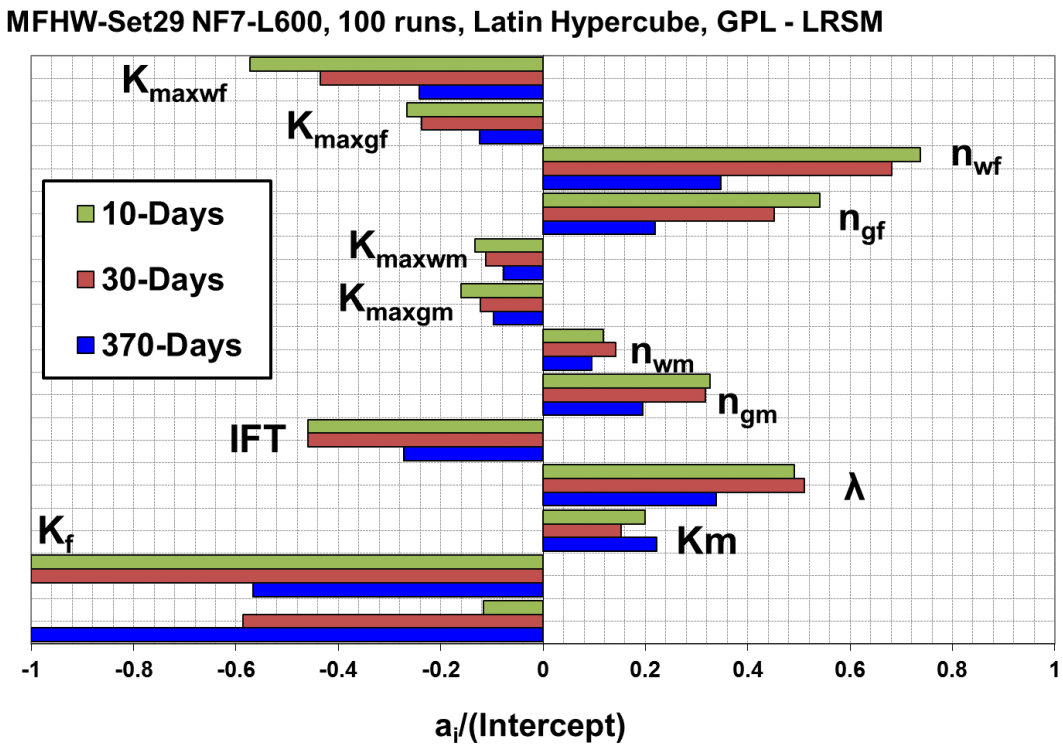

Figure 4.47 Tornado chart comparing LRSM coefficients of all pertinent parameters at three production stages for MFHW-Set29 Nf7 L600m Base Reference sets with LHS with 100 Runs

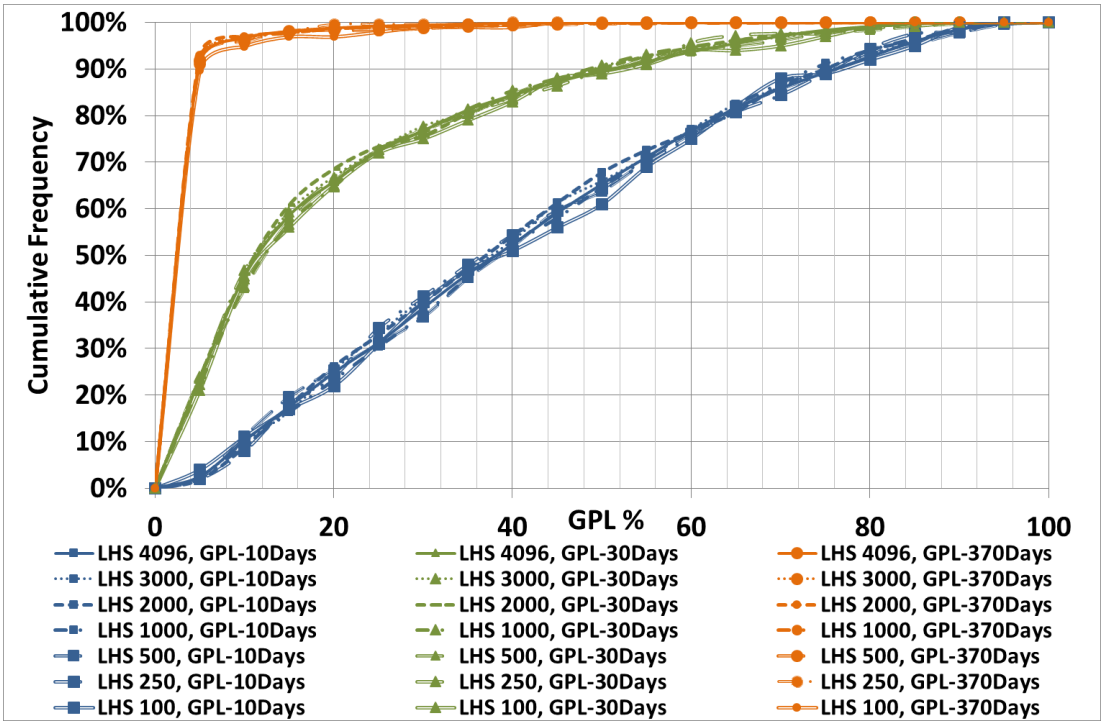

Figure 4.48 : Histogram chart comparing GPL cumulative frequency of MFHW Base reference sets using LHS with different run numbers, (a) LHS with 4096 Runs, (b) LHS with 3000 Runs, (c) LHS with 2000 Runs, (d) LHS with 1000 Runs, (e) LHS with 500 Runs, (f) LHS with 250 Runs and (g) LHS with 100 Runs.

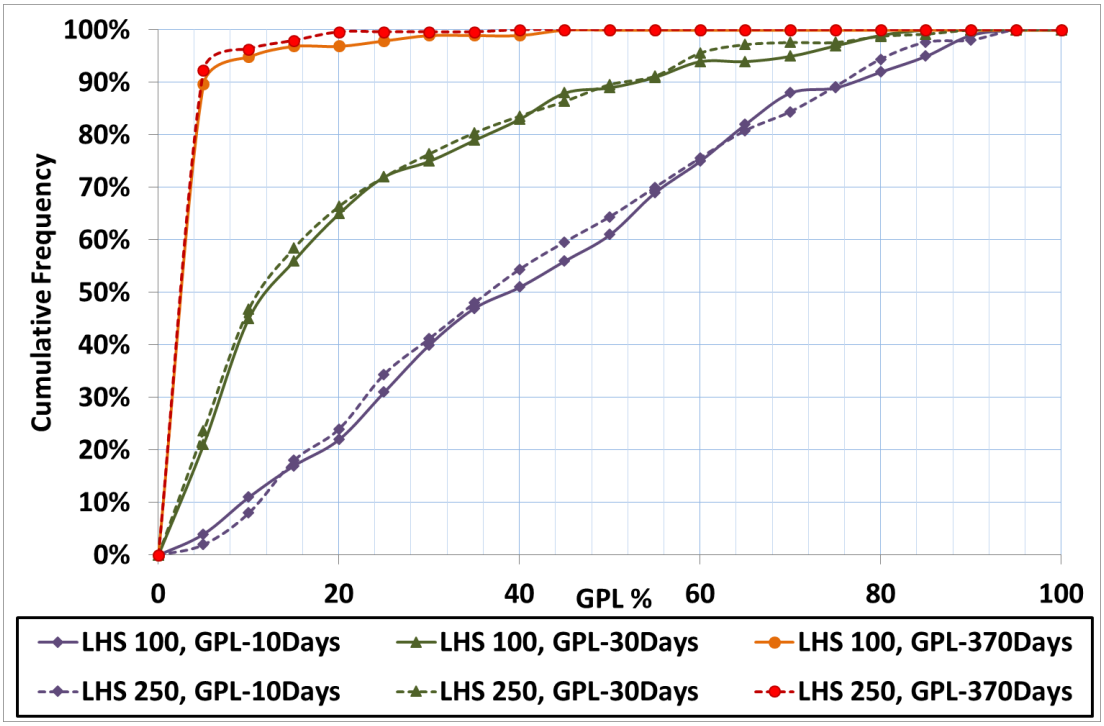

Figure 4.49 Histogram chart comparing GPL cumulative frequency of MFHW Base reference sets using LHS with 250 and 100 run numbers.

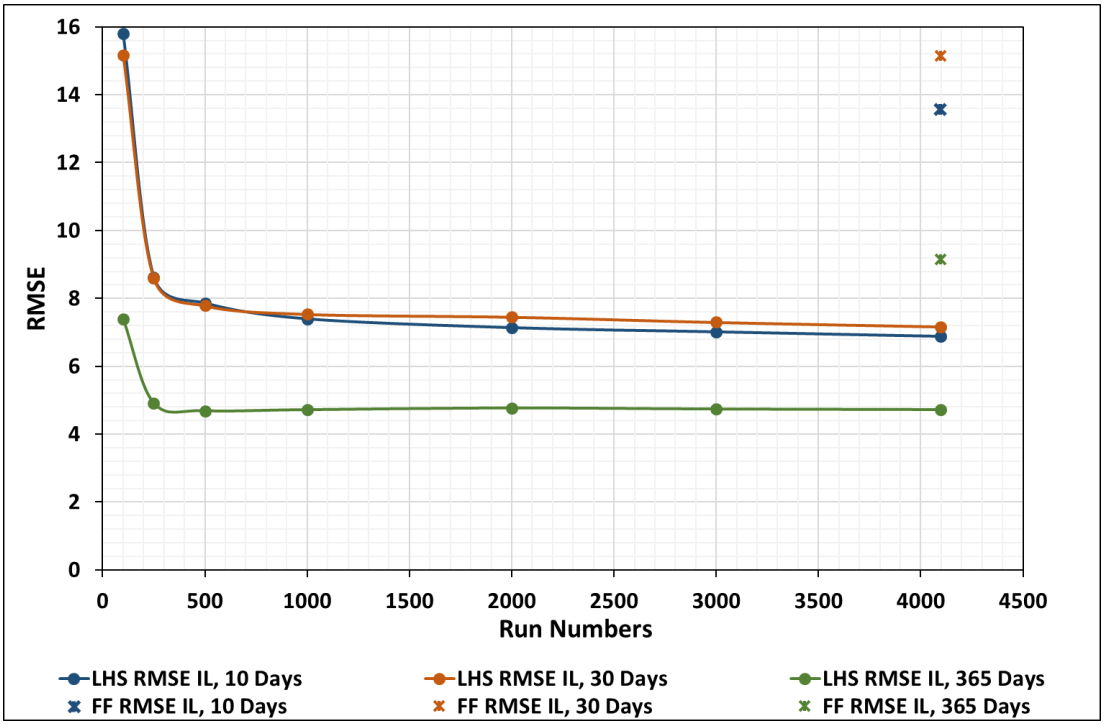

Figure 4.50 RMSE of interactive linear surface models (ILRSM) versus run numbers at three production stages for MFHW Nf7 L600m Base Reference sets with different sampling approaches, i.e., Latin Hyper Cube Sampling, LHS, and two level Full Factorial Sampling, FFS.

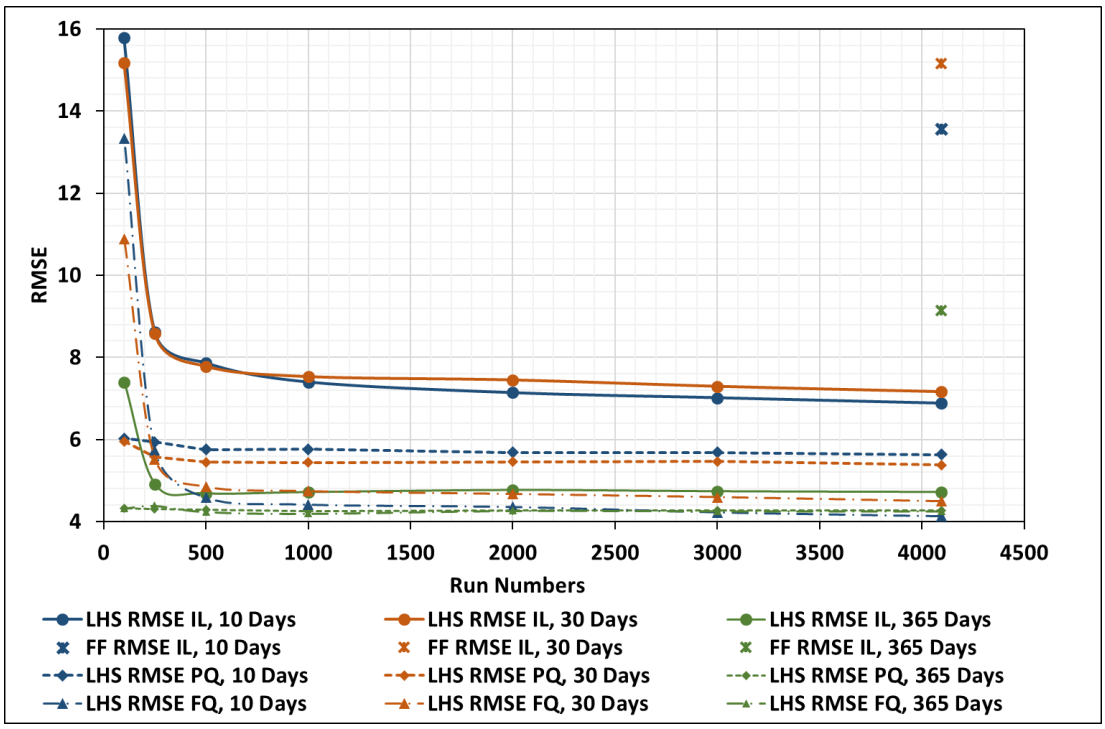

Figure 4.51 RMSE of ILRSM, pure quadratic (PQ) and full quadratic (FQ) models versus run numbers at three production stages for MFHW Nf7 L600m Base Reference sets with different sampling approaches, i.e., Latin Hyper Cube, LHS, and two level Full Factorial Sampling, FFS.

CHAPTER 5 CLEANUP EFFICIENCY OF MFHWS USING UNCONVENTIONAL PC AND RELATIVE PERMEABILITY

A thorough investigation of multiphase mobility at in-situ conditions has highlighted that capillary pressure and relative permeability relationships of tight and ultra-tight reservoirs could significantly deviate from conventional capillary pressure and relative permeability relationships (Shanley et al., 2004).

The most important characteristic of tight and ultra-tight gas reservoirs is their low permeability. The substantially small range of radii of curvature between the grains results in small pore throats in tight and ultra-tight formations (Bennion et al., 2004).The significantly small pore throats in tight and ultra-tight formations will result in larger capillary pressures and higher irreducible water saturations, i.e., Swirr. Wells and Amaefule (1985) conducted a study on tight sandstone samples and demonstrated that the small pore throats of tight and ultra-tight samples will result in high capillary pressure, low porosity, high Swirr and significantly low permeability values. These observations have led to the suggestion of considering unconventional Pc as well as unconventional relative permeability in the presented study of the cleanup efficiency of hydraulic fractures.

In this chapter, following the encouraging results of the work conducted on the cleanup efficiency of SFVWs and MFHWs, this line of research is extended to MFHWs with unconventional Pc and unconventional relative permeability.

In this chapter, a comprehensive evaluation of Pc correlations available for tight and ultra-tight formations is presented. In this exercise, the Go2Flow software (O'Meara Consulting Inc., 2014) was used to investigate the reliability of available Pc correlations models for tight and ultra-tight formations. The result of the study suggested that Brooks and Corey is a simple and accurate one-specific-parameter model to represent Pc data in tight and ultra-tight unconventional formations. However, the range of pore size distribution index used in Brooks and Corey should be limited to 0.3 to 1.5, rather than 1 to 4 used previously, to represent more realistically the unconventional tight/ultra-tight rock behaviours.

Parallel to this, a comprehensive investigation was conducted on the unconventional relative permeability (Kr) with permeability jail effect in unconventional formation. An attractive approach has been adopted to successfully model the weak and strong permeability jail effects in unconventional Kr models. Additionally, a new dimensionless

term, similar to GPL, was defined to capture the impact of same pertinent parameters on the production of fracture fluid (FF), which is an important consideration for HF of unconventional reservoirs.

5.1 MFHW-Sets Analysed

In this chapter, the results of a total of 15 different sets for MFHW-Sets have been analysed. The results have been compared with those of a base reference set and other similar sets. These models have the same reservoir dimensions as those of the MFHW reference set but differ in applied unconventional Pc and relative permeability relationships, heterogeneity, the fracture fluid injection volume (FVR), shut-in time period (ST), matrix permeability variation range (Kmr) and pressure drawdown (DP).

The MFHW sets that have been considered in this chapter are listed in Table 5.1 for reference and convenience.

5.2 Applicability of Pc Correlations for Tight and Ultra-Tight Formations

In this section, the results of a comprehensive evaluation of available Pc correlations that were applied for tight and ultra-tight formations is presented. The study was performed using the Geo2Flow software (O'Meara Consulting Inc., 2014). Geo2Flow is generally used in industry for identifying reservoir compartments, calculating 3D permeabilities consistent with saturation logs, and ensuring 3D saturations that are physically realistic and match their corresponding logs and rock types.

Here 200 Pc data sets were used, which corresponded to tight/ultra-tight formations from western U.S. basins measured by the University of Kansas Centre for Research and submitted to United States Department of Energy (University of Kansas Center for Research and Survey., 2009).

More specifically a comprehensive study was conducted on different J function models to understand ir-reliability for the tight/ultra-tight formations. In this section of Chapter 5, the original and modified leveret J functions, other J function models and the corresponding error in fit indicators when they are applied to unconventional tight and ultra-tight formations are discussed.

5.2.1 Leverett J Function

Leverett (1941) demonstrated that in rocks with the same lithology but of different porosities and permeabilities, one can normalise the capillary pressure described by a single function so-called the Leverett J-Function. That is, instead of plotting Pc versus saturation, Leverett plotted the J Function as described in Equation 5.1.

$$J(S_w) = \frac{P_c}{\gamma cos\theta}\sqrt{\frac{k}{\varphi}} \qquad 5.1$$

Where:

Pc: Capillary pressure

γ: Interfacial tension

θ: Contact angle

k: Permeability

φ: Porosity

Based on the Leverett's work, for a given rock type, most of Pc curves should fit into a single J Function. In other words, a single J Function could be used to describe a large number of Pc curves. The Leverett's approach suggests that Pc characteristics of rocks of an entire reservoir can be described by a limited number of J Functions.

5.2.2 J Function Displacement, J_d

The J Function displacement, J_d, is the value of the J Function that must be overcome in order for the non-wetting phase to enter the rock. It corresponds to the displacement pressure, Pd, (or threshold pressure, Pe), as described in Equation 3.6, on the capillary pressure curve. J_d is determined if Pd is used in Equation 5.1. All Pc functions used in this study rely on J_d, which defines the position of fluid contacts.

5.2.3 Thomeer J Function Model

Thomeer (1960) Showed that plotting the logarithm of the capillary pressure versus the logarithm of the non-wetting phase saturation yields hyperbolas. Thomeer suggested a J function model as described by Equation 5.2.

$$S = 1 - 10^{-(\frac{G}{Log(\frac{J}{J_d})})} \qquad 5.2$$

Where:

S: reduced saturation as described in Equation 3.7

J_d: J Function displacement value

J: J Function value

G: Thomeer's pore geometric factor

The Thomeer's model has one specific parameter, G, the Thomeer's pore geometric factor.

5.2.4 Brooks-Corey J Function Model

Brooks and Corey (1966) considered a bundle of capillary tubes model to represent porous medium and proposed the following expressions:

$$S = (\frac{J_d}{J})^{\lambda} = (\frac{J_d}{J})^{1/a_0} \quad 5.3$$

Where:

S: reduced saturation as described in Equation 3.7

J_d: J Function displacement value

J: J Function value

λ: Pore size distribution index

a_0: The wetting phase saturation exponent

Equation 5.3 corresponds to Equations 3.6 and 3.7 on the capillary pressure curve.

Like Thomeer's model, the Brooks and Corey's model has one model-specific parameter, λ, the pore size distribution index.

5.2.5 Bentsen-Anli J Function Model

Bentsen and Anli (1977) proposed a J Function model, which is described by Equation 5.4.

$$S = e^{(\frac{J_d - J}{a_0})} \quad 5.4$$

Where:

S: reduced saturation as described in Equation 3.7

Jd: J Function displacement value

J: J Function value

a_0: wetting phase saturation exponent

Like Thomeer's and Brooks and Corey's models, the Bentsen and Anli's model has one model-specific parameter, a_0, the wetting phase saturation exponent.

5.2.6 Skelt-Harrison J Function Model

Skelt and Harrison (1995) suggested a J Function model with two model-specific parameters as described by Equation 5.5. Unlike models denoted by Thomeer, Brooks and Corey and Bentsen and Anli, this model has two model-specific parameters, a_0, the capillary pressure scaling factor, and a_1 the exponent for the scaled capillary pressure.

$$S = 1 - e^{-(\frac{a_0}{J-J_d})^{a_1}} \quad 5.5$$

Skelt and Harrison originally introduced their model in terms of height above the free water elevation and Pc. Rearrangement of their correlation in term of J function results in Equation 5.5.

5.2.7 O'Meara Unimodal J Function Model

The O'Meara Unimodal J Function model, like Skelt-Harrison J Function model, has two model-specific parameters, a_0 and a_1. It is described by Equation 5.6.

$$S = \frac{1}{2}\ erfc\ (\frac{Log(\frac{J-J_d}{a_0})}{a_1}) \quad 5.6$$

The erfc function used in the O'Meara's model is a complementary error function. This model has two model-specific parameters labelled a_0 and a_1. The former is equal to the median of the underlying lognormal distribution and the latter is equal to the variance.

5.3 Analysis of Pc Correlations

200 Pc data sets were imported into Geo2Flow to evaluate the suitability of the above mentioned Pc correlations for very tight rocks.

In Geo2Flow Software, the quality of fitting data by either the least squares method or the least absolute deviations method was described by an error in fit. The error in fit is considered for n number of the data points, (xi, yi) with a relationship of y = f(x). For the Least Squares Method, the error is equal to the sum of the squares of the difference between the data and its corresponding point as described by Equation 5.7.

$$\Delta = \sum_{i=1}^{n} [y_i - f(x_i)]^2 \qquad 5.7$$

For the least absolute deviations method, the error is equal to the sum of the difference between the data and its corresponding point in absolute value as expressed by Equation 5.8:

$$\Delta = \sum_{i=1}^{n} |y_i - f(x_i)| \qquad 5.8$$

It should be noted that the lower Δ, the better curve fit is achieved. In this study, the least squares method was applied.

In this exercise, first entire data sets were edited in an excel file to meet the required format by Geo2Flow and next, the excel file was imported into Geo2Flow.

The imported Pc data sets versus saturation are shown in Figure 5.1, it should be noted that here Pc is in Bar. The resulting J functions (using individual permeability, porosity, IFT and contact angle) are shown in Figure 5.2.

As it was discussed previously, 5 different models were considered in this analysis, 3 models with one specific parameter (i.e., Thomeer, Brooks and Corey and the Bentsen and Anli models) and 2 models with two specific parameters (i.e., Skelt-Harrison and the O'Meara Unimodal models). The least squares method was applied to fit the Pc data sets and the final fit to error values of all Pc data sets for 5 models were listed in Table 5.2.

The error in fit for all Pc data sets for Thomeer, Brooks and Corey, the Bentsen and Anli, Skelt-Harrison and O'Meara Unimodal are 6.26E-3, 8.91E-3, 1.49E-2, 6.68E-3 and 7.09E-3, respectively. It is noted that based on these error indicators, Thomeer model and Bentsen and Anli model are the best and worst models, respectively, when all data were considered. It is also noted that models with two model-specific parameters models predict Pc values better than one model-specific parameter models but not the Thomeer model. That is, due to their extra flexibility, i.e. having two model-specific parameters, a better fit is obtained. It should be noted that having two parameters is useful in having a better match, but it implies that a more complicated model is considered. From Table 5.2, it is also shown that Brooks and Corey is the second best one-specific-parameter model.

In order to further investigate the reliability of these J models in unconventional formations, all Pc data sets were divided into three groups of conventional Pc data sets with k>0.1, tight Pc data sets (0.001md<K<0.1md) and ultra-tight Pc data sets

(K<0.001md). The Pc data sets with K>0.1 md were excluded from further analysis. The least squares method was again applied to fit the two groups of Pc data sets corresponding to unconventional rocks, and the final fit to error values of them for 5 models are listed in Table 5.2. The error in fit for tight Pc data sets for Thomeer, Brooks and Corey, the Bentsen and Anli, Skelt-Harrison and O'Meara Unimodal are 9.97E-3, 8.64E-3, 1.21E-2, 7.86E-3 and 8.49E-3, respectively. It is noticed that the Brooks and Corey is the best model with one specific parameter and Skelt-Harrison is the best model with two specific parameters to model tight Pc data sets. The error in fit for ultra-tight Pc data sets for Thomeer, Brooks and Corey, the Bentsen and Anli, Skelt-Harrison and O'Meara Unimodal are 2.89E-2, 2.91E-2, 2.95E-2, 2.87E-2 and 2.86E-2, respectively. It is noticed that the Brooks and Corey and Thomeer are the best models both with one specific parameter and Skelt-Harrison and O'Meara Unimodal are the best models with two specific parameters to model ultra-tight Pc data sets. Table 5.2 also shows that Bentsen and Anli model is the least accurate model for both tight Pc and ultra-tight Pc data sets. Overall based on these results it can be concluded that the Brooks and Corey model is the most suitable for these two groups of data.

5.3.1 Suitability of Brooks and Corey Model for Selected Individual Data Sets

The reliability of five different J models in tight Pc data sets (0.001md<K<0.1md) and ultra-tight Pc data sets (K<0.001md) was investigated as discussed in section 5.2. It was concluded that the Brooks and Corey model was accurate for tight/ultra-tight sets of data. In this part, several data sets from tight/ultra-tight groups were selected and the Brooks and Corey model was fit to them individually to determine the typical range of pore size distribution index for these unconventional data sets.

Some of the data that were analysed are shown in Table 5.3. Table 5.3 shows sample data set name, permeability, porosity and calculated pore size distribution index, j function displacement and error in fit values for the fitted curves. From data of Table 5.3, it is noted that calculated pore size distribution index for these individual data sets varies between 0.313 to 1.49.

Here two sample data sets of tight and ultra-tight sets group, A-IPE-HG-195 and A-IPE-HG-195, were selected to show the good match between Brooks and Corey model and these real data.

A-IPE-HG-195 is a sample data set from tight data sets with K=0.0086 md and porosity=11.8%. The error in fit value for this set is 2.06E-3, which is a very small value.

Figure 5.3 shows a good match between the Fitted Brooks and Corey model and real data for this set. The pore size distribution index and j function displacement values for the fitted curve are 1.08 and 0.054, respectively. A-IPE-HG-14 is a sample data set from ultra-tight data sets with K=0.00016 md and porosity=3%. The error in fit value for this set is 1.99E-4, which is a very small value. Figure 5.4 shows a very good match between the Fitted Brooks and Corey model and real data. The pore size distribution index and j function displacement values for the fitted curve were 0.67 and 0.055 respectively.

5.3.2 Concave down Part of Pc Curves

A concave down part was observed in some Pc (or Leverett J) curves. The dead volume error occurrence was noticed when the apparent capillary displacement pressure or its corresponding J Function displacement value occurred at a wetting phase saturation that was less than 1. Figure 5.5 shows dead volume error observed in dataset A_IPE_HG_103. Some data points of wetting phase saturation show that the non-wetting phase has entered the rock easily when the wetting phase saturation is between 1 and 0.97. However, the characteristic of the curve changes when the value of the J Function exceeds 0.04, where it becomes more difficult for the non-wetting phase to enter the rock. There appears to be a discontinuous break or a change in curvature in the curve at this point. This trend, which cannot be captured by the Brooks and Corey model, relates to the dead volume, has been attributed to the dead volume errors in capillary pressure measurements. Therefore, it should be corrected and not be misinterpreted as a change in characteristics of the rock, Figure 5.6.

The dead volume observed in capillary pressure measurements is expressed as the volume of fluid (mercury) that has been assumed to enter the core sample when, in fact, it has been held up in the core holder or has intruded into vugs or irregularities on the surface of the core. Shafer and Neasham (2000) referred to a correction for the dead volume error as the closure correction. When a dead volume is detected in a capillary pressure measurement, the experimental data must be corrected since it is not representative of the true capillary behaviour of the core sample.

5.3.3 Summary

These observations showed that Brooks and Corey was a simple and accurate one-specific-parameter model to represent Pc data in tight and ultra-tight formations. It should be noted that these results were based on the core samples from western U.S. basins with its range of properties. However, it has to be added that the results of this study suggest that the range of pore size distribution index should be limited to values between 0.3 to 1.5 to represent the unconventional tight/ultra-tight rock behaviours. A wider range (between 1 to 4) was previously considered for the MFHW clean-up study (Chapter 4) that need to be modified, as done for the results presented in the following sections.

5.4 MFHW-Sets using unconventional Pc with Lambda range (0.3-1.5)

The new pore size distribution range suitable for Pc of unconventional formations with different Kmr, DP and FVR were applied and corresponding results were analysed, compared and discussed as presented here in this section. The aim was to observe the impact of these parameters on cleanup efficiency while using unconventional Pc.

5.4.1 Second Response in addition to GPL

After the fracturing stage, some portion of the injected FF flows back to the surface. The volume of FF can vary widely depending on the pertinent parameters and the fracture design. The produced fluid typically consists of a mixture of FF returned to the surface (flowback or FF backflow) and formation water (if any) and include a portion of injected chemicals, therefore, it is important to study how much water is produced. Produced FF management is a key challenge for unconventional gas formations' development and production. The tight regulations regarding the FF flowback and its environmental impacts as well as limited options to dispose FF force operational companies to continually re-visit their existing hydraulic fracturing approach and FF flowback management procedures. Consequently, a new dimensionless terminology, called Produced Fracture Fluid, PFF, has been introduced and the impact of pertinent parameters, same as those on GPL, on PFF has been studied. The produced fracture fluid (PFF, %), as the second response, was defined as a measure of flowback (produced) FF volume compared to the total FF injected into the well at fracturing stage (FF injection stage) as expressed by the following equation.

$$PFF = 100 \times \left[\frac{The\ volume\ of\ produced\ FF\ or\ simply\ Field\ \ water\ production}{Total\ FF\ injected\ at\ fracturing\ stage(FF\ injection\ stage)}\right] \quad 5.9$$

5.4.2 MFHW-Sets 30 Nf7 L600m, Unconventional Pc with Lambda range (0.3 to 1.5)

From this section onward, the results of MFHW-sets using the Latin hypercube sampling (LHS) approach with the optimum 1000 run numbers are discussed. Additionally, the new lambda range (0.3 to 1.5) which represented Pc of tight/ultra-tight formations is applied.

A comparison of the GPL tornado chart of MFHW-set 30 with the new pore size distribution index range, i.e., lambda from 0.3 to 1.5, (Figure 5.7) with that of MFHW-set 26 Nf7 L600m Base Reference set (Figure 4.44) with the only difference being different pore size distribution index range shows that the same trends are observed in both tornado charts for all pertinent parameters. It is also noted that in MFHW-set 30 with lambda range from 0.3 to 1.5, the impact of Pc pertinent parameters (especially that of lambda) on GPL are most important. That is, due to having lower lambda range in set 30, which make Pc values to be much larger than those of set 26.

$$\left.\begin{array}{l} K_m \downarrow \\ IFT \uparrow \\ \lambda \downarrow \\ S_w \downarrow \end{array}\right\} \Rightarrow P_c \uparrow$$

The impact of fluid mobility (especially that of water mobility) in the matrix in MFHW-set 30 is slightly stronger than the one in the MFHW-set 26 with smaller Pc values, this is again due to stronger capillary forces in the matrix, which make the fluid mobility more difficult.

Comparing the PFF tornado chart of MFHW-set 30 with the new lambda from 0.3 to 1.5, (Figure 5.9) with that of MFHW-set 26 Nf7 L600m Base Reference set (Figure 5.8) with the only difference being different lambda range, the same trend is observed in both tornado charts for all pertinent parameters except for Kf, i.e., increasing Kf results in smaller FF production (PFF) in MFHW-Set 30 whilst the opposite was observed in MFHW-Set 26.

In order to further investigate the Kf trend change in PFF tornado chart of MFHW-Set 30, an individual run with a Kf value set at almost maximum value, e.g., run number 29, was selected. A new code in MATLAB was developed, then the water saturation, Swat, values from GRDCL file in Floviz at the end of soaking time was extracted and used. The

aim of plotting the Swat distribution map was to observe the water distribution at the end of soaking time in this max-Kf case and compare it with that of the min-Kf case whereby the Kf was set at its minimum value.

Considering Figure 5.10, Figure 5.11 & Figure 5.12, it is noted that in the case with Max-Kf (Figure 5.10), a region with 30%-70% water saturation (Region B) within the first 45 m of fracture half-length from well is observed. On the other hand, in the case with min-Kf (Figure 5.11), a significant portion of FF is injected/imbibed into the matrix with 60%-100% water saturation (Region A) within almost first 10 m of fracture from well.

This is because during FF injection, in the case with Max-Kf, FF flows significantly easier/faster through the fracture than that of the case of Min-Kf. This results in more distributed FF especially in the matrix in the case with Max-Kf. Consequently, in the Min-Kf case, most of FF is injected/imbibed in a shorter length of the matrix in the vicinity of fracture (i.e., 10m). this resulted in a region (Region A) with higher Sw and lower Pc in which it is easier to be reproduced during the backflow period compared to that of Max-Kf.

Figure 5.12 shows the plotted Pc for MFHW-sets 26 and 30 (run number=29) with different regions that was addressed in Figure 5.10 and Figure 5.11. From Figure 5.12, generally, much larger Pc values are observed for MFHW-Set 30 compared to MFHW-set26. This is because, in set 30, the new lambda range (0.3 to 1.5) is smaller than that used in MFHW-Set 26 (1 to 4) that results in larger Pc. It should also be noted that for MFHW-Set 30 (run number 29), the Pc curve for both Kf-Max and Kf-min were the same.

It is noted from Figure 5.12 that in region A with 60% to 100% water saturation, Pc varies from 100 to 20 psi and from 30 psi to 20psi for MFHW-Set 30 and 26, respectively. In region B with 30% to 70% water saturation, Pc varies from 2100 to 60 psi and from 80 psi to 25 psi for MFHW-Set 30 and 26, respectively. Finally, in region C with 0% to 30% water saturation, Pc varies from infinity to 2100 and from infinity to 80 psi for MFHW-Set 30 and 26 respectively.

It should be noted that considering these three regions (Region A, B & C) with very different Pc values and during the backflow production stage, due to higher Sw values and smaller Pc (less retained FF) for the set with min Kf, more FF production is observed. That is why a negative value for Kf is observed in the relevant tornado chart (Figure 5.9).

According to what was discussed, Kf has two different impacts on FF production:

1. Larger Kf provides better FF mobility inside the fracture during the production stage resulting in more FF production.
2. Larger Kf results in better FF mobility inside fracture during the injection period, this results in more distributed FF and smaller Sw values in the matrix and consequently larger Pc values, which retain more FF during the production stage resulting in less FF production.

According to this and with regard to two different Kf effects, in set 30, the second impact of Kf was dominant and this is why a Kf trend change is observed in PFF tornado chart for this set (Figure 5.9).

It is also noted that in MFHW-set 30 with lambda range from 0.3 to 1.5, the impact of Pc pertinent parameters (especially that one of lambda) on GPL are most important. That is due to having a smaller lambda range, which makes Pc values much larger than those of set 26.

Another important observation in PFF tornado charts of MFHW-Set 26 and 30 (Figure 5.8 and Figure 5.9) is that as water mobility in the matrix increases, the FF production decreases. This is because the water mobility in the matrix has again two different impacts on the FF production:

1. Larger water mobility in the matrix (i.e., maximum K_{maxwm} and minimum n_{wm}) provides better FF mobility inside the matrix during the production stage, i.e. more FF production.
2. Larger water mobility in the matrix (i.e., maximum K_{maxwm} and minimum n_{wm}) results in better FF mobility inside the matrix during the injection period, this results in more distributed FF and smaller Sw values in the matrix and consequently larger Pc values. The larger Pc values retain more FF during the production stage resulting in less FF production.

From data of Figure 5.13, it is noted that in MFHW-Set 30 with stronger Pc values, smaller FF production is observed, which is in line with the fact that larger Pc values retain FF more strongly and consequently less FF flowback.

Figure 5.14 shows the plotted GPL, PFF and FGPT/FWPT (total produced gas-water ratio) for different run numbers for MFHW-sets 30. From Figure 5.14, it is noticed that larger FF production results in more GPL, which is in line with what was previously observed in sets with Kmr=1 that retaining FF inside the matrix results in smaller GPL values.

5.4.3 MFHW-Sets (Nf7 L600m_1000RUNS-newLambda) with different Kmr, FVR & DP

Three additional MFHW-Sets were run to capture the effect of very low Km range (Kmr=100), high FVR and high DP on clean-up efficiency when unconventional Pc is considered. The aim was to observe the impact of these parameters on cleanup efficiency while using unconventional Pc. The effect of extending ST was excluded from further analysis using unconventional Pc since it was clearly observed in SFVW and MFVW sets, that extending ST gives more time to FF to imbibe deeper into the matrix resulting in more distributed FF saturation inside the matrix and less FF flowback. However, it seems this is limited only to the early production time.

5.4.3.1 MFHW-Sets 31 Nf7 L600m_1000RUNS-Kmr=100-newLambda

This MFHW-Set was run to capture the effect of very low Km range (Kmr=100) on clean-up efficiency when unconventional Pc is considered. Km range was reduced from 1 μD-100 μD in MFHW-Set 30 to 0.01 μD-1 μD in this set.

Comparing the GPL tornado chart of MFHW-set 31 with very tight formation, (Figure 5.15) with that of MFHW-set 30 Nf7 L600m Base Reference set (Figure 5.7) with the only difference being different Km ranges applied, the same trend was observed in both tornado charts for all pertinent parameters except for Km. The Km coefficient in MFHW-Set 30 was positive, i.e., increasing Km increases GPL and the Km effect on Pc was important (Figure 5.7). The Km coefficient in MFHW-Set 31 is negative, i.e., increasing Km decreases GPL and the Km effect on mobility is important. This trend change is attributed to very tight nature of the rock in this set which makes the fluid mobility significantly difficult. The effect of fluid mobility in the matrix is more important than that of MFHW-Set 30 and this is in line with what was discussed earlier, i.e. Pc is already high and hence, the effect of fluid mobility is more important.

Considering Figure 5.16 and Figure 5.18, showing the histogram of GPL and PFF for these two sets, almost the same clean-up is observed for these two sets due to very high Pc values for these two sets.

Comparing the PFF tornado chart of MFHW-set 31 with very tight formation, (Figure 5.17) with that of MFHW-set 30 Nf7 L600m Base Reference set (Figure 5.9), the same trend was observed in both tornado charts for all pertinent parameters except for Kf. In MFHW-Set 31, the first effect of Kf is dominant whilst in MFHW-Set 30, the second effect of Kf is dominant.

5.4.3.2 MFHW-Sets 32 Nf7 L600m_1000RUNS-FVR10-newLambda

This MFHW-Set was run to capture the effect of increasing FVR, from 2 in MFHW-Set 30 to 10 in this set with unconventional Pc, on clean-up efficiency.

Comparing the GPL tornado chart of MFHW-set 32 with FVR=10, (Figure 5.19) with that of MFHW-set 30 Nf7 L600m Base Reference set (Figure 5.7) with the only difference being different FF injected at injection stage, the same trend was observed in both tornado charts for all pertinent parameters. It was also noted that:

1. The impact of fluid mobility in the matrix and fracture on GPL was more important in this set than that in MFHW-Set 30.
2. The absolute value of all 12 pertinent parameters at 365 days of production was still large and this observation highlights that clean-up process takes a much longer time, (even up to 1 year) compared to the one for MFHW-set 30.

These two observations in this set were due to much larger FF volume (FVR=10) injected in this set. Figure 5.20 shows that slower clean-up is observed for the high FVR set.

From data of Figure 5.21, which is the PFF tornado chart, it was noted that in MFHW-Set 32, the first effect of Kf on FF production was dominant.

Figure 5.22 shows the histogram chart comparing PFF cumulative frequency of MFHW-set 32 with FVR=10 and MFHW-set 30 with FVR=2 at three production stages. It was noted that unlike MFHW-Set 30, the cumulative frequency curves for MFHW-Set 32 at three different production stages do not overlay each other, this again supports the fact that FF production continues until 1 year of production.

5.4.3.3 MFHW-Sets 33 Nf7 L600m_1000RUNS-DP4000-newLambda

This MFHW-Set was run to investigate the effect of increasing DP, from 1000 in MFHW-Set 30 to 4000 in this set with unconventional Pc, on clean-up efficiency.

Comparing the GPL tornado chart of MFHW-set 33 with DP=4000, (Figure 5.23) with that of MFHW-set 30 Nf7 L600m Base Reference set (Figure 5.7) with the only difference being different DP, the same trend was observed in both tornado charts for all pertinent parameters. It was also noted that the effect of Pc pertinent parameters (lambda, IFT & Km) on GPL was slightly less important than those of MFHW-Set 30. This was due to stronger viscous force (DP=4000 psi) which made retaining FF inside matrix more

difficult. The effect of Kf on FF flowback was minimal due to very large DP applied in this set, Figure 5.23.

From data of Figure 5.24 and Figure 5.26, it is noted that increasing DP does not accelerate the clean-up process in this set with unconventional Pc. This is because although increasing DP generally made clean-up faster in the fracture and matrix in the vicinity of fracture, it resulted in more FF flowback from deeper zones inside the matrix and further away from fracture which had a more detrimental impact on clean-up. This larger FF flowback is shown in Figure 5.26. These two diverse effects balanced each other and almost the same clean-up performance was observed in these two sets.

5.5 Relative Permeabilities in Tight/Ultra-tight Formations

The properties of Tight/Ultra-tight formations are significantly different from conventional formations. A thorough understanding of unconventional formations properties can lead to more accurate production estimates, depletion behaviour and forecast scenarios, which in turn results in more reliable exploration and development.

Generally, tight and ultra-tight sandstones have significantly low values of permeability and porosity with micrometre to nanometer-size pores. A number of suggestions have been put forward about the anomalies associated with unconventional formations.

Rushing et al. (2008) described that the significantly low permeabilities and porosities seen in tight/ultra-tight sandstones can be attributed directly to a massive distribution of small and very small pores. This also could be attributed to a very tortuous system of pore throats connecting these pores in such unconventional rocks. They also discussed that these significantly small pore networks and highly tortuous pore throat systems could be due to initial deposition of fine to very fine grained sediments as well as the existence of dispersed shale and clays in the pores.

Byrnes (1996) addressed the reservoir characteristics of the typical low-permeability sandstones found in the Rocky Mountains. He mentioned that in tight sandstones, porosity is not severely changed by confining stress changes but in-situ effective permeability could be extensively reduced. He highlighted that confining stress decreases the size of the thin pore throats that connect the larger pores, i.e., under confining stress the pore throats' diameter decreases from 50% to 75% and this results in permeability drop of 10 to 40 times.

The impact of massive distribution of small and very small pores, very tortuous system of pore throats and massive confining stresses in the tight and ultra-tight formations may impair the effective permeability to fluids so severely that classical theories for multiphase flow are no longer applicable. Shanley et al. (2004) stated that the water and gas relative permeabilities can be extensively reduced in a way that both phases have minimal relative permeability over some range of saturations. This concept is called the 'permeability jail'.

Figure 5.27 compares the idea for relative permeability and capillary pressure functions of unconventional (tight/ultra-tight formations) and those of conventional formations.

In conventional formations, critical water saturation (Swc) and irreducible water saturation (Swirr) are almost the same or there is a slight difference between these two values, consequently these terms are often used interchangeably, but in tight/ultratight formations, critical water saturation could be significantly greater than the irreducible water saturation. These two terms are further explained below.

- Critical Saturation: Critical saturation, whether water, gas or oil, (Swc, Sgc or Soc) refers to the lowest saturation at which a phase becomes mobile. According to this definition, critical saturations are characteristics of relative permeability curves.
- Irreducible Saturation: irreducible saturation corresponds to the minimum saturation found from capillary pressure curves (in significantly high pressures) determined from special core analysis, consequently irreducible saturation is characteristic of capillary pressure curves.
    - Irreducible water (Swirr), Residual oil (Sor), residual gas and trapped gas (Sgr) and trapped oil saturations (Sor) all refer to the left over saturation of these phases after extensive displacement by other phases. The connate water saturation is the lowest water saturation found in situ and sometimes used for irreducible water saturation.

In tight and ultra-tight formations, critical water saturation is significantly different from (larger than) irreducible water saturation whilst in conventional formations, these two parameters are very close and almost similar. The small water production rates in tight/ultra-tight formations comply with the significantly large values of critical saturation. These extensively tight formations with significantly low permeabilities and very tortuous pore network system lead the two-phases to increasingly intervene to one another's flow in the restricted pore throats of the rock. Consequently, critical gas

saturation also increases and this results in a range of saturations, where all phases have minimal relative permeability values. This is called permeability jail.

Gdanski and Walters (2010) studied the gas and FF relative permeabilities in low permeability gas reservoirs, they also named the 'poor quality matrix relative permeabilities' as relative permeability jail and suggested that hysteresis could be the reason of substantially impaired relative permeabilities. They highlighted that relative permeability hysteresis can happen during imbibition or drainage in fracturing treatment. They considered that an increase in the gas saturation, i.e., post-fracturing cleanup, is a drainage process, whilst a fracturing operation, i.e., FF injection into the matrix, is an imbibition process. They implemented a methodology to model relative permeability hysteresis and its impact on capillary pressure. Relative permeability sets with a crossover from 10% to 0.1% of relative permeability were considered in their study which mostly corresponded to weak jail effect.

Cluff and Byrnes (2010) discussed that in the tight/Ultra-tight formations, water is retained by the substantially large values of capillary pressure and thus decreases the permeability to gas phase extensively. They also mentioned that multiple gas-water drainage/imbibition hysteresis could cause the permeability jail effect. They suggested that this especial hysteresis and consequent jail effect is due to complex pore geometries.

Byrnes (2008) studied the gas relative permeability (Kr) of tight sandstones and showed that Kr of tight sandstones can be modelled using the Corey equation. He used confined mercury injection capillary pressure and coupled electrical resistance measurements on Mesaverde sandstones with various lithology to measure critical saturation of the non-wetting phase.

He performed unconfined mercury intrusion capillary pressure (MICP) analysis on 71 Mesaverde sandstone samples and confined MICP on 54 samples. Samples ranged widely in lithology; grain sizes and sedimentary structures. The tight and ultratight sandstones showed similar porosity and permeability characteristic of western U.S. tight-gas sandstones. In order to understand the critical saturations and the theoretical scale dependence, he studied and applied models of pore architecture and percolation theory analysis. With percolation threshold approach. Although helpful, the most important limitation of this method was that a water-wetting phase was not existing, which can impact the results compared to MICP.

He performed some gas Kr measurements at water saturation values less than the critical water saturation, where water Kr is zero. The gas Kr data in this region displayed

consistency with the relevant data of the region, where water saturation values were more than the critical water saturation. In order to model the Kr data in Corey correlation, he introduced Swc,g whereby water saturations below critical saturation is used. He concluded that that gas Kr can be successfully modelled in low-permeability gas sandstones using the modified Corey equation.

Shaoul et al. (2011) studied the damage mechanisms in stimulation of wells in tight/ultratight formations. They used the idea of permeability jail in unconventional formations to successfully simulate the FF flow-back. They considered two different scenarios, i.e. Strong permeability jail and weak permeability jail.

Strong (total) permeability jail, where the gas and water Kr curves do not intersect and where within a range of 20% in water saturation, both fluids are immobile. This denotes the case of substantially poor reservoir rocks with particularly low permeability, which was addressed in the Shanley et al. (2004) work.

In order to model this case, the Kr curves of both fluids have been shifted through the water saturation region as shown in Figure 5.31. They considered that the initial reservoir water saturation is the same as critical water saturation and at this critical water saturation, gas is mobile, while water is not mobile at all.

The second scenario was called the weak (small) permeability jail and is attributed to significantly low, but limited fluid mobility in the jail saturation region, or jail zone. The Kr curves are created to have a permeability reduction of around 98% through the jail zone.

It has to be highlighted that the idea for the existence of a ‘permeability jail’ has yet to be proven in any laboratory experiments. In this work, in accordance with the approach proposed by Shaoul et al. (2011), three different sets using the weak permeability jail effect have been considered to study the impact of weak jail permeability on clean-up efficiency. In these three sets, i.e., MFHW-Set 34, 35 & 36 with the two-phase regions of 30%, 20% and 10% respectively, significantly low gas and water Kr values across the two-phase region were modelled using the Corey correlation.

To capture the impact of total permeability jail on clean-up efficiency of hydraulic fractures, three additional new sets, i.e., MFHW-Set 37, 38 and 39 with heterogeneous reservoir model were also considered. The strong (total) Kr jail effect causes no production of water or gas after the fracturing operation, and consequently not useful and of no particular interest. Hence, as in real reservoir rocks, the regions with total permeability jail have been distributed throughout the reservoir with other parts using

conventional (without jail effect) and weak permeability jail Kr data. Hydraulic fractures may partially intersect with few of them.

5.6 New MFHW Sets using weak Permeability Jail (MFHW-SETS 34, 35 & 36 NF7 L600m & Base Reference Set)

To capture the effect of unconventional Kr (weak permeability jail) on clean-up efficiency, three sets of MFHW-Set 34, MFHW-Set 35 & MFHW-Set 36 were studied.

In all MFHW-Sets with conventional relative permeability relationship, it was considered that Swirr=Swc=0.15 and Sgc=Sgr=0.1. In three MFHW-Sets with unconventional relative permeability relationship (weak permeability jail effect), it was considered that Swirr= 0.15 and Sgr= 0.1. To represent the weak permeability jail effect in these three sets, relative permeability curves were shifted across the saturation region, i.e., for three sets of MFHW-Set 34, MFHW-Set 35 & MFHW-Set 36, Swc and Sgc were 40% & 30%, 45% & 35% and 50% & 40% respectively (Figure 5.28). This resulted in a restricted two-phase region in MFHW-Set 34, MFHW-Set 35 & MFHW-Set 36 with just 30%, 20% and 10% range of two-phase flow respectively. From Figure 5.28, it was noted that in these weak (small) permeability jail sets, significantly low but limited fluid mobility (relative permeability values) in the jail saturation region, or jail zone was observed. The shorter the two-phase region (jail saturation region, or jail zone), the smaller the relative permeability values of both phases.

These three weak permeability jail sets were compared to each other and their relevant set without weak permeability jail, i.e., MFHW-Set 30. It should be noted that the unconventional Pc was also applied to the model in the MFHW-Sets onward, to capture the realistic cleanup efficiency with both unconventional Kr and Pc.

Comparing the GPL tornado chart of MFHW-Sets 34, 35 and 36, Figure 5.29 a, b and c, with each other with the only difference having different weak jail saturation regions, i.e., 30%, 20% and 10% respectively, and also comparing these GPL tornado chart of weak jail saturation MFHW-Sets with that of MFHW-Set 30 with conventional relative permeability, Figure 5.7, it is noted that the impact of some of the parameters are different but the overall observed trends of all parameters are more or less the same except for Km.

Comparing the GPL tornado chart of MFHW-Sets 34, 35 and 36, Figure 5.29a, b and c, and that of MFHW-Set 30, Figure 5.7, it is noted that the impact of Pc pertinent parameters (IFT & lambda) becomes less important in sets with stronger weak permeability effect, i.e., the stronger the weak jail effect, the less important the impact of

Pc. In line with this observation, the second effect of Km (on Pc) in MFHW-Set 30 is dominant whilst in MFHW-Sets with various jail effect levels, the first effect of Km (on fluid mobility) is dominant. This is due to the fact that the weak permeability jail effect is increased from none in MFHW-Set 30 with conventional Kr (with 75% two-phase region) to progressively larger permeability jail effects in MFHW-Sets 34, 35 and 36 with 30%, 20% and 10% two-phase region, respectively. The increase in the jail effect results in weaker viscous forces. It was noticed before (MFHW-Set 30) that stronger viscous forces help more FF to be injected deeper into the matrix and consequently more distributed FF in the matrix. This results in smaller Sw values in the matrix grids in the vicinity of fracture and resulting in more retained FF inside the matrix due to larger Pc values. Conversely, reducing viscous forces due to increasing the weak jail effect lead FF not to be injected into deeper regions of the matrix. This results in higher FF saturation regions inside the matrix in the vicinity of fracture and consequently less retained FF. This less retained FF due to higher FF saturation lead to more FF flow-back at the production stage, this is because of the stronger the weak jail effect, the less important the impact of Pc pertinent parameters (IFT, lambda and Km) on clean-up efficiency. That also supports the Km trend change, i.e., the second effect of Km (on Pc) in MFHW-Set 30 to be dominant whilst in MFHW-Sets with the jail effect, the first effect of Km (on fluid mobility) becomes dominant.

Figure 5.30 shows the Saturation distribution map (run number 30) at the end of shut-in soaking time (ST) for a) MFHW-Set 34 NF7-L600 with Weak Perm Jail, 30% Two-phase b) MFHW-Set 35 NF7-L600 with Weak Perm Jail, 20%Two-phase and c) MFHW-Set 36 NF7-L600 with Weak Perm Jail, 10%Two-phase. From Figure 5.30, it is noticed that increasing the weak jail effect prevents FF to be injected deeper into the matrix compared to sets with stronger viscous force. In other words, the stronger the weak jail effect, the weaker the viscous force and consequently the shallower injection of FF into the matrix. This resulted in higher FF saturation regions inside the matrix in the vicinity of fracture and consequently less retained FF. As it is shown in Figure 5.30, deepest FF invasion is observed in MFHW-Set 34 with the weakest weak jail effect, i.e. 30% low Kr jail region, whilst the shallowest invasion is observed in MFHW-Set 36 with the strongest weak jail effect, i.e. 10% low Kr jail region.

Comparing the GPL tornado chart of MFHW-Sets 34, 35 and 36, Figure 5.29a, b and c, and that of MFHW-Set 30, Figure 5.7, it is also noted that as the weak permeability jail effect is increased, the impact of fluid mobility in both matrix and fracture (especially

that of matrix) on clean-up efficiency becomes more important. This is because matrix fluid mobility is more critical in MFHW-Sets with the stronger jail effect due to more restricted viscous forces. The impact of fluid mobility inside the fracture also became more important in MFHW-Sets with stronger jail effect and that was due to more FF flow-back at the production stage.

Figure 5.31 shows the histogram chart that compares the GPL cumulative frequency of the runs in MFHW-Sets 36, 35, 34 and 30. It is noted that the stronger, the weak jail effect the slower the clean-up. It should be noted that as weak jail effect is more pronounced, the amount of FF flowback is larger (Figure 5.33) and higher FF flowback results in more GPL values.

Comparing the PFF tornado chart of MFHW-Sets 34, 35 and 36, Figure 5.32a, b and c, similar observations in line with those ones previously noticed in Figure 5.29 were observed, i.e.:

- The stronger, the weak jail effect, the lower the impact of Pc on FF production.
- As weak jail effect became stronger the impact of fluid mobility in both matrix and fracture on FF flow-back became more important.

Figure 5.33 shows the histogram chart that compares the PFF cumulative frequency of the runs in MFHW-Sets 36, 35, 34 and 30. It was noted that the stronger the weak jail effect, the larger the FF flow-back.

5.7 New MFHW Sets using Strong (Total) and Weak (Small) Permeability Jail in Heterogeneous Reservoir Rocks (MFHW-SETS 37, 38 &39 NF7 L600m & Base Reference Set)

The strong (total) Kr jail effect leads to no production of water or gas after stimulation, and consequently not useful and no of particular interest. Hence, as in real unconventional tight/ultra-tight reservoir rocks, the regions with total permeability jail, weak permeability jail and also conventional Kr have been distributed throughout the reservoir. Hydraulic fractures may partially intersect with different regions with different Kr characteristics, i.e., total jail, weak jail and conventional rock. To capture the impact of total permeability jail on clean-up efficiency of hydraulic fractures and to simulate a more realistic case, three new MFHW-Sets, i.e., MFHW-Set 37, 38 & 39 with heterogeneous reservoir model were considered.

For these three MFHW-Sets, the same grid model but with different Kr distribution were constructed. The heterogeneous grid model was divided into 6 different rock type classes with different Kr functions as below:

Rock Type 1. Regions with the total permeability jail effect with 10% total jail range.

It was considered that Swirr= 0.15 and Sgr= 0.1. To represent the total permeability jail effect, Kr curves were shifted further across the saturation region, i.e., Swc and Sgc were 60% & 50%, respectively (Figure 5.34b), this results in a zone of 10% total jail.

Rock Type 2. Regions with the weak permeability jail effect with 10% weak jail saturation zone as discussed in MFHW-Set 36, i.e., Swirr= 0.15, Sgr= 0.1, Swc=50% and Sgc= 40% (Figure 5.28c)

Rock Type 3. Regions with the weak permeability jail effect with 20% weak jail saturation zone as discussed in MFHW-Set 35, i.e., Swirr= 0.15, Sgr= 0.1, Swc=45% and Sgc= 35% (Figure 5.28b)

Rock Type 4. Regions with the weak permeability jail effect with 30% weak jail saturation zone as discussed in MFHW-Set 34, i.e., Swirr= 0.15, Sgr= 0.1, Swc=40% and Sgc= 30% (Figure 5.28a)

Rock Type 5. Regions with a traditional Kr zone as discussed in MFHW-Set 30, i.e., Swirr= 0.15, Sgr= 0.1, Swc=15% and Sgc= 10% (Figure 5.38 a)

Rock Type 6. It should be considered that rock type 6 was only used for the relative permeability function in the hydraulic fractures and the function was kept unchanged (Swirr= 0.15, Sgc= 0.1, Swc=15% and Sgr= 10%) for all MFHW-Sets with either conventional or unconventional Kr.

For the three MFHW-Sets, the reservoir models with different Kr distribution were built and visualised using PETREL software (Schlumberger, 2014). Truncated normal distribution was utilised to randomly distribute different Kr functions throughout the reservoir model. The truncated normal distribution is the probability distribution of a normally distributed random variable whose value is either bounded below or above (or both).

Figure 5.35 shows different rock type contributions for MFHW-Set 37 NF7-L600 with mixed 1, MFHW-Set 38 NF7-L600 with mixed 2 and MFHW-Set 39 NF7-L600 with mixed 3. From Figure 5.35 a, it is noted that the heterogeneous model of MFHW-Set 37 consists of 10.1% Rock type 1, 23.9% Rock type 2, 27.4% Rock type 3, 26.7% Rock type

4 and 12% Rock type 5. It should be noted that rock type 6 was just used for fracture grid blocks. Figure 5.35 b also shows the contribution of different rock types of the heterogeneous model of MFHW-Set 38 (17.1% Rock type 1, 31.7% Rock type 2, 26.3% Rock type 3, 18.6% Rock type 4 and 6.4% Rock type 5). Finally, Figure 5.35c shows the contribution of different rock types of the heterogeneous model of MFHW-Set 39 (21.3% Rock type 1, 36.5% Rock type 2, 24.7% Rock type 3, 13.4% Rock type 4 and 4% Rock type 5). It should be considered that the contribution of rock types with total and weak Kr jail in MFHW-set 39 is more than that of MFHW-set 38 and MFHW-set 38 is more than that of MFHW-set 37, in other words, the Kr jail effect is most pronounced in MFHW-Set 39 compared to MFHW-Sets 38& 37.

Figure 5.36 displays the different rock type distribution in the heterogeneous reservoir model of MFHW-Set 37 NF7-L600, MFHW-Set 38 NF7-L600 and MFHW-Set 39 NF7-L600.

Comparing the GPL tornado chart of MFHW-Sets 37, 38 and 39 with the only difference was more/most pronounced Kr jail effect in MFHW-Set 38 and MFHW-Set 39, Figure 5.37a and b, and that of MFHW-Set 30, Figure 5.7, the same observations as those discussed in the previous section, were noted:

- The more pronounced the Kr jail effect, the lower the impact of Pc on clean-up efficiency.
- As the Kr jail effect becomes more pronounced, the impact of gas mobility in both matrix and fracture on clean-up efficiency becomes more significant. In line with this, the impact of Km (that of on mobility) on clean-up efficiency turns out to be more important.

Figure 5.38 shows the Saturation distribution map (run number 30) at the end of ST for a simulation run with different Kr curves or set of Kr curves; using a) conventional Kr, b) Kr curves shown in Figure 5.38b for the whole reservoir, i.e. which has a 10% total permeability jail effect, c) mixed 1 Kr curves corresponding to MFHW-Set 37 NF7-L600 s, d) mixed 2 Kr sets corresponding to MFHW-Set 38 NF7-L600s and e) mixed 3 Kr sets corresponding to MFHW-Set 39 NF7-L600s. Figure 5.39 shows the SATNUM distribution map corresponding to the data of Figure 5.38c, it was noted from these two Figures that in grids with total jail effect (as shown in Figure 5.38c with red circles), FF was effectively blocked and was not injected into the neighboring matrix grid in Y direction due to lack of viscous force. From these matrix grid blocks with total jail effect, FF could be imbibed into the neighbouring matrix grid blocks in Y direction by Pc force,

that is why the neighbouring matrix grid in the Y direction next to matrix grid blocks with total jail effect had substantially smaller Sw values.

From Figure 5.38 and Figure 5.30, it was noticed that increasing the Kr jail effect leads FF into shallower regions of the matrix as well as a significant amount of FF being left inside the fracture due to weaker viscous forces. This resulted in higher FF saturation regions in the fracture and inside the matrix in the vicinity of fracture and consequently less retained FF.

It was noted that when the whole reservoir was affected by the total permeability jail, it did not produce any gas or FF at production stage due to total jail, whereby all FF were accumulated in the fracture and matrix grids around fracture (Figure 5.38 b) and the well was effectively killed.

Figure 5.38c, Figure 5.38d and Figure 5.38e display an asymmetrical saturation distribution due to heterogeneity which was introduced to the models of the corresponding three sets. There was a high FF saturation region in the fracture and inside matrix around the fracture due to more pronounced jail effect.

Comparing the data of Figure 5.38 c, d and e, it is noted that in grids with total jail effect, FF is effectively blocked and not injected into the matrix due to lack of viscous force. It should be noted that in grids with total jail effect, the only force driving FF to be imbibed into the matrix is Pc.

Figure 5.40 and Figure 5.42 display the histogram chart that compares the GPL and PFF cumulative frequency of the runs in MFHW-Sets 36, 37, 38,39 and 30 respectively. It was noted that generally the stronger the jail effect the slower the clean-up and larger FF flow-back.

Comparing the PFF tornado chart of MFHW-Sets 37, 38 and 39, Figure 5.41a, b and c, similar observations in line with those previously noticed in MFHW-Sets 34, 35 and 36 were observed.

5.8 MFHW-Sets in Heterogeneous Reservoir Rocks with high FVR, different STs, and DPs and low Km range

In this section, the cleanup efficiency of MFHWs in heterogeneous formations, while changing some of the pertinent parameters, was investigated. 5 MFHW-Sets were simulated considering different injection volumes (FVR=10), ST=20, applied pressure drawdown (DP) during production and Km range, i.e., MFHW-Sets 40, 41, 42, 43 and 44. The aim was to observe the impact of these parameters on cleanup efficiency while

using heterogeneous reservoir rocks with unconventional Pc and Kr. MFHW Set 38 (mixed 2 with 17.1% total relative permeability jail, 76.5% of different weak permeability jails and 6.4% with conventional Kr) was selected as a base reference set for these new sets.

5.8.1 Increased FVR MFHW-Set 40

In MFHW-Set 40, the fracture volume ratio has been increased from 2 in the MFHW-Set 38 to 10. Comparing the tornado chart of MFHW-Set 40, Figure 5.43, with that of MFHW-Set 38 (FVR=2) with the only difference being a higher FVR for MFHW-Set 40, Figure 5.37b, it is noted that the observed trends are more or less the same.

The Km and gas mobility the matrix in both sets have the most significant impact on GPL and the sequences of the importance of other parameters are somewhat similar. It is also noted that Pc pertinent parameters and FF mobility in fracture are less important in the MFHW-Set 40, this is due to higher FF volume being injected compared to that one of MFHW-Set 38. In line with this, the impact of Km and Kf is less pronounced in MFHW-Set 40.

Since the model geometry of MFHWs is different from that of SFVWs, a new MATLAB code has been developed which uses the adjacent grid blocks saturation as input and give the map in a standardised format for MFHWs. The MATLAB code is included in Appendix 7.5.

Figure 5.44 shows the saturation distribution map (run number 30) at the end of ST for MFHW-Set 40 NF7-L600s with heterogeneous rock (mixed 2). The larger volume of injected FF results in higher GPL values and requires a longer time to flowback. This can clearly be seen in the water saturation map of this set, Figure 5.44, after two days of shut-in. Comparing data of this Figure with those of Figure 5.38d in the base reference set, it is noted that the FF saturation in the matrix and fracture is much greater than that of MFHW-Set 38 due to larger FVR.

Figure 5.45 and Figure 5.46 show Pc versus water saturation, Sw, for MFHW-Set40 at early and later production periods. It is demonstrated that although higher Pc values were observed for best case than worst case at all Sw in MFHW-Set40 at early production times (indicating that keeping FF in matrix is better and results in less GPL), higher Pc values were observed in MFHW-Set40 for worst case than best case at Sws above 28% at longer production time, i.e.,365days, (it is best to backflow the FF out of the matrix).

In other words, at longer production time, unlike previous two early times, using chemicals (IFT reducing agents) to reduce Pc could reduce GPL.

Figure 5.47 is the histogram chart that compares the GPL cumulative frequency of the runs in MFHW -Sets 40 (MFHW with FVR=10) and MFHW-Set 38. Similar to what was reported previously (Chapter 3) for the SFVW sets and MFHW-Sets, faster clean-up is observed for the MFHW-Set 38 FVR=2 compared to the MFHW-Set40 FVR=10. This is due to less FF injected in the MFHW-Set 38, which requires less time to clean.

5.8.2 Extended ST MFHW-Set 41

In MFHW-Set 41, the shut-in time has been extended from 2 days in the MFHW-Set 38 to 20 days. A comparison of the tornado chart of MFHW-Set 41 (ST=20), Figure 5.49, with that of MFHW-Set 38 (ST=2), Figure 5.37b, with the only difference being a longer soaking time for MFHW-Set 41, shows the same observation that was noted in chapter 3 for SFVW sets and in chapter 4 for MFHW sets (using conventional Pc and Kr), i.e., the observed magnitude and trends of all pertinent parameters are more or less the same. However, the absolute value of Pc pertinent parameters, i.e. IFT and λ, are larger than those of MFHW-Set 38, confirming the observation reported for the corresponding SFVW sets and MFHW-Sets (using conventional Pc and Kr) that extending soaking time makes the effect of Pc on GPL to be more important (Chapter 3 and Chapter 4).

Figure 5.50 shows the Saturation distribution map (run number 30) at the end of ST for MFHW-Set 41 NF7-L600s with heterogeneous rock (mixed 2). The longer applied ST in this set results in more FF imbibition deeper into the matrix and consequently lower GPL values. This can clearly be seen in the water saturation map of this set, Figure 5.50, after twenty days of a shut-in. Comparing data of this Figure with those of Figure 5.38d in MFHW-Set 38, it is noted that FF is imbibed into the matrix more than those of shorter ST (ST=2 days). This results in more distributed FF saturation in the matrix and smaller FF saturations in the fracture due to longer ST and consequently better cleanup.

The histogram chart that compares the GPL cumulative frequency of the runs in MFHW-Set 41 (ST=20 days) and MFHW-Set 38 (ST=2 days), Figure 5.51, shows that faster clean-up is observed for the extended ST MFHW set compared to the MFHW-Set 38 but only at early production time, the same observation as the one noted for SFVWs and MFHWs (Chapter 3 and Chapter 4). The PFF histogram chart that compares the PFF cumulative frequency of the runs in MFHW-Set 41 (ST=20 days) and MFHW-Set 38 (ST=2 days), Figure 5.53, shows that smaller FF flowback is observed for the extended

ST MFHW set compared to the MFHW-Set 38, this is in line with having a longer ST that allows FF to be imbibed more into the matrix and consequently more retained in the matrix.

5.8.3 MFHW-Sets with reduced/increased DP (DP=100 and 4000 psi)

In this section, DP has been decreased/increased from 1000 psi in the MFHW -Set 38 to 100 and 4000 psi in MFHW-Sets 42 & 43 respectively.

Comparing the tornado chart of MFHW-Set 42 (DP=100), Figure 5.54a, with that of MFHW-Set 38 (DP=1000) with the only difference being a lower DP by a factor of 10 for MFHW-Set 42, Figure 5.37b, it is noted that the observed trends of pertinent parameters are the same with the exception of an increase in the absolute value of Pc pertinent parameters in the lower DP set. This is in line with what was reported previously for low DP MFHW sets (using conventional Pc and Kr) and low DP SFVW sets, i.e., in low DP sets the effect of Pc on GPL is more pronounced (Chapter 4 and Chapter 3).

In MFHW-Set 42, the impact of the end points and exponents of Corey type relative permeability curves for gas and FF in the matrix is more pronounced than that of these parameters in MFHW-Set 38 confirming the observation noted in the corresponding SFVW sets and MFHW sets (using conventional Pc and Kr). That is, in low DP sets, it is more important how fluid (Gas and FF) flows from the matrix to fracture than how it flows from fracture to the wellbore.

In MFHW-Set 43, DP has been increased from 1000 psi in the MFHW-Set 38 to 4000 psi. Comparing the tornado chart of MFHW-Set 43 (DP=4000), Figure 5.54b, with that of MFHW-Set 38 (DP=1000) with the only difference being a higher DP by a factor of 4 for MFHW-Set 43, Figure 5.37b, it is noted that the observed trends of pertinent parameters are more or less similar with the exception of a decrease in the absolute value of Pc pertinent parameters. This is in line with what was reported previously for high DP SFVW sets and MFHW sets (using conventional Pc and Kr), i.e., in high DP sets the effect of Pc on GPL is less pronounced. (Chapter 3 and Chapter 4)

The impact of the end points and exponents of Corey type relative permeability curves for gas and FF in the matrix is slightly less pronounced than that of these parameters in MFHW-Set 38 confirming the observation noted in SFVW sets and MFHW sets (using conventional Pc and Kr), that is, in high DP sets it is less important how fluid (Gas and FF) flows from the matrix to fracture than how it flows from fracture to the wellbore. This follows the same trend as what was observed above for the low DP set, MFHW-42. In line with these observations, the same observations are noted when the PFF tornado charts

of MFHW-Set 42 and 43 are compared to the relevant one on MFHW-Set 38 with DP=1000 (Figure 5.55).

Figure 5.56 is the histogram chart that compares the GPL cumulative frequency of the runs in MFHW-Set 42 with DP=100 psi, MFHW-Set 38 with DP=1000psi and MFHW-Set 43 with DP=4000psi. Slower/faster clean-up is observed for this lower/higher DP set compared to the MFHW-Set 38. Figure 5.57 is the PFF histogram chart that compares the FF cumulative frequency of the runs in MFHW-Set 42 with DP=100 psi, MFHW-Set 38 with DP=1000psi and MFHW-Set 43 with DP=4000psi. Smaller/Larger FF flowback is observed for this lower/higher DP set compared to the MFHW-Set 38. These observations are in line with was previously observed in chapter 3 and 4 in SFVW sets and MFHW sets (using conventional Pc and Kr) respectively.

5.8.4 Tighter Formations by a Factor of 10 MFHW-Sets 44

In this section, the range of matrix permeability variation has been lowered from 1 μD-100 μD in the MFHW-Set 38 to 0.1 μD-10 μD in MFHW-Set 44.

Comparing the tornado charts of MFHW-Set 44 (Kmr=10), Figure 5.58 with that of MFHW-Set 38 (Kmr=1) with the only difference being tighter formations by a factor of 10 for MFHW-Sets 44, Figure 5.37b, it is noted that the observed trends are the same except for the IFT coefficient at 365 days. Since in MFHW-Set 44, the matrix permeability range has been reduced by a factor of 10, fluid mobility in the heterogeneous matrix rock is more difficult, hence the effect of gas mobility pertinent parameters in the matrix on cleanup efficiency is more pronounced.

Comparing the PFF tornado charts of MFHW-Set 44 (Kmr=10), Figure 5.60 with that of MFHW-Set 38 (Kmr=1) with the only difference being tighter formations by a factor of 10 for MFHW-Sets 44, Figure 5.41b, the same observations are noted in line with GPL tornado charts.

It is noted that in MFHW-Sets 44, the IFT coefficient trend changes as production time increases. This highlights that using IFT reducing agent could improve the cleanup efficiency. Figure 5.62 and Figure 5.63 show Pc versus water saturation in MFHW-Set 44 with heterogeneous rock (mixed 2), Sw, for MFHW-Set44 at early and later production periods. It is concluded that although higher Pc values were observed for best case than worst case at all Sw in MFHW-Set44 at early production times, i.e., 10 and 30 days, (indicating that keeping FF in matrix is better and results in less GPL), higher Pc values were observed in MFHW-Set44 for worst case than best case at Sws above 26% at longer

production time, i.e.,365days, (it is best to backflow the FF out of the matrix). In other words, at longer production time, unlike previous two early times, using chemicals (IFT reducing agents) to reduce Pc could reduce GPL, this is in line with what was previously observed in section 5.7.1 for high FVR sets.

Considering the histogram charts that compare the GPL cumulative frequency of the runs in MFHW-Set 44 & 38 with Kmr=10 &1 respectively, Figure 5.59, the same observation is observed similar to what was reported previously for the SFVW sets (Chapter 3) and MFHW sets using conventional Pc and Kr (Chapter 4), i.e., slower clean-up is observed for the tighter formation compared to the MFHW base reference set.

5.9 Summary and Conclusions

In order to further improve the current understanding of hydraulic fracturing treatment for practical field applications, this study has expanded the previous works that were done in chapter 4 to capture the impact of unconventional Pc and Kr on the MFHWs clean-up efficiency. In this chapter, a comprehensive evaluation of Pc correlations available for tight and ultra-tight formations was performed using the Go2Flow software. Additionally, a comprehensive investigation was conducted on unconventional relative permeability (Kr) and permeability jail effects in unconventional formation.

For these 10 sets, a new dimensionless term, similar to GPL, was defined to capture the impact the same pertinent parameters on the production of FF, which was an important consideration for HF of unconventional reservoirs.

A summary of the main conclusions are given below:

1. The results of Pc model evaluations (using 200 conventional, tight and ultra-tight Pc data sets) showed that Brooks and Corey was a simple and accurate one-specific-parameter model to represent Pc data in tight and ultra-tight unconventional formations.
2. The result of this study suggested that the range of pore size distribution index should be limited to values between 0.3 to 1.5 to represent the unconventional tight/ultra-tight rock behaviours. This new pore size distribution range was applied in the model to account for unconventional Pc.
3. In this study a concave down part in some Pc (or Leverett J) curves was observed, this concave down effect was attributed to the dead volume errors in capillary pressure measurements. The dead volume must be corrected and should not be misinterpreted as a change in a characteristic of the rock.

4. In MFHW-sets with unconventional Pc, the impact of Pc pertinent parameters (especially that of lambda) on GPL was most important. This was attributed to having a lower lambda range in the unconventional Pc MFHW-Sets, which made Pc values to be much larger than those of conventional Pc MFHW-Sets.
5. Kf had two different impacts on the FF production:
    - Larger Kf provided better FF mobility inside the fracture during the production stage. This resulted in more FF production.
    - Larger Kf resulted in better FF mobility inside the fracture during the injection period. This resulted in more distributed FF and smaller Sw values in the matrix and consequently larger Pc values. The larger Pc values retain more FF during the production stage resulting in less FF production.
6. PFF tornado charts showed that as water mobility in the matrix increased, the FF production decreased. This is because the water mobility in the matrix, which has again two different impacts on the FF production:
    - Larger water mobility in the matrix provides better FF mobility inside the matrix during the production stage resulting in more FF production.
    - Larger water mobility in the matrix results in better FF mobility inside the matrix during the injection period. This results in more distributed FF and smaller Sw values in the matrix and consequently larger Pc values. The larger Pc values retain more FF during the production stage resulting in less FF production.
7. For the sets with unconventional Pc, reducing the permeability range (Km) or increasing the injected FF volume to fracture volume ratio (FVR), resulted in the same observations as those, when conventional Pc was employed, the main ones are:
    a. Reducing the Km range or increasing FVR slowed down the clean-up.
    b. The Km coefficient in the set with Kmr=1 was positive, i.e., increasing Km increased GPL, which indicated that the Km effect reducing Pc which results in increased FF production, was important. Km coefficient in the set with Kmr=100 was negative, i.e., increasing Km decreased GPL, which indicated that the Km effect on mobility was important. This trend change is due to very tight nature of the rock in this set, which makes the matrix fluid mobility significantly difficult.
    c. In the set with significantly high FVR, the impact of fluid mobility in the matrix and fracture on GPL was more important than those sets with lower FVR.

8. However, increasing DP did not accelerate the clean-up process in the MFHW-Set with unconventional Pc. This is because although increasing DP generally makes clean-up faster in the fracture and matrix in the fracture vicinity, it results in more FF flowback from deeper zones inside the matrix and further away from fracture which has a more detrimental impact on clean-up. This two diverse effects balanced each other and almost the same clean-up performance was observed in the two sets with conventional an unconventional Pc curves. More FF flowback in this high DP set with unconventional Pc is due to larger viscous force, which leads to more FF flow-back whilst in the relevant set but with conventional Pc most of the FF flow-back occurs at moderate DP since the Pc values are not as significant as the ones for unconventional Pc to retain the FF inside matrix as strongly as the unconventional Pc does.
9. Although the idea for the existence of a 'permeability jail' has yet to be proven in any laboratory experiments, Kr jail is an emerging topic that offers insights to tight/ultra-tight reservoirs' behaviour that could explain many of the observations made in unconventional formations.
10. A comprehensive investigation was conducted on the unconventional (Kr) with jail effect in unconventional formations. An attractive approach was adopted to successfully model the weak and strong permeability jail effects in unconventional Kr models, i.e. Corey type model was used albeit with a large difference between critical (phase mobilisation in the increasing saturation direction) and trap end point (is in the decreasing saturation direction) saturation.
11. In MFHW-Sets with unconventional Kr it was noted that:
    a. The more pronounced the relative permeability jail effect, the lower the impact of Pc on both clean-up efficiency and FF flow-back.
    b. As the Kr jail effect became more pronounced, the impact of fluid mobility in both matrix and fracture on both clean-up efficiency and FF flow-back became more significant.
        i. In line with this, the impact of Km (that on mobility) on clean-up efficiency turned out to be more important, i.e. it had a negative coefficient.
    c. The stronger the Kr jail effect, the slower the clean-up was also noted.
12. In heterogeneous formations with unconventional Pc and Kr, when other pertinent parameters like FVR, DP, ST and Km range were changed, the same observations were

observed in line with what was previously observed in chapter 3 and 4 for SFVW sets and MFHW sets (using conventional Pc and Kr) respectively.

5.10 References

BENNION, D. B., THOMAS, F. B., SCHULMEISTER, B. E. & SUMANI, M. 2004. Determination of true effective in situ gas permeability in subnormally water-saturated tight gas reservoirs. *Journal of Canadian Petroleum Technology,* 43**,** 27-32.

BENTSEN, R. G. & ANLI, J. 1977. Using Parameter Estimation Techniques To Convert Centrifuge Data Into a Capillary-Pressure Curve.

BROOKS, R. H. & COREY, A. 1966. Properties of porous media affecting fluid flow. *Journal of the Irrigation and Drainage Division,* 92**,** 61-90.

BYRNES, A. P. 1996. Reservoir characteristics of low-permeability sandstones in the Rocky Mountains. *Mountain Geologist,* 34**,** 39-48.

BYRNES, A. P. 2008. Issues with gas relative permeability in low-permeability sandstones. *AAPG Hedberg Series, no. 3, p. 63–76.*

CLUFF, R. M. & BYRNES, A. P. 2010. Relative Permeability In Tight Gas Sandstone Reservoirs - The "Permeability Jail" Model. *Society of Petrophysicists and Well-Log Analysts.* Society of Petrophysicists and Well-Log Analysts.

GDANSKI, R. D. & WALTERS, H. G. 2010. Impact of Fracture Conductivity and Matrix Relative Permeability on Load Recovery. Society of Petroleum Engineers.

JURUS, W. J., WHITSON, C. H. & GOLAN, M. 2013. Modeling Water Flow in Hydraulically-Fractured Shale Wells. Society of Petroleum Engineers.

LEVERETT, M. 1941. Capillary behavior in porous solids. *Transactions of the AIME,* 142**,** 152-169.

MCKAY, M. D., BECKMAN, R. J. & CONOVER, W. J. 1979. A Comparison of Three Methods for Selecting Values of Input Variables in the Analysis of Output from a Computer Code. *Technometrics,* 21**,** 239-245.

O'MEARA Consulting Inc. 2014. Geo2Flow, Release 2014.5.4, *Geo2Flow*.

RUSHING, J. A., NEWSHAM, K. E. & BLASINGAME, T. A. 2008. Rock Typing: Keys to Understanding Productivity in Tight Gas Sands. Society of Petroleum Engineers.

SCHLUMBERGER. 2014. Petrel E&P Software Platform 2014.1 (64-bit), *Schlumberger Company*.

SHAFER, J. & NEASHAM, J. Mercury porosimetry protocol for rapid determination of petrophysical and reservoir quality properties. International Symposium of the Society of Core Analysts, SCA, 2000. 12.

SHANLEY, K. W., CLUFF, R. M. & ROBINSON, J. W. 2004. Factors controlling prolific gas production from low-permeability sandstone reservoirs: Implications for resource assessment, prospect development, and risk analysis. *AAPG bulletin,* 88**,** 1083-1121.

SHAOUL, J. R., VAN ZELM, L. F. & DE PATER, C. J. 2011. Damage Mechanisms in Unconventional-Gas-Well Stimulation--A New Look at an Old Problem.

SKELT, C. & HARRISON, B. 1995. An Integrated Approach To Saturation Height Analysis. Society of Petrophysicists and Well-Log Analysts.

THOMEER, J. H. M. 1960. Introduction of a Pore Geometrical Factor Defined by the Capillary Pressure Curve.

UNIVERSITY OF KANSAS CENTER FOR RESEARCH, I. & SURVEY., T. K. G. 2009. Analysis Of Critical Permeability, Capillary Pressure And Electrical Properties For Mesaverde Tight Gas Sandstones From Western U.S. Basins. *Final Scientific/Technical Report for United States Department of Energy and National Energy Technology Laboratory*.

WANG, J. Y., HOLDITCH, S. A. & MCVAY, D. 2009. Modeling Fracture Fluid Cleanup in Tight Gas Wells. Society of Petroleum Engineers.

5.11 Tables

Table 5.1 Unconventional MFHW-Sets analysed

Set Name	No. of fractures	Horizontal Length (m)	DP (Psi)	FVR	Shut-in time (days)	Kf (D)	Km (μD)	lam
Default Values	3	600	1000	2	2	1-30	1-100	1-4
MFHW-Set 30	7	✓	✓	✓	✓	✓	✓	0.3-1.5
MFHW-Set 31	7	✓	✓	✓	✓	✓	0.01-1	0.3-1.5
MFHW-Set 32	7	✓	✓	10	✓	✓	✓	0.3-1.5
MFHW-Set 33	7	✓	4000	✓	✓	✓	✓	0.3-1.5
MFHW-Set 34 weak jail, two phase 30%	7	✓	✓	✓	✓	✓	✓	0.3-1.5
MFHW-Set 35 weak jail, two phase 20%	7	✓	✓	✓	✓	✓	✓	0.3-1.5
MFHW-Set 36 weak jail, two phase 10%	7	✓	✓	✓	✓	✓	✓	0.3-1.5
MFHW-Set 37 mixed 1	7	✓	✓	✓	✓	✓	✓	0.3-1.5
MFHW-Set 38 mixed 2	7	✓	✓	✓	✓	✓	✓	0.3-1.5
MFHW-Set 39 mixed 3	7	✓	✓	✓	✓	✓	✓	0.3-1.5
MFHW-Set 40 mixed 2	7	✓	✓	10	✓	✓	✓	0.3-1.5
MFHW-Set 41 mixed 2	7	✓	✓	✓	20	✓	✓	0.3-1.5
MFHW-Set 42 mixed 2	7	✓	100	✓	✓	✓	✓	0.3-1.5
MFHW-Set 43 mixed 2	7	✓	4000	✓	✓	✓	✓	0.3-1.5
MFHW-Set 44 mixed 2	7	✓	✓	✓	✓	✓	0.1-10	0.3-1.5

Table 5.2 Error in fit of different J function models for all Pc data sets, tight and Ultra-tight data sets

	J Function Model Name	Error in Fit for All Pc Datasets	Error in Fit for Tight Pc Datasets	Error in Fit for Ultra-Tight Pc Datasets
Models with one model-specific parameter	Thomeer	6.26E-03	9.97E-03	2.89E-02
	Brooks and Corey	8.91E-03	8.64E-03	2.91E-02
	Bentsen and Anli	1.49E-02	1.21E-02	2.95E-02
Models with two model-specific parameters	Skelt-Harrison	6.68E-03	7.86E-03	2.87E-02
	O'Meara Unimodal	7.09E-03	8.49E-03	2.86E-02

Table 5.3 Pore size distribution index, Error in fit and j function displacement values of Brooks and Corey model for different individual data sets of tight and ultra-tight groups

Sample data set name	Permeability, md	Porosity %	λ	Jd	Error in fit
A-IPE-HG-195	0.0086	11.8	1.080	0.0540	2.06E-03
A-IPE-HG-120	0.00062	5.5	0.462	0.0326	3.23E-05
A-IPE-HG-141	0.0011	12.8	1.062	0.0228	8.80E-04
A-IPE-HG-142	0.0062	7.3	1.042	0.0377	1.40E-03
A-IPE-HG-112	0.008	10.5	1.179	0.0546	2.01E-04
A-IPE-HG-114	0.00957	10.2	1.497	0.0703	8.60E-04
A-IPE-HG-128	0.0199	12	0.458	0.0555	4.63E-04
A-IPE-HG-168	0.0364	9	0.613	0.0776	5.50E-04
A-IPE-HG-77	0.0416	9.5	0.386	0.0345	7.41E-04
A-IPE-HG-76	0.0512	9.8	0.492	0.0394	5.18E-04
A-IPE-HG-60	0.067	15.4	0.565	0.0827	2.79E-04
A-IPE-HG-101	0.0728	14.1	0.575	0.1242	3.16E-04
A-IPE-HG-167	0.0978	9.8	0.743	0.1016	1.99E-04
A-IPE-HG-9	0.137	11.4	0.556	0.0492	3.63E-04
A-IPE-HG-14	0.00016	3	0.670	0.0550	1.99E-04
A-IPE-HG-34	0.00025	4.5	0.766	0.0079	5.04E-04
A-IPE-HG-130	0.000064	8.2	0.694	0.0231	2.84E-04
A-IPE-HG-52	0.000343	5.5	0.704	0.0489	4.46E-05
A-IPE-HG-132	0.00028	4.2	0.951	0.0875	4.00E-03
A-IPE-HG-137	0.000374	3.7	0.357	0.1016	1.36E-03
A-IPE-HG-19	0.00039	4.2	0.826	0.0560	7.43E-04
A-IPE-HG-93	0.00025	7.8	0.664	0.0348	7.17E-04
A-IPE-HG-27	0.00021	4.3	0.487	0.0173	5.43E-04
A-IPE-HG-31	0.00034	5.7	0.475	0.0493	7.57E-06
A-IPE-HG-110	0.00117	8.4	0.513	0.0341	7.42E-04
A-IPE-HG-55	0.000088	3	0.749	0.0500	7.31E-04
A-IPE-HG-37	0.00227	10.2	0.538	0.0252	1.13E-04
A-IPE-HG-109	0.00029	4	0.313	0.0351	1.18E-04
A-IPE-HG-118	0.0189	10.2	0.921	0.0525	6.27E-05
A-IPE-HG-119	0.00247	9.7	0.561	0.0320	2.36E-04

5.12 Figures

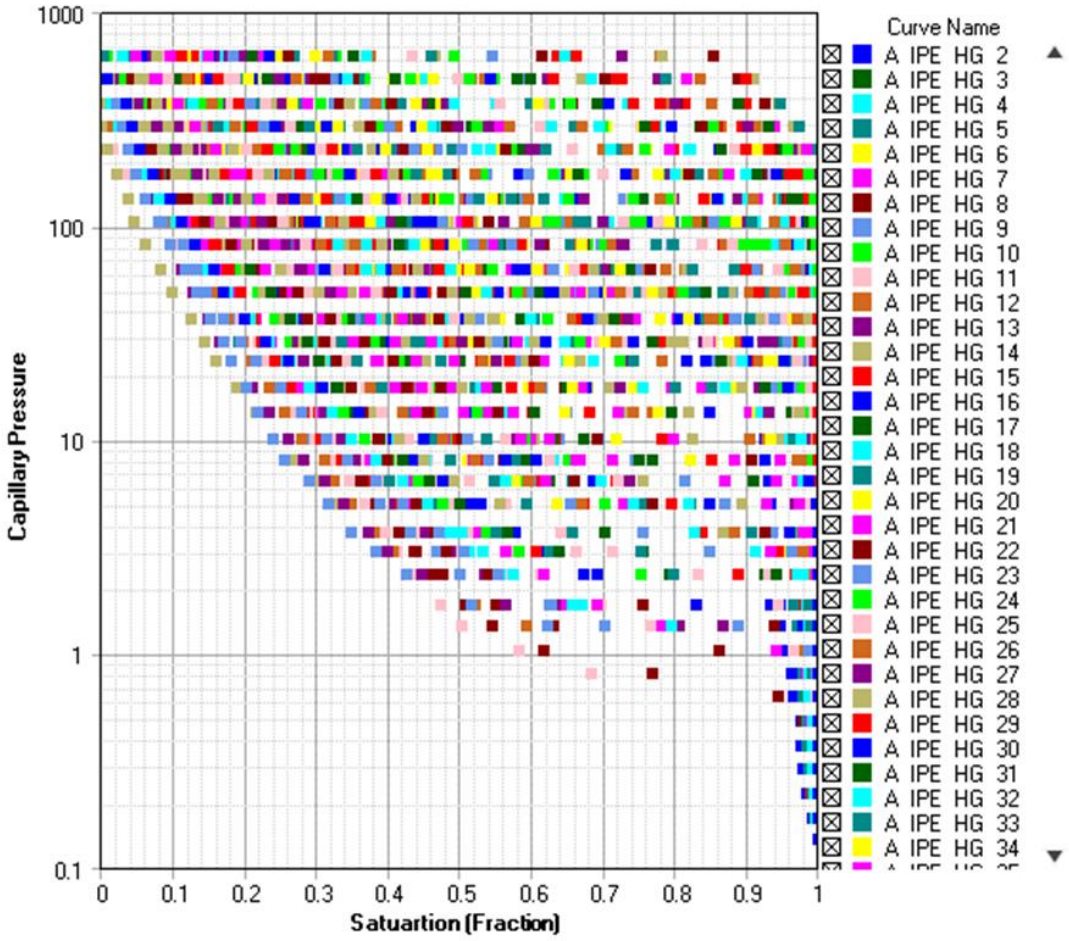

Figure 5.1 200 Pc data sets versus saturation found in the literature and used in this study. (It should be noted that the Pc is in Bar)

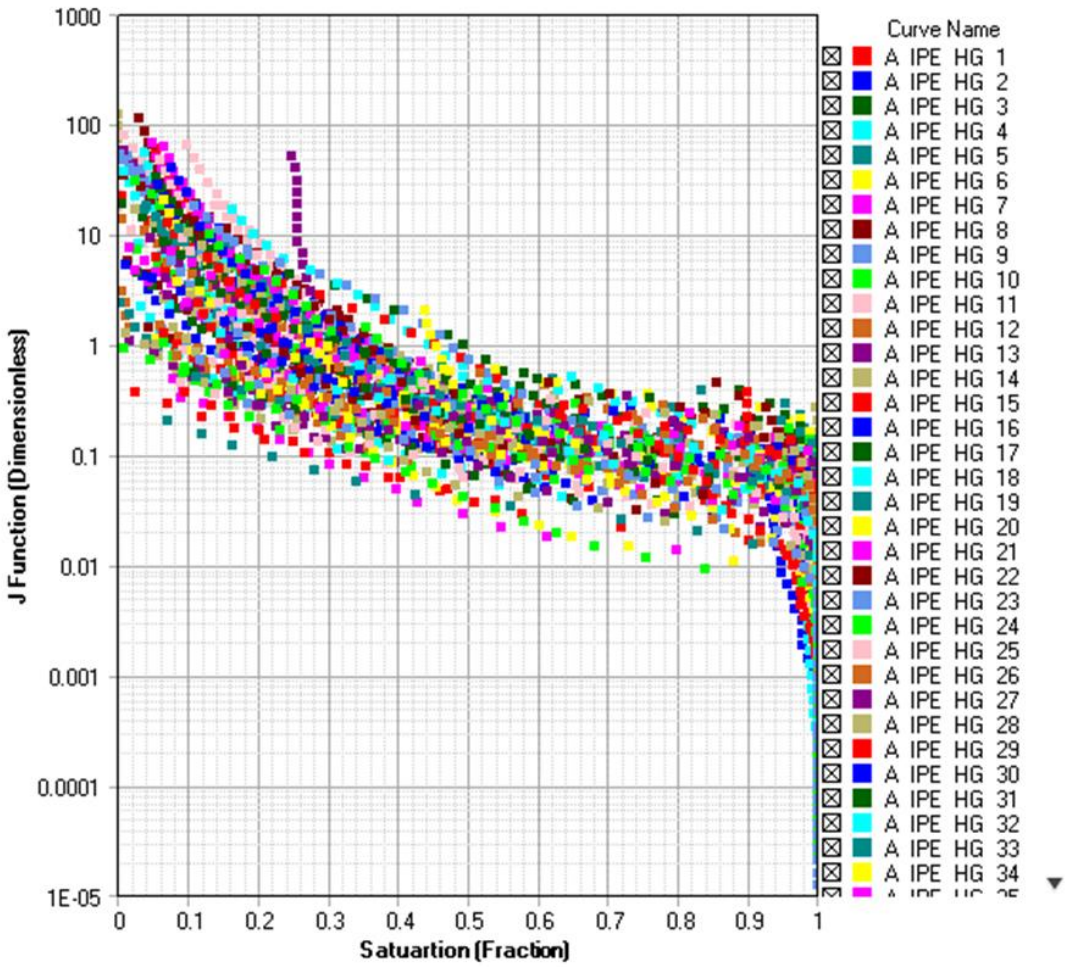

Figure 5.2 J functions versus saturation for the 200 Pc data sets of Figure 5.1

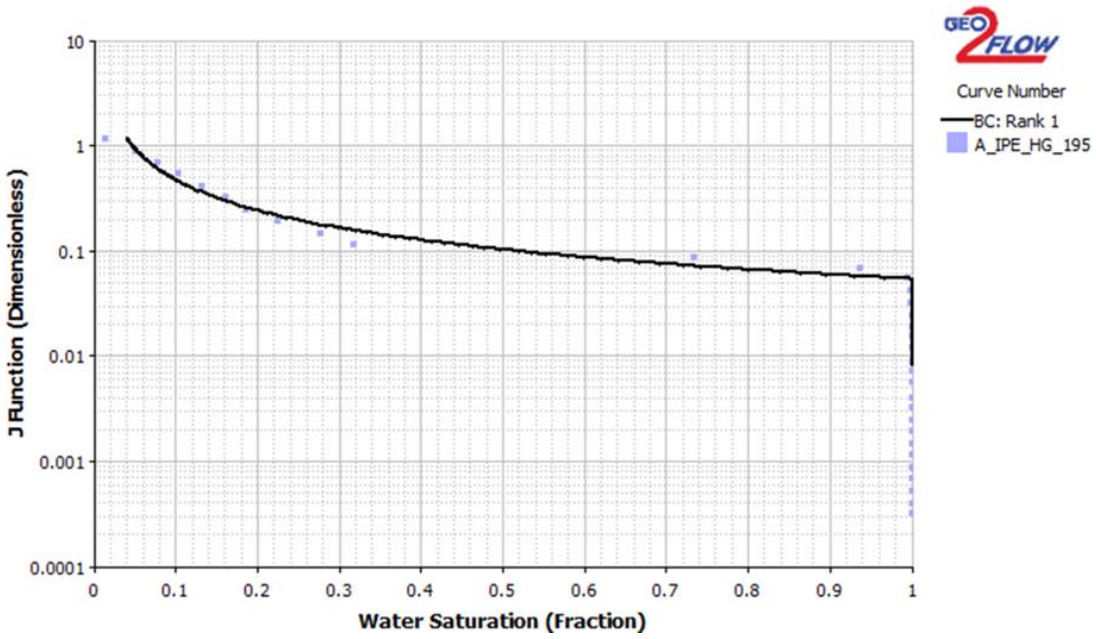

Figure 5.3 Real and fitted J functions versus saturation for a Pc sample data set (A-IPE-HG-195) from tight sets.

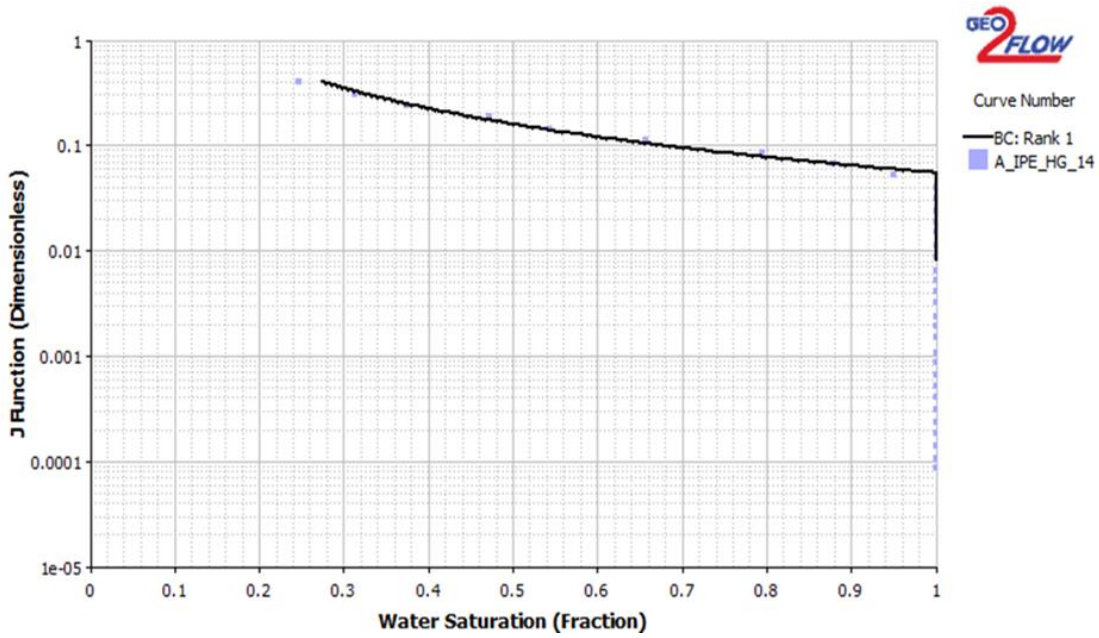

Figure 5.4 Real and fitted J functions versus saturation for a Pc sample data set (A-IPE-HG-14) from ultra-tight sets.

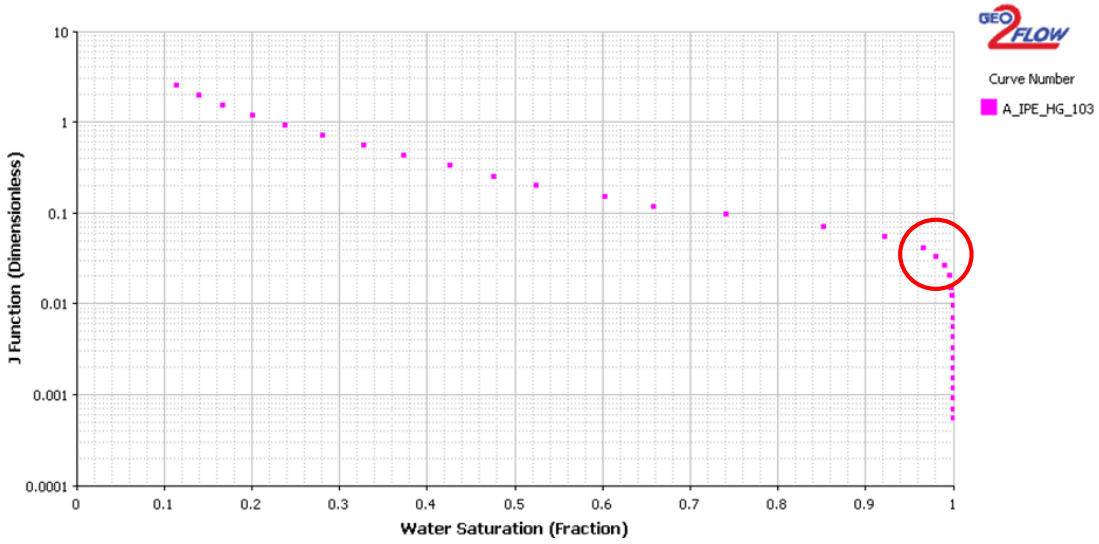

Figure 5.5 A Pc sample data set (A_IPE_HG_103) with dead volume error highlighted with a red coloured circle.

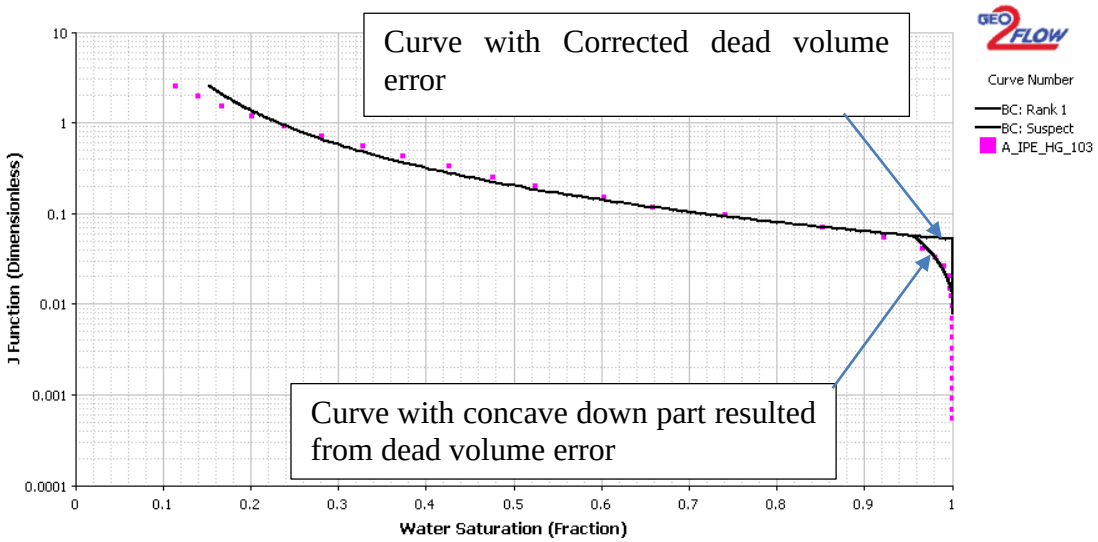

Figure 5.6 A Pc sample data set (A_IPE_HG_103) with corrected dead volume error.

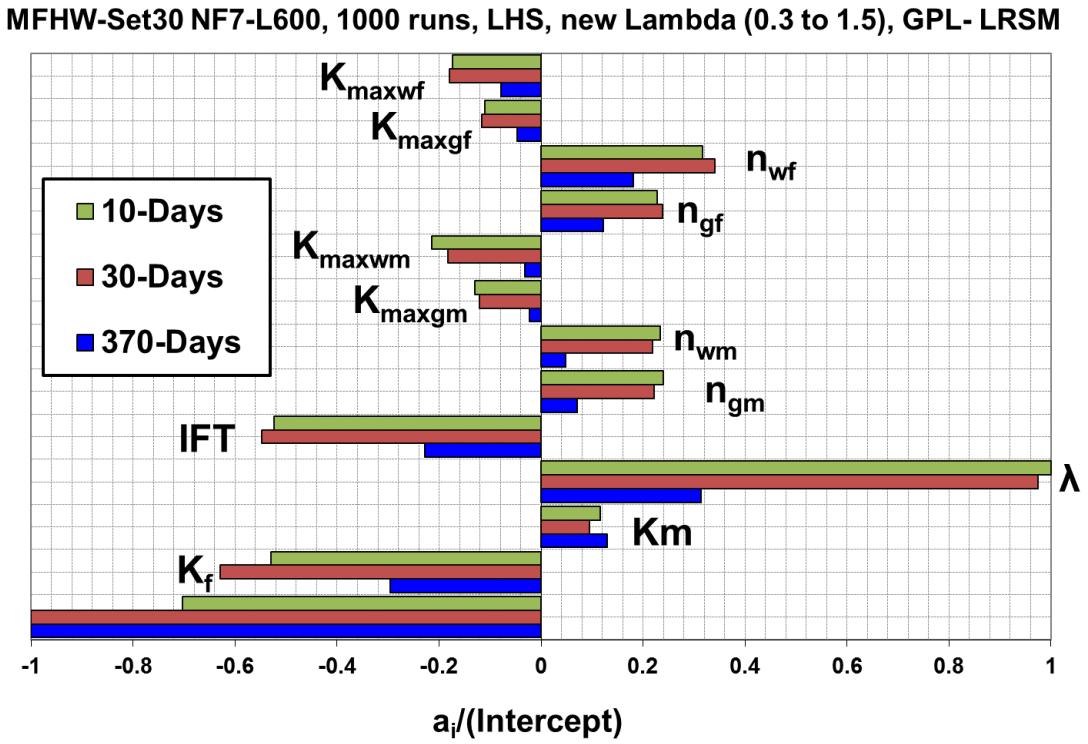

Figure 5.7 GPL Tornado chart comparing LRSM coefficients of all pertinent parameters at three production stages for MFHW-set30 using new lambda range (0.3 to 1.5)

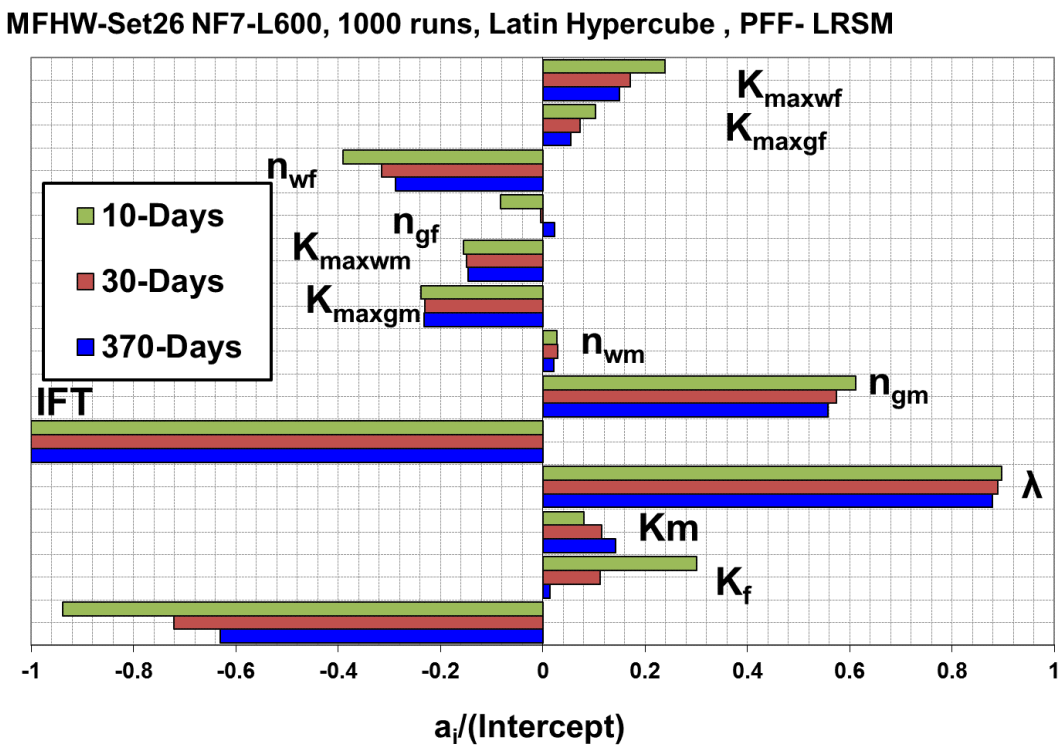

Figure 5.8 PFF Tornado chart comparing LRSM coefficients of all pertinent parameters at three production stages for MFHW-set26 Base Reference sets with LHS & 1000 Runs

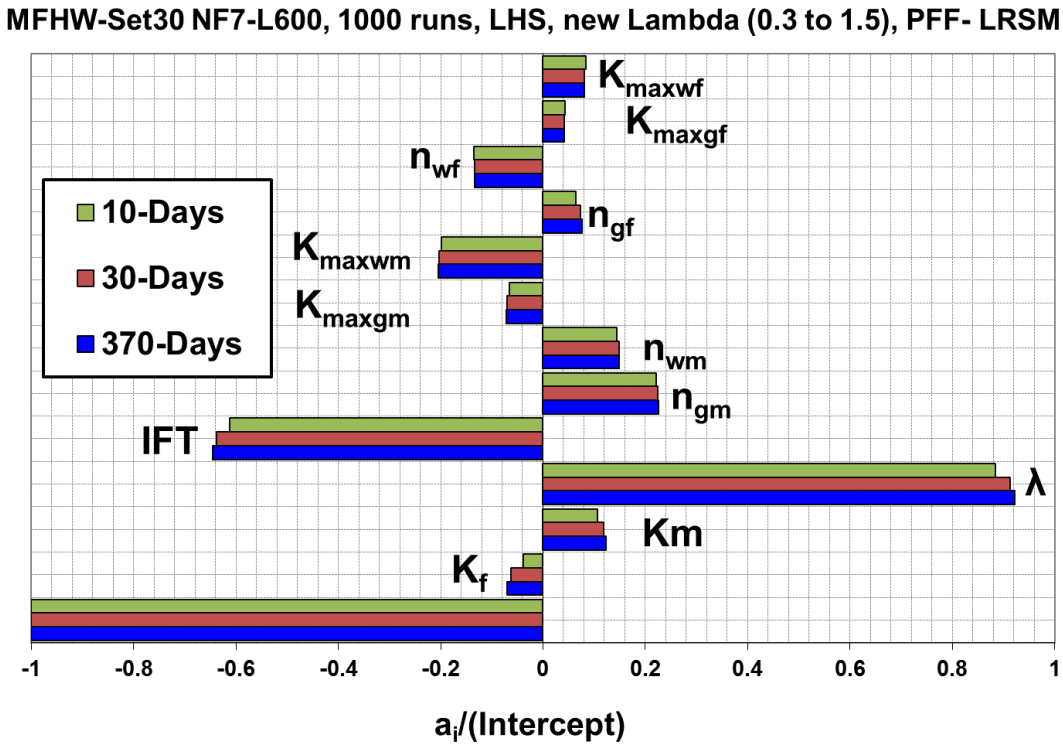

Figure 5.9 PFF Tornado chart comparing LRSM coefficients of all pertinent parameters at three production stages for MFHW-set30 using new lambda range (0.3 to 1.5)

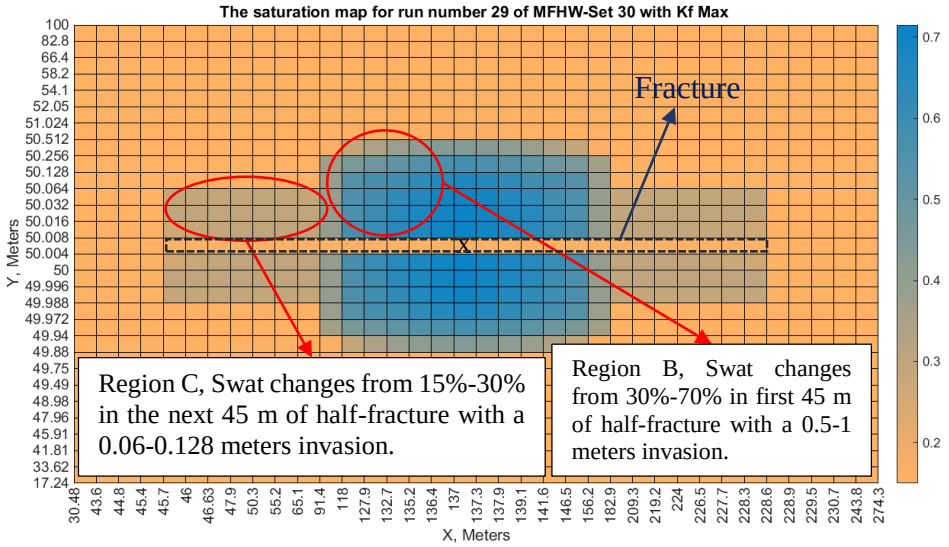

Figure 5.10 Fracturing Fluid saturation map for run number 29 with maximum Kf of MFHW-Set 30 after 2 days of shut-in period.

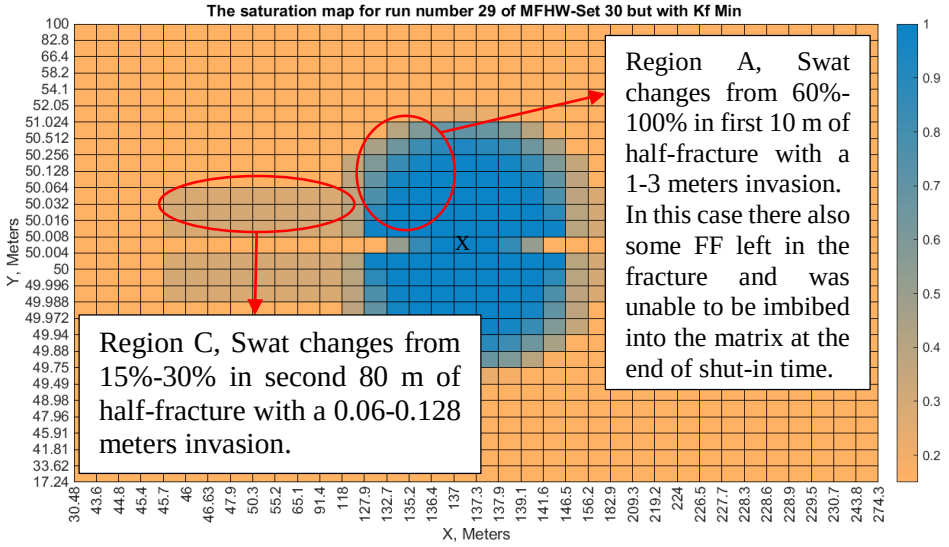

Figure 5.11 Fracturing Fluid saturation map for run number 29 with minimum Kf of MFHW-Set 30 after 2 days of shut-in period.

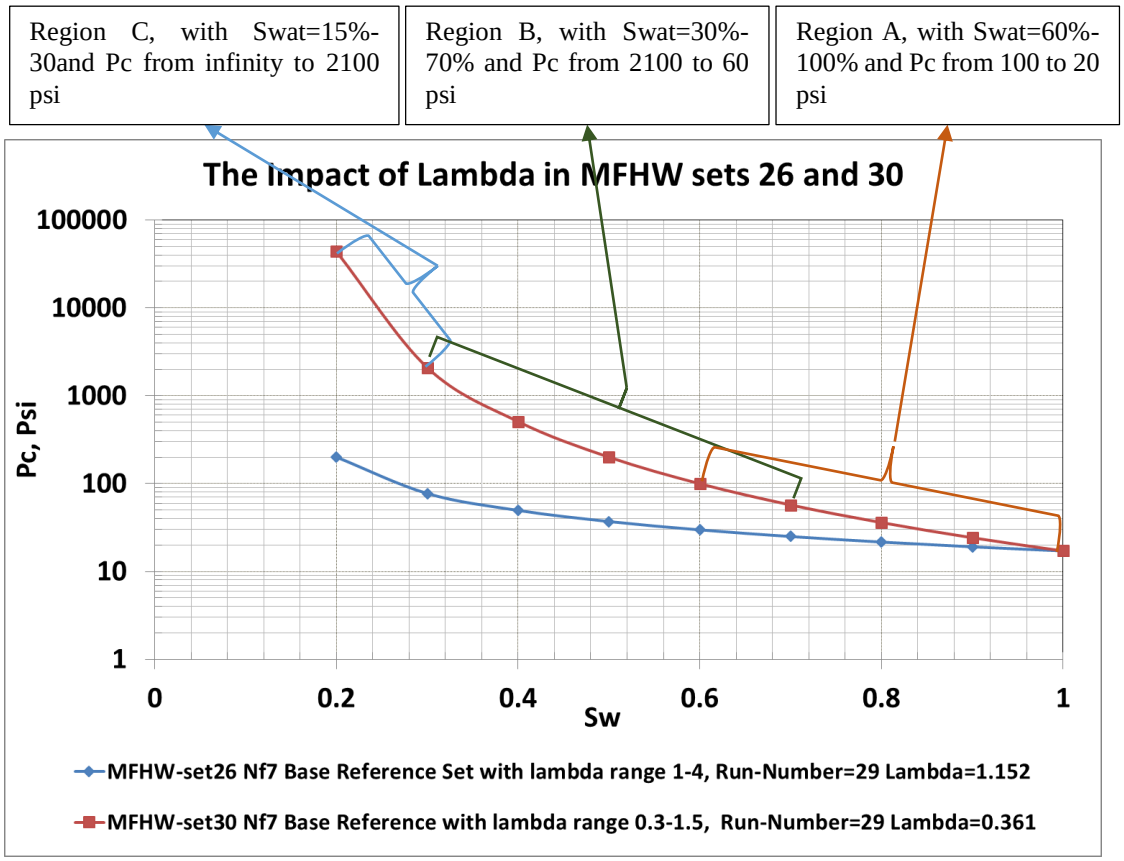

Figure 5.12 the plotted Pc for MFHW-sets 26 and 30 (run number=29) with different regions that was addressed in Figure 5.11 and Figure 5.10.

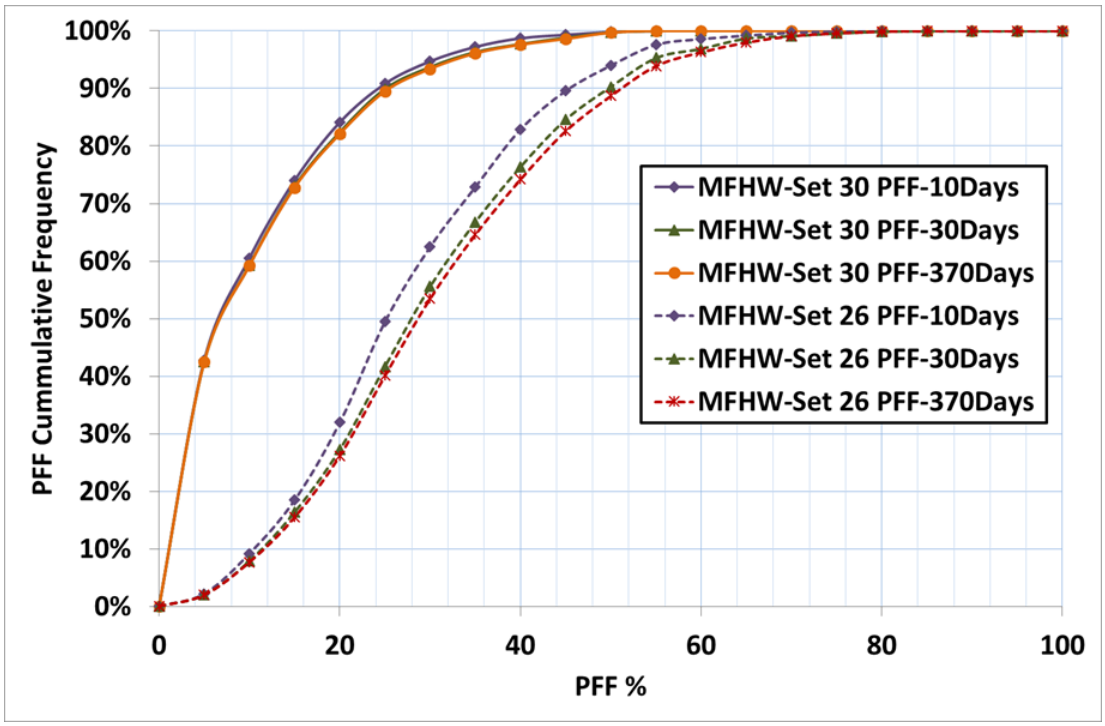

Figure 5.13 Histogram chart comparing PFF cumulative frequency of MFHW-set 30 using new lambda range (0.3 to 1.5) and MFHW-Set 26 at three production stages.

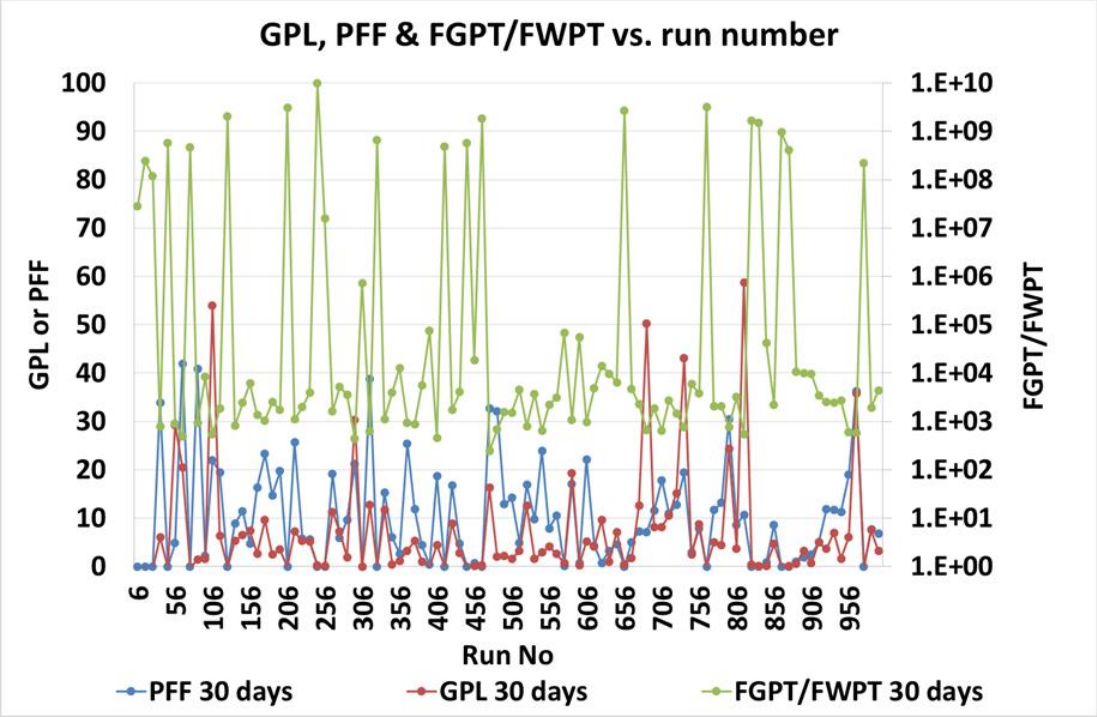

Figure 5.14 GPL, PFF and FGPT/FWPT versus run numbers in MFHW-set 30 using new lambda range (0.3 to 1.5) at 30 days of production.

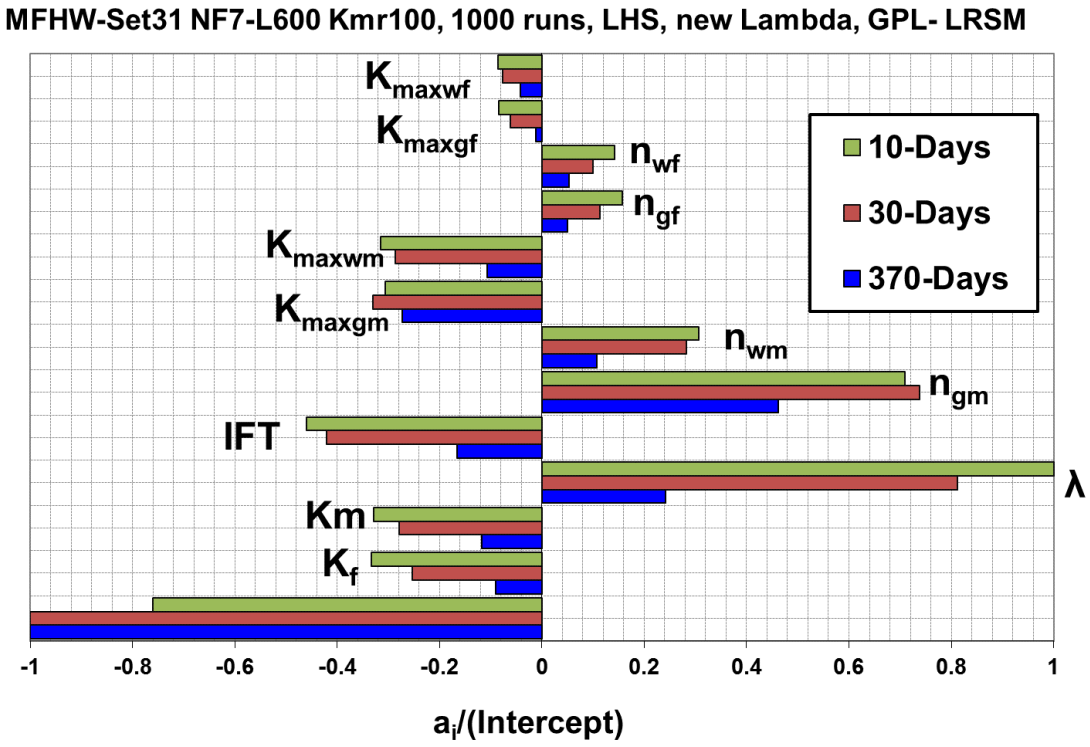

Figure 5.15 GPL Tornado chart comparing LRSM coefficients of all pertinent parameters at three production stages for MFHW-set31 with Kmr=100 and using new lambda range (0.3 to 1.5)

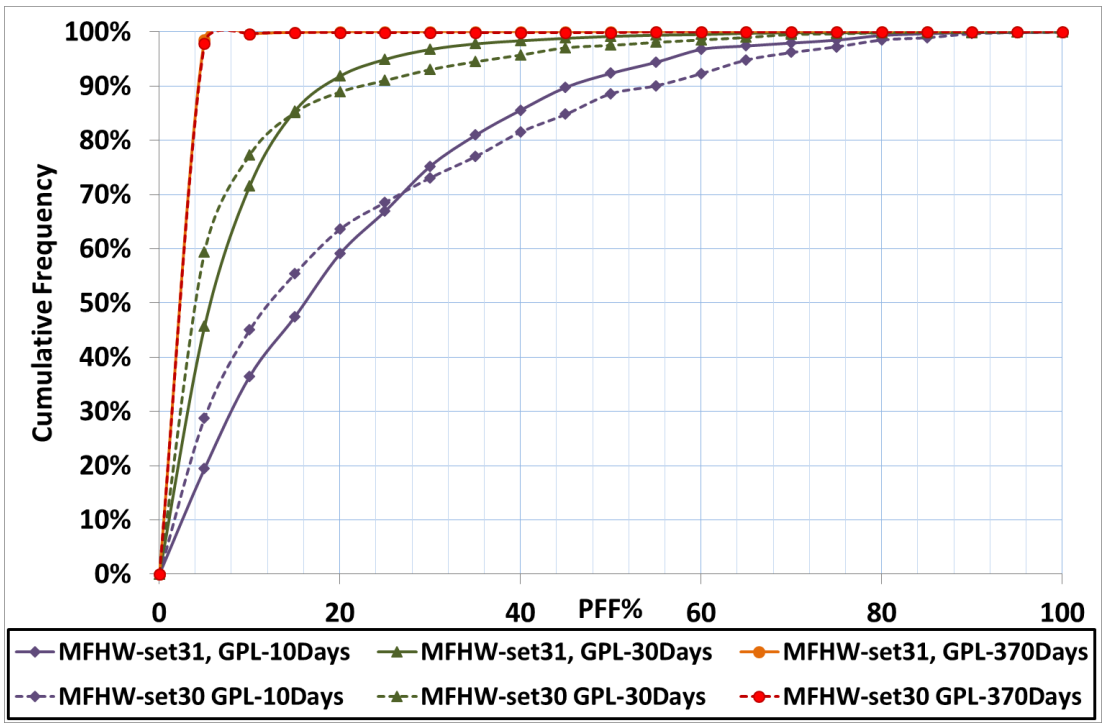

Figure 5.16 Histogram chart comparing GPL cumulative frequency of MFHW-set 31 with Kmr=100 and MFHW-Set 30 at three production stages.

Figure 5.20

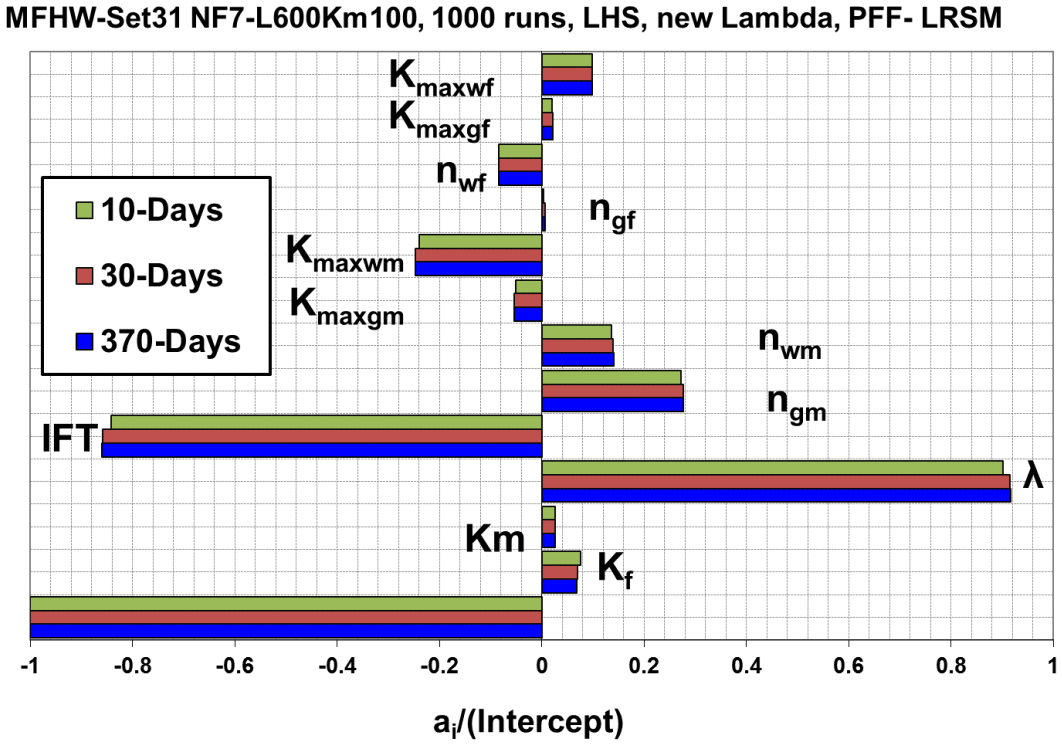

Figure 5.17 PFF Tornado chart comparing LRSM coefficients of all pertinent parameters at three production stages for MFHW-set31 with Kmr=100 and using new lambda range (0.3 to 1.5)

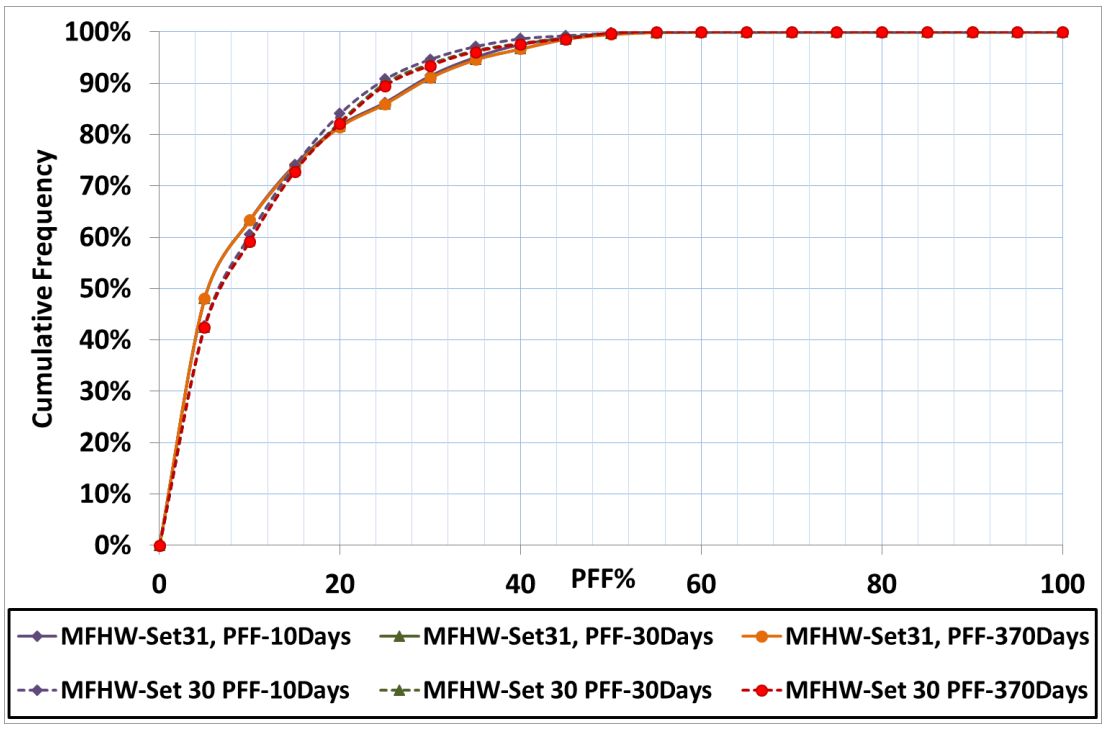

Figure 5.18 Histogram chart comparing PFF cumulative frequency of MFHW-set 31 with Kmr=100 and MFHW-Set 30 at three production stages.

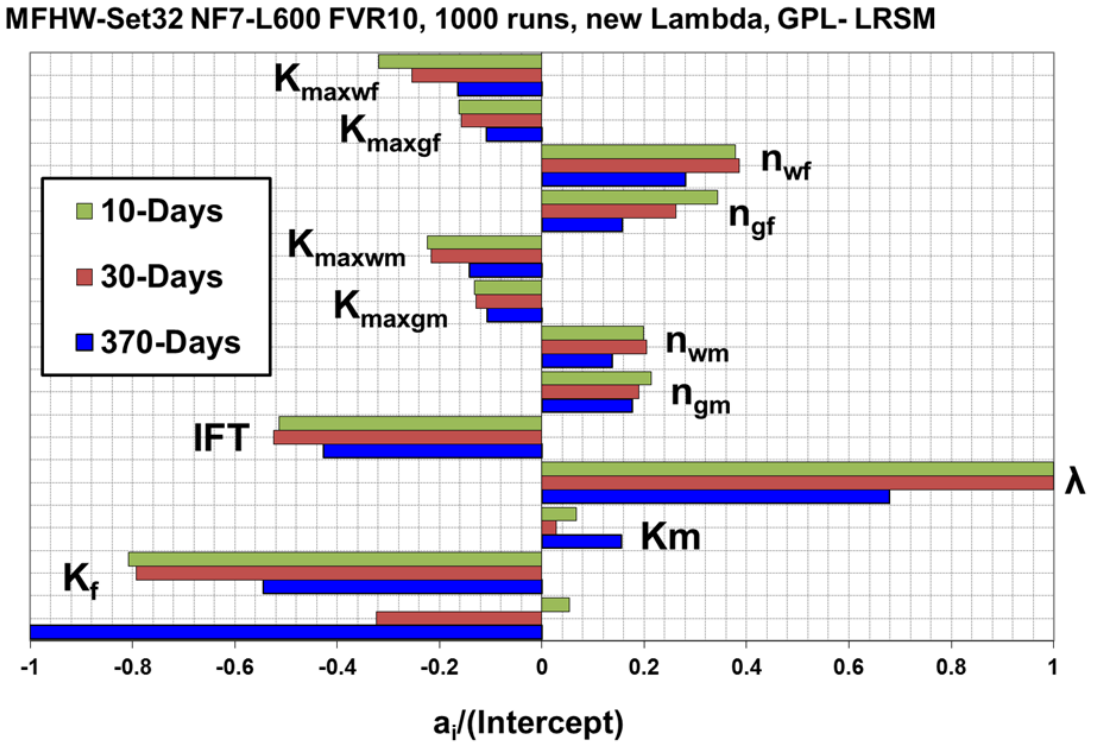

Figure 5.19 GPL Tornado chart comparing LRSM coefficients of all pertinent parameters at three production stages for MFHW-set32 with FVR=10 and using new lambda range (0.3 to 1.5)

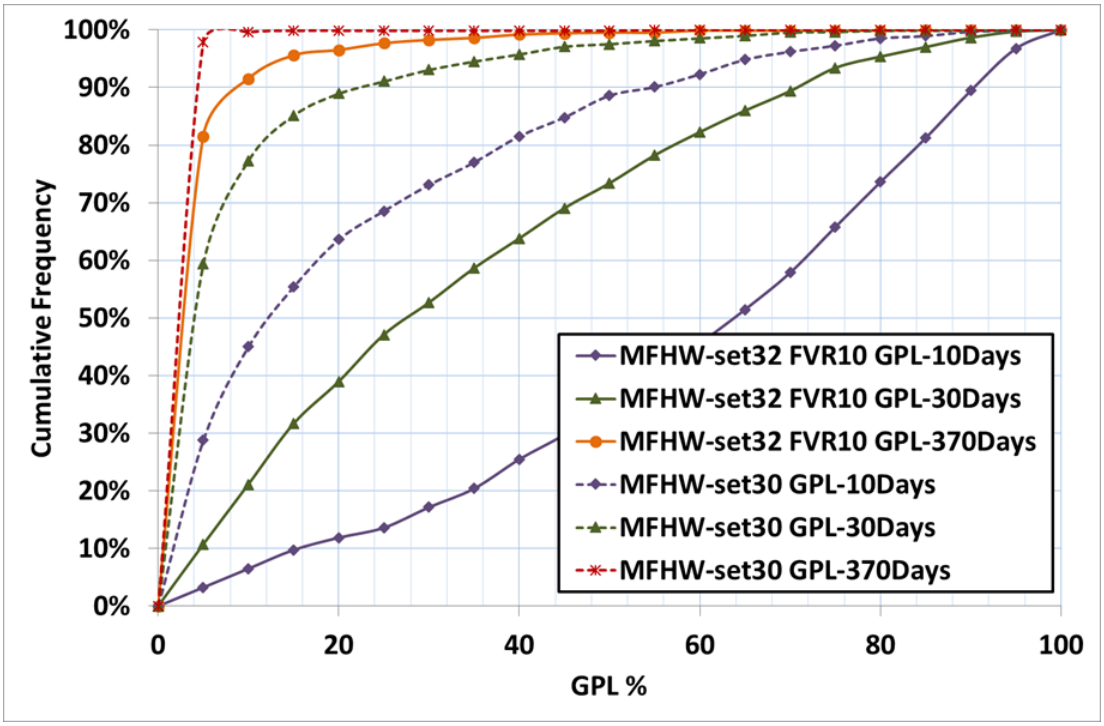

Figure 5.20 Histogram chart comparing GPL cumulative frequency of MFHW-set 32 with FVR=10 and MFHW-Set 30 at three production stages.

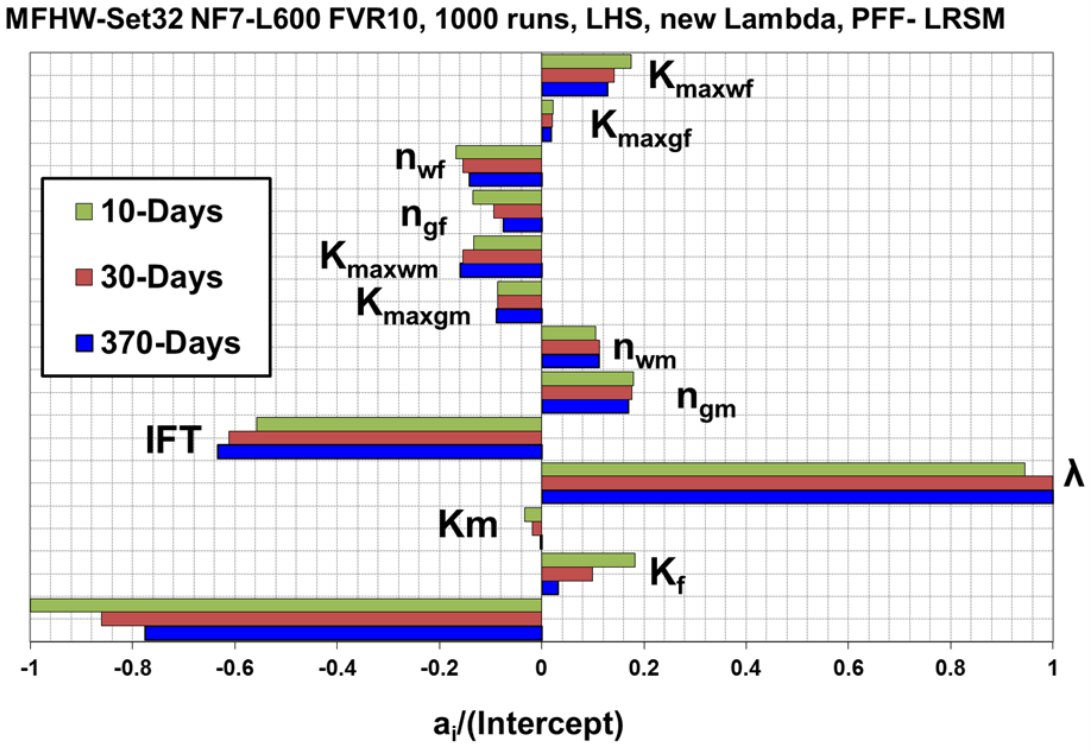

Figure 5.21 PFF Tornado chart comparing LRSM coefficients of all pertinent parameters at three production stages for MFHW-set32 with FVR=10 and using new lambda range (0.3 to 1.5)

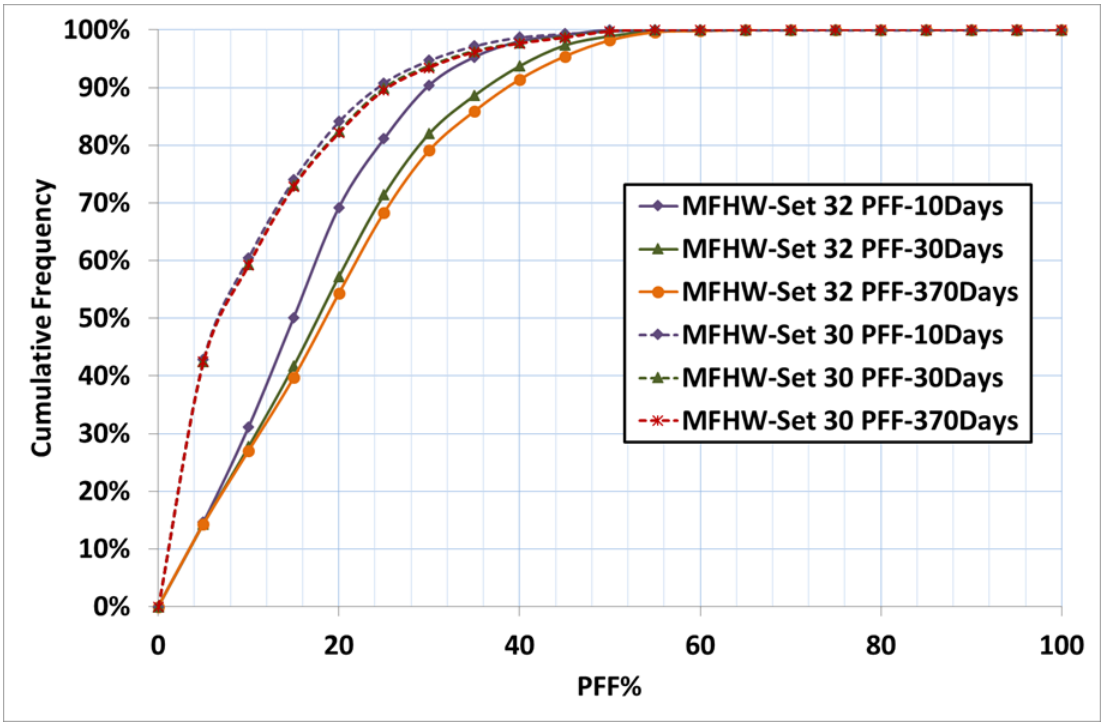

Figure 5.22 Histogram chart comparing PFF cumulative frequency of MFHW-set 32 with FVR=10 and MFHW-set 30 at three production stages.

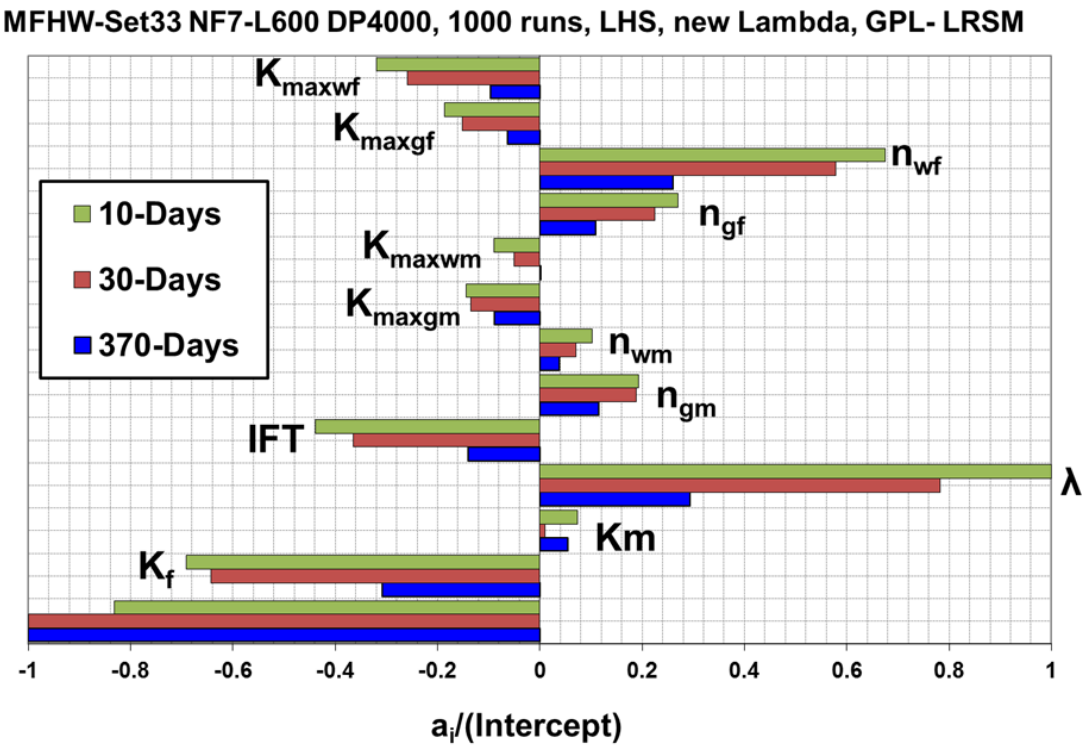

Figure 5.23 GPL Tornado chart comparing LRSM coefficients of all pertinent parameters at three production stages for MFHW-set33 with DP=4000psi and using new lambda range (0.3 to 1.5)

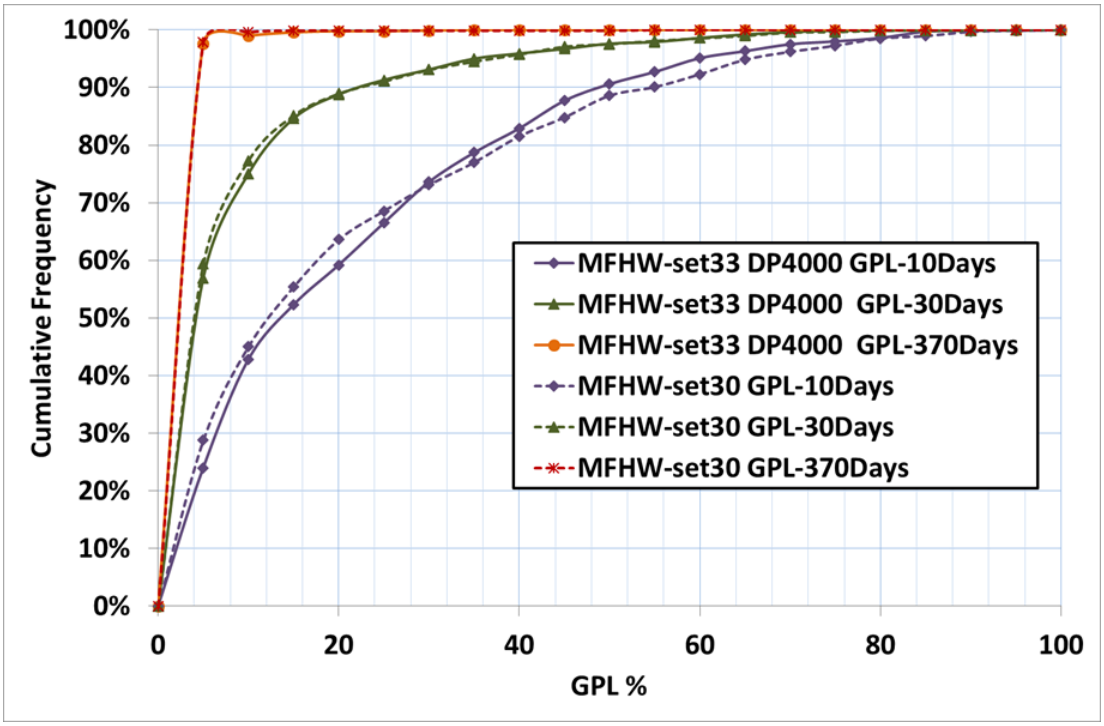

Figure 5.24 Histogram chart comparing GPL cumulative frequency of MFHW-set 33 with DP=4000psi and MFHW-Set 30 at three production stages.

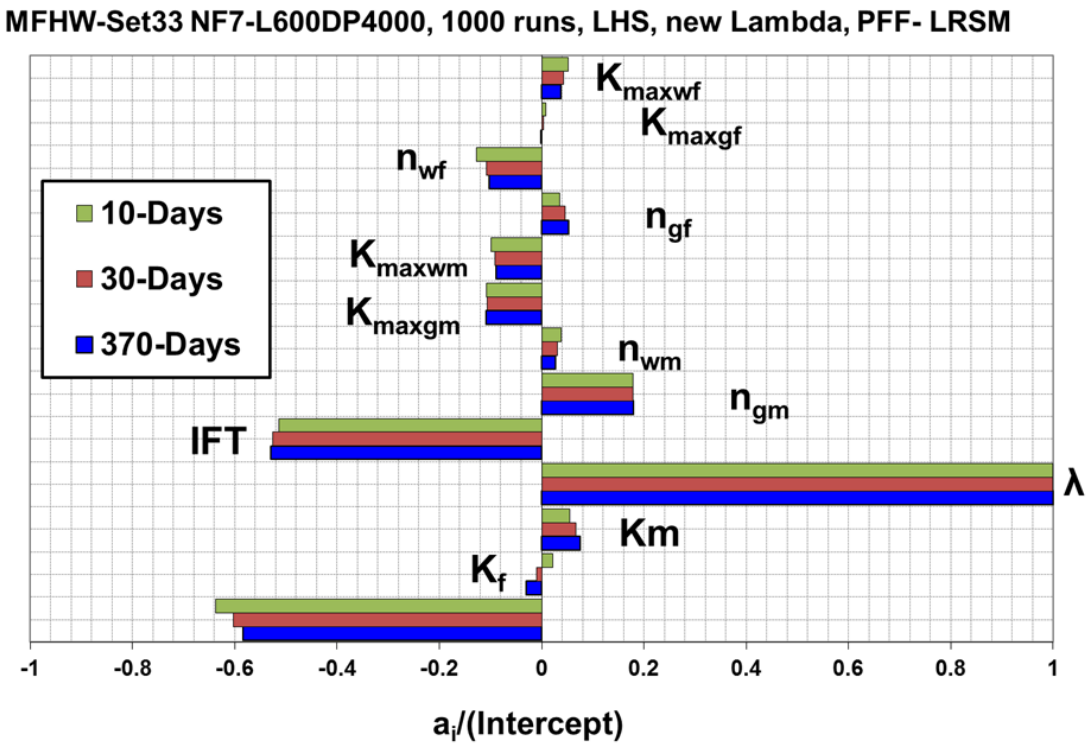

Figure 5.25 PFF Tornado chart comparing LRSM coefficients of all pertinent parameters at three production stages for MFHW-set33 with DP=4000psi and using new lambda range (0.3 to 1.5)

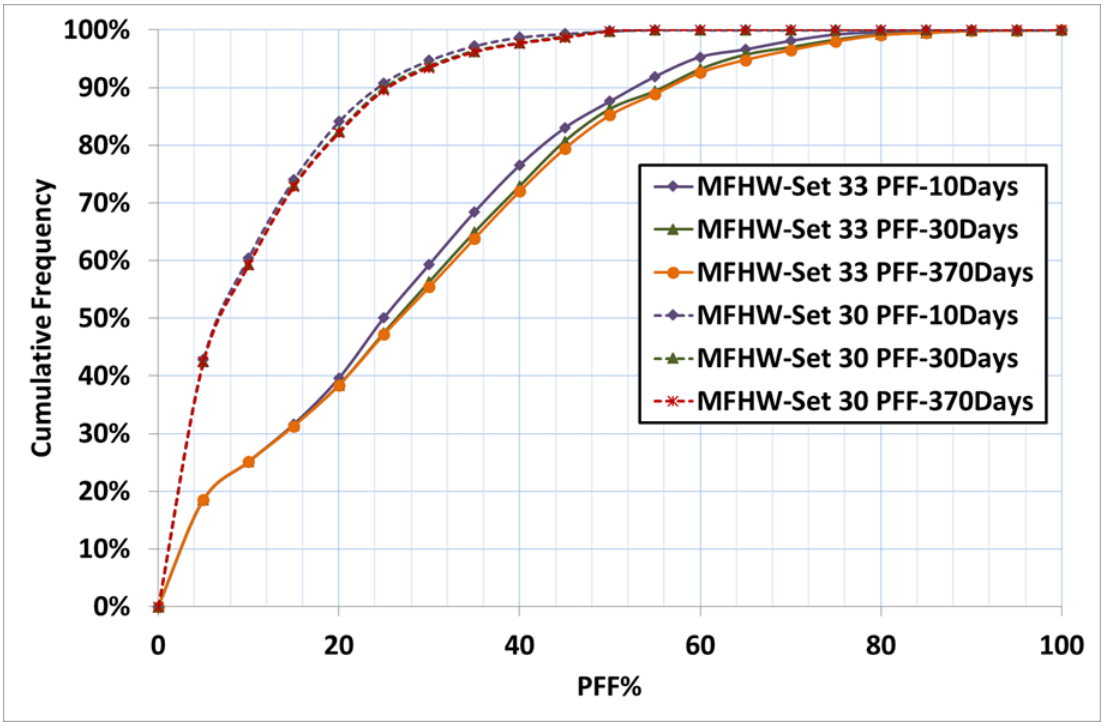

Figure 5.26 Histogram chart comparing PFF cumulative frequency of MFHW-set 33 with DP=4000psi and MFHW-Set 30 at three production stages.

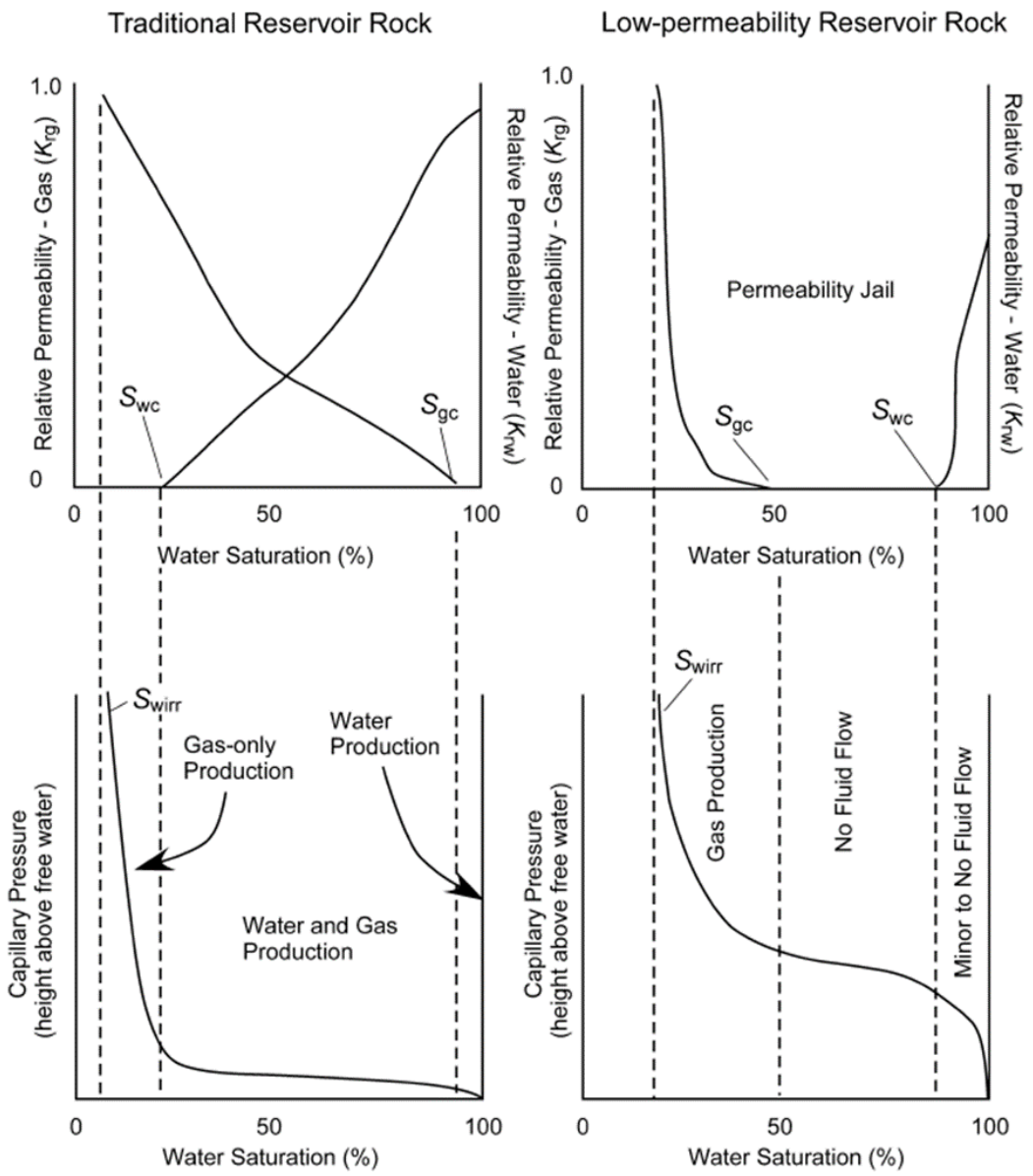

Figure 5.27 Illustration of capillary pressure and relative permeability curves in conventional and tight/ultra tight reservoir rocks. Critical water saturation (Swc), critical gas saturation (Sgc), and irreducible water saturation (Swirr) are shown. (Shanley et al. 2004)

- In conventional rocks, Swirr and Swc are similar. However, in tight/ultra tight reservoir rocks, Swirr and Swc can be extensively different.
- Although in conventional reservoirs, there is a wide range of water saturations at which both water and gas can flow, in tight/ultra tight reservoir rocks, there is a broad range of water saturations in which neither gas nor water can flow.

a) MFHW-Set 34 NF7-L600 with Weak Perm Jail, Two-phase 30%

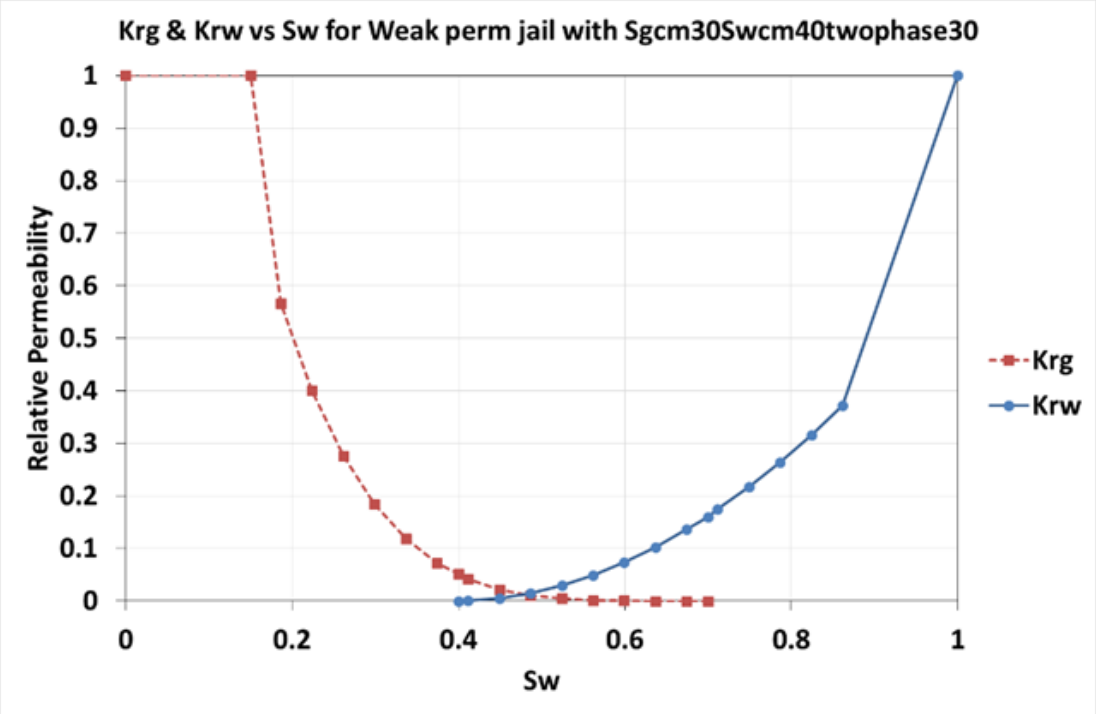

b) MFHW-Set 35 NF7-L600 with Weak Perm Jail, Two-phase 20%

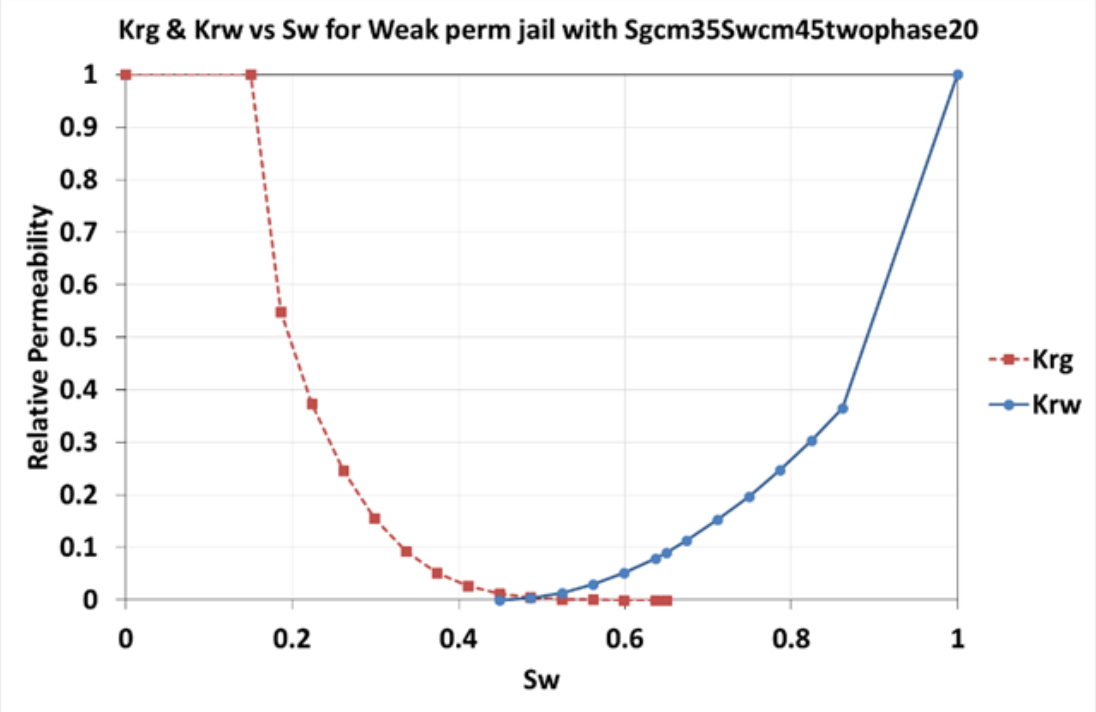

c) MFHW-Set 36 NF7-L600 with Weak Perm Jail, Two-phase 10%

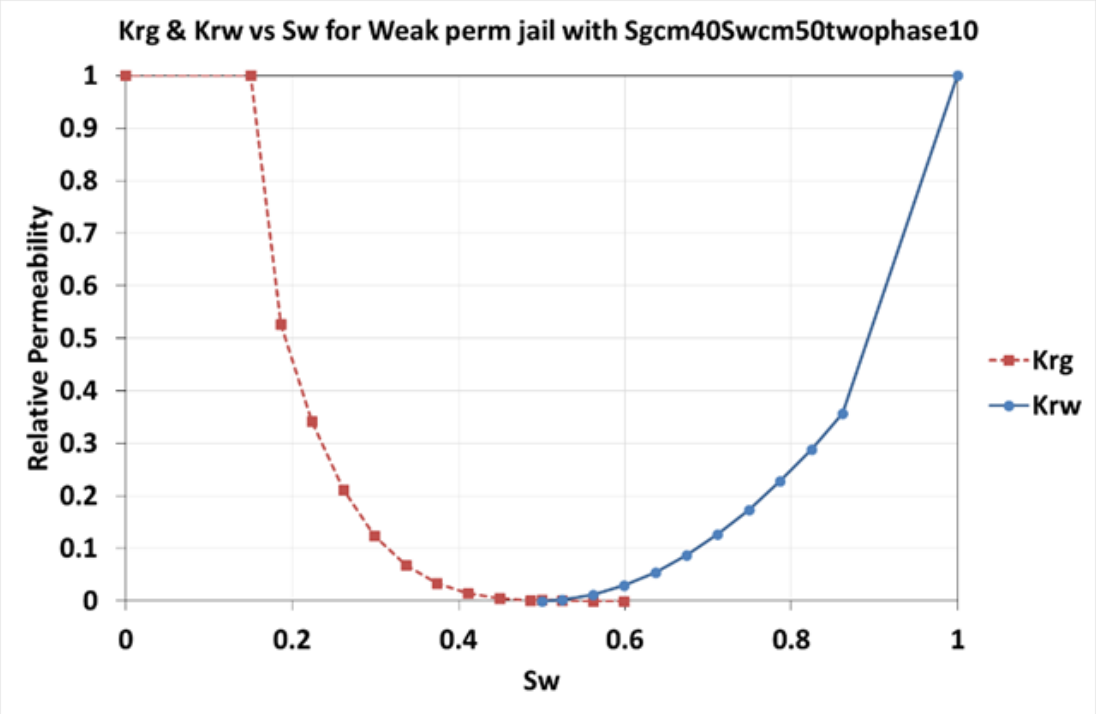

Figure 5.28 Relative permeability curves for weak jail effect, a) MFHW-Set 34 NF7-L600 with Weak Perm Jail, Two-phase 30%, b) MFHW-Set 35 NF7-L600 with Weak Perm Jail, Two-phase 20% & c) MFHW-Set 36 NF7-L600 with Weak Perm Jail, Two-phase 10%.

a) MFHW-Set 34 NF7-L600 with Weak Perm Jail, Two-phase 30%

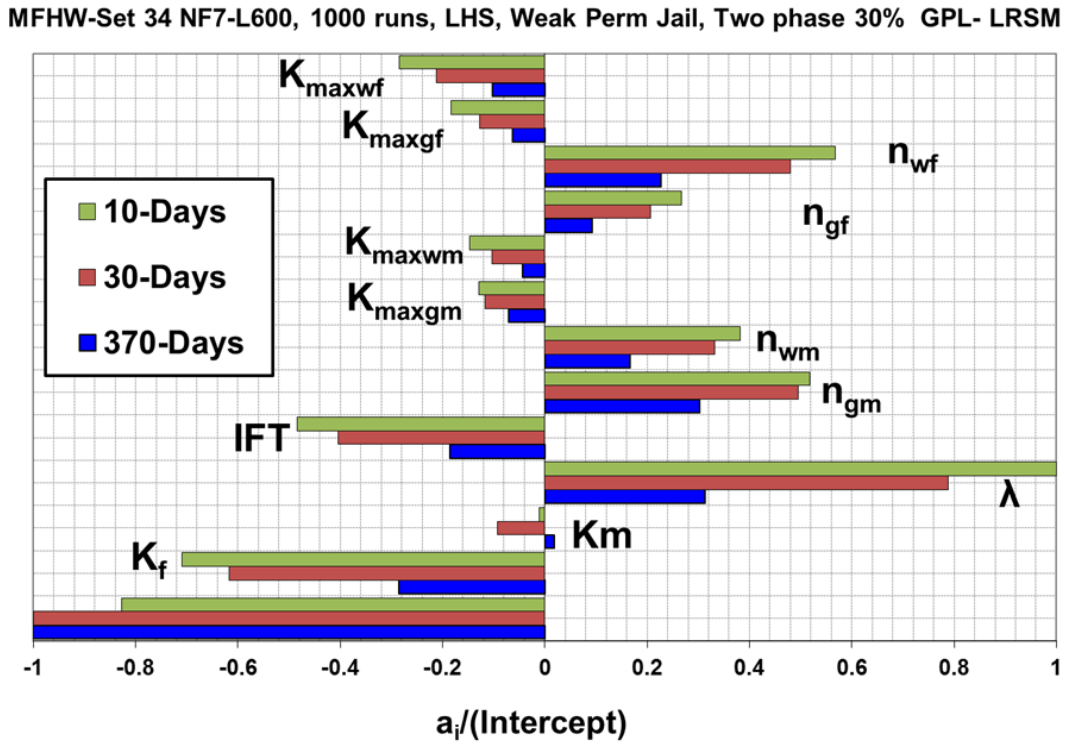

b) MFHW-Set 35 NF7-L600 with Weak Perm Jail, Two-phase 20%

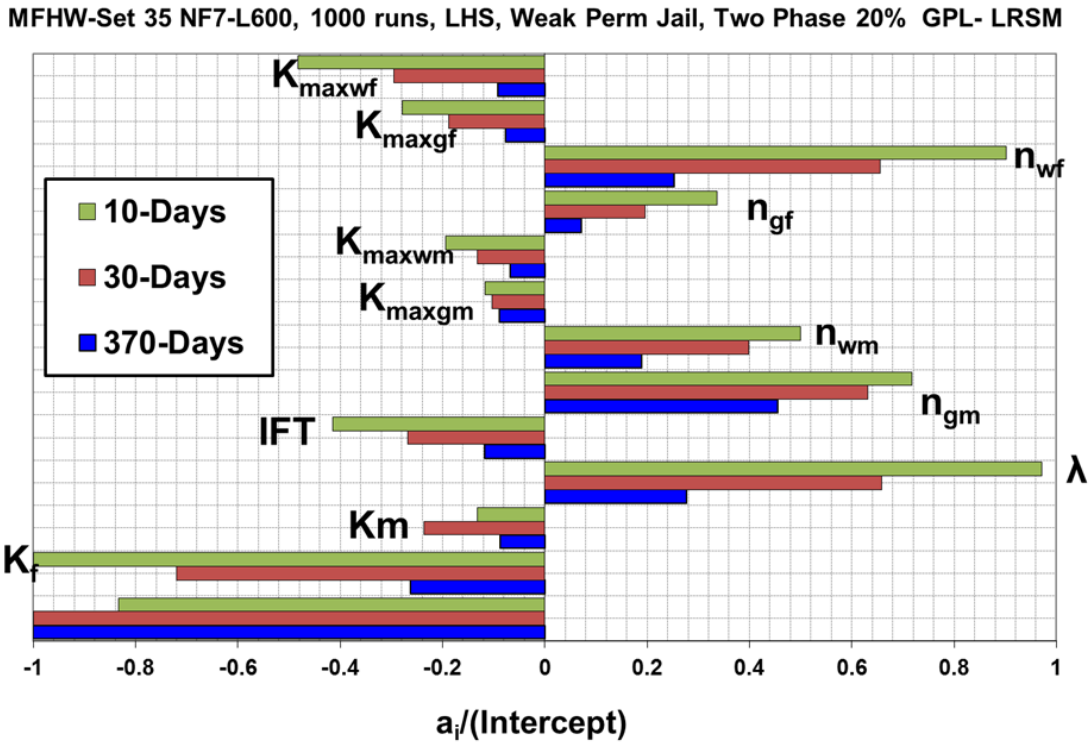

c) MFHW-Set 36 NF7-L600 with Weak Perm Jail, Two-phase 10%

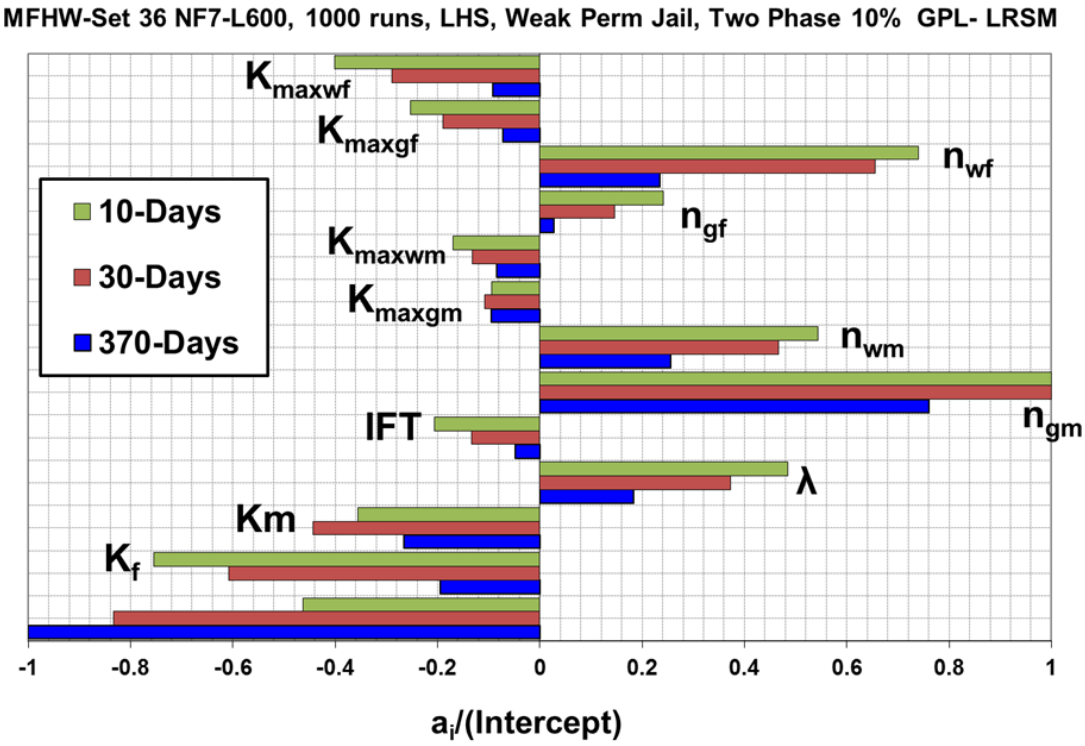

Figure 5.29 GPL Tornado chart comparing LRSM coefficients of all pertinent parameters at three production stages for a) MFHW-Set 34 NF7-L600 with Weak Perm Jail, Two-phase 30% b) MFHW-Set 35 NF7-L600 with Weak Perm Jail, Two-phase 20% c) MFHW-Set 36 NF7-L600 with Weak Perm Jail, Two-phase 10% at three production stages.

a) MFHW-Set 34 NF7-L600 with Weak Perm Jail, Two-phase 30%

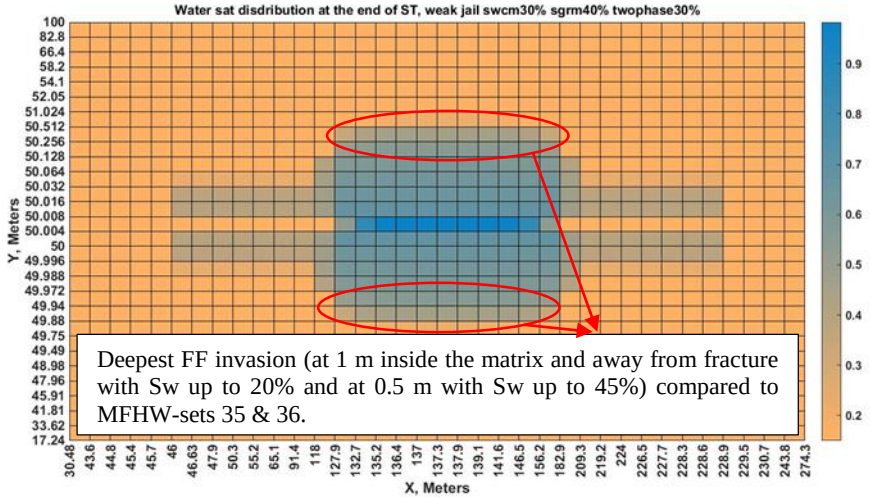

b) MFHW-Set 35 NF7-L600 with Weak Perm Jail, Two-phase 20%

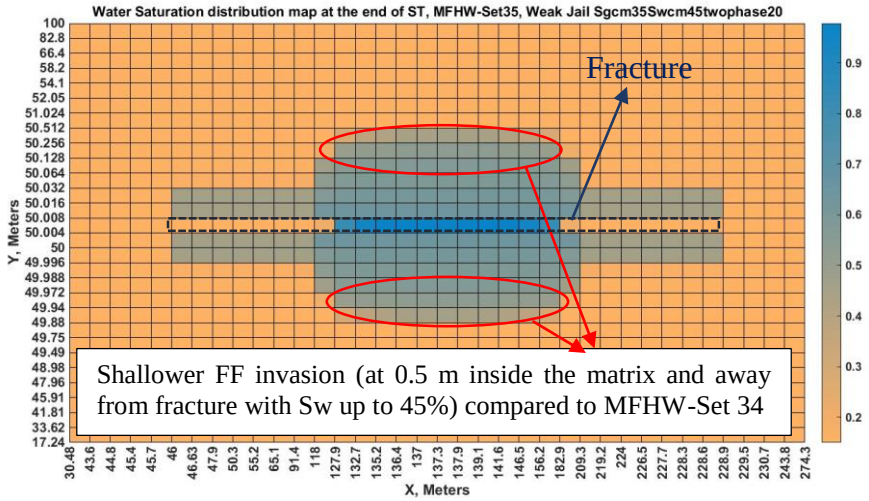

c) MFHW-Set 36 NF7-L600 with Weak Perm Jail, Two-phase 10%

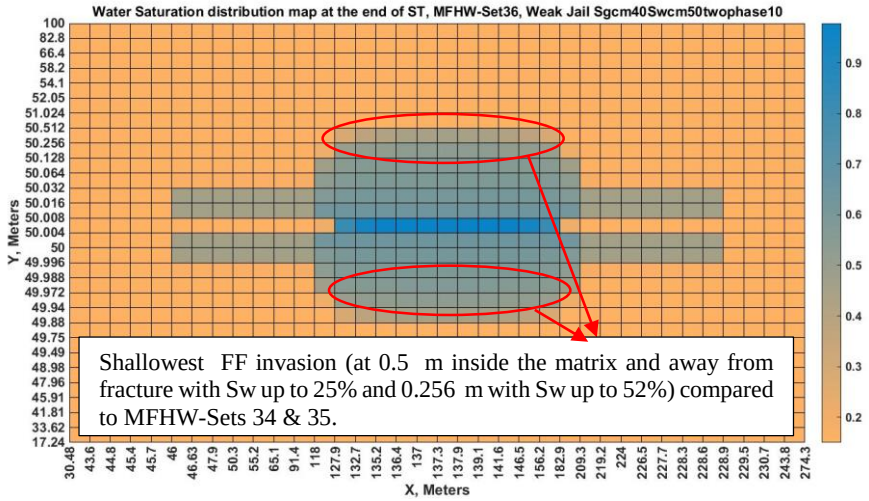

Figure 5.30 Saturation distribution map (run number 30) at the end of ST for a) MFHW-Set 34 NF7-L600 with Weak Perm Jail, Two-phase 30% b) MFHW-Set 35 NF7-L600 with Weak Perm Jail, Two-phase 20% c) MFHW-Set 36 NF7-L600 with Weak Perm Jail, Two-phase 10%

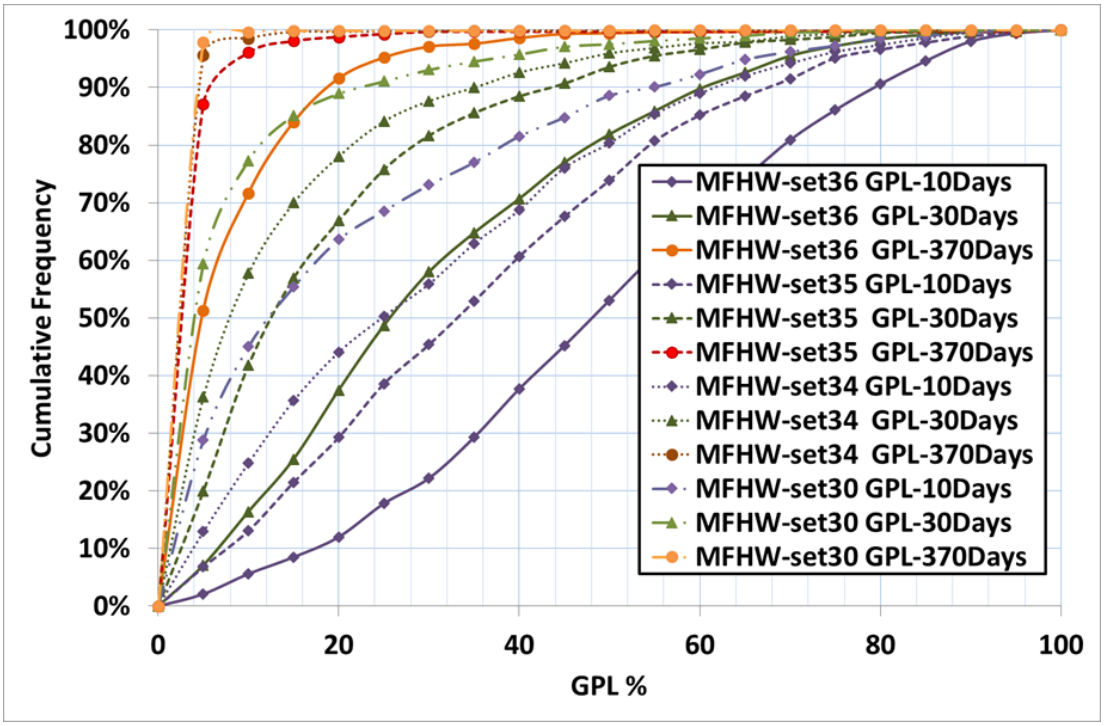

Figure 5.31 GPL Histogram chart comparing a) MFHW-Set 34 NF7-L600 with Weak Perm Jail, Two-phase 30% b) MFHW-Set 35 NF7-L600 with Weak Perm Jail, Two-phase 20% c) MFHW-Set 36 NF7-L600 with Weak Perm Jail, Two-phase 10% with MFHW-Set 30 NF7-L600 at three production stages

a) MFHW-Set 34 NF7-L600 with Weak Perm Jail, Two-phase 30%

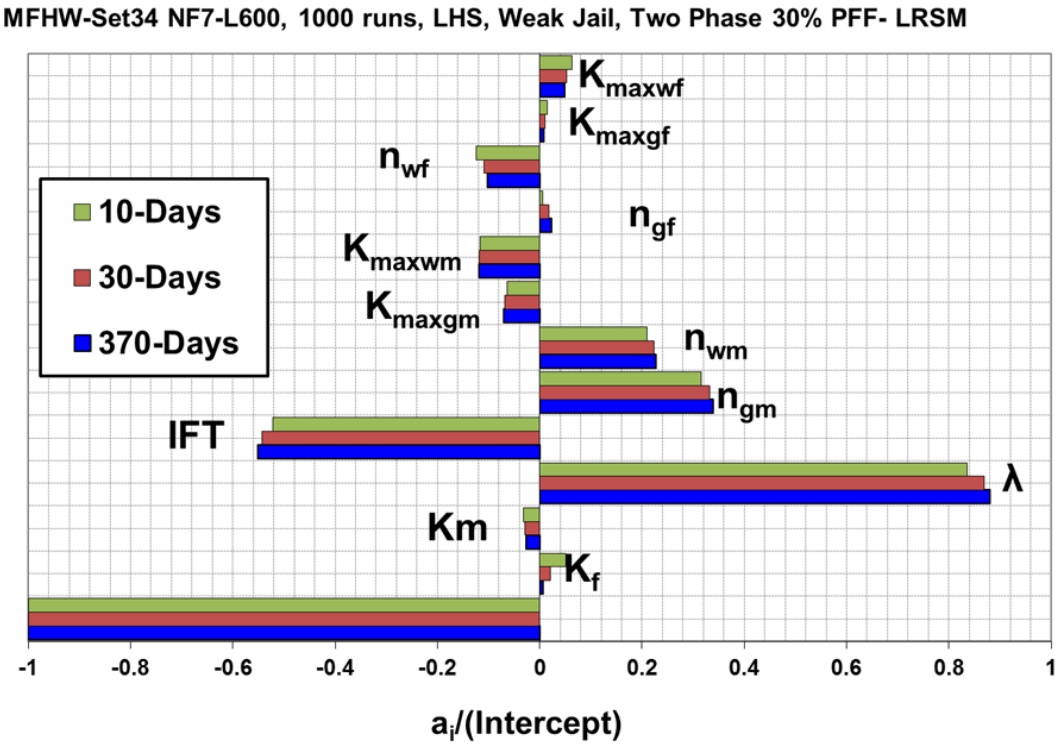

b) MFHW-Set 35 NF7-L600 with Weak Perm Jail, Two-phase 20%

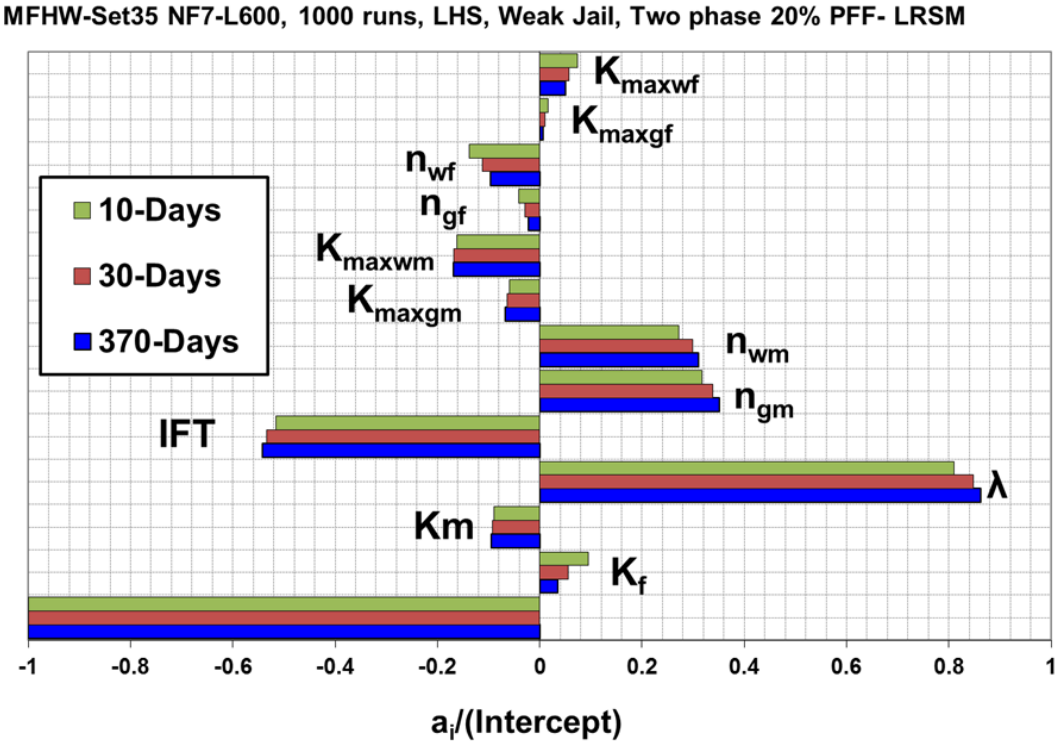

c) MFHW-Set 36 NF7-L600 with Weak Perm Jail, Two-phase 10%

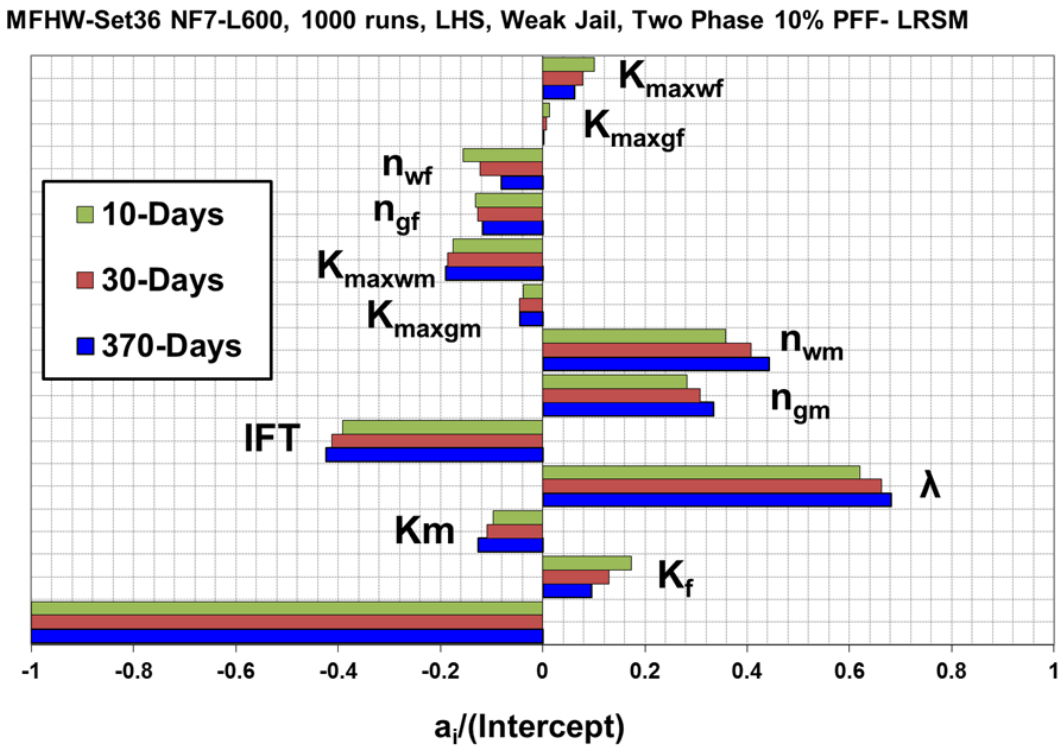

Figure 5.32 PFF Tornado chart comparing LRSM coefficients of all pertinent parameters at three production stages for a) MFHW-Set 34 NF7-L600 with Weak Perm Jail, Two-phase 30% b) MFHW-Set 35 NF7-L600 with Weak Perm Jail, Two-phase 20% c) MFHW-Set 36 NF7-L600 with Weak Perm Jail, Two-phase 10% at three production stages.

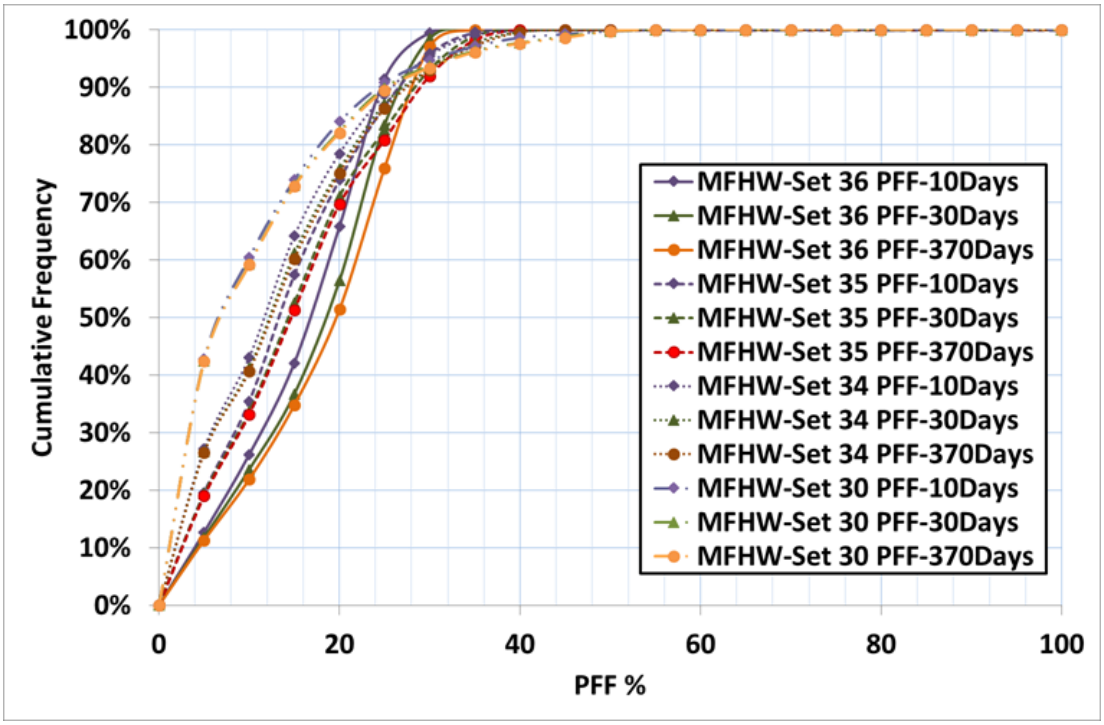

Figure 5.33 PFF Histogram chart comparing a) MFHW-Set 34 NF7-L600 with Weak Perm Jail, Two-phase 30% b) MFHW-Set 35 NF7-L600 with Weak Perm Jail, Two-phase 20% c) MFHW-Set 36 NF7-L600 with Weak Perm Jail, Two-phase 10% with MFHW-Set 30 NF7-L600 at three production stages

a) Normal rock with conventional relative permeability

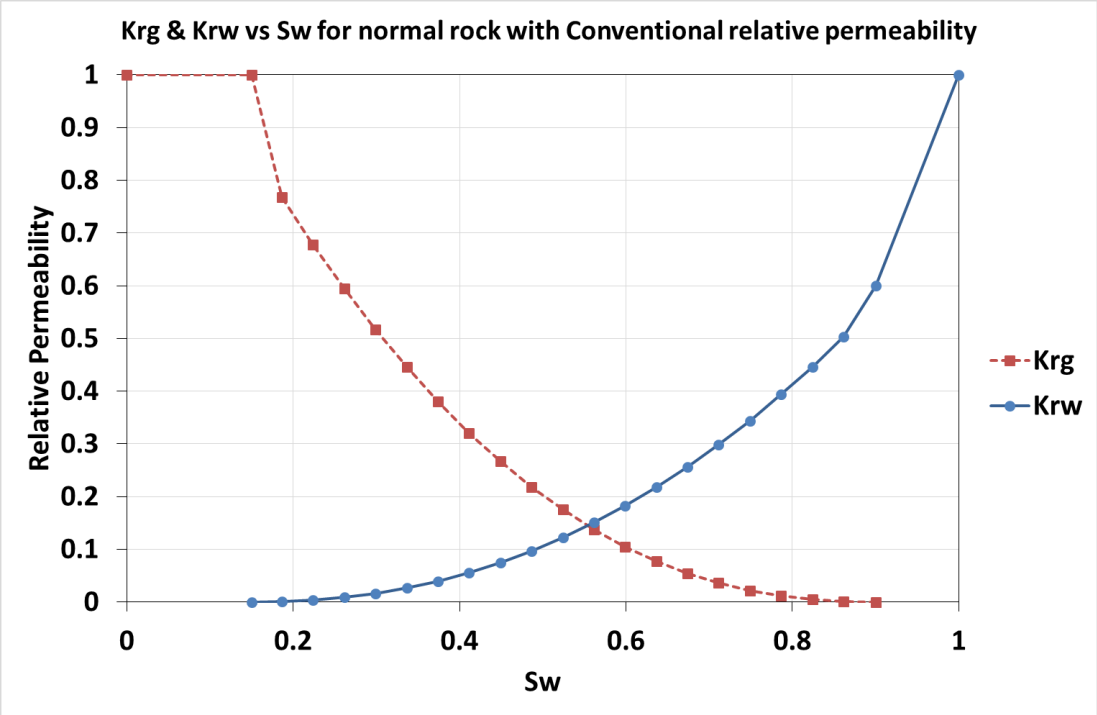

b) Total permeability jail effect with 10% total jail

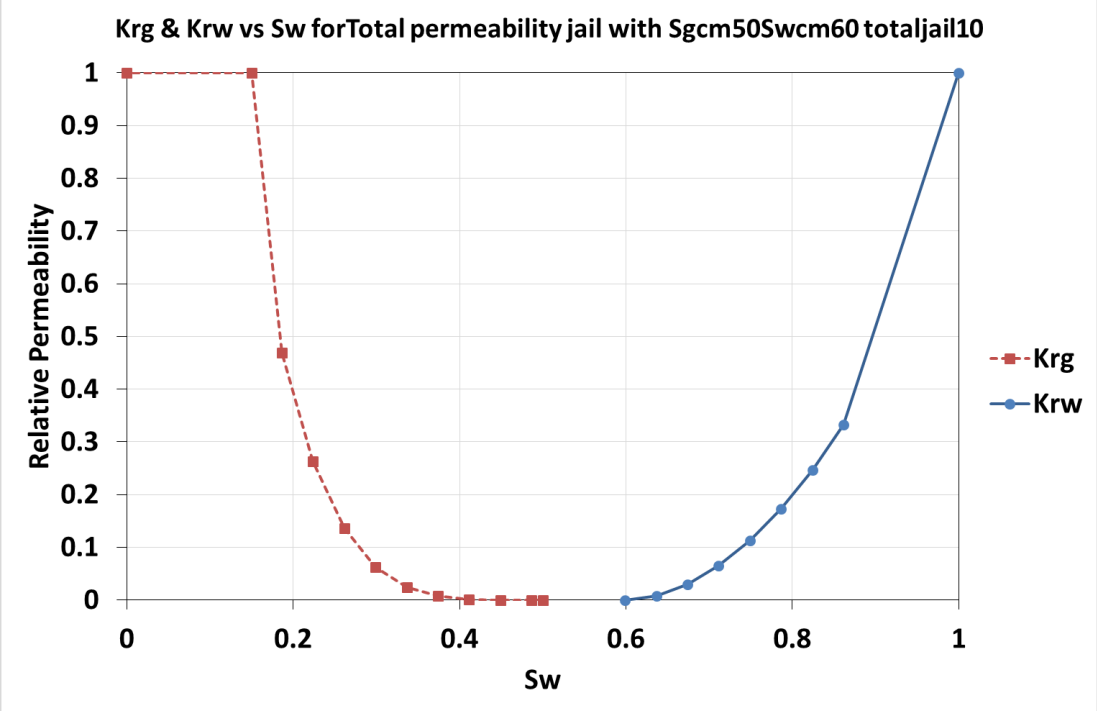

Figure 5.34 Relative permeability curves for a) normal conventional rock & b) total permeability jail effect with 10% total jail.

a) MFHW-Set 37 NF7-L600 with mixed 1

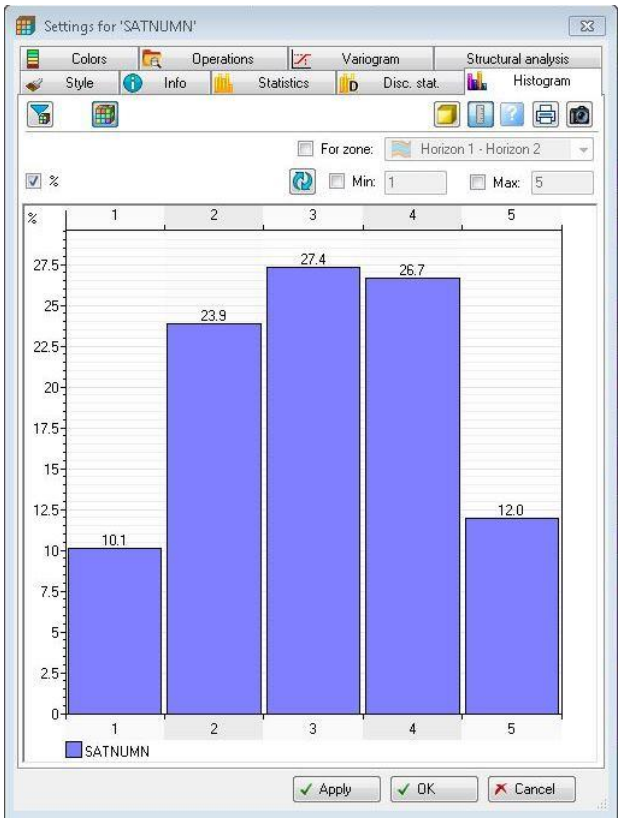

b) MFHW-Set 38 NF7-L600 with mixed 2

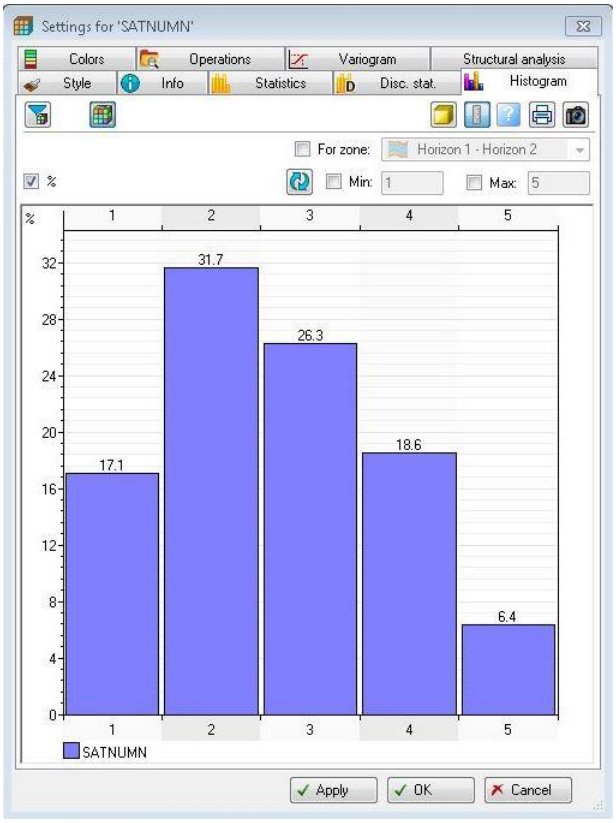

c) MFHW-Set 39 NF7-L600 with mixed 3

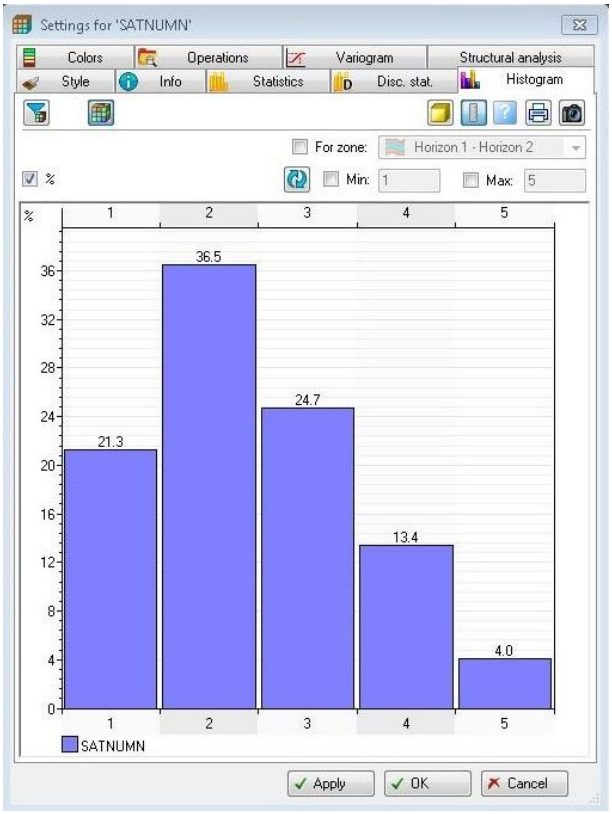

Figure 5.35: Different Rock type contribution to a) MFHW-Set 37 NF7-L600 with mixed 1, b) MFHW-Set 38 NF7-L600 with mixed 2. & c) MFHW-Set 39 NF7-L600 with mixed 3 (Rock types: 1. Total jail, 2. Weak jail as that of MFHW-Set 36, 3. Weak jail as that of MFHW-Set 35, 4. Weak jail as that of MFHW-Set 34 & 5. Conventional permeability as shown in Figure 5.34 a)

MFHW-Set 37 NF7-L600 with mixed 1

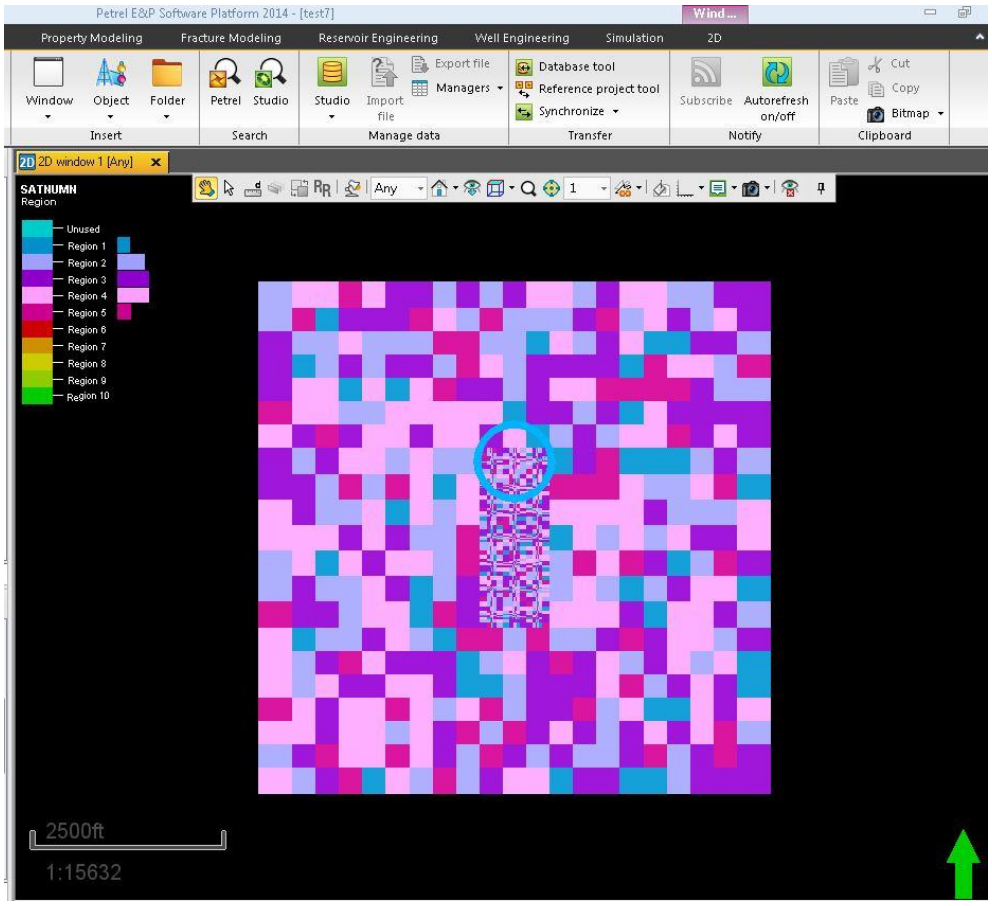

b) MFHW-Set 38 NF7-L600 with mixed 2

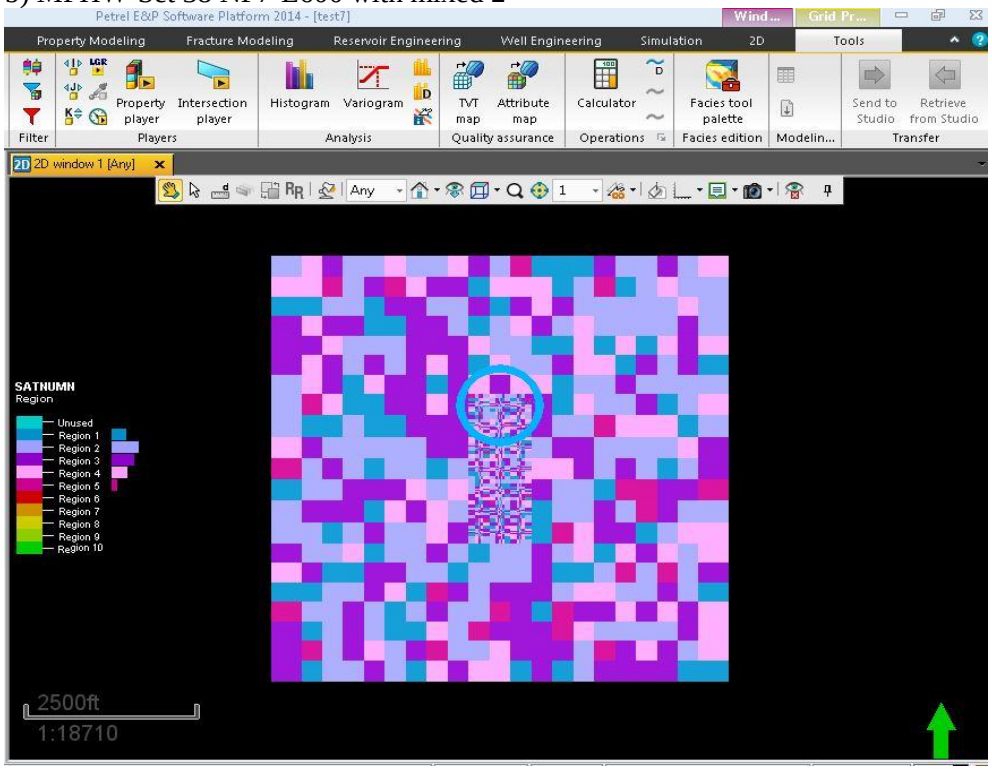

c) MFHW-Set 39 NF7-L600 with mixed 3

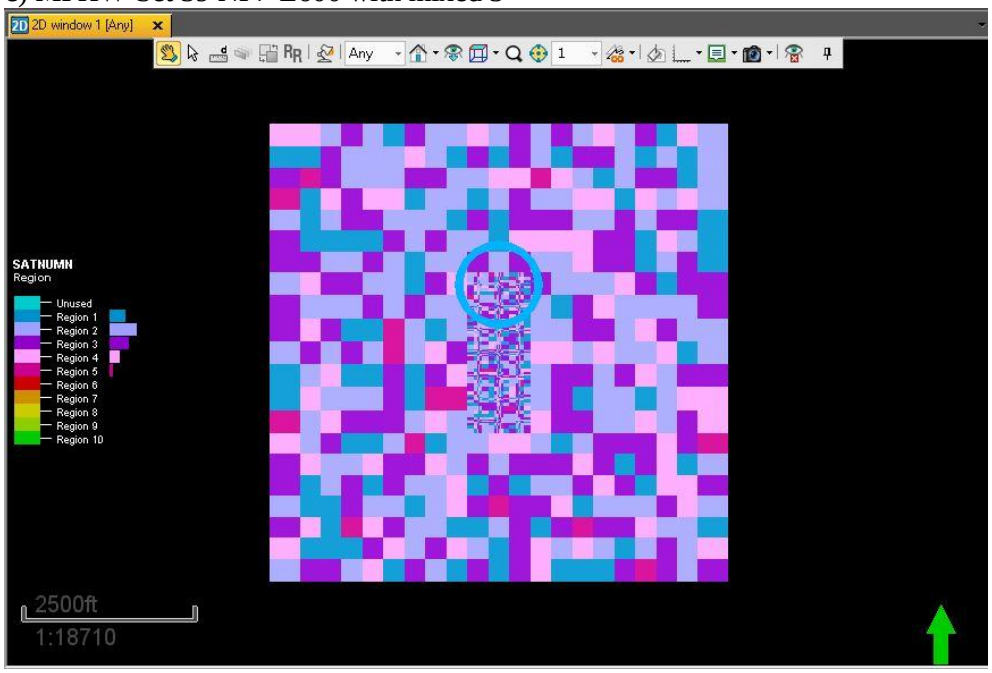

Figure 5.36: Different Rock type distribution in a) MFHW-Set 37 NF7-L600 with mixed 1 & b) MFHW-Set 38 NF7-L600 with mixed 2. (Rock types: 1. Total jail 10%, 2. Weak jail as that of MFHW-Set 36, 3. Weak jail as that of MFHW-Set 35, 4. Weak jail as that of MFHW-Set 34 & 5. Conventional permeability as shown in Figure 5.45 a)

MFHW-Set 37 NF7-L600 with mixed 1

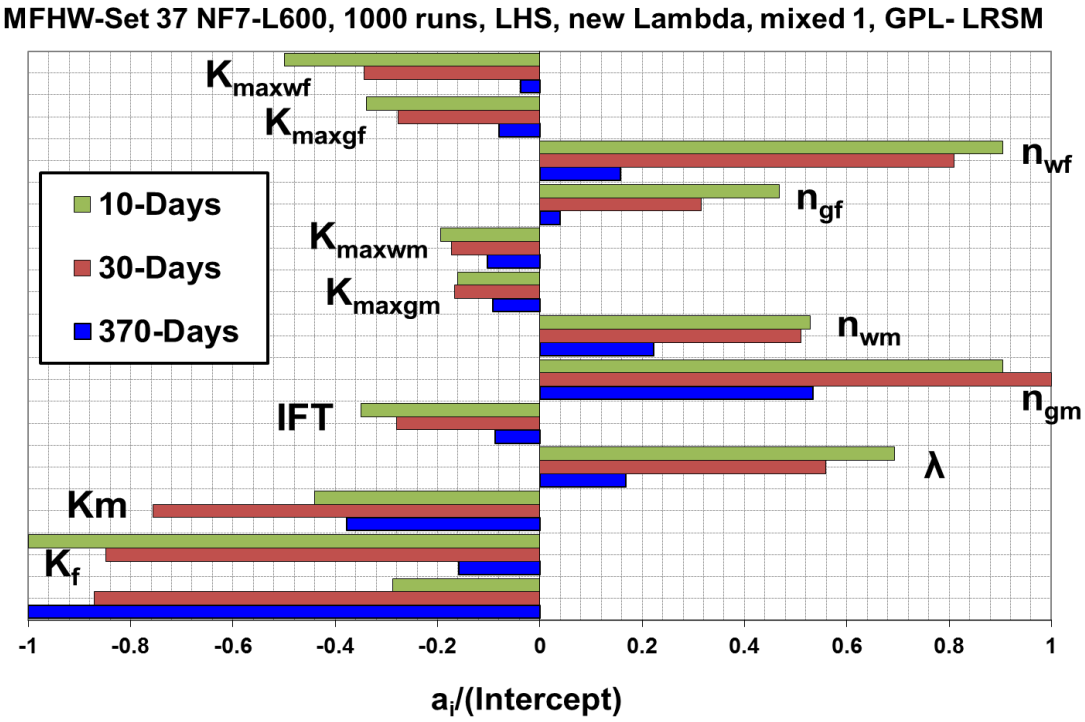

b) MFHW-Set 38 NF7-L600 with mixed 2

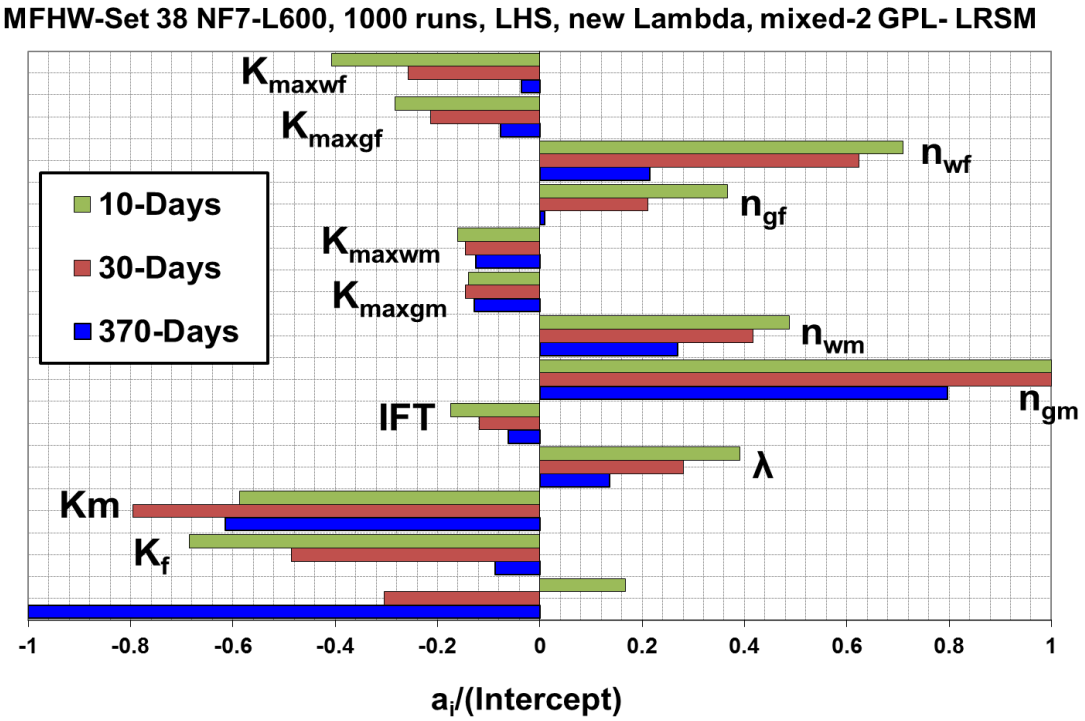

C) MFHW-Set 39 NF7-L600 with mixed 2

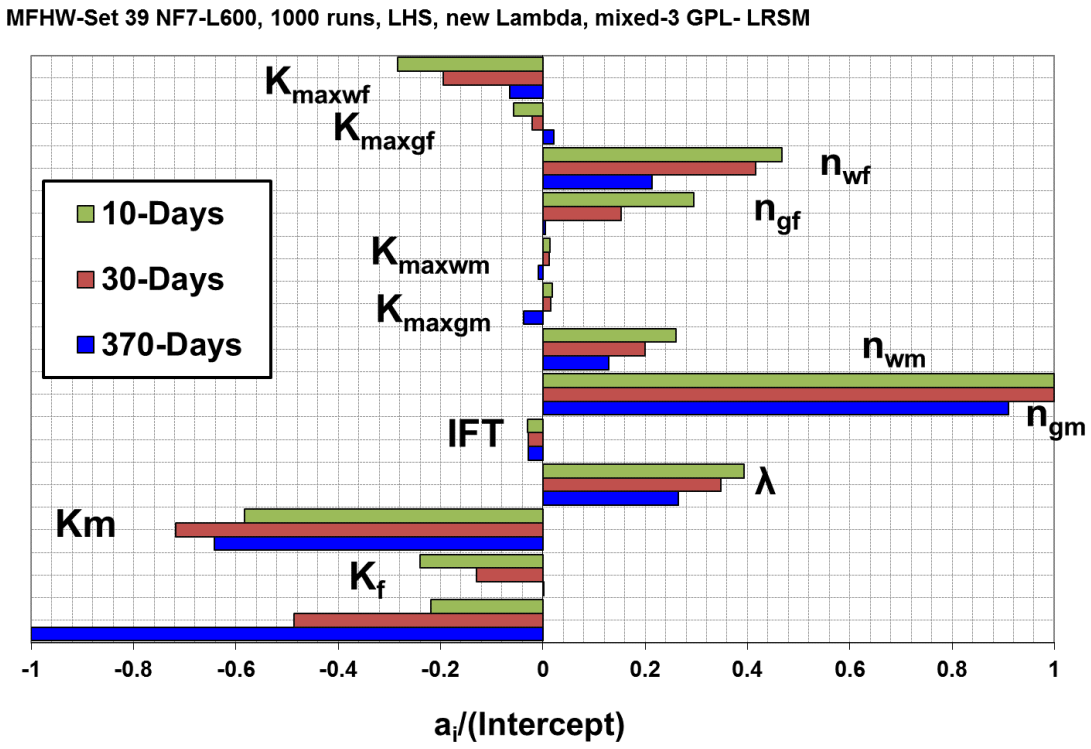

Figure 5.37 GPL Tornado chart comparing LRSM coefficients of all pertinent parameters at three production stages for a) MFHW-Set 37 NF7-L600 with mixed 1 & b) MFHW-Set 38 NF7-L600 with mixed 2 at three production stages

a) Normal rock with conventional relative permeability

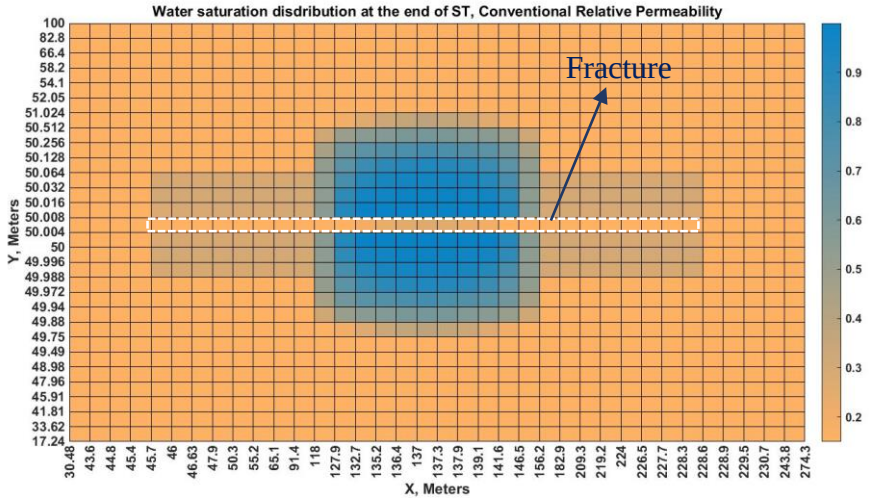

b) Total permeability jail effect with 10% total jail

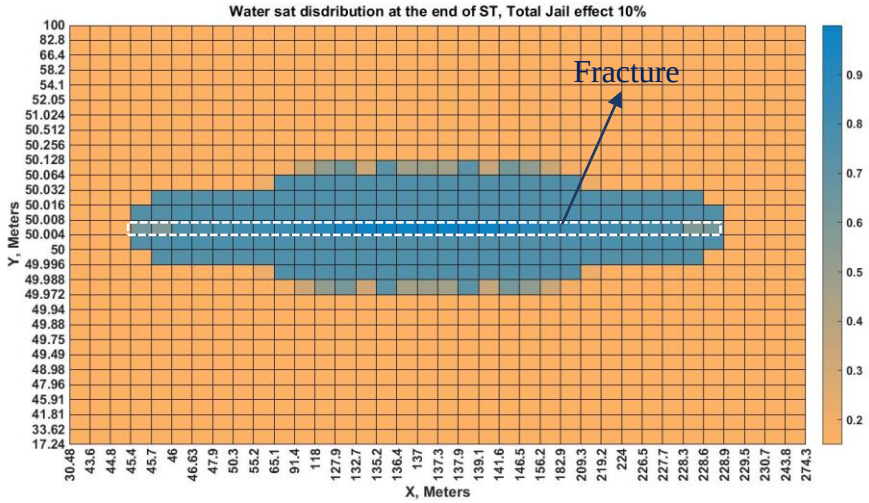

c) MFHW-Set 37 NF7-L600 with mixed 1

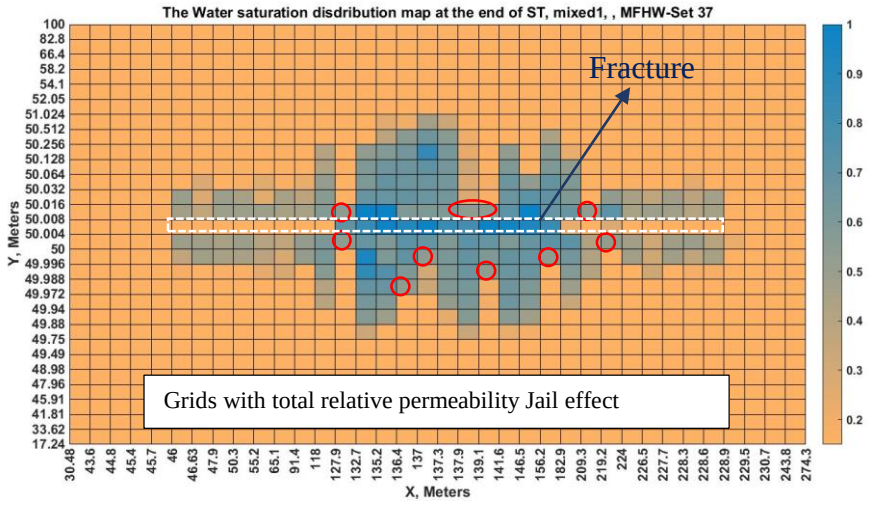

d) MFHW-Set 38 NF7-L600 with mixed 2

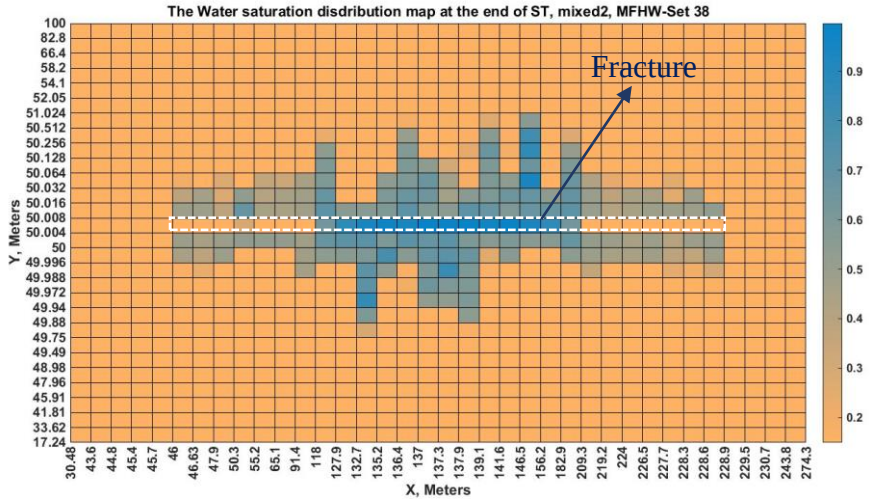

e) MFHW-Set 39 NF7-L600 with mixed 3

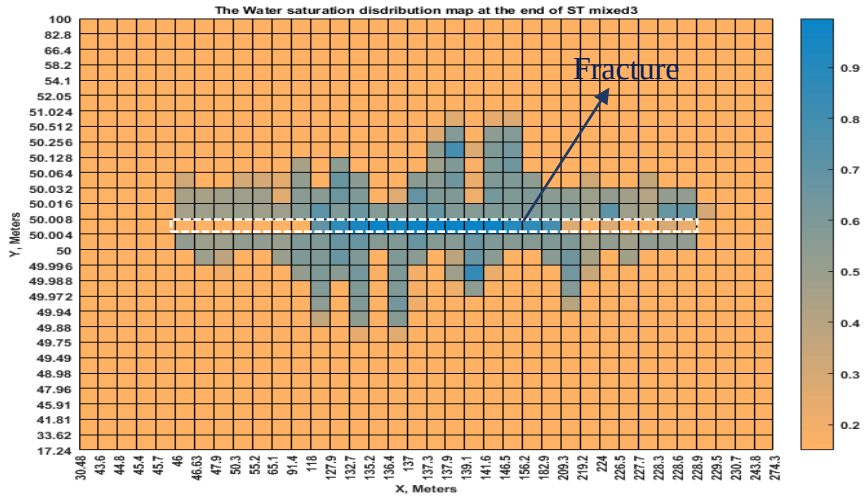

Figure 5.38: Saturation distribution map (run number 30) at the end of ST for a) conventional Kr b) Kr curves shown in Figure 5.38b for the whole reservoir, i.e. which has a 10% total permeability jail effect c) mixed 1 Kr curves corresponding to MFHW-Set 37 NF7-L600 d) mixed 2 Kr sets corresponding to MFHW-Set 38 NF7-L600s & e) mixed 3 Kr sets corresponding to MFHW-Set 39 NF7-L600s.

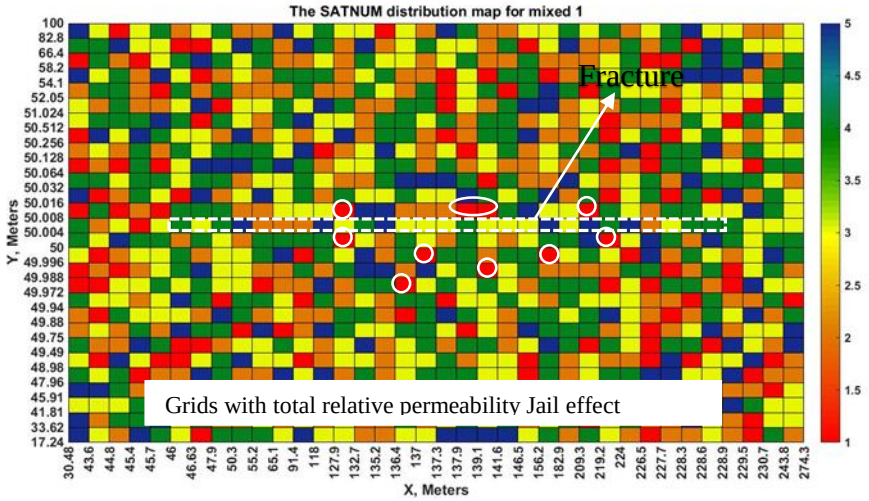

Figure 5.39 SATNUM distribution map (run number 30) for MFHW-Set 37 NF7-L600 with mixed 1.

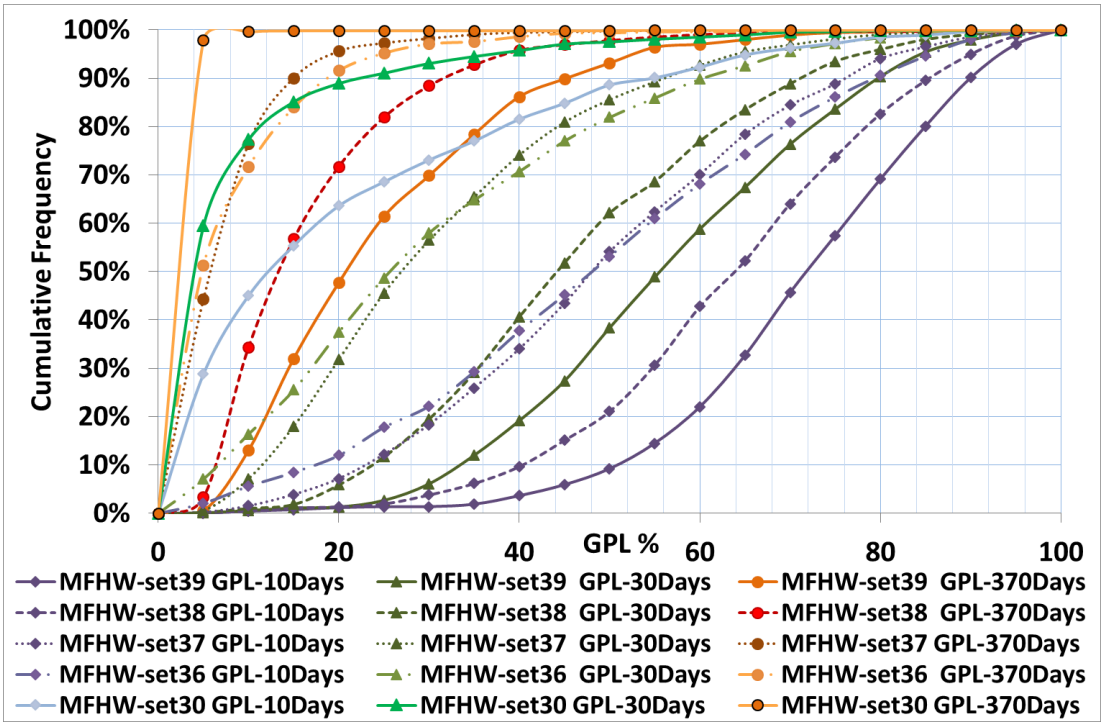

Figure 5.40 GPL Histogram chart comparing a) MFHW-Set 37 NF7-L600 with mixed 1, b) MFHW-Set 38 NF7-L600 with mixed 2 & c) MFHW-Set 39 NF7-L600 with mixed 3 with Weak Perm Jail set 36 and also with MFHW-Set 30 NF7-L600 at three production stages

a) MFHW-Set 37 NF7-L600 with mixed 1

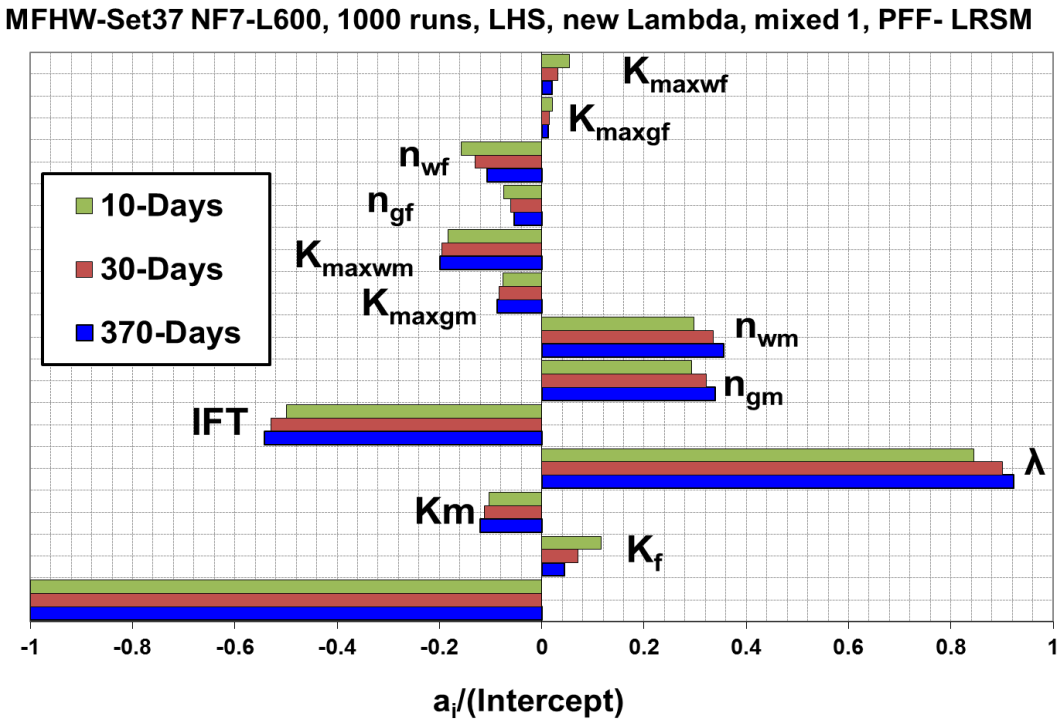

b) MFHW-Set 38 NF7-L600 with mixed 2

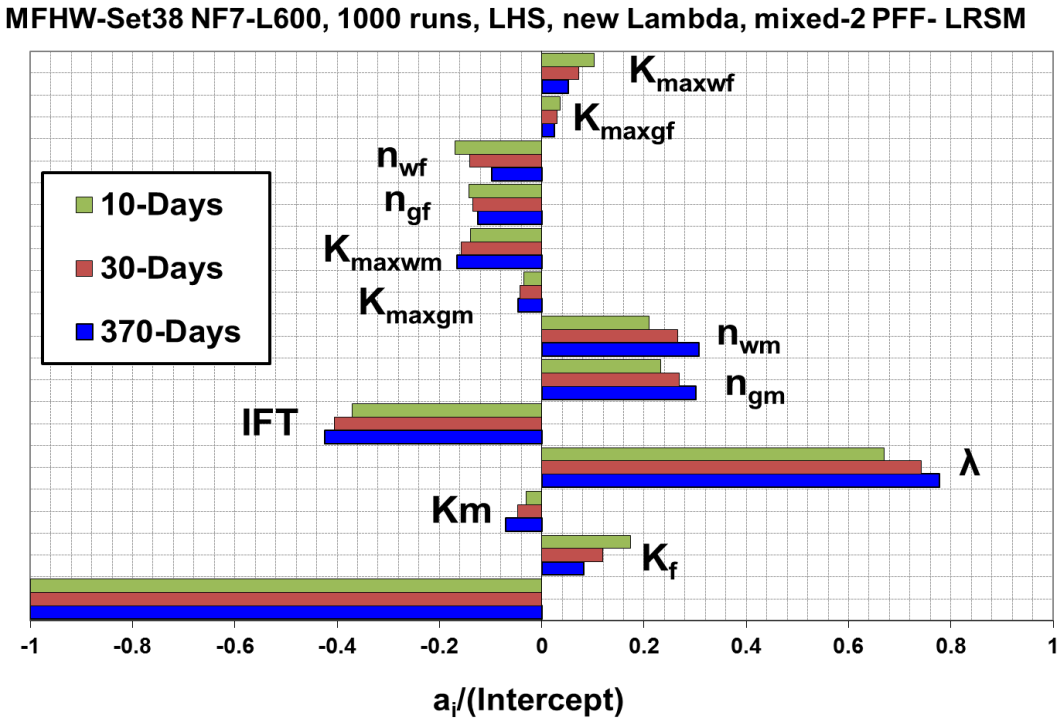

c) MFHW-Set 39 NF7-L600 with mixed 3

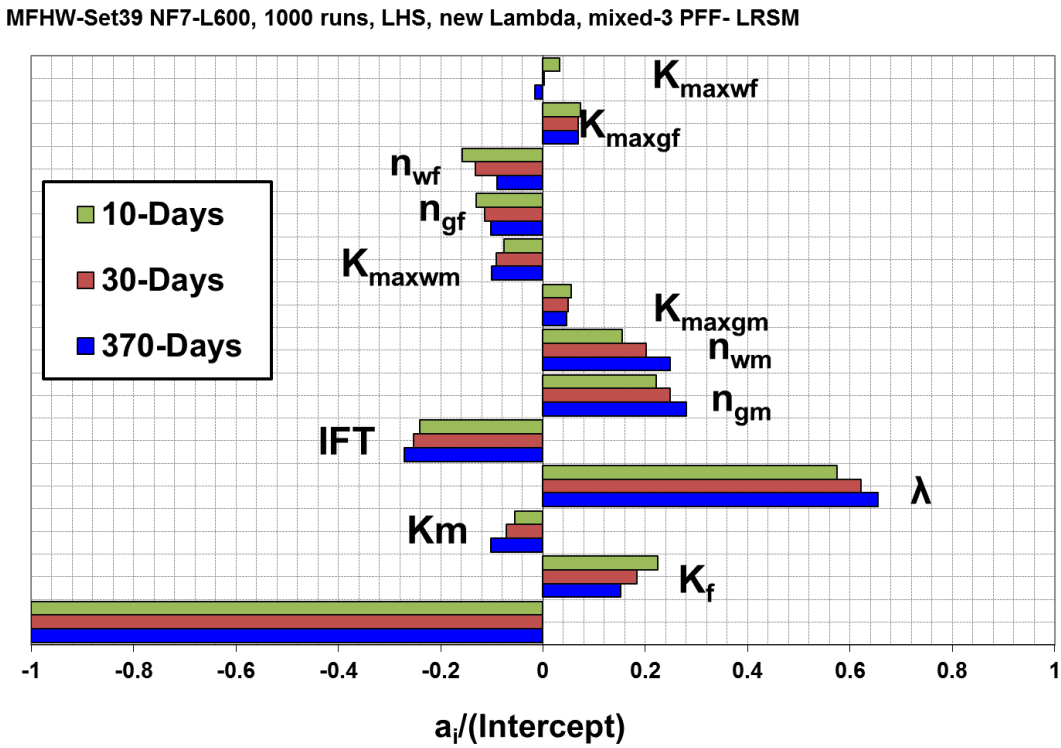

Figure 5.41: PFF Tornado chart comparing LRSM coefficients of all pertinent parameters at three production stages for a) MFHW-Set 37 NF7-L600 with mixed 1, b) MFHW-Set 38 NF7-L600 with mixed 2 & c) MFHW-Set 39 NF7-L600 with mixed3 at three production stages.

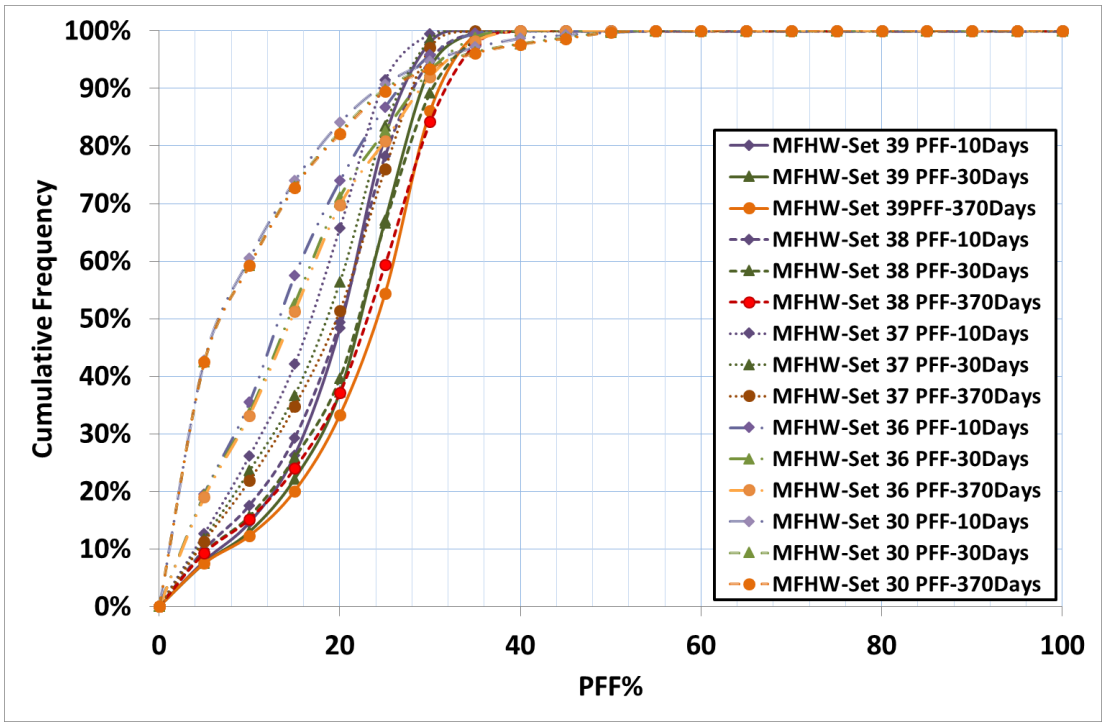

Figure 5.42 PFF Histogram chart comparing a) MFHW-Set 37 NF7-L600 with mixed 1, b) MFHW-Set 38 NF7-L600 with mixed 2 & c) MFHW-Set 39 NF7-L600 with mixed 3 with Weak Perm Jail sets and also with MFHW-Set 30 NF7-L600 at three production stages

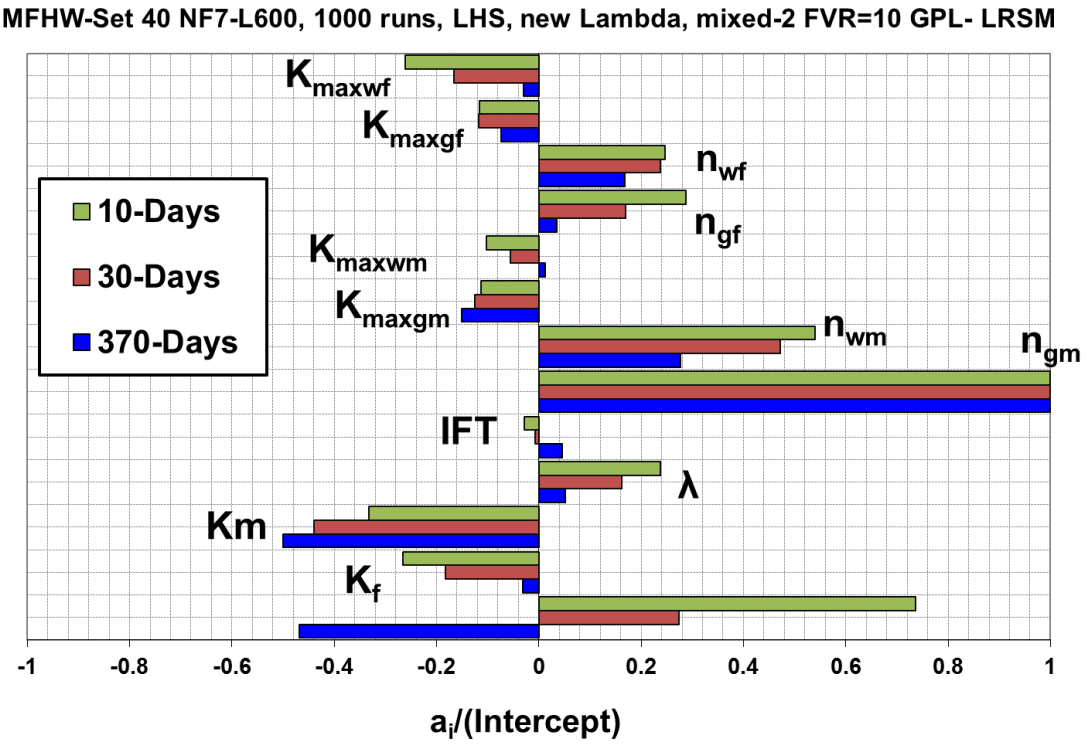

Figure 5.43 GPL Tornado chart comparing LRSM coefficients of all pertinent parameters at three production stages for MFHW-Set 40 NF7-L600 with heterogeneous rock (mixed 2) and FVR=10 at three production stages

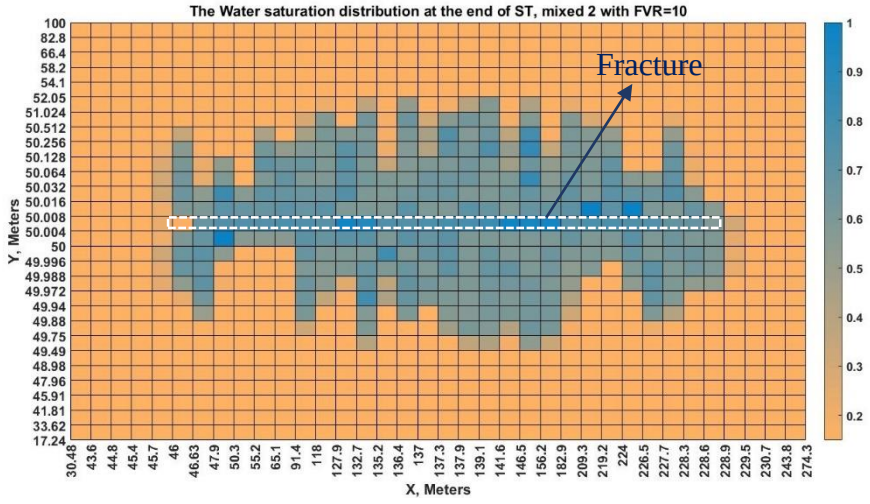

Figure 5.44 Saturation distribution map (run number 30) at the end of ST for MFHW-Set 40 FVR=10.

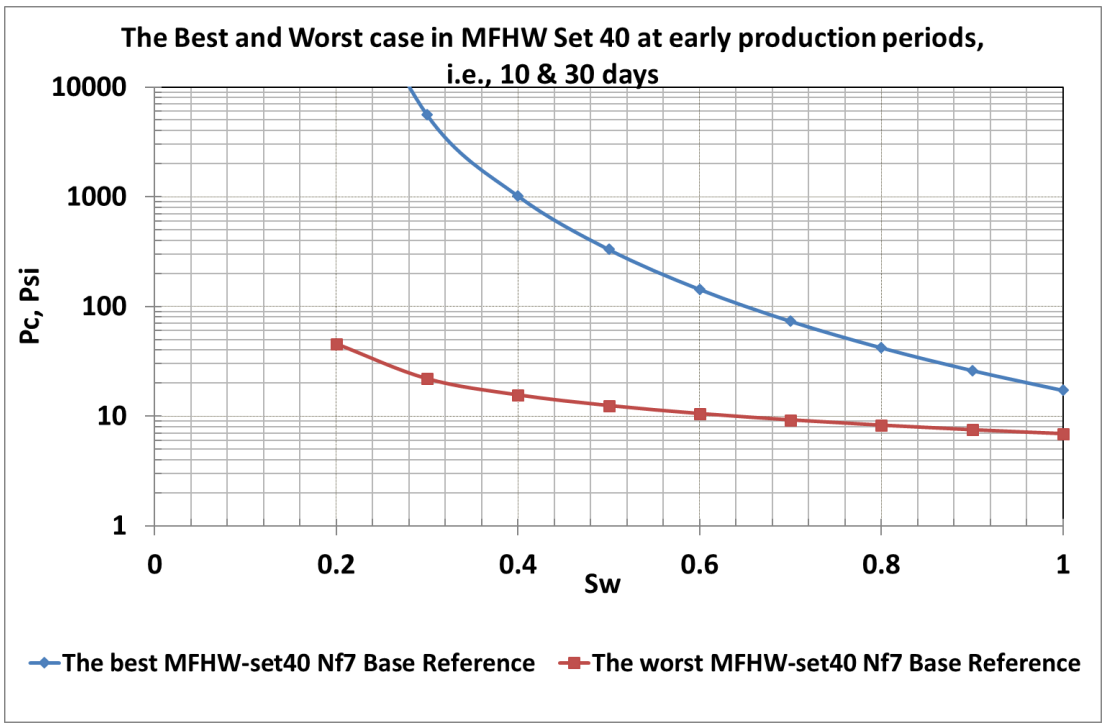

Figure 5.45 Pc vs. Sw in the best and worst case of MFHW-Set 40 at early production periods, i.e., 10 and 30 days

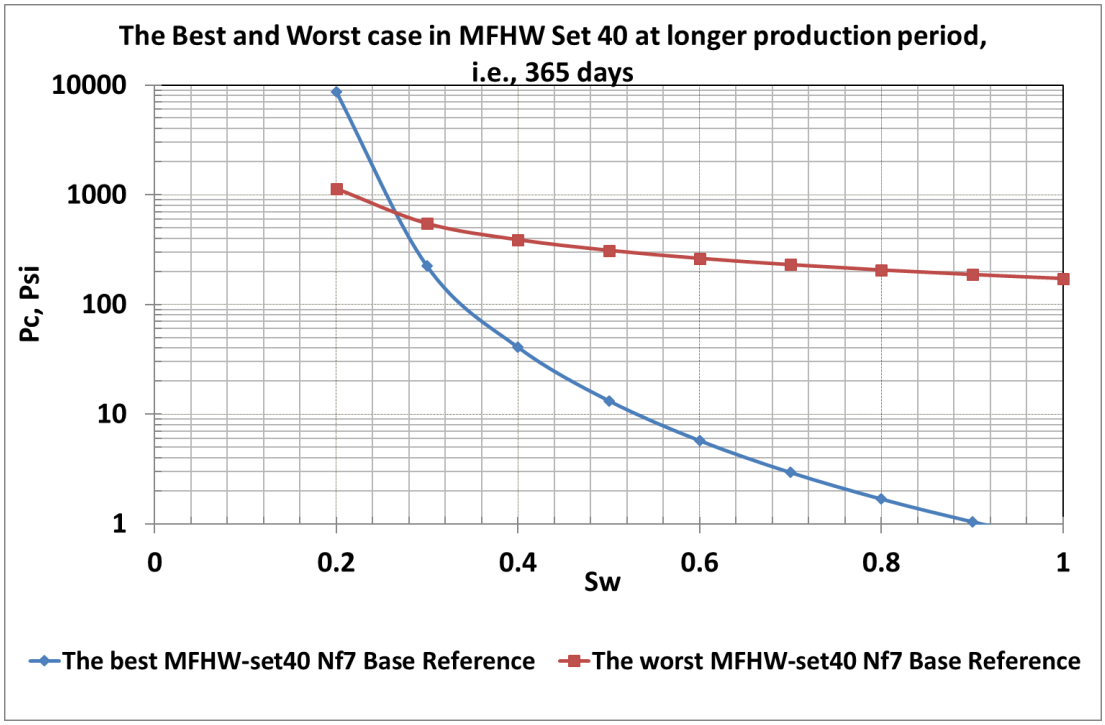

Figure 5.46 Pc vs. Sw in the best and worst case of MFHW-Set 40 at longer production period, i.e., 365 days

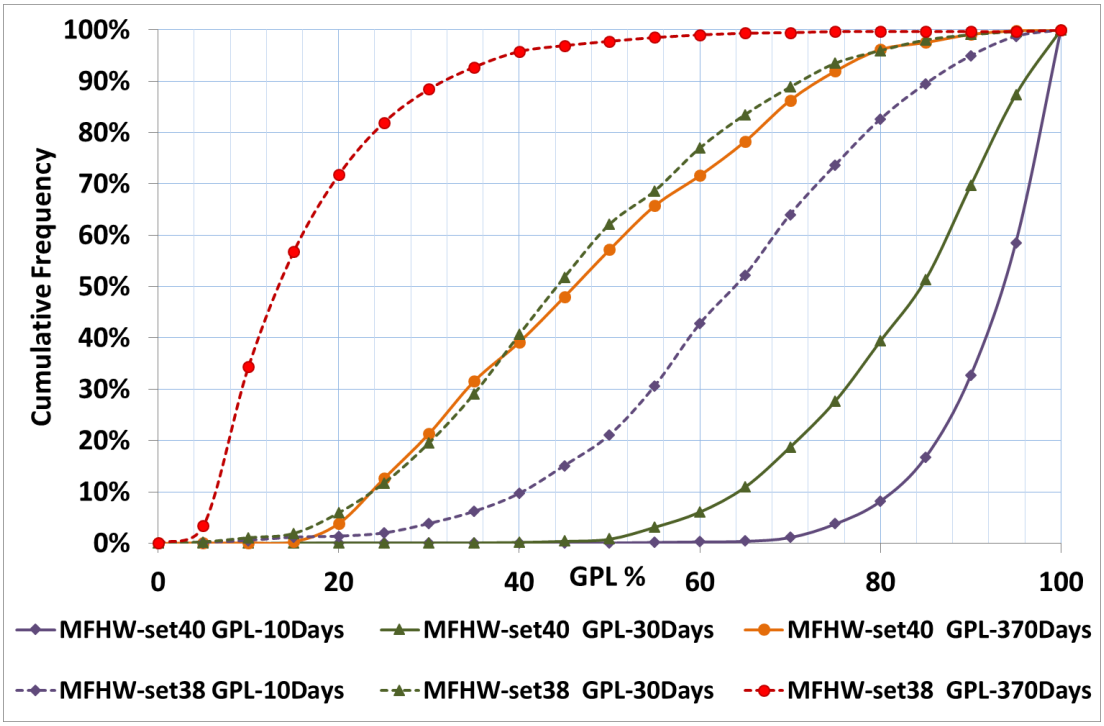

Figure 5.47 GPL Histogram chart comparing a) MFHW-Set 40 NF7-L600 with mixed 2, FVR=10 and b) MFHW-Set 38 NF7-L600 with mixed 2 at three production stages

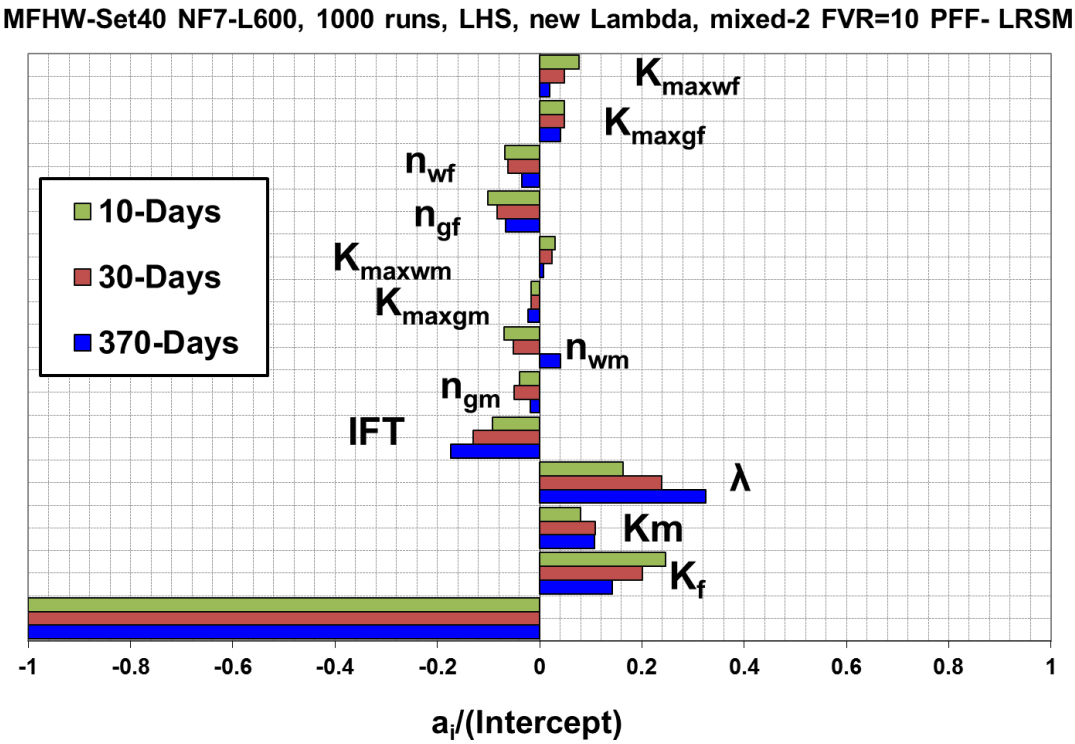

Figure 5.48 PFF Tornado chart comparing LRSM coefficients of all pertinent parameters at three production stages for MFHW-Set 40 NF7-L600 with heterogeneous rock (mixed 2) and FVR=10 at three production stages

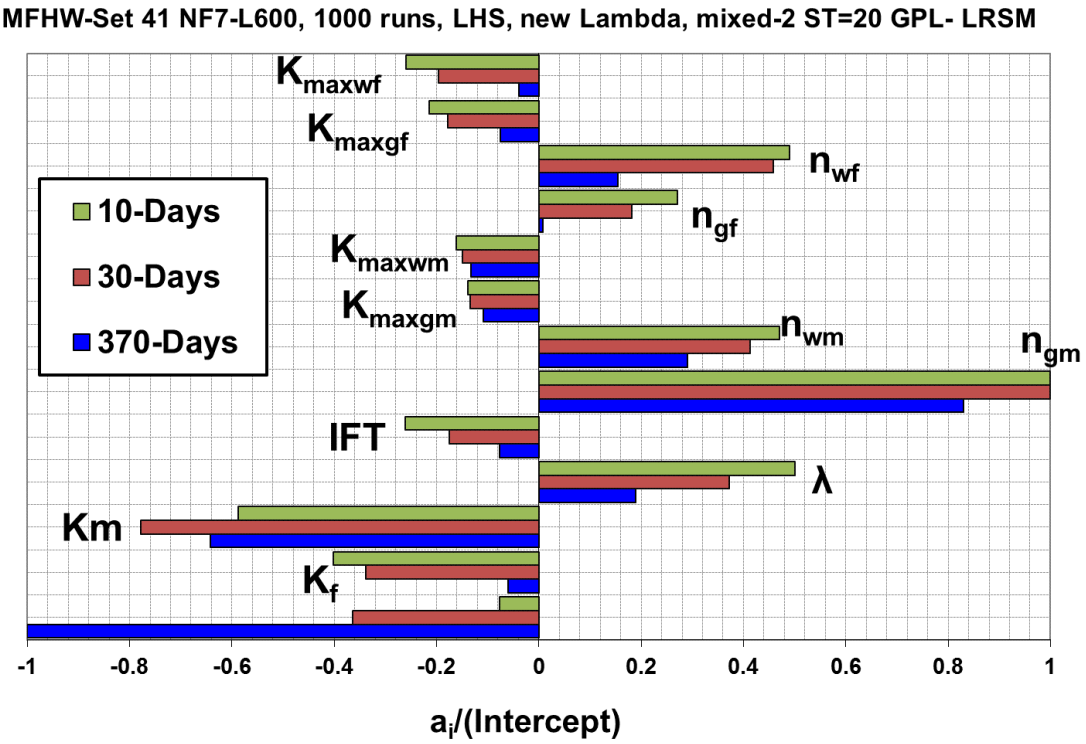

Figure 5.49 GPL Tornado chart comparing LRSM coefficients of all pertinent parameters at three production stages for MFHW-Set 41 NF7-L600 with heterogeneous rock (mixed 2) and ST=20 at three production stages

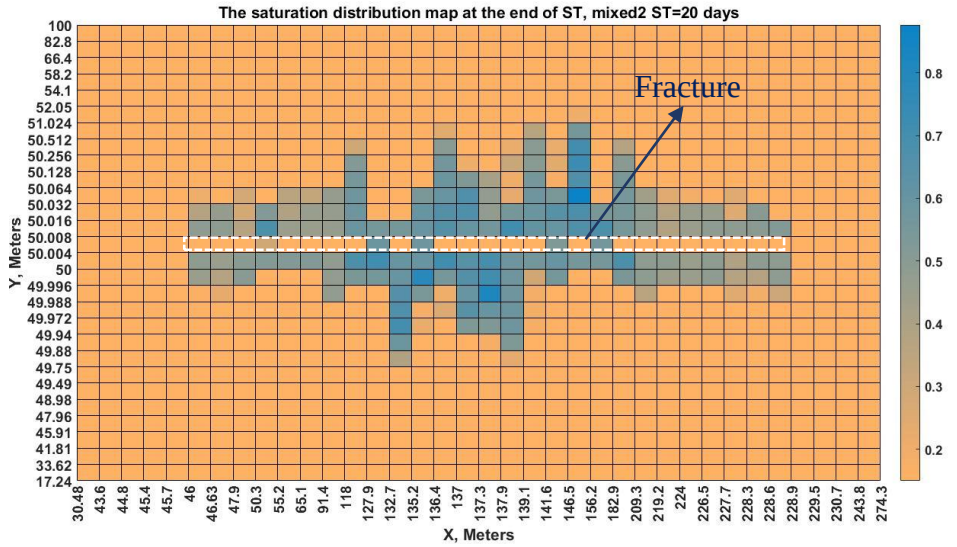

Figure 5.50 Saturation distribution map (run number 30) at the end of ST for MFHW-Set 41 FVR=10.

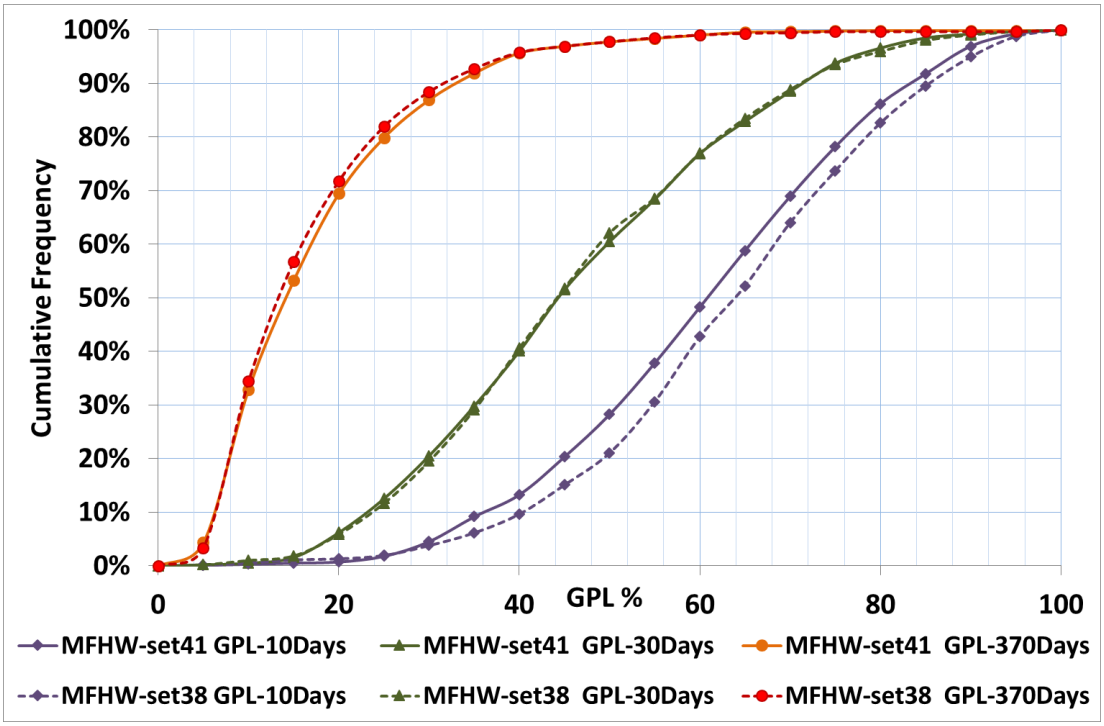

Figure 5.51 GPL Histogram chart comparing a) MFHW-Set 41 NF7-L600 with mixed 2, ST=20 and b) MFHW-Set 38 NF7-L600 with mixed 2 at three production stages

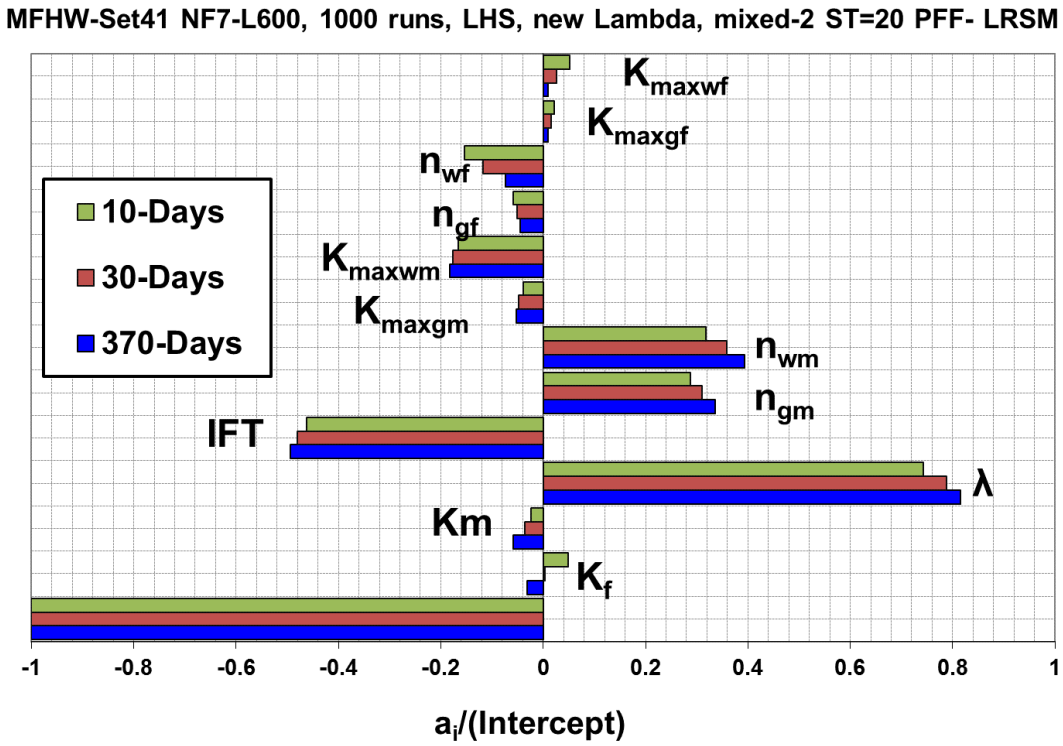

Figure 5.52 PFF Tornado chart comparing LRSM coefficients of all pertinent parameters at three production stages for MFHW-Set 41 NF7-L600 with heterogeneous rock (mixed 2) and ST=20 at three production stages

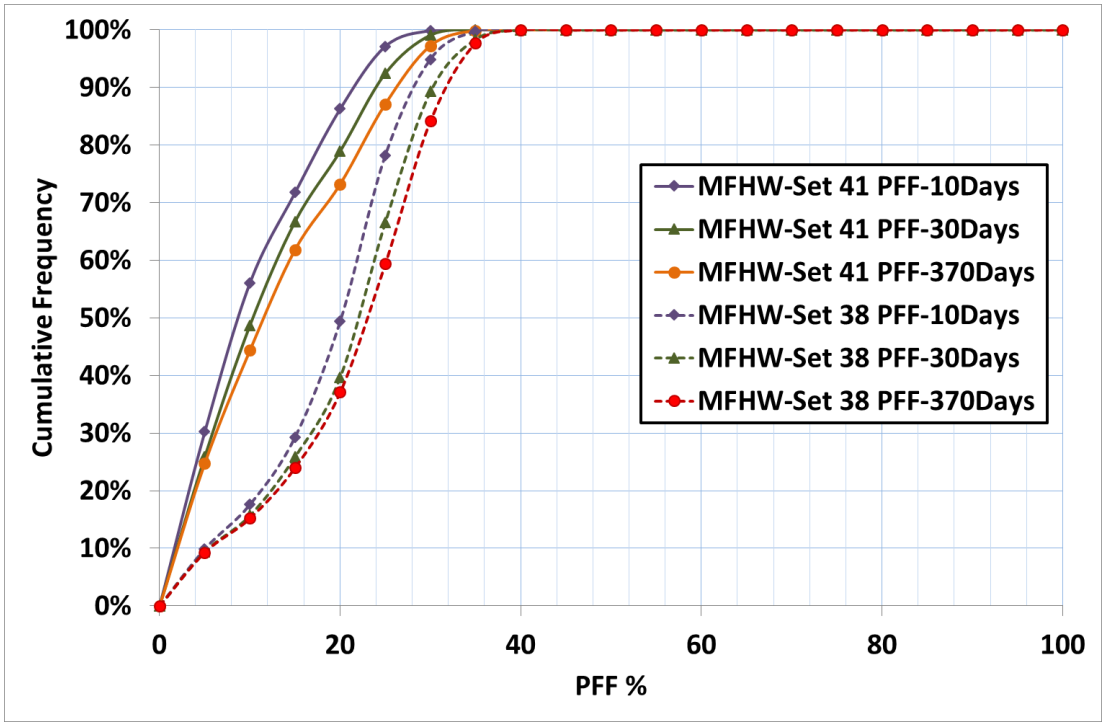

Figure 5.53 PFF Histogram chart comparing a) MFHW-Set 41 NF7-L600 with mixed 2, ST=20 and b) MFHW-Set 38 NF7-L600 with mixed 2 at three production stages

a) MFHW-Set 42 NF7-L600 with mixed 2 and DP100

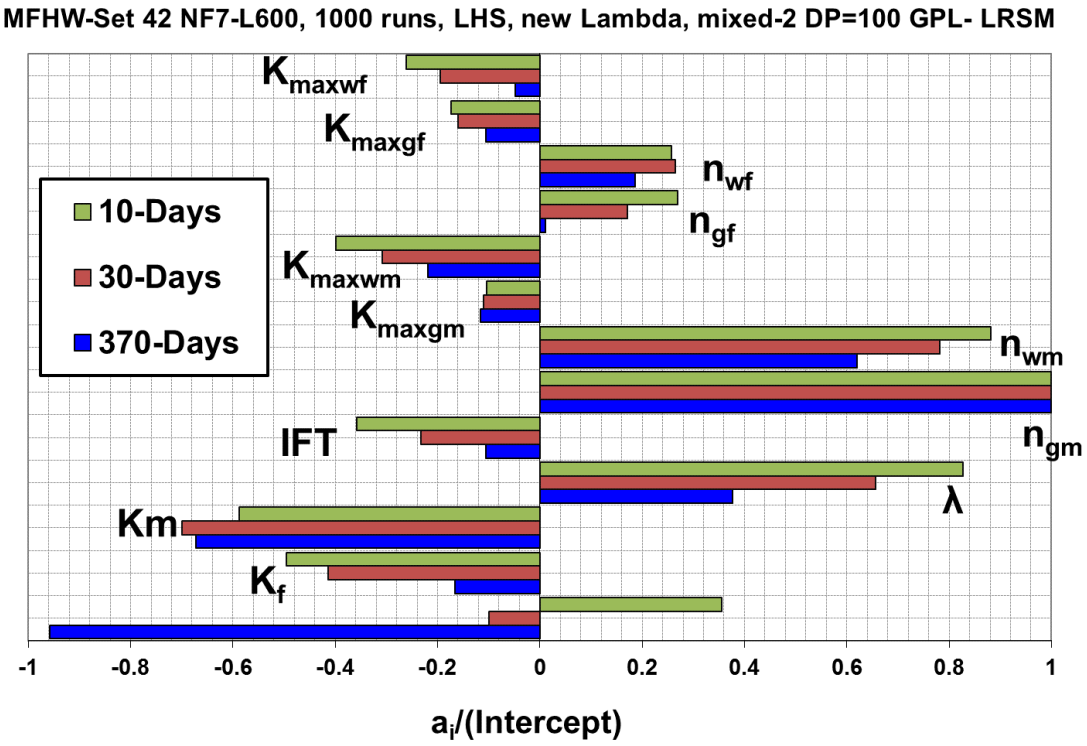

b) MFHW-Set 43 NF7-L600 with mixed 2 and DP4000

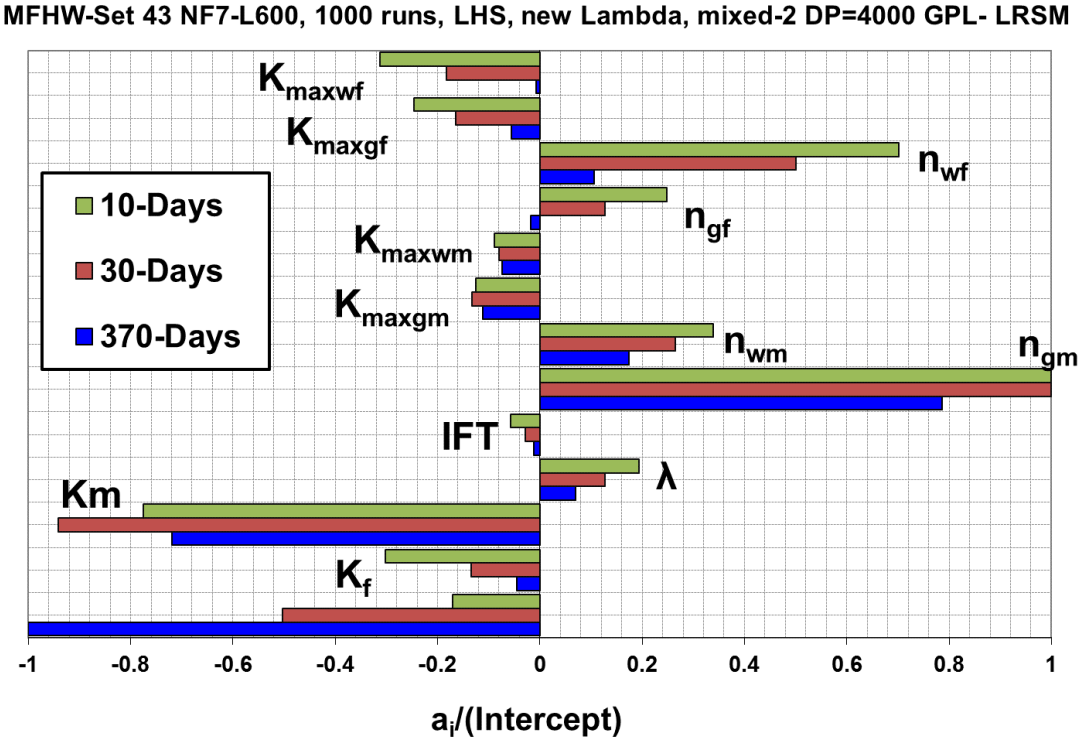

Figure 5.54 GPL Tornado chart comparing LRSM coefficients of all pertinent parameters at three production stages for a) MFHW-Set 42 NF7-L600 with mixed 2 and DP100, b) MFHW-Set 43 NF7-L600 with mixed 2 and DP4000 at three production stages.

a) MFHW-Set 42 NF7-L600 with mixed 2 and DP100

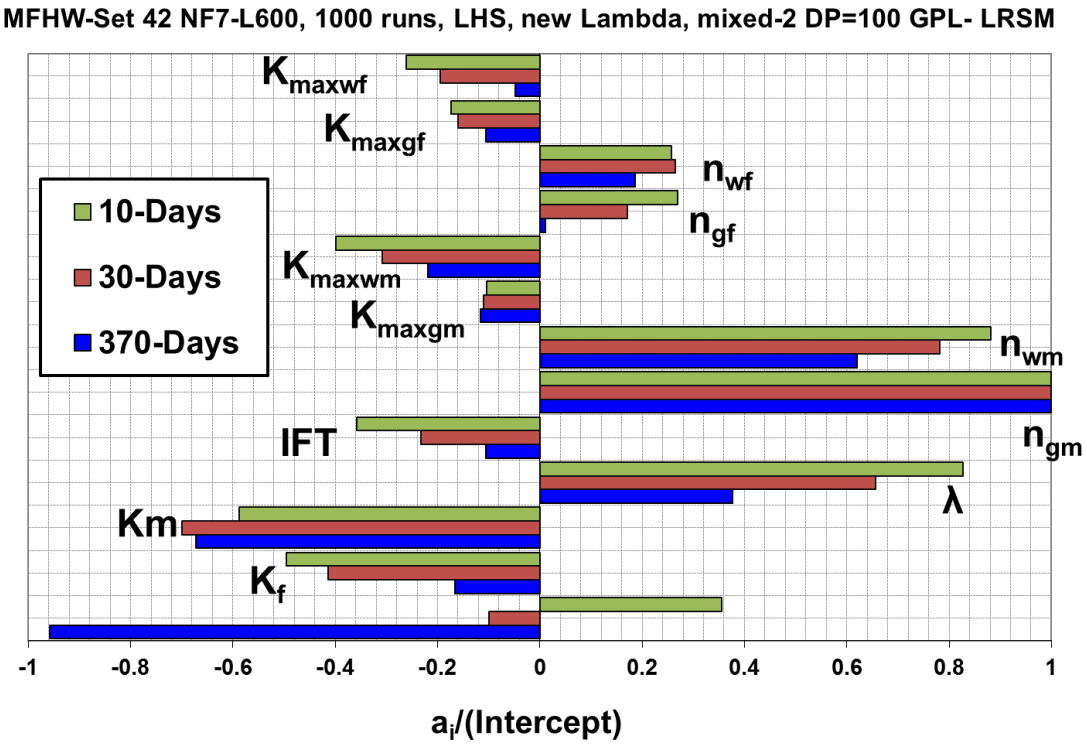

b) MFHW-Set 43 NF7-L600 with mixed 2 and DP4000

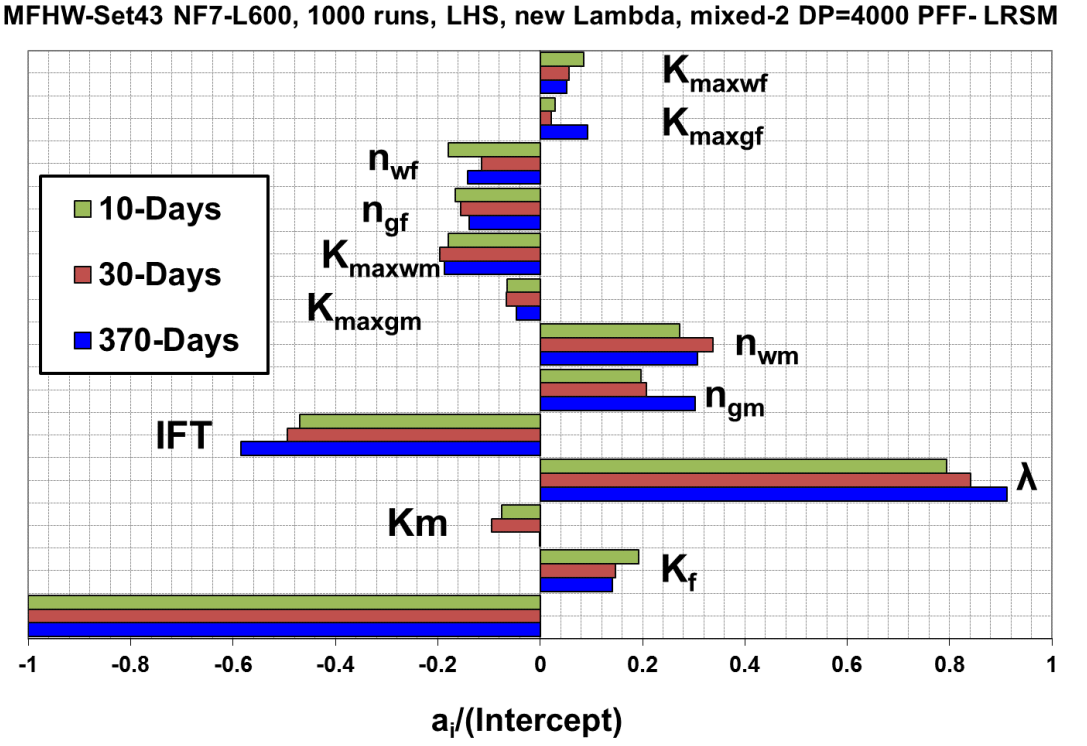

Figure 5.55 PFF Tornado chart comparing LRSM coefficients of all pertinent parameters at three production stages for a) MFHW-Set 42 NF7-L600 with mixed 2 and DP100, b) MFHW-Set 43 NF7-L600 with mixed 2 and DP4000 at three production stages.

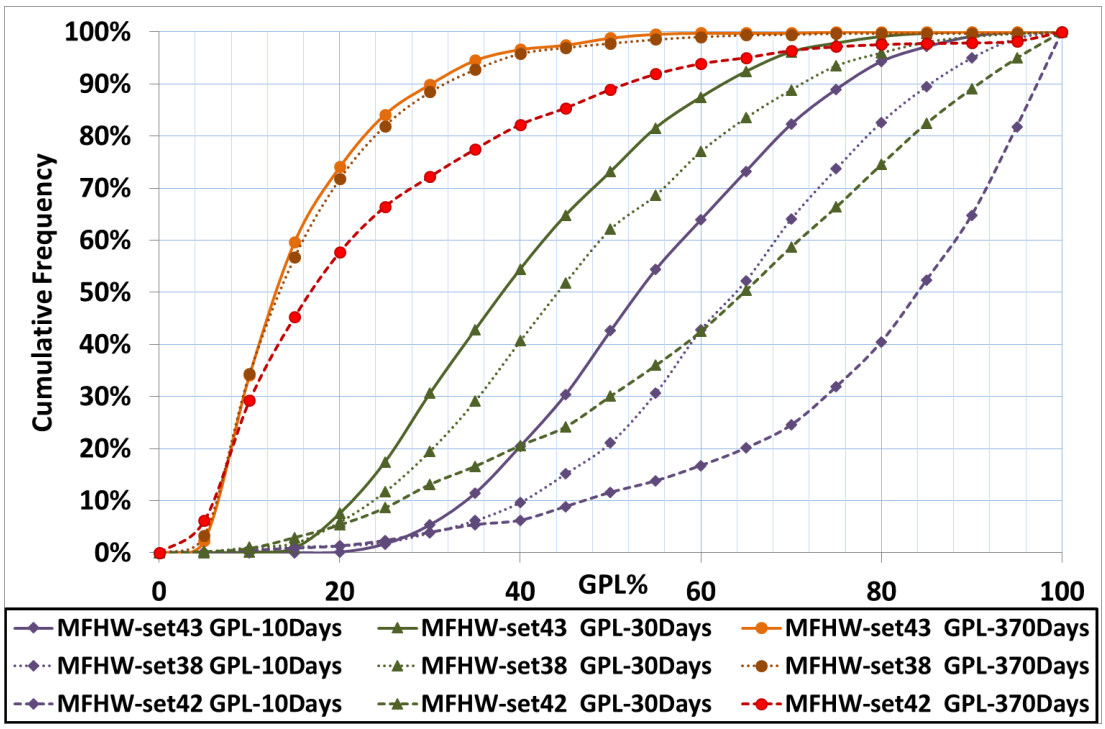

Figure 5.56 GPL Histogram chart comparing a) MFHW-Set 42 NF7-L600 with mixed 2 and DP100, b) MFHW-Set 43 NF7-L600 with mixed 2 and DP4000 and c) MFHW-Set 38 NF7-L600 with mixed 2 at three production stages

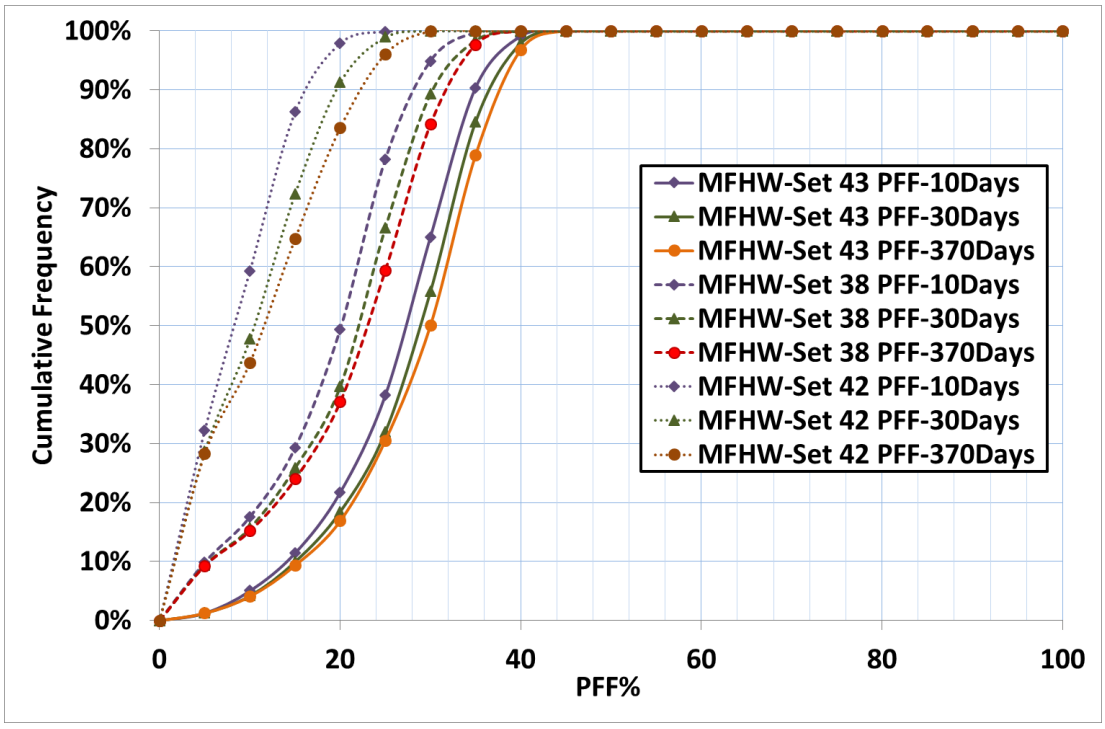

Figure 5.57 PFF Histogram chart comparing a) MFHW-Set 42 NF7-L600 with mixed 2 and DP100, b) MFHW-Set 43 NF7-L600 with mixed 2 and DP4000 and c) MFHW-Set 38 NF7-L600 with mixed 2 at three production stages

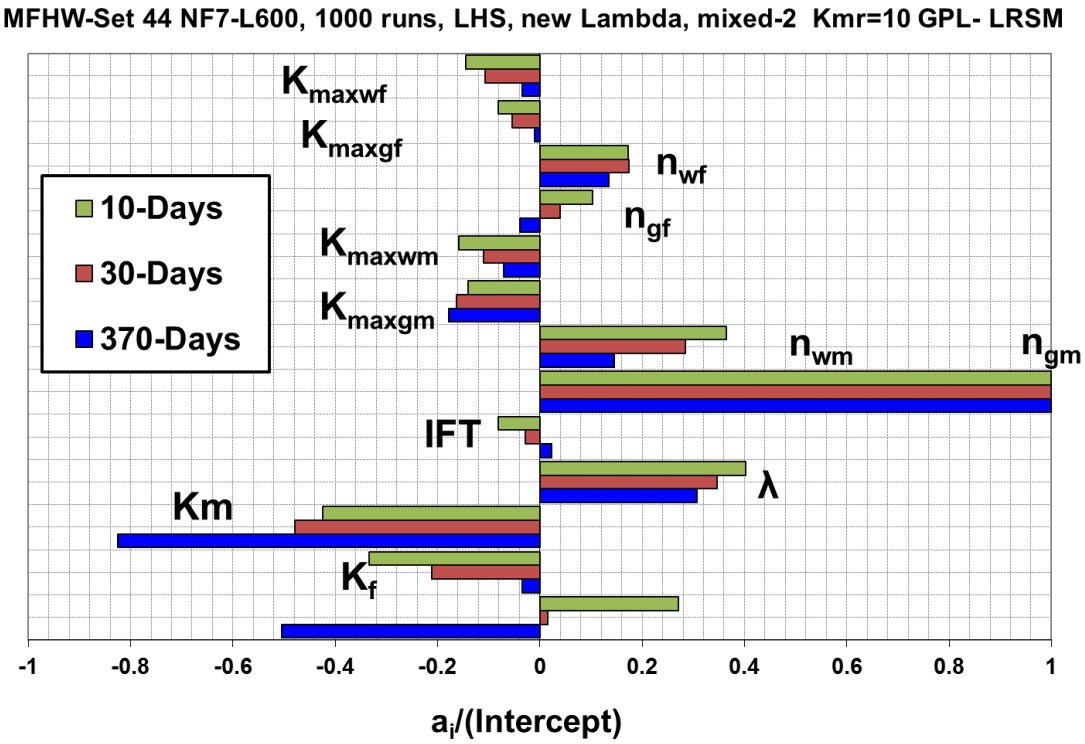

Figure 5.58 GPL Tornado chart comparing LRSM coefficients of all pertinent parameters at three production stages for MFHW-Set 44 NF7-L600 with mixed 2 and Kmr=10 at three production stages.

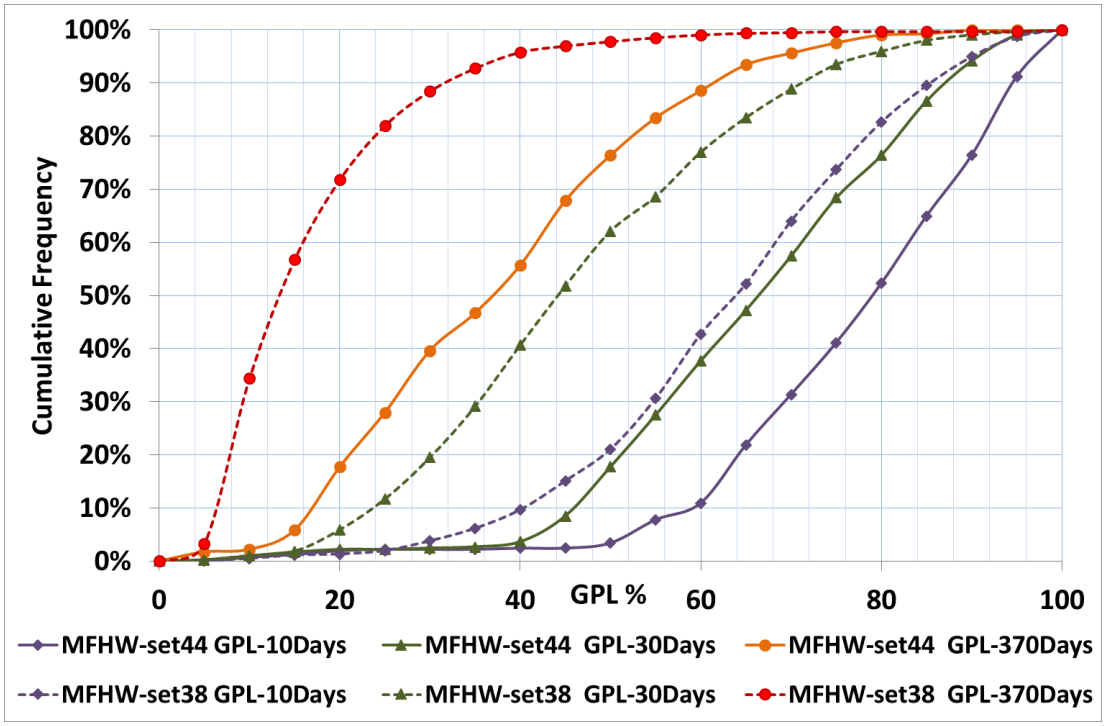

Figure 5.59 GPL Histogram chart comparing a) MFHW-Set 44 NF7-L600 with mixed 2 and Kmr=10 and b) MFHW-Set 38 NF7-L600 with mixed 2 at three production stages

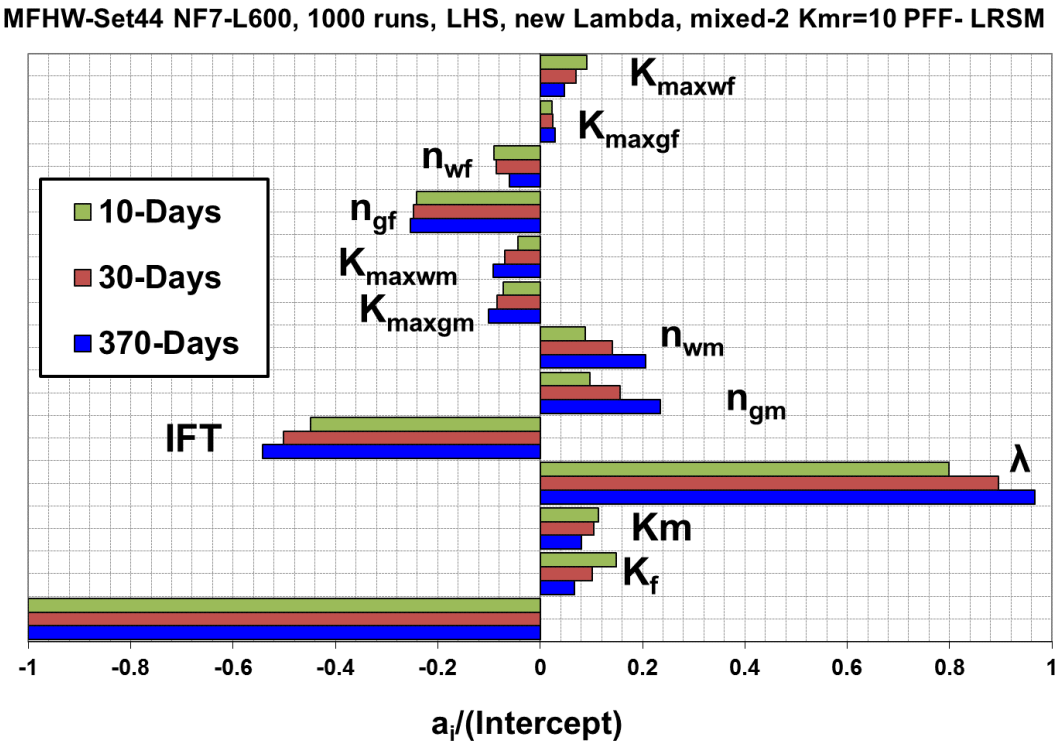

Figure 5.60 PFF Tornado chart comparing LRSM coefficients of all pertinent parameters at three production stages for MFHW-Set 44 NF7-L600 with mixed 2 and Kmr=10 at three production stages.

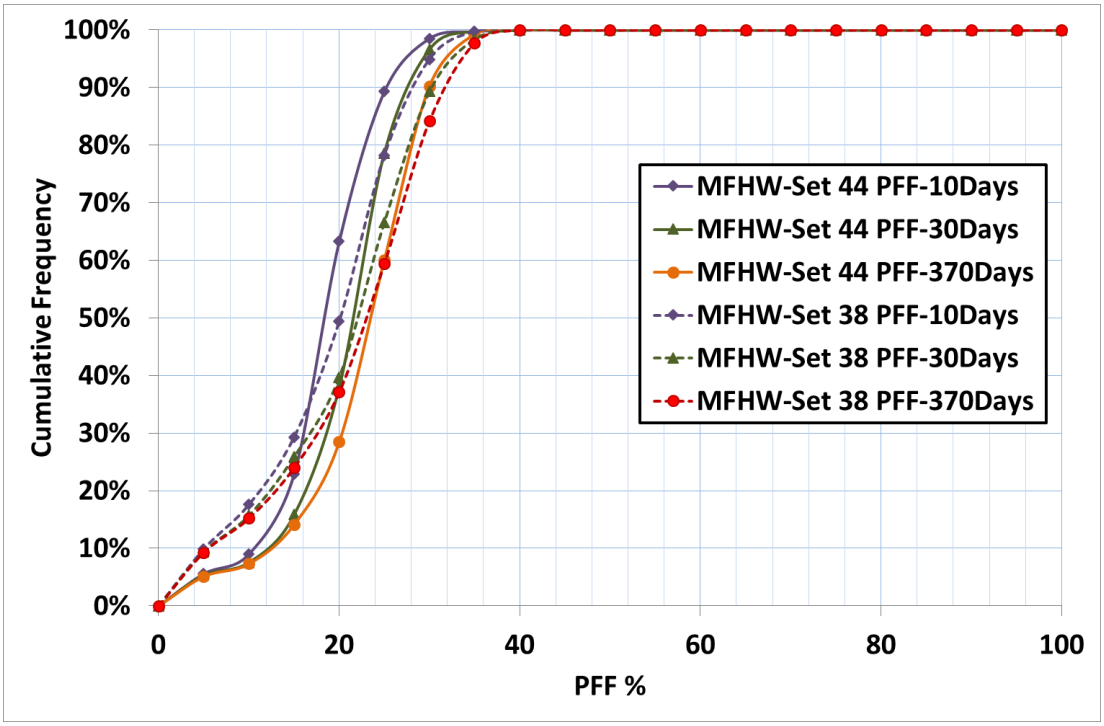

Figure 5.61 PFF Histogram chart comparing a) MFHW-Set 44 NF7-L600 with mixed 2 and Kmr=10 and b) MFHW-Set 38 NF7-L600 with mixed 2 at three production stages

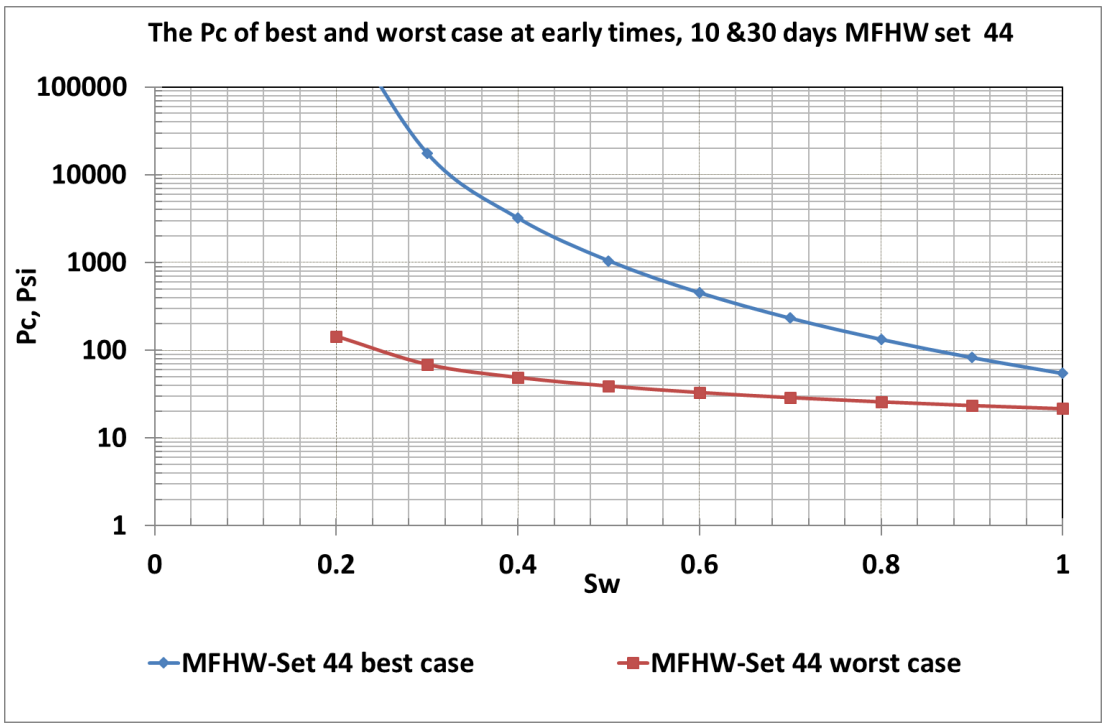

Figure 5.62 Pc vs. Sw in the best and worst case of MFHW-Set 44 at early production periods, i.e., 10 and 30 days

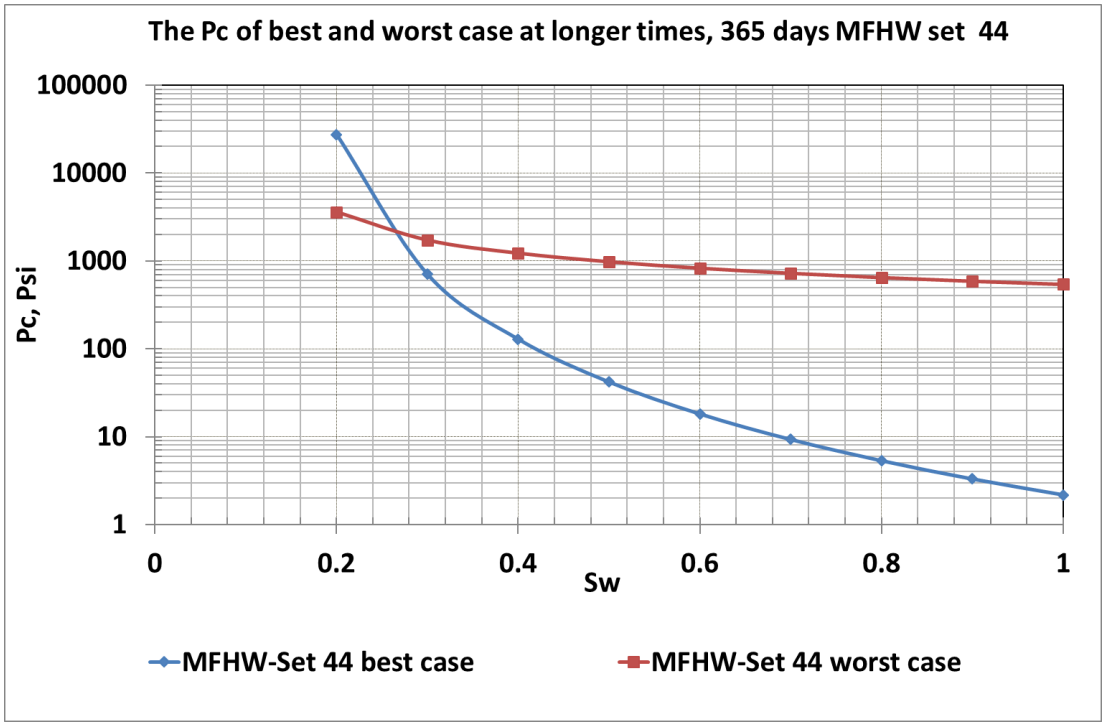

Figure 5.63 Pc vs. Sw in the best and worst case of MFHW-Set 44 at longer production period, i.e., 365 days

CHAPTER 6 CONCLUSIONS AND RECOMMENDATIONS

6.1 Summary

Hydraulic fracturing also known as hydrofracturing, hydrofracking and fracking is the most important stimulation procedures, particularly for tight and ultratight gas reservoirs. Over the last 6 decades, many researchers studied the underperformance of some of the hydraulically fractured wells in tight and ultratight gas fields. It is highlighted by some studies that poor cleanup efficiency of the injected FF is one of the reasons for low productivity of hydraulically fractured wells.

There are some parametric studies in literature, estimating the impact of few related parameters affecting the FF cleanup efficiency of hydraulic fractured wells in tight and ultratight gas fields.

Due to the different assumptions made by researchers to simulate the hydraulic fracturing process, some contradictory observations in some of the reports are presented. To address these issues, Jamiolahmady et al. (2009) studied the cleanup efficiency in single fractured vertical wells, SFVW, of gas and gas-condensate fields. They further investigated some of the uncertainty on the impact of pertinent parameters affecting the cleanup efficiency in tight and ultra-tight formations. Ghahri et al. (2011) extended the work conducted by Jamiolahmady et al. (2009). They conducted a wide-ranging investigation of variation of all pertinent parameters using experimental design combined with the response surface methodology (RSM). They demonstrated that gas production loss, GPL, is significantly affected by parameters linked to FF cleanup inside the fracture. particularly Kf.

The 16 pertinent parameters they used were: the exponent of Corey type (gas or fracture fluid) relative permeability curve (ngi and nwi), the end point of (gas or fracture fluid) relative permeability (Kmaxgi and Kmaxwi), Km, Kf, IFT, Lambda, DP, Porosity, Sgrm and Sgrf. Out of the 16 pertinent parameters, Alajmi (2012) considered four parameters constant in each simulation set, i.e., porosity, residual gas and water saturations in the matrix and fracture and pressure drawdown (DP). The impact of pressure drop (DP), which was considered constant, was treated separately, i.e. different sets of simulations were considered for each pressure drop. Among the 16 parameters, the three least important parameters on cleanup efficiency (i.e., porosity, Sgrm and Sgrf) were considered constant. Porosity was fixed at a value of 0.15 and both residual gas saturation in the matrix (Sgrm) and fracture (Sgrf) were fixed at a value of 0.1. This brings

the total number of variables from 16 in Ghahri's work (Ghahri (2010)) to 12 in Alajmi's work (Alajmi (2012)) and this work for both pre- and post-treatment simulations.

This thesis extends the line of work conducted by Jamiolahmady et al. (2009) and Ghahri et al. (2011) to the areas that are not addressed in their work as below:

- Identifying the gaps in SFVW study and conducting new SFVW sets that were not addressed before (sets with different parameters, i.e., tight and very tight sets, shorter fracture, different Swi, DP, FVR, etc.).
- Extending the cleanup efficiency study to MFHWs systems with conventional Pc and Kr as well as unconventional Pc & Kr).
- Applying new sampling approach to increase the accuracy of RSM and reduce CPU time (i.e., the LHS method rather than the old FFS) and conducting new MFHW-Sets using the new approach
- Conducting a comprehensive evaluation of Pc correlations available for tight and ultra-tight formations to identify the most suitable one used in this study.
- Conducting a comprehensive investigation on unconventional relative permeability (Kr) and permeability jail effects in unconventional formations and conducting new MFHW-Sets to propose a suitable method to model them for the purpose of this work.

In other words, this thesis extends the line of work conducted by Jamiolahmady et al. (2009) and Ghahri et al. (2011) on SFVW to sets with different fracture fluid injection volume (FVR), shut-in time period (ST), matrix permeability variation range (Kmr), pressure drawdown (DP), initial water saturation (Swi) and length of hydraulic fracture. Additionally, in order to further improve the current understanding of hydraulic fracturing treatment for practical field applications, this study has expanded the previous work that has been done on SFVW sets to MFHWs systems with different fracture spacing (300m, 100m, 75m and 50m), different fracture length (600m and 900m), different permeability variation range (Kmr=0.01, 1,10 and 100), different pressure drawdowns (DP=100, 1000 and 4000psi) and different STs. In order to increase the accuracy of the fitted response surface models and to reduce the CPU time, instead of FFS experimental design used in the previous simulations (SFVW sets and MFHW sets 1 to 22), the LHS method has been used to decrease the required number of runs. It should be noted that the response surface model fitted to the results based on the FFS is a linear whereas that fitted based on LHS could be either linear or quadratic, which increases the accuracy of the fitted response

surface models. In addition, a comprehensive evaluation of Pc correlations available for tight and ultra-tight formations was performed using the Go2Flow and identify the most suitable model. Parallel to this, a comprehensive investigation was conducted on the unconventional Kr with relative permeability jail effect in unconventional formation. An attractive approach has been adopted to successfully model the weak and strong permeability jail effects in unconventional Kr models. Finally, several new MFHW-Sets were run capturing the impact of unconventional Pc and Kr on the MFHWs clean-up efficiency. It should be noted that some of the conclusions are due to assumptions or limitations in the model, i.e., independent variation of parameters without using dependency function between them, lack of enhanced permeability zone around then fracture and permeability jail effect.

6.2 Conclusions

The first part of this thesis was devoted to evaluating the impact of pertinent parameters on the clean-up efficiency of SFVWs. A series of numerical simulation runs (4096 runs in each SFVW-Set) were conducted using a MATLAB code coupled with ECLIPSE100. The key conclusions of studying these SFVW-Sets are listed in Table 6.1.

Table 6.1 The key conclusions of the SFVW-Sets

Investigated SFVW scenarios	Impacts
Base Reference set	• FF mobility parameters in the fracture, were the key drivers of GPL improvement • A reduction of Pc increases GPL. • Higher IFT is favourable to have higher production rates.
Higher injection volumes of Fracturing Fluid	• The larger the FVR, the slower the cleanup
Extension of Soak time	• Extended shut-in time results in better gas production. • Extension of the Soak period has a short term impact.
Tighter/Tightest Matrix Formation	• In tighter gas formations, generally more production loss and slower cleanup were observed.
Increasing the pressure drawdown during production stage.	• When DP was increased, the impact of Pc on cleanup became less pronounced and vice versa. • The larger the drawdown, the faster the cleanup.
Shorter fractures	• As fracture length decreased, the effect of fracture parameters on GPL decreased and the effect of matrix parameters on GPL increased.

The second part of this thesis was focused on the impact of pertinent parameters on the clean-up efficiency of MFHW systems (using conventional Pc and Kr similar to those of SFVW) with different fracture spacing (300m, 100m, 75m and 50m), different fracture length (600m and 900m), different permeability variation range (Kmr=0.01, 1,10 and 100), different pressure drawdowns (DP=100, 1000 and 4000psi) and different STs. Series of numerical simulation runs (4096 runs in each MFVW-Set using FFS and 1000 runs in MFHW-sets using LHS) were conducted using either a MATLAB code (FFS approach) or a Python transcript (LHS approach) coupled with ECLIPSE100. The main listed conclusions of SFVW-Sets are: For the MFHW sets23 to 29, instead of two-level full factorial linear (FFS) experimental design used in the previous simulations (MFHW sets 1 to 22 and SFVW-Sets 1-66), the LHS method was used to decrease the required number of runs and to increase the accuracy of the fitted response surface models.

The key conclusions of studying these MFHW-Sets are listed in Table 6.2.

Table 6.2 The key conclusions of the MFHW-Sets

Investigated Scenarios	Impacts
MFHW Base Reference set	• A reduction of Pc increases GPL. The near well bore choking effect in MFHWs makes the effect of Pc even more pronounced. • Higher IFT is even more favourable to have higher production rates in MFHWs relative to SFVWs. • Faster clean-up was observed for MFHWs compared to SFVWs.
Higher injection volumes	• The larger the FVR, the slower the cleanup
Tighter/Tightest Matrix Formation	• The negative impact of the near well bore choking effect on cleanup is less pronounced in tighter formations.
Increasing the pressure drawdown	• When pressure drawdown was increased, the impact of Pc on cleanup became less pronounced and vice versa. • The larger the drawdown, the faster the cleanup.
Shorter fractures	• As fracture length decreased, the effect of fracture parameters on GPL decreased and the effect of matrix parameters on GPL increased.
Reducing the fracture spacing	• Similar cleanup efficiency is observed for different fracture spacing. • Increasing horizontal well length while the fracture spacing was fixed, did not change the fracture clean-up efficiency at all.
Use of Chemicals	• In MFHW sets with conventional and tight formations, using chemicals (IFT reducing agents) could increase GPL whilst in ultra-tight formations, it is recommended to use chemicals in order to reduce Pc and consequently reduce GPL.
Latin Hypercube sampling versus full factorial sampling	• Using LHS with an optimum run number reduced the CPU time significantly compared to two-level FFS sets. • The optimum (minimum) required number of MFHW-Nf7L600 runs for FQRSMs was 1000.

The third part of this thesis was devoted to capturing the impact of unconventional Pc and Kr on the MFHWs clean-up efficiency. a comprehensive evaluation of Pc correlations available for tight and ultra-tight formations has been performed using Go2Flow software to investigate the reliability of available Pc correlations models for tight and ultra-tight formations. Furthermore, a comprehensive investigation was conducted on unconventional relative permeability (Kr) and permeability jail effects in unconventional formation. An attractive approach has been adopted to successfully model weak and strong permeability jail effects.

The key conclusions of studying these MFHW-Sets with unconventional Pc and Relative permeability are listed in Table 6.3.

Table 6.3 The key conclusions of the MFHW-Sets

Investigated MFHW Scenarios		Impacts
MFHW sets with unconventional Pc	Comprehensive evaluation of Pc correlations	• The Brooks and Corey is a simple and accurate model to represent Pc data in unconventional formations. • The range of pore size distribution index should be limited to values between 0.3 to 1.5 to represent the unconventional formations.
	MFHW-sets with unconventional Pc	The same observations were noted as MFHWs with conventional Pc apart from following: • The impact of Pc pertinent parameters (especially that of lambda) on GPL was most important. • The lower lambda range in the unconventional formations resulted in larger Pc values.
		• Reducing the Km range or increasing FVR slowed down the clean-up performance.
MFHW sets with unconventional Pc & Kr	Unconventional relative permeability	• A Corey type model with a large difference between critical and trap end point saturation was used.
	MFHW-Sets with unconventional Pc & Kr	• The more pronounced the jail effect, the lower the impact of Pc on clean-up efficiency. • The stronger the Kr jail effect, the slower the clean-up was also noted
	Heterogeneous MFHW-Sets	• In heterogeneous formations with unconventional Pc and Kr, when FVR, DP, ST and Km range were changed, the same observations were observed in line with what was previously observed in chapter 3 and 4

6.3 Recommendations

The research that has been undertaken for this thesis has highlighted a number of topics on which further research would be beneficial.

- Tight and ultra-tight low permeability reservoirs typically have large initial water saturation (Swi), However, this is not always the case in many fields where they have "sub-irreducible" Swi. the irreducible water saturation (Swirr) in these tight gas reservoirs tends to be higher than the Swi. This is attributed to desiccation (Bennion et al., 2004).

i. In this thesis, the impact of Swi on cleanup efficiency was studied when it was equal to/larger than Swirr. But the impact of Swi when it is smaller than Swirr, i.e., desiccation, was not studied.
    a. It is recommended that this case will be captured in future cleanup efficiency studies and its impact on post-fracturing cleanup will be investigated.

- Following the promising results of the work conducted on the cleanup efficiency of SFVWs, MFHW-Sets and MFHW-Sets with unconventional Pc and Kr in tight and ultra-tight formations, it is recommended that the line of research will be extended to shale gas formations.
- In this thesis, a pre-fractured well was considered to model hydraulically fracturing process. To model the hydraulically fracturing process more realistically it is recommended that geomechanics of hydraulic fracturing will be considered in addition to the flow dynamics to capture the impact of fluid flow and geomechanics on the cleanup efficiency simultaneously.
- The statistical and sampling approaches in this thesis to capture the impact of parameters on the GPL for a fractured well can be extended to gas condensate reservoirs.

6.4 References

ALAJMI, E 2012. Modelling of Gas-Condensate Flow around Complex Well Geometries and Cleanup Efficiency in Heterogeneous Systems. PhD thesis, Heriot-Watt University Petroleum Engineering, Edinburgh, UK

BENNION, D. B., THOMAS, F. B., SCHULMEISTER, B. E. & SUMANI, M. 2004. Determination of true effective in situ gas permeability in subnormally water-saturated tight gas reservoirs. *Journal of Canadian Petroleum Technology,* 43**,** 27-32.

ECONOMIDES, M. J. & MARTIN, A. N. How to decide between horizontal transverse, horizontal longitudinal and vertical fractured completion. Proceedings - SPE Annual Technical Conference and Exhibition, 2010. 2474-2491.

GHAHRI, P., JAMIOLAHMADY, M. & SOHRABI, M. 2011. A Thorough Investigation Of Cleanup Efficiency Of Hydraulic Fractured Wells Using Response Surface Method. Society of Petroleum Engineers.

GHAHRI, P 2010. Modelling of Gas-condensate flow around horizontal and deviated wells and cleanup efficiency of hydraulically fractured wells. PhD thesis, Heriot-Watt University Petroleum Engineering, Edinburgh, UK

JAMIOLAHMADY, M., SOHRABI, M. & GHAHRI, P. 2009. Investigation of Cleanup Efficiency of Hydraulically Fractured Wells in Gas Condensate Reservoirs. Society of Petroleum Engineers.

CHAPTER 7 APPENDIX

7.1 The developed MATLAB code for SFVWs

```
function CleanupEfficiencyMultilayer

clear
clc
tic
% ------------------------------------------------------------------------
------------------------------------------------------ %
% define variables
%
% ------------------------------------------------------------------------
------------------------------------------------------ %
% global inputfileRoot;
%name of file
% inputfileRootf = ['1phase_wf4mm_xf100m_BFT'];

inputfileRootp2 = ['1phase_wf4mm_xf400m_Multilayer'];

inputfileRootcl = ['1phase_wf4mm_xf400m_MultilayerClean'];

fid1=fopen('Eout1-Multilayer-L400.inc', 'a');
fprintf(fid1,'No.file,x1 x3 x4 x5 x9 x10 x11 x12 x15 x16 x17
x18,PRtime(days),GPTL1(MSCF),WPTL1(STB),WITL1(STB),GPTL2(MSCF),WPTL2(S
TB),WITL2(STB),PRtime_Cl(days),GPT_Cl_L1(MSCF),GPT_Cl_L2(MSCF)\n');
fid2=fopen('Eout2-Multilayer-L400.inc', 'a');
fprintf(fid2,'No.file,x1 x3 x4 x5 x9 x10 x11 x12 x15 x16 x17
x18,PRtime(days),GPTL1(MSCF),WPTL1(STB),WITL1(STB),GPTL2(MSCF),WPTL2(S
TB),WITL2(STB),PRtime_Cl(days),GPT_Cl_L1(MSCF),GPT_Cl_L2(MSCF)\n');
fid3=fopen('Eout3-Multilayer-L400.inc', 'a');
fprintf(fid3,'No.file,x1 x3 x4 x5 x9 x10 x11 x12 x15 x16 x17
x18,PRtime(days),GPTL1(MSCF),WPTL1(STB),WITL1(STB),GPTL2(MSCF),WPTL2(S
TB),WITL2(STB),PRtime_Cl(days),GPT_Cl_L1(MSCF),GPT_Cl_L2(MSCF)\n');
fid4=fopen('Eout4-Multilayer-L400.inc', 'a');
fprintf(fid4,'No.file,x1 x3 x4 x5 x9 x10 x11 x12 x15 x16 x17
x18,PRtime(days),GPTL1(MSCF),WPTL1(STB),WITL1(STB),GPTL2(MSCF),WPTL2(S
TB),WITL2(STB),PRtime_Cl(days),GPT_Cl_L1(MSCF),GPT_Cl_L2(MSCF)\n');

% Number of Fractured Well Model
neclfile1=1;

% no. fracture cells
NFG=[15];
%Fracture lenght
Lf=[100];
wf=[4];
Cfd=[1];
Nolayers=1;

RPdataNo=4096; %32801-repeatdata2index.inc
nfileffei=1;
nfileffee=RPdataNo;%2^13
Noexp=2^12;

% 2^18 , 18 is the number of paramters
NY=[36];
NX=[33];
% fracture permeability(mD), X1, Y
```

```
kf=[1000 (1000+30000)/2 30000];
%pressure drawdown (psi),X2,N
dp=[1000 (1000+1000)/2 1000];
% matrix permeability,X3,Y
km=[0.001 (0.001+0.1)/2 0.1];
%pore size disturbution,X4, Y
lam=[1 (1+4)/2 4];
%matrix interfacial tension,X5, Y
IFT=[2 (2+50)/2 50];
%porosity,X6,N
poros=[0.15 (0.15+0.15)/2 0.15];
%Sgr matrix,X7,N
Sgrm=[0.1 (0.1+0.1)/2 0.1];
%Swr matrix,X8,N
Swcm=[0.15 (0.15+0.15)/2 0.15];
%core exponent krg,X9, Y
ngm=[1.5 (1.5+5)/2 5];
%core exponent krw,X10, Y
nwm=[1.2 (1.2+4)/2 4];
%endpoint krg,X11, Y
Kmaxgm=[0.5 (0.5+1.0)/2 1.0];
%endpoint krw,X12, Y
Kmaxwm=[0.05 (0.05+0.6)/2 0.6];
%Sgr fracture,X13,N
Sgrf=[0.1 (0.1+0.1)/2 0.1];%
%Swr fracture,X14,N
Swcf=[0.15 (0.15+0.15)/2 0.15];
%core exponent krg fracture,X15,Y
ngf=[1.5 (1.5+5)/2 5];
%core exponent krw fracture,X16,Y
nwf=[1.2 (1.2+4)/2 4];
%endpoint krg fracture,X17, Y
Kmaxgf=[0.5 (0.5+1.0)/2 1.0];
%endpoint krw fracture,X18, Y
Kmaxwf=[0.10 (0.1+0.75)/2 0.75];
pi=7500;
% fracture porosity
porosf=[0.35 (0.35+0.35)/2 0.35];
%k1/k2 ,x19
k1k2=[1    (1+1)/2     1];
%kvkh,x20
kvkh=[1    (1+1)/2     1];
%Cf variation vertical, x21
Iv=[1 (1+1)/2     1];

% for interpolating data
x=[0 0.5 1];
% Report time RSM file
timer=[13.67 34.43 181.43 371.4373];

%[x1 x3 x4 x5 x9 x10 x11 x12 x15 x16 x17
x18]=readmatrixexpdesignm3(Noexp);

%[RPdata]=readmatrixexpRP(RPdataNo);
load('fullfactorialdesign1.mat');
x0=dCC(:,1);x1=dCC(:,2);x3=dCC(:,3);x4=dCC(:,4);x5=dCC(:,5);x9=dCC(:,6
);x10=dCC(:,7);x11=dCC(:,8);x12=dCC(:,9);
x15=dCC(:,10);x16=dCC(:,11);x17=dCC(:,12);x18=dCC(:,13);

fidd=fopen('PREMX.INC','w+');
fidd1=fopen('PORO.INC','w+');
fidd2=fopen('krm.INC','w');
```

```
fidd3=fopen('WCONPROD.INC','w');
% fidd4=fopen('PERMZ.INC','w+');

for neclfile=nfileffei:nfileffee
neclfile
x1f=x1(neclfile);x2f=0.5;x3f=x3(neclfile);x4f=x4(neclfile);x5f=x5(neclfile);x6f=0.5;x7f=0.5;x8f=0;
x9f=x9(neclfile);x10f=x10(neclfile);x11f=x11(neclfile);x12f=x12(neclfile);x13f=0.5;x14f=0;x15f=x15(neclfile);
x16f=x16(neclfile);x17f=x17(neclfile);x18f=x18(neclfile);x19f=1;x20f=1;x21f=1;

kfint= interp1(x,kf,x1f,'linear');
dpint=interp1(x,dp,x2f,'linear');
kmint= interp1(x,km,x3f,'linear');
lamint= interp1(x,lam,x4f,'linear');
IFTint= interp1(x,IFT,x5f,'linear');
porosint= interp1(x,poros,x6f,'linear');
Sgrmint= interp1(x,Sgrm,x7f,'linear');
Swcmint= interp1(x,Swcm,x8f,'linear');
ngmint= interp1(x,ngm,x9f,'linear');
nwmint= interp1(x,nwm,x10f,'linear');
Kmaxgmint= interp1(x,Kmaxgm,x11f,'linear');
Kmaxwmint= interp1(x,Kmaxwm,x12f,'linear');
Sgrfint= interp1(x,Sgrf,x13f,'linear');
Swcfint= interp1(x,Swcf,x14f,'linear');
ngfint= interp1(x,ngf,x15f,'linear');
nwfint= interp1(x,nwf,x16f,'linear');
Kmaxgfint= interp1(x,Kmaxgf,x17f,'linear');
Kmaxwfint= interp1(x,Kmaxwf,x18f,'linear');
k1k2fint= interp1(x,k1k2,x19f,'linear');
kvkhfint= interp1(x,kvkh,x20f,'linear');
Ivfint=interp1(x,Iv,x21f,'linear');

writekxmE100Multilayer(porosint,porosf(1),kmint,kfint,k1k2fint,Ivfint,kvkhfint,NY,NX,NFG,fidd,fidd1);

krmfm1Multilayer(Sgrmint,Swcmint,ngmint,nwmint,Kmaxgmint,Kmaxwmint,kmint,k1k2fint,lamint,IFTint,Sgrfint,Swcfint,ngfint,nwfint,Kmaxgfint,Kmaxwfint,fidd2);

PRDRAWDOWN(dpint,pi,fidd3)

!runEclipseTUD.bat;
%read production time-second time
filenameRSM=inputfileRootp2(neclfile1,:);
% [para1ti parawit para3gpt
para4wpt]=eclreadRSMMultilayer(filenameRSM,timer,neclfile);
[para1ti paragpt1 paragpt2  parawpt1 parawpt2 parawit1
parawit2]=eclreadRSMMulti(filenameRSM,timer,neclfile);
productiont(1, neclfile)=para1ti(1,neclfile);
FGPTff(1, neclfile)=paragpt1(1,neclfile);
FWPTff(1, neclfile)=parawpt1(1,neclfile);
FWITff(1, neclfile)=parawit1(1,neclfile);

FGPTff2(1, neclfile)=paragpt2(1,neclfile);
FWPTff2(1, neclfile)=parawpt2(1,neclfile);
FWITff2(1, neclfile)=parawit2(1,neclfile);

productiont(2, neclfile)=para1ti(2,neclfile);
FGPTff(2, neclfile)=paragpt1(2,neclfile);
```

```
FWPTff(2, neclfile)=parawpt1(2,neclfile);

FGPTff2(2, neclfile)=paragpt2(2,neclfile);
FWPTff2(2, neclfile)=parawpt2(2,neclfile);

productiont(3, neclfile)=para1ti(3,neclfile);
FGPTff(3, neclfile)=paragpt1(3,neclfile);
FWPTff(3, neclfile)=parawpt1(3,neclfile);

FGPTff2(3, neclfile)=paragpt2(3,neclfile);
FWPTff2(3, neclfile)=parawpt2(3,neclfile);


productiont(4, neclfile)=para1ti(4,neclfile);
FGPTff(4, neclfile)=paragpt1(4,neclfile);
FWPTff(4, neclfile)=parawpt1(4,neclfile);

FGPTff2(4, neclfile)=paragpt2(4,neclfile);
FWPTff2(4, neclfile)=parawpt2(4,neclfile);

filenameRSM=inputfileRootcl(neclfile1,:);
% read RSM file-clean file
% [para1ti parawit para3gpt
para4wpt]=eclreadRSMMultilayer(filenameRSM,timer,neclfile);
[para1ti paragpt1 paragpt2  parawpt1 parawpt2 parawit1
parawit2]=eclreadRSMMulti(filenameRSM,timer,neclfile);

productiontc(1, neclfile)=para1ti(1,neclfile);
FGPTffc(1, neclfile)=paragpt1(1,neclfile);
FWPTffc(1, neclfile)=parawpt1(1,neclfile);
FWITffc(1, neclfile)=parawit1(1,neclfile);

FGPTff2c(1, neclfile)=paragpt2(1,neclfile);
FWPTff2c(1, neclfile)=parawpt2(1,neclfile);
FWITff2c(1, neclfile)=parawit2(1,neclfile);

productiontc(2, neclfile)=para1ti(2,neclfile);
FGPTffc(2, neclfile)=paragpt1(2,neclfile);
FWPTffc(2, neclfile)=parawpt1(2,neclfile);

FGPTff2c(2, neclfile)=paragpt2(2,neclfile);
FWPTff2c(2, neclfile)=parawpt2(2,neclfile);

productiontc(3, neclfile)=para1ti(3,neclfile);
FGPTffc(3, neclfile)=paragpt1(3,neclfile);
FWPTffc(3, neclfile)=parawpt1(3,neclfile);

FGPTff2c(3, neclfile)=paragpt2(3,neclfile);
FWPTff2c(3, neclfile)=parawpt2(3,neclfile);

productiontc(4, neclfile)=para1ti(4,neclfile);
FGPTffc(4, neclfile)=paragpt1(4,neclfile);
FWPTffc(4, neclfile)=parawpt1(4,neclfile);

FGPTff2c(4, neclfile)=paragpt2(4,neclfile);
FWPTff2c(4, neclfile)=parawpt2(4,neclfile);

% productiontc(4, neclfile)=para1ti(4,neclfile);
% FGPTffc(4, neclfile)=paragpt1(4,neclfile);
```

```
% FWPTffc(4, neclfile)=parawpt1(4,neclfile);
%
% FGPTff2c(4, neclfile)=paragpt2(4,neclfile);
% FWPTff2c(4, neclfile)=parawpt2(4,neclfile);
%
% productiontc(1, neclfile)=para1ti(1,neclfile);
% FGPTffc(1, neclfile)=para3gpt(1,neclfile);
%
% productiontc(2, neclfile)=para1ti(2,neclfile);
% FGPTffc(2, neclfile)=para3gpt(2,neclfile);
%
% productiontc(3, neclfile)=para1ti(3,neclfile);
% FGPTffc(3, neclfile)=para3gpt(3,neclfile);
%
% productiontc(4, neclfile)=para1ti(4,neclfile);
% FGPTffc(4, neclfile)=para3gpt(4,neclfile);

fprintf(fid1,'%3f %3f %3f %3f %3f %3f %3f %3f %3f %3f %3f %3f %3f %3f %3f
%3f %3f %3f %3f %3f %3f %3f %3f %3f %3f %3f %3f %3f %3f %3f\n',x0(neclfile),x1(neclfile), ...
x3(neclfile),x4(neclfile),x5(neclfile),x9(neclfile),x10(neclfile),x11(
neclfile) ...
,x12(neclfile),x15(neclfile),x16(neclfile),x17(neclfile),x18(neclfile)
...
,productiont(1, neclfile),FGPTff(1, neclfile),FWPTff(1,
neclfile),FWITff(1, neclfile),FGPTff2(1, neclfile),FWPTff2(1,
neclfile),FWITff2(1, neclfile), ...
productiontc(1, neclfile), FGPTffc(1, neclfile), FGPTff2c(1,
neclfile));
% fprintf(fid1,'\n');


fprintf(fid2,'%3f %3f %3f %3f %3f %3f %3f %3f %3f %3f %3f %3f %3f %3f %3f
%3f %3f %3f %3f %3f %3f %3f %3f %3f %3f %3f %3f %3f %3f %3f\n',x0(neclfile),x1(neclfile), ...
x3(neclfile),x4(neclfile),x5(neclfile),x9(neclfile),x10(neclfile),x11(
neclfile) ...
,x12(neclfile),x15(neclfile),x16(neclfile),x17(neclfile),x18(neclfile)
...
,productiont(2, neclfile),FGPTff(2, neclfile),FWPTff(2,
neclfile),FWITff(1, neclfile),FGPTff2(2, neclfile),FWPTff2(2,
neclfile),FWITff2(1, neclfile), ...
productiontc(2, neclfile), FGPTffc(2, neclfile), FGPTff2c(2,
neclfile));
% fprintf(fid2,'\n');


fprintf(fid3,'%3f %3f %3f %3f %3f %3f %3f %3f %3f %3f %3f %3f %3f %3f %3f
%3f %3f %3f %3f %3f %3f %3f %3f %3f %3f %3f %3f %3f %3f %3f\n',x0(neclfile),x1(neclfile), ...
x3(neclfile),x4(neclfile),x5(neclfile),x9(neclfile),x10(neclfile),x11(
neclfile) ...
,x12(neclfile),x15(neclfile),x16(neclfile),x17(neclfile),x18(neclfile)
...
,productiont(3, neclfile),FGPTff(3, neclfile),FWPTff(3,
neclfile),FWITff(1, neclfile),FGPTff2(3, neclfile),FWPTff2(3,
neclfile),FWITff2(1, neclfile), ...
productiontc(3, neclfile), FGPTffc(3, neclfile), FGPTff2c(3,
neclfile));
% fprintf(fid3,'\n');

fprintf(fid4,'%3f %3f %3f %3f %3f %3f %3f %3f %3f %3f %3f %3f %3f %3f %3f
%3f %3f %3f %3f %3f %3f %3f %3f %3f %3f %3f %3f %3f %3f %3f\n',x0(neclfile),x1(neclfile), ...
```

```
x3(neclfile),x4(neclfile),x5(neclfile),x9(neclfile),x10(neclfile),x11(
neclfile) ...
,x12(neclfile),x15(neclfile),x16(neclfile),x17(neclfile),x18(neclfile)
...
,productiont(4, neclfile),FGPTff(4, neclfile),FWPTff(4,
neclfile),FWITff(1, neclfile),FGPTff2(4, neclfile),FWPTff2(4,
neclfile),FWITff2(1, neclfile), ...
productiontc(4, neclfile), FGPTffc(4, neclfile), FGPTff2c(4,
neclfile));
% fprintf(fid4,'\n');

% !del 1PHASE_WF4MM_XF400M_BFT.RSM
% !del 1PHASE_WF4MM_XF400M_AFT.RSM
% !del 1PHASE_WF4MM_XF400M_CLEAN.RSM
% !del 1PHASE_WF4MM_XF400M_BFT.UNRST
% !del 1PHASE_WF4MM_XF400M_AFT.UNRST
% !del 1PHASE_WF4MM_XF400M_CLEAN.UNRST
% !del 1PHASE_WF4MM_XF400M_BFT.UNSMRY
% !del 1PHASE_WF4MM_XF400M_AFT.UNSMRY
% !del 1PHASE_WF4MM_XF400M_CLEAN.UNSMRY

end %neclfile
fclose(fid1);
fclose(fid2);
fclose(fid3);
fclose(fid4);
fclose(fidd);
fclose(fidd1);
fclose(fidd2);
fclose(fidd3);
% fclose(fidd4);
toc

end


function
ecloutputwriten(Cfd,Lf,wf,productiont,FGPTff,FWPTff,productiontc,FGPTf
fc,nif)
timer=[14 21 41 382];
if abs (productiontc-timer(1))<=0.001;
filenameoutputf='ECLIPSEoutcomes1.inc';end
if abs (productiontc-timer(2))<=0.001;
filenameoutputf='ECLIPSEoutcomes2.inc';end
if abs (productiontc-timer(3))<=0.001;
filenameoutputf='ECLIPSEoutcomes3.inc';end
if abs (productiontc-timer(4))<=0.001;
filenameoutputf='ECLIPSEoutcomes4.inc';end

fid=fopen(filenameoutputf, 'w');
for i=1:nif
if i==1;

fprintf(fid,'No.file,PRtime(days),GPT(MSCF),WPT(STB),PRtime_Cl(days),G
PT_Cl(MSCF),Cfd,Lf(m),wf(mm)\n');
end
fprintf(fid,'%3f %3f %5f %3f %3f %3f %3f %3f %3f %3f %3f %3f
%3f\n',i,productiont(i),FGPTff(i),FWPTff(i),productiontc(i),FGPTffc(i)
,Cfd,Lf,wf);
fprintf(fid,'\n');
end
```

```
fclose(fid);

end



function [para1ti paragpt1 paragpt2  parawpt1 parawpt2 parawit1
parawit2]=eclreadRSMMulti(filenameRSM, restarttime,nfileff)
% global Timerpt
% global FWITrpt
% global FGPTrpt
% global FWPTrpt

% filenameRSM1='1phase_wf5mm_xf417m_Cfd_1_p1_f_n1';

filenameRSM=[filenameRSM,'.RSM'];

fid = fopen(filenameRSM,'r');
flag = 0;
p=1;
NOTimestep=9100;
%statment = '';
%keywords = '';
para1 = [0.0];
para2 = [0.0];
para3 = [0.0];
para4 = [0.0];
para5 = [0.0];
para6 = [0.0];
para7 = [0.0];
para8 = [0.0];
para9 = [0.0];
para10 = [0.0];
if fid ==-1;

    para1ti(1:4,nfileff)=para1(1);
    paragpt1(1:4,nfileff)=para3(1);
    paragpt2(1:4,nfileff)=para4(1);
    parawpt1(1:4,nfileff)=para5(1);
    parawpt2(1:4,nfileff)=para6(1);
    parawit1(1:4,nfileff)=para7(1);
    parawit2(1:4,nfileff)=para8(1);
else
while 1 && p<5
    tline = fgetl(fid);
    flag = flag +1;
    %%%% read the correct line
    if(flag > NOTimestep) ;

       [para1(flag-6) para2(flag-6) para3(flag-6) para4(flag-6)
para5(flag-6) para6(flag-6) para7(flag-6) para8(flag-6) para9(flag-6)]
= strread(tline, '%f %f %f %f %f %f %f %f %f');
%  if p==1;
%        if abs (para1((flag-6))-((restarttime-
10)*0.041667+2))<=0.05;break;end
%
%  else
    if abs (para1((flag-6))-restarttime(p))<=0.05;
    para1ti(p,nfileff)=para1((flag-6));
    paragpt1(p,nfileff)=para3((flag-6));
    paragpt2(p,nfileff)=para4((flag-6));
```

```
    parawpt1(p,nfileff)=para5((flag-6));
    parawpt2(p,nfileff)=para6((flag-6));
    parawit1(p,nfileff)=para7((flag-6));
    parawit2(p,nfileff)=para8((flag-6));

    if p==1;
    NOTimestep=NOTimestep+420;
    end
    if p==2;
    NOTimestep=NOTimestep+746;
    end
    if p==3;
    NOTimestep=NOTimestep+15;
    end
    p=p+1;

        end
%  end
    end

    if ~ischar(tline), break, end
%      disp(tline);
    tline = '';
end
fclose(fid);


end
end


function
krmfm1Multilayer(Sgrm,Swcm,ngm,nwm,Kmaxgm,Kmaxwm,Km,k1k2,lam,IFT,Sgrf,
Swcf,ngf,nwf,Kmaxgf,Kmaxwf,fid);
% fid=fopen('krm.INC','w');
frewind(fid);
fprintf(fid,'SGWFN \n');

for k=1:1

% if k==2;Km=Km/k1k2;end

iSg=Sgrm+0.001;
i=1;

while  (1-Swcm-iSg)>0

Swt(i)=1-iSg;
Sgt(i)=iSg;
krmgt(i)= Kmaxgm*((Sgt(i)- Sgrm)/(1- Swcm- Sgrm))^ngm;
krmwt(i)=Kmaxwm*((Swt(i)- Swcm)/(1- Swcm- Sgrm))^nwm;
Pd(i)=0.0075*IFT*Km^(-0.5);
Pc(i)=Pd(i)/((Swt(i)-Swcm)/(1-Swcm))^(1/lam)*14.5038;

if i==1;
fprintf(fid,'%6.3f %6.3f %6.3f %6.3f\n',0,0,1.0,Pc(i));
else
fprintf(fid,'%6.3f %6.3f %6.3f
%6.3f\n',Sgt(i),krmgt(i),krmwt(i),Pc(i));
end
```

```
i=i+1;
iSg=iSg+(1-Swcm-Sgrm)/5;
end
numcol=i;

fprintf(fid,'%6.3f %6.3f %6.3f %6.3f\n',0.85,1.0,0,Pc(i-1));
fprintf(fid,'%6.3f %6.3f %6.3f %6.3f\n',1.0,1.0,0,Pc(i-1));
fprintf(fid,'/ \n');

end

iSg=Sgrf+0.001;
i=1;
while  (1-Swcf-iSg)>0
Swt(i)=1-iSg;
Sgt(i)=iSg;
krmgt(i)= Kmaxgf*((Sgt(i)- Sgrf)/(1- Swcf- Sgrf))^ngf;
krmwt(i)=Kmaxwf*((Swt(i)- Swcf)/(1- Swcf- Sgrf))^nwf;
% Pd(i)=0.0075*IFT*Km^(-0.5);
Pc(i)=0;

if i==1;
fprintf(fid,'%6.3f %6.3f %6.3f %6.3f\n',0,0,1.0,Pc(i));
else
fprintf(fid,'%6.3f %6.3f %6.3f
%6.3f\n',Sgt(i),krmgt(i),krmwt(i),Pc(i));
end

i=i+1;
iSg=iSg+(1-Swcf-Sgrf)/5;
end

fprintf(fid,'%6.3f %6.3f %6.3f %6.3f\n',0.85,1.0,0,Pc(i-1));
fprintf(fid,'%6.3f %6.3f %6.3f %6.3f\n',1.0,1.0,0,Pc(i-1));
fprintf(fid,'/ \n');

% fclose(fid);
end


function PRDRAWDOWN(dp,pi,fiddd)
% fiddd=fopen('WCONPROD.INC','w');
frewind(fiddd);
fprintf(fiddd,'WCONPROD \n');
BHP=pi-dp;
fprintf(fiddd,'PROD1 OPEN BHP %3.0f* %3.2f/ \n',5,BHP);
fprintf(fiddd,'/ \n');

end


function writekxmE100Multilayer(poros,porosf,km,kf,k1k2,Iv,
NY,NX,NFG,fid,fid1)

kmd=km;
kfd=kf;
frewind(fid);
frewind(fid1);
% fid=fopen('PREMX.INC','w');
```

```
% fid1=fopen('PORO.INC','w');
fprintf(fid,'PERMX \n');
fprintf(fid1,'PORO \n');

for k=1:2

if k==2; kmd=km/k1k2 ;end
if k==2; kfd=kfd*Iv ;end
for i=1:NY
    for j=1:NX
        if i==1 & j<=NFG
fprintf(fid,'%6.0f \n',kfd);
fprintf(fid1,'%6.2f \n',porosf);
Km2(j,i)=kfd;
        else
fprintf(fid,'%6.4f \n',kmd);
fprintf(fid1,'%6.2f \n',poros);
Km2(j,i)=kmd;
    end
    end
end
end
fprintf(fid,'/ \n');
fprintf(fid1,'/ \n');

end
```

7.2 The developed MATLAB code to generate saturation maps for SFVW-Sets

```
% function createfigure(ZData1, YData1, XData1, CData1)
%CREATEFIGURE(ZDATA1,YDATA1,XDATA1,CDATA1)
%  ZDATA1:  surface zdata
%  YDATA1:  surface ydata
%  XDATA1:  surface xdata
%  CDATA1:  surface cdata

%  Auto-generated by MATLAB on 07-Feb-2013 16:10:10

% Create figure
figure1 = figure('Colormap',...
    [1 0.694117665290833 0.39215686917305;0.984811723232269
0.691316545009613 0.398319333791733;0.969623386859894
0.688515424728394 0.404481798410416;0.954435110092163
0.685714304447174 0.410644263029099;0.939246833324432
0.682913184165955 0.416806727647781;0.924058496952057
0.680112063884735 0.422969192266464;0.908870220184326
0.677310943603516 0.429131656885147;0.893681943416595
0.674509823322296 0.43529412150383;0.87849360704422 0.671708703041077
0.441456586122513;0.863305330276489 0.668907582759857
0.447619050741196;0.848117053508759 0.666106462478638
0.453781515359879;0.832928717136383 0.663305342197418
0.459943979978561;0.817740440368652 0.660504221916199
0.466106444597244;0.802552103996277 0.657703101634979
0.472268909215927;0.787363827228546 0.65490198135376
0.47843137383461;0.772175550460815 0.65210086107254
0.484593838453293;0.75698721408844 0.649299740791321
0.490756303071976;0.741798937320709 0.646498620510101
0.496918767690659;0.726610660552979 0.643697500228882
0.503081262111664;0.711422324180603 0.640896379947662
0.509243726730347;0.696234047412872 0.638095259666443
0.51540619134903;0.681045770645142 0.635294139385223
0.521568655967712;0.665857434272766 0.632493019104004
0.527731120586395;0.650669157505035 0.629691898822784
0.533893585205078;0.635480880737305 0.626890778541565
0.540056049823761;0.620292544364929 0.624089658260345
0.546218514442444;0.605104267597198 0.621288537979126
0.552380979061127;0.589915990829468 0.618487417697906
0.55854344367981;0.574727654457092 0.615686297416687
0.564705908298492;0.559539377689362 0.612885177135468
0.570868372917175;0.544351100921631 0.610084056854248
0.577030837535858;0.529162764549255 0.607282936573029
0.583193302154541;0.513974487781525 0.604481816291809
0.589355766773224;0.498786181211472 0.60168069601059
0.595518231391907;0.483597874641418 0.59887957572937
0.60168069601059;0.468409597873688 0.596078455448151
0.607843160629272;0.453221291303635 0.593277335166931
0.614005625247955;0.438032984733582 0.590476214885712
0.620168089866638;0.422844707965851 0.587675094604492
0.626330554485321;0.407656401395798 0.584873974323273
0.632493019104004;0.392468094825745 0.582072854042053
0.638655483722687;0.377279788255692 0.579271733760834
0.64481794834137;0.362091511487961 0.576470613479614
0.650980412960052;0.346903204917908 0.573669493198395
0.657142877578735;0.331714898347855 0.570868372917175
0.663305342197418;0.316526621580124 0.568067252635956
0.669467806816101;0.301338315010071 0.565266132354736
0.675630271434784;0.286150008440018 0.562465012073517
0.681792736053467;0.270961731672287 0.559663891792297
0.68795520067215;0.255773425102234 0.556862771511078
```

```
0.694117665290833;0.240585118532181 0.554061651229858
0.700280129909515;0.225396826863289 0.551260530948639
0.706442594528198;0.210208535194397 0.548459410667419
0.712605059146881;0.195020228624344 0.5456582903862
0.718767523765564;0.179831936955452 0.54285717010498
0.724929988384247;0.164643630385399 0.540056049823761
0.73109245300293;0.149455338716507 0.537254929542542
0.737254917621613;0.134267047047615 0.534453809261322
0.743417382240295;0.119078740477562 0.531652688980103
0.749579846858978;0.10389044880867 0.528851568698883
0.755742311477661;0.0887021496891975 0.526050448417664
0.761904776096344;0.073513850569725 0.523249328136444
0.768067240715027;0.0583255551755428 0.520448207855225
0.77422970533371;0.0431372560560703 0.517647087574005
0.780392169952393]);

% Create axes
axes1 = axes('Parent',figure1,...

'YTickLabel',{'','0.002','0.006','0.014','0.03','0.062','0.126','0.254
','0.51','1.022','2.046','4.094','8.19','16.382','32.766'},...
    'YTick',[1 2 3 4 5 6 7 8 9 10 11 12 13 14 15],...

'XTickLabel',{'','0.61','1.83','4.27','9.14','18.9','57','133.2','267.
01','343.21','381.31','391.06','395.94','398.37','399.4','400','400.81
','402.03','404.47','409.35'},...
    'XTick',[1 2 3 4 5 6 7 8 9 10 11 12 13 14 15 16 17 18 19 20],...
    'CLim',[0 1]);
% Uncomment the following line to preserve the X-limits of the axes
xlim(axes1,[1 20]);
% Uncomment the following line to preserve the Y-limits of the axes
ylim(axes1,[1 15]);
box(axes1,'on');
hold(axes1,'all');

% Create xlabel
xlabel('X, Meters');

% Create ylabel
ylabel('Y, Meters');

% Create title
title('The worst case saturation map for');

% % Create surface
%
surface('Parent',axes1,'ZData',ZData1,'YData',YData1,'XData',XData1,..
.
%     'CData',CData1);

% Create colorbar
colorbar('peer',axes1);
pcolor (unnamed)
```

7.3 The developed MATLAB code for MFHWs

```
function CleanupEfficiencyMFHWMehrzad

clear
clc
tic
xlswrite('Results.xlsx',{'Run_No', 'Kf', 'Km', 'Lam', 'IFT', 'ngm',
'nwm', 'Kmaxgm', 'Kmaxwm', 'ngf', 'nwf', 'Kmaxgf', 'Kmaxwf',
'PRtime(days)', 'FGPT(MSCF)', 'FWPT(STB)', 'FWIT(STB)',
'FGPR(MSCF/DAY)', 'FWIR(STB/DAY)', 'FPR(PSIA)', 'PRtime_Cl(days)',
'FGPT_CL(MSCF)', 'FGPR_CL(MSCF/DAY)', 'FPR_CL(PSIA)'} ,'10 days','a1')
xlswrite('Results.xlsx',{'Run_No', 'Kf', 'Km', 'Lam', 'IFT', 'ngm',
'nwm', 'Kmaxgm', 'Kmaxwm', 'ngf', 'nwf', 'Kmaxgf', 'Kmaxwf',
'PRtime(days)', 'FGPT(MSCF)', 'FWPT(STB)', 'FWIT(STB)',
'FGPR(MSCF/DAY)', 'FWIR(STB/DAY)', 'FPR(PSIA)', 'PRtime_Cl(days)',
'FGPT_CL(MSCF)', 'FGPR_CL(MSCF/DAY)', 'FPR_CL(PSIA)'} ,'30 days','a1')
xlswrite('Results.xlsx',{'Run_No', 'Kf', 'Km', 'Lam', 'IFT', 'ngm',
'nwm', 'Kmaxgm', 'Kmaxwm', 'ngf', 'nwf', 'Kmaxgf', 'Kmaxwf',
'PRtime(days)', 'FGPT(MSCF)', 'FWPT(STB)', 'FWIT(STB)',
'FGPR(MSCF/DAY)', 'FWIR(STB/DAY)', 'FPR(PSIA)', 'PRtime_Cl(days)',
'FGPT_CL(MSCF)', 'FGPR_CL(MSCF/DAY)', 'FPR_CL(PSIA)'} ,'180
days','a1')
xlswrite('Results.xlsx',{'Run_No', 'Kf', 'Km', 'Lam', 'IFT', 'ngm',
'nwm', 'Kmaxgm', 'Kmaxwm', 'ngf', 'nwf', 'Kmaxgf', 'Kmaxwf',
'PRtime(days)', 'FGPT(MSCF)', 'FWPT(STB)', 'FWIT(STB)',
'FGPR(MSCF/DAY)', 'FWIR(STB/DAY)', 'FPR(PSIA)', 'PRtime_Cl(days)',
'FGPT_CL(MSCF)', 'FGPR_CL(MSCF/DAY)', 'FPR_CL(PSIA)'} ,'370
days','a1')

first_Run_No=577;
last_Run_No=1000;%2^12

% Model Dimensions used in PERMX generation
NY=[21];
NX=[21];

% fracture permeability(mD), X1, Y
kf=[1000 (1000+30000)/2 30000];
%pressure drawdown (psi),X2,N
dp=[1000 (1000+1000)/2 1000];
% matrix permeability,X3,Y
km=[0.001 (0.001+0.1)/2 0.1];
%pore size disturbution,X4, Y
lam=[1 (1+4)/2 4];
%matrix interfacial tension,X5, Y
IFT=[2 (2+50)/2 50];
%porosity,X6,N
poros=[0.15 (0.15+0.15)/2 0.15];
%Sgr matrix,X7,N
Sgrm=[0.1 (0.1+0.1)/2 0.1];
%Swr matrix,X8,N
Swcm=[0.15 (0.15+0.15)/2 0.15];
%core exponent krg,X9, Y
ngm=[1.5 (1.5+5)/2 5];
%core exponent krw,X10, Y
nwm=[1.2 (1.2+4)/2 4];
%endpoint krg,X11, Y
Kmaxgm=[0.5 (0.5+1.0)/2 1.0];
%endpoint krw,X12, Y
Kmaxwm=[0.05 (0.05+0.6)/2 0.6];
```

```
%Sgr fracture,X13,N
Sgrf=[0.1 (0.1+0.1)/2 0.1];%
%Swr fracture,X14,N
Swcf=[0.15 (0.15+0.15)/2 0.15];
%core exponent krg fracture,X15,Y
ngf=[1.5 (1.5+5)/2 5];
%core exponent krw fracture,X16,Y
nwf=[1.2 (1.2+4)/2 4];
%endpoint krg fracture,X17, Y
Kmaxgf=[0.5 (0.5+1.0)/2 1.0];
%endpoint krw fracture,X18, Y
Kmaxwf=[0.10 (0.1+0.75)/2 0.75];
pi=7500;
% fracture porosity
porosf=[0.35 (0.35+0.35)/2 0.35];
%k1/k2 ,x19
k1k2=[1    (1+1)/2     1];
%kvkh,x20
kvkh=[1    (1+1)/2     1];
%Cf variation vertical, x21
Iv=[1 (1+1)/2     1];

% for interpolating data
x=[0 0.5 1];

load('fullfactorialdesign1.mat');
x0=dCC(:,1);x1=dCC(:,2);x3=dCC(:,3);x4=dCC(:,4);x5=dCC(:,5);x9=dCC(:,6
);x10=dCC(:,7);x11=dCC(:,8);x12=dCC(:,9);
x15=dCC(:,10);x16=dCC(:,11);x17=dCC(:,12);x18=dCC(:,13);

kxfile=fopen('PREMX.INC','w+');
poro_file=fopen('PORO.INC','w+');
krm_file=fopen('krm.INC','w');
WCONPROD_file=fopen('WCONPROD.INC','w');
REFINE_file=fopen('PREMX-PORO-REF.INC','w');


for Run_No=first_Run_No:last_Run_No
Run_No
x1f=x1(Run_No);x2f=0.5;x3f=x3(Run_No);x4f=x4(Run_No);x5f=x5(Run_No);x6
f=0.5;x7f=0.5;x8f=0;
x9f=x9(Run_No);x10f=x10(Run_No);x11f=x11(Run_No);x12f=x12(Run_No);x13f
=0.5;x14f=0;x15f=x15(Run_No);
x16f=x16(Run_No);x17f=x17(Run_No);x18f=x18(Run_No);x19f=1;x20f=1;x21f=
1;

kfint= interp1(x,kf,x1f,'linear');
dpint=interp1(x,dp,x2f,'linear');
kmint= interp1(x,km,x3f,'linear');
lamint= interp1(x,lam,x4f,'linear');
IFTint= interp1(x,IFT,x5f,'linear');
porosint= interp1(x,poros,x6f,'linear');
Sgrmint= interp1(x,Sgrm,x7f,'linear');
Swcmint= interp1(x,Swcm,x8f,'linear');
ngmint= interp1(x,ngm,x9f,'linear');
nwmint= interp1(x,nwm,x10f,'linear');
Kmaxgmint= interp1(x,Kmaxgm,x11f,'linear');
Kmaxwmint= interp1(x,Kmaxwm,x12f,'linear');
Sgrfint= interp1(x,Sgrf,x13f,'linear');
Swcfint= interp1(x,Swcf,x14f,'linear');
ngfint= interp1(x,ngf,x15f,'linear');
```

```
nwfint= interp1(x,nwf,x16f,'linear');
Kmaxgfint= interp1(x,Kmaxgf,x17f,'linear');
Kmaxwfint= interp1(x,Kmaxwf,x18f,'linear');
k1k2fint= interp1(x,k1k2,x19f,'linear');
kvkhfint= interp1(x,kvkh,x20f,'linear');
Ivfint=interp1(x,Iv,x21f,'linear');

writekxm(porosint,porosf(1),kmint,kfint,k1k2fint,Ivfint,kvkhfint,NY,NX
,kxfile,poro_file);

writekrm_krf(Sgrmint,Swcmint,ngmint,nwmint,Kmaxgmint,Kmaxwmint,kmint,k
1k2fint,lamint,IFTint,Sgrfint,Swcfint,ngfint,nwfint,Kmaxgfint,Kmaxwfin
t,krm_file);

PRDRAWDOWN(dpint,pi,WCONPROD_file);

refinementproperties(porosint,porosf(1),kmint,kfint,k1k2fint,Ivfint,kv
khfint,NY,NX,REFINE_file);

!runEclipseTUD.bat;
Results=importdata('MFHW.RSM');
Results_clean=importdata('MFHWClean.RSM');

% Report time RSM file for Soaking time ST=2 days, prod times
are:[13.62165 34.43728 181.4373 371.4373]and these production times
are equivalent to these Tsteps: 9109, 9544,10289, 10308
%for Soaking time ST=20 days prod times are:[31.6218 52.43742 199.4374
389.4373] and these production times are equivalent to these
Tsteps(540 in addition to number of tsteps for ST=2)
%i.e. 9643, 10084, 10829, 10848

Eout1=[Run_No, x1f, x3f, x4f, x5f, x9f, x10f, x11f, x12f, x15f, x16f,
x17f, x18f, Results.data(9109,2), Results.data(9109,4:9),
Results_clean.data(9109,2), Results_clean.data(9109,4),
Results_clean.data(9109,7), Results_clean.data(9109,9)];
Eout2=[Run_No, x1f, x3f, x4f, x5f, x9f, x10f, x11f, x12f, x15f, x16f,
x17f, x18f, Results.data(9544,2), Results.data(9544,4:9),
Results_clean.data(9544,2), Results_clean.data(9544,4),
Results_clean.data(9544,7), Results_clean.data(9544,9)];
Eout3=[Run_No, x1f, x3f, x4f, x5f, x9f, x10f, x11f, x12f, x15f, x16f,
x17f, x18f, Results.data(10289,2), Results.data(10289,4:9),
Results_clean.data(10289,2), Results_clean.data(10289,4),
Results_clean.data(10289,7), Results_clean.data(10289,9)];
Eout4=[Run_No, x1f, x3f, x4f, x5f, x9f, x10f, x11f, x12f, x15f, x16f,
x17f, x18f, Results.data(10308,2), Results.data(10308,4:9),
Results_clean.data(10308,2), Results_clean.data(10308,4),
Results_clean.data(10308,7), Results_clean.data(10308,9)];

my_cell = sprintf( 'a%s',num2str(1+Run_No) );
xlswrite('Results.xlsx',Eout1,'10 days',my_cell)
xlswrite('Results.xlsx',Eout2,'30 days',my_cell)
xlswrite('Results.xlsx',Eout3,'180 days',my_cell)
xlswrite('Results.xlsx',Eout4,'370 days',my_cell)

end %Run_No
toc
end
```

```
function
refinementproperties(poros,porosf,km,kf,k1k2,Iv,kvkh,NY,NX,REFINE_file
)

kmd=km;
kfd=kf;

frewind(REFINE_file);


fprintf(REFINE_file,'REFINE\r\n');
fprintf(REFINE_file,'REF1  / \r\n');
fprintf(REFINE_file,'EQUALS\r\n');
fprintf(REFINE_file,'PERMX %6.4f 6 32 15 15 1 1 /\r\n',kfd);
fprintf(REFINE_file,'PORO %6.4f 6 32 15 15 1 1 /\r\n',porosf);
fprintf(REFINE_file,'/\r\n');
fprintf(REFINE_file,'COPY \r\n');
fprintf(REFINE_file,'PERMX PERMY /\r\n');
fprintf(REFINE_file,'PERMX PERMZ /\r\n');
fprintf(REFINE_file,'/\r\n');
fprintf(REFINE_file,'ENDFIN\r\n');

fprintf(REFINE_file,'REFINE\r\n');
fprintf(REFINE_file,'REF2  / \r\n');
fprintf(REFINE_file,'EQUALS\r\n');
fprintf(REFINE_file,'PERMX %6.4f 6 32 15 15 1 1 /\r\n',kfd);
fprintf(REFINE_file,'PORO %6.4f 6 32 15 15 1 1 /\r\n',porosf);
fprintf(REFINE_file,'/\r\n');
fprintf(REFINE_file,'COPY \r\n');
fprintf(REFINE_file,'PERMX PERMY /\r\n');
fprintf(REFINE_file,'PERMX PERMZ /\r\n');
fprintf(REFINE_file,'/\r\n');
fprintf(REFINE_file,'ENDFIN\r\n');

fprintf(REFINE_file,'REFINE\r\n');
fprintf(REFINE_file,'REF3  / \r\n');
fprintf(REFINE_file,'EQUALS\r\n');
fprintf(REFINE_file,'PERMX %6.4f 6 32 15 15 1 1 /\r\n',kfd);
fprintf(REFINE_file,'PORO %6.4f 6 32 15 15 1 1 /\r\n',porosf);
fprintf(REFINE_file,'/\r\n');
fprintf(REFINE_file,'COPY \r\n');
fprintf(REFINE_file,'PERMX PERMY /\r\n');
fprintf(REFINE_file,'PERMX PERMZ /\r\n');
fprintf(REFINE_file,'/\r\n');
fprintf(REFINE_file,'ENDFIN\r\n');

fprintf(REFINE_file,'REFINE\r\n');
fprintf(REFINE_file,'REF4  / \r\n');
fprintf(REFINE_file,'EQUALS\r\n');
fprintf(REFINE_file,'PERMX %6.4f 6 32 15 15 1 1 /\r\n',kfd);
fprintf(REFINE_file,'PORO %6.4f 6 32 15 15 1 1 /\r\n',porosf);
fprintf(REFINE_file,'/\r\n');
fprintf(REFINE_file,'COPY \r\n');
fprintf(REFINE_file,'PERMX PERMY /\r\n');
fprintf(REFINE_file,'PERMX PERMZ /\r\n');
fprintf(REFINE_file,'/\r\n');
fprintf(REFINE_file,'ENDFIN\r\n');

fprintf(REFINE_file,'REFINE\r\n');
fprintf(REFINE_file,'REF5  / \r\n');
fprintf(REFINE_file,'EQUALS\r\n');
```

```
fprintf(REFINE_file,'PERMX %6.4f 6 32 15 15 1 1 /\r\n',kfd);
fprintf(REFINE_file,'PORO %6.4f 6 32 15 15 1 1 /\r\n',porosf);
fprintf(REFINE_file,'/\r\n');
fprintf(REFINE_file,'COPY \r\n');
fprintf(REFINE_file,'PERMX PERMY /\r\n');
fprintf(REFINE_file,'PERMX PERMZ /\r\n');
fprintf(REFINE_file,'/\r\n');
fprintf(REFINE_file,'ENDFIN\r\n');

fprintf(REFINE_file,'REFINE\r\n');
fprintf(REFINE_file,'REF6  / \r\n');
fprintf(REFINE_file,'EQUALS\r\n');
fprintf(REFINE_file,'PERMX %6.4f 6 32 15 15 1 1 /\r\n',kfd);
fprintf(REFINE_file,'PORO %6.4f 6 32 15 15 1 1 /\r\n',porosf);
fprintf(REFINE_file,'/\r\n');
fprintf(REFINE_file,'COPY \r\n');
fprintf(REFINE_file,'PERMX PERMY /\r\n');
fprintf(REFINE_file,'PERMX PERMZ /\r\n');
fprintf(REFINE_file,'/\r\n');
fprintf(REFINE_file,'ENDFIN\r\n');

fprintf(REFINE_file,'REFINE\r\n');
fprintf(REFINE_file,'REF7  / \r\n');
fprintf(REFINE_file,'EQUALS\r\n');
fprintf(REFINE_file,'PERMX %6.4f 6 32 15 15 1 1 /\r\n',kfd);
fprintf(REFINE_file,'PORO %6.4f 6 32 15 15 1 1 /\r\n',porosf);
fprintf(REFINE_file,'/\r\n');
fprintf(REFINE_file,'COPY \r\n');
fprintf(REFINE_file,'PERMX PERMY /\r\n');
fprintf(REFINE_file,'PERMX PERMZ /\r\n');
fprintf(REFINE_file,'/\r\n');
fprintf(REFINE_file,'ENDFIN\r\n');

end



function
writekrm_krf(Sgrm,Swcm,ngm,nwm,Kmaxgm,Kmaxwm,Km,k1k2,lam,IFT,Sgrf,Swcf
,ngf,nwf,Kmaxgf,Kmaxwf,krm_file);
% krm_file=fopen('krm.INC','w');
frewind(krm_file);
fprintf(krm_file,'SGWFN \r\n');

for k=1:1

% if k==2;Km=Km/k1k2;end

iSg=Sgrm+0.001;
i=1;

while  (1-Swcm-iSg)>0

Swt(i)=1-iSg;
Sgt(i)=iSg;
krmgt(i)= Kmaxgm*((Sgt(i)- Sgrm)/(1- Swcm- Sgrm))^ngm;
krmwt(i)=Kmaxwm*((Swt(i)- Swcm)/(1- Swcm- Sgrm))^nwm;
Pd(i)=0.0075*IFT*Km^(-0.5);
Pc(i)=Pd(i)/((Swt(i)-Swcm)/(1-Swcm))^(1/lam)*14.5038;

if i==1;
```

```
fprintf(krm_file,'%6.3f %6.3f %6.3f %6.3f\r\n',0,0,1.0,Pc(i));
else
fprintf(krm_file,'%6.3f %6.3f %6.3f
%6.3f\r\n',Sgt(i),krmgt(i),krmwt(i),Pc(i));
end

i=i+1;
iSg=iSg+(1-Swcm-Sgrm)/5;
end
numcol=i;

fprintf(krm_file,'%6.3f %6.3f %6.3f %6.3f\r\n',0.85,1.0,0,Pc(i-1));
fprintf(krm_file,'%6.3f %6.3f %6.3f %6.3f\r\n',1.0,1.0,0,Pc(i-1));
fprintf(krm_file,'/ \r\n');

end

iSg=Sgrf+0.001;
i=1;
while  (1-Swcf-iSg)>0
Swt(i)=1-iSg;
Sgt(i)=iSg;
krmgt(i)= Kmaxgf*((Sgt(i)- Sgrf)/(1- Swcf- Sgrf))^ngf;
krmwt(i)=Kmaxwf*((Swt(i)- Swcf)/(1- Swcf- Sgrf))^nwf;
% Pd(i)=0.0075*IFT*Km^(-0.5);
Pc(i)=0;

if i==1;
fprintf(krm_file,'%6.3f %6.3f %6.3f %6.3f\r\n',0,0,1.0,Pc(i));
else
fprintf(krm_file,'%6.3f %6.3f %6.3f
%6.3f\r\n',Sgt(i),krmgt(i),krmwt(i),Pc(i));
end

i=i+1;
iSg=iSg+(1-Swcf-Sgrf)/5;
end

fprintf(krm_file,'%6.3f %6.3f %6.3f %6.3f\r\n',0.85,1.0,0,Pc(i-1));
fprintf(krm_file,'%6.3f %6.3f %6.3f %6.3f\r\n',1.0,1.0,0,Pc(i-1));
fprintf(krm_file,'/ \r\n');

% fclose(krm_file);
end
```

7.4 The developed Python code for MFHWs

```
def KmMaker(km):
    NY=21
    NX=21

    # kf=1000
    # km=0.001
    # lam=1
    # IFT=50
    # ngm=3
    # nwm=3
    # Kmaxgm=0.9
    # Kmaxwm=1
    # ngf=2
    # nwf=2
    # Kmaxgf=1
    # Kmaxwf=1

    # poros=0.15
    # porosf=0.35
    PERMX=open('C:\Mehrzad MEPO MFHW Nf7 L600m Base Reference
Set\source\PERMX.INC','w')
    PERMX.write('PERMX \n')
    for k in range (1,2,1):
        for i in range (1,NY+1,1):
            for j in range (1,NX+1,1):
                PERMX.write(''+str(km)+' \n')
    PERMX.write('/ \n')
    PERMX.close()
    try:
        f3 = open('C:\Mehrzad MEPO MFHW Nf7 L600m Base Reference
Set\source\PERMX.INC', "r")
        try:
            # Read the entire contents of a file at once.
            string3 = f3.read()
        finally:
            f3.close()
    except IOError:
        pass
    return string3



def RefineMaker(kf):
    porosf=0.35

    PERMX_PORO_REF=open('C:\Mehrzad MEPO MFHW Nf7 L600m Base Reference
Set\source\PERMX_PORO_REF.INC','w')

    PERMX_PORO_REF.write('REFINE\n')
    PERMX_PORO_REF.write('REF1  / \n')
    PERMX_PORO_REF.write('EQUALS\n')
    PERMX_PORO_REF.write('PERMX '+str(kf)+' 6 32 15 15 1 1 /\n')
    PERMX_PORO_REF.write('PORO '+str(porosf)+' 6 32 15 15 1 1 /\n')
    PERMX_PORO_REF.write('/\n')
    PERMX_PORO_REF.write('COPY \n')
    PERMX_PORO_REF.write('PERMX PERMY /\n')
    PERMX_PORO_REF.write('PERMX PERMZ /\n')
    PERMX_PORO_REF.write('/\n')
```

```
PERMX_PORO_REF.write('ENDFIN\n')

PERMX_PORO_REF.write('REFINE\n')
PERMX_PORO_REF.write('REF2  / \n')
PERMX_PORO_REF.write('EQUALS\n')
PERMX_PORO_REF.write('PERMX '+str(kf)+' 6 32 15 15 1 1 /\n')
PERMX_PORO_REF.write('PORO '+str(porosf)+' 6 32 15 15 1 1 /\n')
PERMX_PORO_REF.write('/\n')
PERMX_PORO_REF.write('COPY \n')
PERMX_PORO_REF.write('PERMX PERMY /\n')
PERMX_PORO_REF.write('PERMX PERMZ /\n')
PERMX_PORO_REF.write('/\n')
PERMX_PORO_REF.write('ENDFIN\n')

PERMX_PORO_REF.write('REFINE\n')
PERMX_PORO_REF.write('REF3  / \n')
PERMX_PORO_REF.write('EQUALS\n')
PERMX_PORO_REF.write('PERMX '+str(kf)+' 6 32 15 15 1 1 /\n')
PERMX_PORO_REF.write('PORO '+str(porosf)+' 6 32 15 15 1 1 /\n')
PERMX_PORO_REF.write('/\n')
PERMX_PORO_REF.write('COPY \n')
PERMX_PORO_REF.write('PERMX PERMY /\n')
PERMX_PORO_REF.write('PERMX PERMZ /\n')
PERMX_PORO_REF.write('/\n')
PERMX_PORO_REF.write('ENDFIN\n')

PERMX_PORO_REF.write('REFINE\n')
PERMX_PORO_REF.write('REF4  / \n')
PERMX_PORO_REF.write('EQUALS\n')
PERMX_PORO_REF.write('PERMX '+str(kf)+' 6 32 15 15 1 1 /\n')
PERMX_PORO_REF.write('PORO '+str(porosf)+' 6 32 15 15 1 1 /\n')
PERMX_PORO_REF.write('/\n')
PERMX_PORO_REF.write('COPY \n')
PERMX_PORO_REF.write('PERMX PERMY /\n')
PERMX_PORO_REF.write('PERMX PERMZ /\n')
PERMX_PORO_REF.write('/\n')
PERMX_PORO_REF.write('ENDFIN\n')

PERMX_PORO_REF.write('REFINE\n')
PERMX_PORO_REF.write('REF5  / \n')
PERMX_PORO_REF.write('EQUALS\n')
PERMX_PORO_REF.write('PERMX '+str(kf)+' 6 32 15 15 1 1 /\n')
PERMX_PORO_REF.write('PORO '+str(porosf)+' 6 32 15 15 1 1 /\n')
PERMX_PORO_REF.write('/\n')
PERMX_PORO_REF.write('COPY \n')
PERMX_PORO_REF.write('PERMX PERMY /\n')
PERMX_PORO_REF.write('PERMX PERMZ /\n')
PERMX_PORO_REF.write('/\n')
PERMX_PORO_REF.write('ENDFIN\n')

PERMX_PORO_REF.write('REFINE\n')
PERMX_PORO_REF.write('REF6  / \n')
PERMX_PORO_REF.write('EQUALS\n')
PERMX_PORO_REF.write('PERMX '+str(kf)+' 6 32 15 15 1 1 /\n')
PERMX_PORO_REF.write('PORO '+str(porosf)+' 6 32 15 15 1 1 /\n')
PERMX_PORO_REF.write('/\n')
PERMX_PORO_REF.write('COPY \n')
PERMX_PORO_REF.write('PERMX PERMY /\n')
PERMX_PORO_REF.write('PERMX PERMZ /\n')
PERMX_PORO_REF.write('/\n')
PERMX_PORO_REF.write('ENDFIN\n')
```

```
    PERMX_PORO_REF.write('REFINE\n')
    PERMX_PORO_REF.write('REF7  / \n')
    PERMX_PORO_REF.write('EQUALS\n')
    PERMX_PORO_REF.write('PERMX '+str(kf)+' 6 32 15 15 1 1 /\n')
    PERMX_PORO_REF.write('PORO '+str(porosf)+' 6 32 15 15 1 1 /\n')
    PERMX_PORO_REF.write('/\n')
    PERMX_PORO_REF.write('COPY \n')
    PERMX_PORO_REF.write('PERMX PERMY /\n')
    PERMX_PORO_REF.write('PERMX PERMZ /\n')
    PERMX_PORO_REF.write('/\n')
    PERMX_PORO_REF.write('ENDFIN\n')
    PERMX_PORO_REF.close()
    try:
        f2 = open('C:\Mehrzad MEPO MFHW Nf7 L600m Base Reference
Set\source\PERMX_PORO_REF.INC', "r")
        try:
            # Read the entire contents of a file at once.
            string2 = f2.read()
        finally:
            f2.close()
    except IOError:
        pass
    return string2


def SchMaker(kf, km, lam, IFT, ngm, nwm, Kmaxgm, Kmaxwm, ngf, nwf,
Kmaxgf, Kmaxwf):
    Sgrm=0.1
    Swcm=0.15
    Sgrf=0.1
    Swcf=0.15
    krm=open('C:\Mehrzad MEPO MFHW Nf7 L600m Base Reference
Set\source\krm.INC','w')
    krm.write('SGWFN \n')

    iSg=Sgrm+0.001
    i=1
    while  (1-Swcm-iSg)>0:
        Swt=1-iSg
        Sgt=iSg
        krmgt=Kmaxgm*((Sgt-Sgrm)/(1.0-Swcm-Sgrm))**ngm
        krmwt=Kmaxwm*((Swt-Swcm)/(1.0-Swcm- Sgrm))**nwm
        Pd=0.0075*IFT*km**(-0.5)
        Pc=Pd/((Swt-Swcm)/(1-Swcm))**(1.0/lam)*14.5038
        if i==1:
            krm.write(' 0 0 1.0 '+str(Pc)+' \n')
        else:
            krm.write(' '+str(Sgt)+' '+str(krmgt)+' '+str(krmwt)+'
'+str(Pc)+' \n')
        i=i+1
        iSg=iSg+(1-Swcm-Sgrm)/5

    krm.write(' 0.85 1.0 0 '+str(Pc)+' \n')
    krm.write(' 1.0  1.0 0 '+str(Pc)+' \n')
    krm.write('/ \n')

    iSg=Sgrf+0.001
    i=1
    while  (1-Swcf-iSg)>0:
        Swt=1-iSg
```

```
        Sgt=iSg
        krmgt=Kmaxgf*((Sgt-Sgrf)/(1-Swcf-Sgrf))**ngf
        krmwt=Kmaxwf*((Swt-Swcf)/(1-Swcf- Sgrf))**nwf
        Pc=0
        if i==1:
            krm.write(' 0 0 1.0 '+str(Pc)+' \n')
        else:
            krm.write(' '+str(Sgt)+' '+str(krmgt)+' '+str(krmwt)+'
'+str(Pc)+' \n')
        i=i+1
        iSg=iSg+(1-Swcf-Sgrf)/5

    krm.write(' 0.85 1.0 0 '+str(Pc)+' \n')
    krm.write(' 1.0  1.0 0 '+str(Pc)+' \n')
    krm.write('/ \n')
    krm.close()
    try:
        f1 = open('C:\Mehrzad MEPO MFHW Nf7 L600m Base Reference
Set\source\krm.INC', "r")
        try:
            # Read the entire contents of a file at once.
            string1 = f1.read()
        finally:
            f1.close()
    except IOError:
        pass
    return string1
```

7.5 The developed MATLAB code to generate saturation maps for MFHW-Sets

```
% function createfigure(CData1, ZData1, YData1, XData1)
%CREATEFIGURE(CDATA1, ZDATA1, YDATA1, XDATA1)
%  CDATA1:  surface cdata
%  ZDATA1:  surface zdata
%  YDATA1:  surface ydata
%  XDATA1:  surface xdata

%  Auto-generated by MATLAB on 28-Jan-2016 12:49:16

% Create figure
figure1 = figure('Colormap',...
    [1 0.694117665290833 0.39215686917305;0.984811723232269
0.691316545009613 0.398319333791733;0.969623386859894
0.688515424728394 0.404481798410416;0.954435110092163
0.685714304447174 0.410644263029099;0.939246833324432
0.682913184165955 0.416806727647781;0.924058496952057
0.680112063884735 0.422969192266464;0.908870220184326
0.677310943603516 0.429131656885147;0.893681943416595
0.674509823322296 0.43529412150383;0.87849360704422 0.671708703041077
0.441456586122513;0.863305330276489 0.668907582759857
0.447619050741196;0.848117053508759 0.666106462478638
0.453781515359879;0.832928717136383 0.663305342197418
0.459943979978561;0.817740440368652 0.660504221916199
0.466106444597244;0.802552103996277 0.657703101634979
0.472268909215927;0.787363827228546 0.65490198135376
0.47843137383461;0.772175550460815 0.65210086107254
0.484593838453293;0.75698721408844 0.649299740791321
0.490756303071976;0.741798937320709 0.646498620510101
0.496918767690659;0.726610660552979 0.643697500228882
0.503081262111664;0.711422324180603 0.640896379947662
0.509243726730347;0.696234047412872 0.638095259666443
0.51540619134903;0.681045770645142 0.635294139385223
0.521568655967712;0.665857434272766 0.632493019104004
0.527731120586395;0.650669157505035 0.629691898822784
0.533893585205078;0.635480880737305 0.626890778541565
0.540056049823761;0.620292544364929 0.624089658260345
0.546218514442444;0.605104267597198 0.621288537979126
0.552380979061127;0.589915990829468 0.618487417697906
0.55854344367981;0.574727654457092 0.615686297416687
0.564705908298492;0.559539377689362 0.612885177135468
0.570868372917175;0.544351100921631 0.610084056854248
0.577030837535858;0.529162764549255 0.607282936573029
0.583193302154541;0.513974487781525 0.604481816291809
0.589355766773224;0.498786181211472 0.60168069601059
0.595518231391907;0.483597874641418 0.59887957572937
0.60168069601059;0.468409597873688 0.596078455448151
0.607843160629272;0.453221291303635 0.593277335166931
0.614005625247955;0.438032984733582 0.590476214885712
0.620168089866638;0.422844707965851 0.587675094604492
0.626330554485321;0.407656401395798 0.584873974323273
0.632493019104004;0.392468094825745 0.582072854042053
0.638655483722687;0.377279788255692 0.579271733760834
0.64481794834137;0.362091511487961 0.576470613479614
0.650980412960052;0.346903204917908 0.573669493198395
0.657142877578735;0.331714898347855 0.570868372917175
0.663305342197418;0.316526621580124 0.568067252635956
0.669467806816101;0.301338315010071 0.565266132354736
0.675630271434784;0.286150008440018 0.562465012073517
0.681792736053467;0.270961731672287 0.559663891792297
```

```
0.68795520067215;0.255773425102234 0.556862771511078
0.694117665290833;0.240585118532181 0.554061651229858
0.700280129909515;0.225396826863289 0.551260530948639
0.706442594528198;0.210208535194397 0.548459410667419
0.712605059146881;0.195020228624344 0.5456582903862
0.718767523765564;0.179831936955452 0.54285717010498
0.724929988384247;0.164643630385399 0.540056049823761
0.73109245300293;0.149455338716507 0.537254929542542
0.737254917621613;0.134267047047615 0.534453809261322
0.743417382240295;0.119078740477562 0.531652688980103
0.749579846858978;0.10389044880867 0.528851568698883
0.755742311477661;0.0887021496891975 0.526050448417664
0.761904776096344;0.073513850569725 0.523249328136444
0.768067240715027;0.0583255551755428 0.520448207855225
0.77422970533371;0.0431372560560703 0.517647087574005
0.780392169952393]);

% Create axes
axes1 = axes('Parent',figure1,...

'YTickLabel',{'17.24','33.62','41.81','45.91','47.96','48.98','49.49',
'49.75','49.88','49.94','49.972','49.988','49.996','50','50.004','50.0
08','50.016','50.032','50.064','50.128','50.256','50.512','51.024','52
.05','54.1','58.2','66.4','82.8','100'},...
    'YTick',[1 2 3 4 5 6 7 8 9 10 11 12 13 14 15 16 17 18 19 20 21 22
23 24 25 26 27 28 29],...

'XTickLabel',{'30.48','43.6','44.8','45.4','45.7','46','46.63','47.9',
'50.3','55.2','65.1','91.4','118','127.9','132.7','135.2','136.4','137
','137.3','137.9','139.1','141.6','146.5','156.2','182.9','209.3','219
.2','224','226.5','227.7','228.3','228.6','228.9','229.5','230.7','243
.8','274.3'},...
    'XTickLabelRotation',90,...
    'XTick',[1 2 3 4 5 6 7 8 9 10 11 12 13 14 15 16 17 18 19 20 21 22
23 24 25 26 27 28 29 30 31 32 33 34 35 36 37]);
%% Uncomment the following line to preserve the X-limits of the axes
xlim(axes1,[1 37]);
%% Uncomment the following line to preserve the Y-limits of the axes
ylim(axes1,[1 29]);
box(axes1,'on');
hold(axes1,'on');

% Create ylabel
ylabel('Y, Meters');

% Create xlabel
xlabel('X, Meters');

% Create title
title('The saturation map for Kf Max');

% % Create surface
% surface('Parent',axes1,'AlignVertexCenters','on','CData',CData1,...
%     'ZData',ZData1,...
%     'YData',YData1,...
%     'XData',XData1);

% Create colorbar
colorbar('peer',axes1);
```

pcolor (unnamed)